IMPACTS OF POTENTIAL SEISMIC LANDSLIDES ON LIFELINE CORRIDORS

Final Report

SPR 740

RESEARCH

IMPACTS OF POTENTIAL SEISMIC LANDSLIDES ON LIFELINE CORRIDORS

Final Report

SPR 740

by

Michael J. Olsen, Assistant Professor, Ph.D., E.I.T.
Scott A. Ashford, Professor and School Head, Ph.D., P.E.
Rubini Mahlingam, Graduate Research Assistant
Mahyar Sharifi-Mood, Graduate Research Assistant
Matt O'Banion, Graduate Research Assistant
Daniel T. Gillins, Assistant Professor, Ph.D.
Oregon State University, 101 Kearney Hall
Corvallis, OR 97331

for

Oregon Department of Transportation
Research Section
555 13th Street NE, Suite 1
Salem OR 97301

and

Federal Highway Administration
400 Seventh Street, SW
Washington, DC 20590-0003

February 2015

Technical Report Documentation Page

1. Report No. FHWA-OR-RD-15-06	2. Government Accession No.	3. Recipient's Catalog No.
4. Title and Subtitle Impacts of Potential Seismic Landslides on Lifeline Corridors		5. Report Date February 2015
		6. Performing Organization Code
7. Author(s) Michael J. Olsen, Ph.D. Scott A. Ashford, Ph.D., Rubini Mahlingam, Mahyar Sharifi-Mood, Matt O'Banion, Daniel T. Gillins		8. Performing Organization Report No. SPR 740
9. Performing Organization Name and Address School of Civil and Construction Engineering Oregon State University 101 Kearney Hall Corvallis, Oregon 97331		10. Work Unit No. (TRAIS)
		11. Contract or Grant No.
12. Sponsoring Agency Name and Address Oregon Dept. of Transportation Research Section and Federal Highway Admin. 555 13th Street NE, Suite 1 400 Seventh Street, SW Salem, OR 97301 Washington, DC 20590-0003		13. Type of Report and Period Covered Final Report
		14. Sponsoring Agency Code
15. Supplementary Notes		

16. Abstract

This report presents a fully probabilistic method for regional seismically induced landslide hazard analysis and mapping. The method considers the most current predictions for strong ground motions and seismic sources through use of the U.S.G.S. seismic hazard curves in conjunction with topographic, geologic, and other geospatial information. Probabilistic landslide triggering analysis is performed based on Newmark's sliding block theory. Because strength parameters are difficult to obtain in detail for a large regional area, friction angles for each lithological unit are estimated from histograms of the terrain slope at locations of previously mapped landslides within the unit. Afterwards, empirical models are used to predict the probability of a landslide triggering and the probability of horizontal displacement from a landslide exceeding specific thresholds (i.e., 0.1, 0.3, 1.0 m) relevant to engineering and planning purposes.

The probabilistic landslide-triggering map is evaluated by comparing its predictions with previously mapped landslides from the Statewide Landslide Inventory Database of Oregon (SLIDO). Over 99.8% of the landslides in SLIDO are located in areas mapped with very high probability (i.e., 80-100%) of a landslide triggering.

The created landslide hazard maps are suitable for regional resilience and planning studies by various agencies, as well as integration with maps of other types of hazards for probabilistic-based multi-hazard calculations and risk assessment. The maps should not be used in place of site-specific analyses, but may be used to prioritize where site-specific analyses and new geotechnical investigations are most needed. Finally, the maps can be used to identify which sections of the highway corridors would be likely be least affected by landslides, enabling it to serve as a lifeline route.

17. Key Words Landslides, earthquakes, lifelines, lidar	18. Distribution Statement Copies available from NTIS, and online at http://www.oregon.gov/ODOT/TD/TP_RES/	
19. Security Classification (of this report) Unclassified	20. Security Classification (of this page) Unclassified	21. No. of Pages 240 22. Price

SI* (MODERN METRIC) CONVERSION FACTORS

APPROXIMATE CONVERSIONS TO SI UNITS

Symbol	When You Know	Multiply By	To Find	Symbol
LENGTH				
in	inches	25.4	millimeters	mm
ft	feet	0.305	meters	m
yd	yards	0.914	meters	m
mi	miles	1.61	kilometers	km
AREA				
in^2	square inches	645.2	millimeters squared	mm^2
ft^2	square feet	0.093	meters squared	m^2
yd^2	square yards	0.836	meters squared	m^2
ac	acres	0.405	hectares	ha
mi^2	square miles	2.59	kilometers squared	km^2
VOLUME				
fl oz	fluid ounces	29.57	milliliters	ml
gal	gallons	3.785	liters	L
ft^3	cubic feet	0.028	meters cubed	m^3
yd^3	cubic yards	0.765	meters cubed	m^3

NOTE: Volumes greater than 1000 L shall be shown in m^3.

Symbol	When You Know	Multiply By	To Find	Symbol
MASS				
oz	ounces	28.35	grams	g
lb	pounds	0.454	kilograms	kg
T	short tons (2000 lb)	0.907	megagrams	Mg
TEMPERATURE (exact)				
°F	Fahrenheit	(F-32)/1.8	Celsius	°C

APPROXIMATE CONVERSIONS FROM SI UNITS

Symbol	When You Know	Multiply By	To Find	Symbol
LENGTH				
mm	millimeters	0.039	inches	in
m	meters	3.28	feet	ft
m	meters	1.09	yards	yd
km	kilometers	0.621	miles	mi
AREA				
mm^2	millimeters squared	0.0016	square inches	in^2
m^2	meters squared	10.764	square feet	ft^2
m^2	meters squared	1.196	square yards	yd^2
ha	hectares	2.47	acres	ac
km^2	kilometers squared	0.386	square miles	mi^2
VOLUME				
ml	milliliters	0.034	fluid ounces	fl oz
L	liters	0.264	gallons	gal
m^3	meters cubed	35.315	cubic feet	ft^3
m^3	meters cubed	1.308	cubic yards	yd^3
MASS				
g	grams	0.035	ounces	oz
kg	kilograms	2.205	pounds	lb
Mg	megagrams	1.102	short tons (2000 lb)	T
TEMPERATURE (exact)				
°C	Celsius	1.8C+32	Fahrenheit	°F

*SI is the symbol for the International System of Measurement

ACKNOWLEDGEMENTS

DISCLAIMER

TABLE OF CONTENTS

APPENDIX A: LIST OF SYMBOLS

APPENDIX B: ANALYSIS OF DEM PIXEL SIZE AND DATA SOURCE AND CONTRIBUTION TO LANDSLIDE DETECTION

APPENDIX C: A MAXIMUM ENTROPY APPROACH TO SEISMIC SLOPE STABILITY ANALYSIS AND MAPPING

APPENDIX D: OUTPUT AMBRASEYS AND MENU (1988) DISPLACEMENT

APPENDIX E: REMEDIATION TECHNIQUES

LIST OF TABLES

LIST OF FIGURES

Executive Summary

Landslides are ubiquitous within the state of Oregon, imposing an annual estimated cost of more than $10 million. Weak, saturated soils and steep slopes combined with persistent rainfall throughout most of the year provide a dangerous environment for this natural disaster in western Oregon. This grim situation is intensified due to the nearby presence of the Cascadia Subduction Zone, which is capable of generating large and powerful earthquakes.

This report presents a fully probabilistic method for regional seismically induced landslide hazard analysis and mapping. The method considers the most current predictions for strong ground motions and seismic sources through use of the U.S. Geological Survey's Next Generation Attenuation seismic hazard curves in conjunction with topographic, geologic, and other geospatial information. Probabilistic landslide triggering analysis is performed based on Newmark's sliding block theory. Because strength parameters are difficult to obtain in detail for a large regional area, friction angles for each lithological unit are estimated from histograms of the terrain slope at locations of previously mapped landslides within the unit. Afterwards, empirical models are used to predict the probability of a landslide triggering and the probability of horizontal displacement from a landslide exceeding specific thresholds (i.e., 0.1, 0.3, 1.0 m) relevant to engineering and planning purposes.

The probabilistic landslide-triggering map is evaluated by comparing its predictions with previously mapped landslides from the Statewide Landslide Inventory Database of Oregon (SLIDO). Over 99.8% of the landslides in SLIDO are located in areas mapped with very high probability (i.e., 80-100%) of a landslide triggering.

The created landslide hazard maps are suitable for regional resilience and planning studies by various agencies, as well as integration with maps of other types of hazards for probabilistic-based multi-hazard calculations and risk assessment. The maps should not be used in place of site-specific analyses, but may be used to prioritize where site-specific analyses and new geotechnical investigations are most needed. Finally, the maps can be used to identify which sections of the highway corridors would be likely be least affected by landslides, enabling it to serve as a lifeline route.

1.0   INTRODUCTION

1.1   PROBLEM STATEMENT

Coastal communities depend on Highway 101 and the state highways crossing the Coast Range to connect them with the rest of the State of Oregon. Unfortunately, landslides have the potential to isolate these communities by blocking narrow roadways adjacent to the steep slopes. The Oregon Coast Range is likewise home to weak soils, steep slopes, high groundwater, and substantial rainfall that can combine to produce landslides. "Sunken Grade" signs testify to the chronic nature of these slope movements throughout western Oregon.

The eventual certainty of one or more large earthquakes striking and triggering landslides adds to the considerable existing hazard described above. Seismic events produce additional inertial loading that may trigger landslides on slopes that are normally stable, or may reactivate dormant, pre-existing landslides. Because the Cascadia Subduction Zone (CSZ) is capable of generating powerful and long-lasting ground shaking across western Oregon, the geographic scope of potential seismically induced landslides is particularly broad. In addition to damaging and disrupting the state highway system, seismically induced landslides will inhibit the response to the damage and disruption caused by other earthquake hazards, such as strong ground shaking, liquefaction, and tsunami waves. The human and economic costs of earthquakes are multiplied by delayed response and recovery *(Gordon et al. 2004).*

State leaders and the general public expect the state highway system to serve as an important lifeline, facilitating post-earthquake response and recovery. In order to prepare effectively for the post-shaking use of the highway system, this report assesses the vulnerability of the various state highway routes to landslides. This will help the Oregon Department of Transportation (ODOT) identify key sites for seismic retrofit and to prioritize debris removal and repairs. In this way, ODOT can better ensure that critical lifeline corridors remain operational after a disaster, and can better plan how best to quickly and rationally restore other parts of the highway system after an earthquake.

1.2   BACKGROUND

This study focuses on the Oregon Coast Range, a 30- to 40-mile-wide swath of steep, rugged topography that extends for 300 miles along the Oregon coast. The Coast Range is heavily vegetated, receives substantial rainfall (up to 70 inches annually, typically during the winter months), and has a varied geology including Cenozoic marine sedimentary and volcanic rocks and Mesozoic accreted terranes *(Orr and Orr 2012).*

Recent landslide mapping in the Coast Range by DOGAMI using high-resolution lidar topography (*Burns and Madin 2009; Burns et al. 2010, 2012b,c,d, 2013a,b*) has determined that many parts of the Coast Range are 20-30% landslide material by area. The Cascadia subduction zone, a convergent plate boundary extending from Vancouver Island to northern California, has

produced powerful (magnitude 8-9) earthquakes at least 40 times over the last 10,000 years (*Goldfinger et al. 2012*). The paleoseismic record suggests that there is a strong likelihood that a rupture of the northern (7-12% chance) or southern (37-42%) margins of the Cascadia Subduction Zone in next 50 years (*Goldfinger et al. 2012*). This mix of topography, climate, geology, and seismicity make the Oregon Coast Range a zone of great instability—thereby threatening infrastructure and those who depend on that infrastructure.

Figure 1.1 shows the extents of the study area, which is bounded by the northern and southern borders of the State of Oregon, the I-5 corridor on the east, and the Pacific Ocean on the west. Coastal communities in the study area are connected by one major north-south route: Highway 101. Highway 101 is connected to the Interstate 5 freeway and the Willamette Valley by the following east-west routes: US Routes 30, 26, and 20; and, Oregon State Routes 6, 18, 22, 34, 126, 36, 38, and 42. There are some additional, minor routes to the coast. It is critical that these lifeline routes be accessible following an earthquake and/or tsunami to allow vital supplies and rescuers to reach the coast and allow people to escape, if needed. Even during common traffic conditions, recent landslides have caused major delays on these routes. Conditions following an major earthquake can be expected to compound such problems.

Lifelines are vital factors for the effective economy of a region and include highways, railroads, fiber optics, water conveyance infrastructure, other pipelines, utility transmission lines, and goods. Hence, special attention is required to analyze the effects of landslides in lifeline corridors *(Wilson et al.* 2008*)*. Crespo et al. *(Crespo et al.* 1987*)* studied the earthquake effects on lifelines in Ecuador, where both qualitative and quantitative methods were used. These impacts include direct losses on property, utility services, disruption of economic activity, delay in recovery options, release of hazardous products, and structural failures (*US Earthquake Consortium 2000*). Such studies will help us to determine the likelihood of survival of lifelines during various magnitudes of earthquakes, so that emergency/evacuation plans can be framed effectively (*Borchardt 1998*).

Landslides occur in the coastal regions of Oregon at irregular intervals. These landslides result in movement of material that affects coastal lifelines and structures. Coastal communities rely on a relatively few lifeline corridors (specially designated highways for evacuation and supply transport during emergencies), particularly following disastrous events when corridors provide critical access for rescue operations and for economic rebuilding activities. It is therefore important to identify which lifeline corridors are safe and can be relied on at the time of adversity. It is also important that rescue teams and citizens know the safest and least vulnerable routes to take during a disaster .

This study focuses solely on the landslide hazard, although it should be noted that a variety of additional considerations (including other hazards) exist for determining prioritization for lifeline routes. The Oregon Department of Transportation (ODOT) has recently completed an overview study that prioritizes lifeline routes as part of a broader analysis (*CH2M Hill 2012*) and considers many other factors. Nonetheless, this information can be used to identify sections that are irrecoverable and too expensive to mitigate as well as sections that will be expected to have a lower extent of damage. Hence, Oregon DOT can use this information for optimal allocation of limited funds for mitigation efforts.
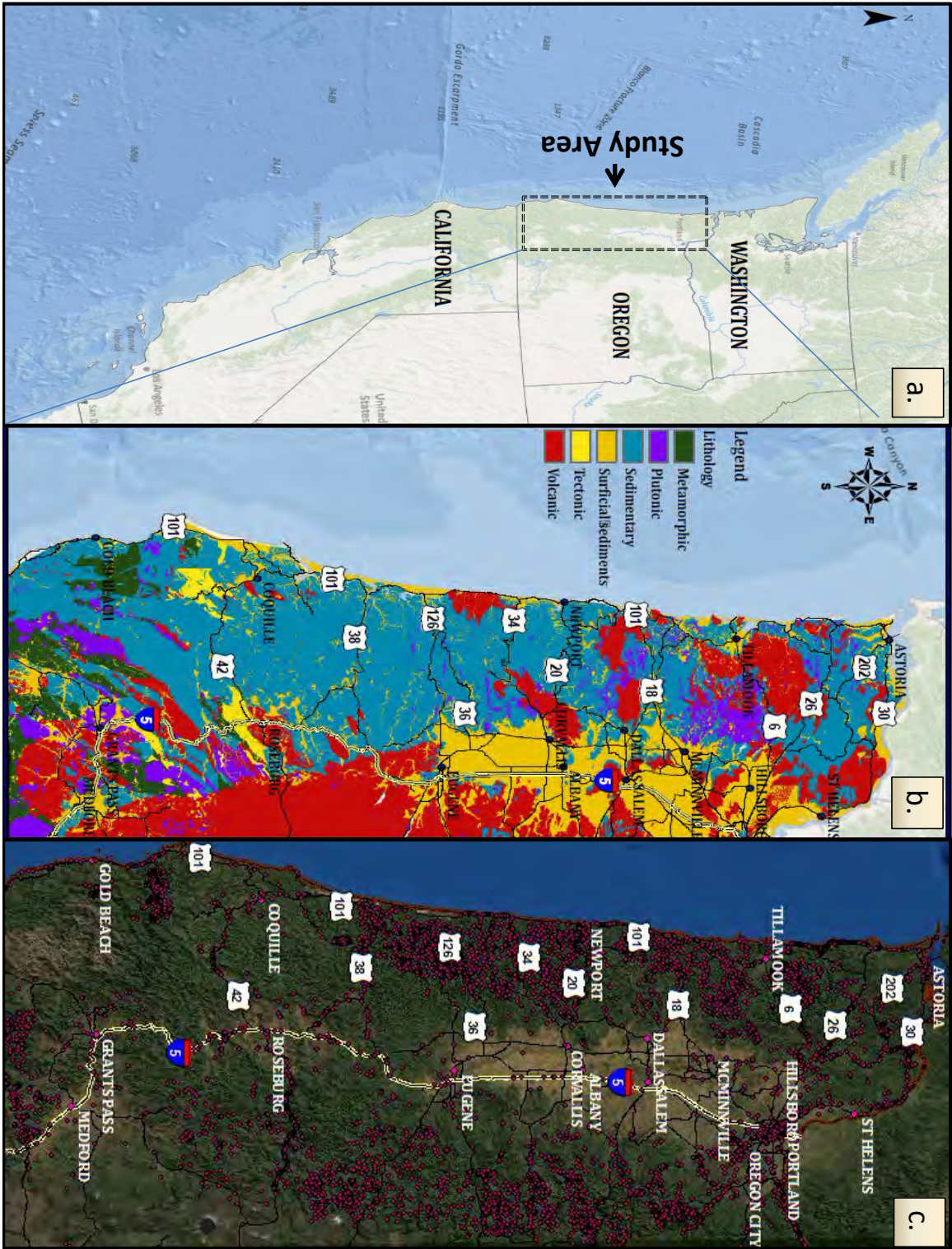
Figure 1.1: a. Study area b. Lithology map in Oregon coast c. Landslide inventory map.

1.3 OBJECTIVES OF THE STUDY

The objective of this research was to quantify the seismically induced landslide hazard along critical lifeline corridors in western Oregon. Understanding how landslides can affect these lifeline corridors is important for planning, preparation, and resilience purposes. The objective of this study was accomplished by:

1. Compiling available geospatial data regarding numerous factors that potentially contribute to the landslide hazard. Several datasets are compiled into a Geographic Information System (GIS), including: (1) vector datasets, such as highway locations, faults, folds, geology/lithology, streams, and land use; and (2) raster datasets, such as slope, aspect, slope roughness, terrain ruggedness, probabilistic seismic hazard data from the USGS (*2008*), and precipitation.

2. Analyzing the level of correlation of the numerous available factors with previously mapped landslides in western Oregon. Those factors most correlated with the previously mapped landslides are selected as predictor variables of the landslide hazard.

3. Developing new, or selecting existing, empirical models that use the predictor variables to predict the probability of a seismically induced landslide triggering and the probability of displacement from the landslide exceeding specified threshold distances.

4. Applying the empirical models using tools in GIS to produce new probabilistic landslide hazard maps of western Oregon. Such maps will allow better visualization of the landslide hazard along the critical lifeline corridors. These maps will help ODOT to locate and prioritize landslide-hazard mitigation efforts and future site-specific analyses. The maps will also inform ODOT of the least-vulnerable routes following a major event.

1.4 SIGNIFICANCE OF WORK

It is anticipated that the results of this project will be of significant economic benefit to ODOT and the State of Oregon, including:

1. Cost savings by determining which lifelines corridors can be hardened with the least resources.

2. Improvement of post-disaster operation plans resulting in quicker emergency response and economic recovery.

3. Selection of sites for quantitative monitoring that cannot be safely accessed by conventional means.

4. Advancement of the understanding of the current, historic, and ancient landslides on the highway system to manage their impacts on construction and maintenance better.

5. Compilation of LIDAR data, which can be used for future purposes, including routine monitoring of slopes and infrastructure, as well as supporting future roadway improvement projects

6. Development of a method to assess landslide hazards. Although the study area was western Oregon, the developed methodology can be applied elsewhere. Further, the developed methodology consists of a modular approach that inputs readily available data at the most basic level for broad applicability and consistency.

While the potential for disaster is high, quantification of hazard can lead to improved decision making and planning. Disaster preparation and management are key actions, which can be performed when effective tools and accurate data are available. A landslide hazard map enables governmental agencies to delineate vulnerable lifeline routes and utilities so that they will be able to optimally allocate resources for mitigation, plan safer routes, design structures that are more resilient, develop disaster preparation and response strategies, and identify sites that warrant more detailed monitoring and investigation.

1.5 IMPLEMENTATION

This project and the resulting landslide hazard maps can improve and shape work products from two relevant initiatives already underway within ODOT. The first is the Engineering and Asset Management Section's Unstable Slope Program. The second is the update and revision of ODOT's Lifeline Routes.

The information from this study will also be combined with ongoing work of the ODOT Bridge Section related to the seismic vulnerability of bridges along these lifeline routes to gain a better understanding of the total vulnerability and seismic risk of these corridors. This will aid in understanding which routes are currently the most resilient and in deciding which routes to invest retrofit funds into upgrades.

1.6 ORGANIZATION OF THIS REPORT

This report presents an analysis of seismic slope stability in western Oregon as well as a new methodology for fully probabilistic regional landslide hazard analysis and mapping.

Chapter 2 contains general background information on landslides and seismic slope stability.

Chapter 3 discusses landslide and seismic hazards in Oregon as well as current resilience and mapping efforts.

Chapter 4 presents background information on common landslide hazard mapping techniques.

Chapter 5 discusses the data sources used and compiled for this effort.

Chapter 6 presents a statistical approach to quantify the relative contribution of several factors to the landslide hazard in western Oregon. Numerous factors, such as slope, aspect, and a vegetation index were investigated. The study found that some factors are correlated with lithology.

Chapter 7 assesses soil erosion susceptibility throughout the study area and its correlation with landslides.

Chapter 8 presents regional seismic slope stability evaluations using multivariate regression techniques to develop coefficients for a logit function. It also discusses development of a GIS-based model tool, which enables one to quickly generate a series of maps based on multiple factors and evaluate their reliability.

Chapter 9 describes a newly developed methodology for a regional, probabilistic analysis for landslide hazard mapping based on readily available data. This methodology also enables one to consider the hazard in context of estimated displacements.

Chapter 10 applies the methodology to create a series of landslide triggering and displacement exceedance maps for the State of Oregon. Two displacement empirical models were used and compared.

Chapter 11 presents a series of landslide triggering and displacement exceedance maps for western Oregon based on a Cascadia Subduction Zone scenario event. Both a series of probabilistic maps showing the probability of exceeding displacement thresholds and a displacement map showing the estimated displacement (based on mean strength from the prior analyses) is provided.

Chapter 12 provides conclusions to the report, discussing the key outcomes of previous chapters and describing the potential use of produced maps and results derived within this study. Finally, Chapter 12 also discusses topics for future work and considerations.

Appendix A provides a list of symbols and abbreviations.

Appendix B evaluates the influence of DEM resolution and source for landslide prediction.

Appendix C shows the results of an alternative approach, maximum entropy, used for regional slope stability evaluation. This approach produced similar results to the generated maps.

Appendix D contains output maps using the Ambraseys and Menu *(Ambraseys and Menu 1988)* displacement model. Note that this model did not perform as well as the presented models and is only included for comparative purposes.

Appendix E describes potential remediation techniques.

2.0   LANDSLIDES AND SEISMIC SLOPE STABILITY

This chapter presents a review of landslides and seismic slope stability analyses.

2.1   OVERVIEW OF LANDSLIDES

Considered as one of the most devastating natural hazards, landslides are responsible for tremendous societal and economic harms, including fatalities and infrastructure damage. The United States Geologic Survey considers landslides to be the foremost geologic hazard, which are exceptionally common in all 50 states of United States, creating an average numeral of 25 fatalities and $1-2 billion cost in a typical year.

Landslides can be described as a downward movement of a mass of earth materials such as rocks and soils from a slope when the applied loads (driving forces) exceeds the strength (resisting forces) of the slope materials. For a synthesized overview of landslides including types, consequences, causative factors, and remediation, the reader is referred to USGS Circular 1325: "The Landslide Handbook – A Guide to Understanding Landslides" (*Highland and Bobrowksy 2008*).

2.1.1 Types

Typically, landslides may be classified in to seven basic types (Table 2.1), depending upon the type of movement and the type of materials carried. Cruden and Varnes *(Cruden and Varnes* 1996*)* classify the mechanisms of slope failures as falls, topples, slides (rotational and translational), lateral spreads, flows, or a combination. Of the many different ways landslides can occur, for the purposes of slope stability evaluation, each is designated as one of two types: shallow (<5m) and deep (>5m). Figure 2.1 shows an example of surficial slope failures, which have been problematic for the US Highway 20 realignment project. Landslides are often further classified by the rate of movement, predominant material type, failure mechanism, or triggering mechanism (e.g. rainfall or seismic).

Cornforth *(Cornforth 2005)* grouped earthquake-induced landslides in to the following three categories:

> Failure of marginally stable slopes.
> Translational-slide movements in clay soils.
> Liquefaction of saturated, cohesionless soils (e.g., lateral spreading).

Table 2.1: Type of landslides (modified from *Varnes 1978*)

Type of Movement		Bedrock	Engineering Soils	
			> 50% Coarse	> 50% Fine
	FALLS	Rock fall	Debris fall	Earth fall
	TOPPLES	Rock topple	Debris slide	Earth slide
SLIDES	ROTATIONAL	Rock slide	Debris slide	Earth slide
	TRANSLATIONAL			
	LATERAL SPREADS	Rock spread	Debris spread	Earth spread
	FLOWS	Rock flow (deep creep)	Debris flow (e.g., lahar, avalanche)	Earth flow
			(soil creep)	
	COMPLEX	Combination of two or more principal types of movement		

Figure 2.1: Shallow landslides at the US 20 Highway re-alignment project

2.1.2 Consequences

Disaster assistance, road maintenance, relocation, and repair following landslides result in the largest public costs (*US Search and Rescue Task Force 2011*). The USGS estimates that landslides in U.S cause an annual loss of about $3.5 billion (2001 dollars) and at least 25 fatalities, with other factors contributing to indirect losses (*USGS 2004*). For example, the recent landslide in Zhougqu County in China killed 1,144 people (*Boston.com 2010*), left thousands homeless, and posed a high threat for many epidemic diseases. Landslides are often associated with heavy infrastructure damage, loss of transportation accessibility, and freezing economic and domestic activities in mountainous regions. The most expensive landslide in U.S history occurred in Thistle, Utah during the spring of 1983, with a total cost exceeding $500 million. This large landslide spanned about 2000 m from top to bottom and varied in width up to about 300 m. Table 2.2 presents losses from various landslides.

Seismically induced landslides can also have devastating impacts. For example, the Loma Prieta earthquake triggered thousands of landslides, in October 1989, causing more than $30 million dollars in damage to over 200 houses, other structures, and utilities (*US Search and Rescue Task Force 2011*). Many of the landslides blocking critical transportation routes also impeded relief and rescue efforts. Experts felt that event served as a wakeup call to prepare for more devastating earthquakes that are likely to occur in future. In addition to landslides, liquefaction-induced lateral spreading of flood plain deposits along the Pajaro and Salinas rivers in the Monterey Bay region (*Holzer et al. 1989*) caused significant damage. Liquefaction accounted for $99.2 million of the total loss of $5.9 billion. The earthquake also significantly affected lifeline utilities, requiring 123 substantial repairs of pipelines in the municipal water supply system and replacement of 13.6 km of gas distribution lines (*Holzer et al. 1989*).

9

While high-velocity landslides can cause heavy damage to lives and buildings, slow moving landslides can cause cracking in buildings, road surfaces, utilities, pipes, etc. Quantifying many environmental impacts (e.g. landslide derived sediment creating turbidity in streams and other bodies of water, spoiling the fish habitats) in financial terms is nearly impossible since the impact is proportional to time and other variables (e.g. materials carried by the landslides, nature of the water body, etc. (*Leiba 1999*)).

Construction of the highways themselves can often create unstable cuts, leading to rockfalls, particularly during seismic events. Xinpo and Siming *(Xinpo and Siming* 2009*)* provide a discussion of several types of landslides observed along roadways following the 2008 Sichuan earthquake and potential repairs for these landslides (Table 2.3). Appendix F provides a more detailed discussion of remediation techniques.

Table 2.2: Consequences of mass earth movements (dry and wet), sorted by continent, from 1980-2010 (*EM-DAT 2013*). Note that values of zero (0) may mean that no data are available.

Continent	Type	# Events	# Killed	# Injured	# Affected	# Homeless	Total Affected	Damage (1,000 US$)
Africa	Landslide	23	440	98	15704	17600	33402	0
	Rockfall	2	129	72	0	625	697	0
	Subsidence	1	34	0	300	0	300	0
Americas	Avalanche	4	95	37	117	0	154	0
	Debris flow	1	10	0	0	0	0	0
	Landslide	109	6031	3745	1256386	183886	1444017	2000000
	Rockfall	3	216	0	0	0	0	0
Asia	Avalanche	43	2602	561	15810	38690	55061	50000
	Debris flow	1	106	0	0	0	0	0
	Landslide	223	12712	3635	1642318	3902278	5548231	1890838
	Rockfall	1	50	0	0	0	0	0
	Subsidence	1	287	38	2800	0	2838	0
Europe	Avalanche	28	772	61	14313	60	14434	757489
	Landslide	22	641	375	24894	3099	28368	2323000
Oceania	--	1	10	0	0	0	0	0
	Landslide	15	449	52	2663	18000	20715	0
Totals		478	24,584	8,674	2,975,305	4,164,238	7,148,217	7,021,327

Table 2.3: Landslide types and potential remediation techniques (after *Xinpo and Siming 2009*).

Landslide Type	Remediation
Shallow slope failures	Retaining walls
Deep landslides	Tie-backs
Rock avalanches	Tie backs, shotcrete
Surficial rock failures	Short rock bolts, shotcrete
Rock falls	Rock traps, fences
Instability of down-slope of road	Retaining walls, piles, etc. Change course of road

2.1.3 Causative Factors

Predicting landslides is complicated because of the numerous factors and conditions contributing to soil failure. Van Westen *(Van Westen* 1993*)* describes the use of many factors in a geospatial landslide analyses. This section will discuss many of these and other relevant factors considered in the literature.

2.1.3.1 Geologic

The type, permeability and strength of soil and rock found in the slope, subsurface lithology and geologic variability, jointing, structure, inter bedding, and interfaces between soil layers all play a role in the type and size of landslides. Unfortunately, aside from surficial geologic information, much of this information is not available on a regional scale in detail.

2.1.3.2 Topographic

Existing slope (topographic gradient), slope height, shape, slope face direction (aspect), and terrain ruggedness are important driving forces for landslides.

Slope: several researchers have found that slope (i.e. gradient of the ground surface) is correlated with landslide triggering (e.g., *Rahardjo et al. 2007*). For example, Rahardjo et al. *(Rahardjo et al.* 2007*)* concluded that with every increase of 1 degree, the initial factor of safety against landslide triggering is reduced by 2.32% for a given soil material.

Slope height: Rahardjo et al. *(Rahardjo et al.* 2007*)* also found that for slope heights greater than 5m the initial factor of safety decreases exponentially as the slope height increases.

Slope shape also has a considerable effect on its stability and resistance to movement. There are three principal types of slope shapes: planar (i.e. consistent gradient), divergent (e.g. the brow of a hill), convergent (e.g. a vale or hollow). With other site variables held constant, divergent landforms are generally most stable in steep terrain, followed by planar hillslope segments, and finally convergent hillslopes are the least stable (*Sidle and Ochiai 2006*). Divergent landforms allow subsurface and surface waters to evaporate, reducing pore water pressures throughout the slope. In contrast, convergent slopes create rapid pore water pressure increases during storms or periods of snowmelt (*Sidle 1984, Montgomery* et al. *1997; Tsuboyama* et al. *2000, Fernandes* et al. *2004Gillins*).

2.1.3.3 Hydrologic

Climate, persistent or intense rainfall, depth to ground water table, and pore water pressures can create unstable conditions and trigger landslides. Rainfall characteristics affecting stability include: (1) total amount of rainfall, (2) short-term intensity, (3) antecedent storm precipitation, and (4) storm duration. Generally, landslides are widespread in regions with steep slopes where the soil is weak, weathered, saturated due to heavy rainfall, and/or the groundwater table is relatively close to the ground surface. High intensity or long duration rainfall typically results in smaller, shallow failures. In contrast, medium to massive landslides generally result from long-term rainfall accumulation (*Yu et al. 2006*) or seismic influences (*Heynekamp et al. 1999*). Further, continued rainfall over long time spans leads to weathering and weakening of rock or soil.

The permeability of the soil also influences the potential for sliding. For example, Pradel and Raad *(Pradel and Raad 1993)* found that soils with a low critical hydraulic conductivity threshold (k_{lim} <10^{-4} cm/sec for the Southern California area) are more **likely** to develop a shear failure plane parallel to the slope surface due to a loss of adhesion between soil particles from saturation.

2.1.3.4 Vegetation

Vegetation (grasses and trees in particular) can help stabilize areas through evapotranspiration (*Bishop and Stevens 1964*) and can add reinforcement to the soil (*Sidle and Ochiai 2006*). Added reinforcement from trees is generally close (within 1m) to the ground surface (*Greenwood et. al. 2004*). As such, removal of vegetation can have adverse effects. Many studies (e.g., *Bishop and Stevens 1964, Endo and Tsuruta 1969, Fujiwara 1970, Swanson and Dyrness 1975*) have found a 2 to 10 fold increase in rates of soil erosion within 3 to 15 years after timber was harvested from soil slopes.

However, in some cases, vegetation can weaken an area and increase landslide susceptibility. For example, vegetation may add weight and thereby driving forces to a slope, or root growth may break apart soil cementation. Root systems may also increase hydraulic gradients, leading to further subsurface erosion and weakening.

2.1.3.5 External influences

Seismic activity, volcanic activity, or human actions can also lead to slope failures. Seismic slope stability will be discussed in more detail in Section 2.2.1.

Human terrain modifications and land use such as over-steepened cut slopes, fills, excavations, tree harvesting, and other changes in loading or resistance also contribute to landslide triggering.

2.2   SLOPE STABILITY

Landslides can be analyzed as a slope stability problem. In geotechnical engineering practice, slope stability is often characterized by computing the ratio of stresses resisting failure (shear strength) and stresses driving failure (from mass and gravity, and other loads). This ratio is termed the Factor of Safety (FS). The shear strength of the soil is commonly described by its friction angle (ϕ') and cohesion intercept (c') in Mohr-Coulomb Theory. The Mohr-Coulomb failure envelope is a function of these strength parameters and approximates the stress conditions at which the driving stresses have become equal to the resisting stresses of the soil. Such an envelope is depicted by plotting the shear strength of a material versus the applied normal stresses (Figure 2.2).

When the driving loads exceed the shear strength of the soil, failure occurs or the slope becomes unstable (i.e., FS < 1). Material on an unstable slope will then displace, along a failure surface.
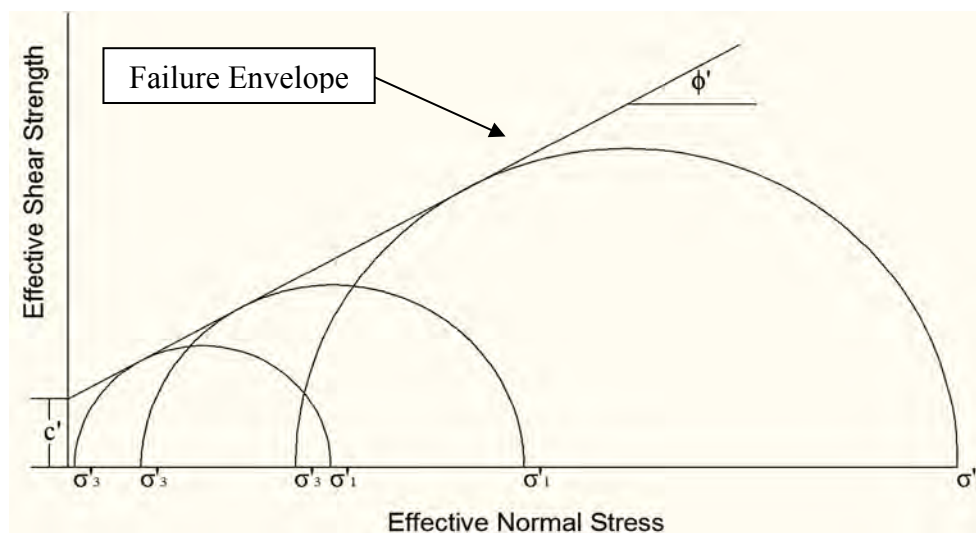
Figure 2.2: Mohr-Coulomb failure envelope (from *Rikli 2011*)

For slope stability analysis of very long (or "infinite") slopes, a potential failure surface is along a plane, parallel to the soil surface. Lambe and Whitman *(Lambe and Whitman* 1969*)* derived an equation (1-1) to compute the factor of safety along this failure plane, which results from seepage parallel to the slope face.

$$FS = \frac{c' + (\gamma_t - \gamma_w)d_w \cos^2(\alpha) \tan(\varphi')}{\gamma_t d \sin(\alpha) \cos(\alpha)} \qquad (1\text{-}1)$$

where: FS = factor of safety, c' = cohesion intercept, γt = total unit weight of soil, γw = unit weight of water, d = depth of the sliding mass above the failure plane, dw = depth of the groundwater table above the failure plane, ф' = effective friction angle, and α = slope inclination.

For stability analysis of finite slopes, failure surfaces are commonly divided into circular rotational slip, non-circular rotational slip, translational slip, and compound slip (*Craig 1997*).

Geotechnical engineers frequently use limit equilibrium methods of analysis when studying finite slope stability problems. They commonly use computation based on the method of slices because such an approach allows simple analysis of complex geometries, and can incorporate varying soil and groundwater conditions. A method of slices approach considers the stability of the slope in two dimensions and can be iterated to a potential failure surface. The sliding mass above an assumed failure surface is divided into slices, and the forces acting on each side (e.g., normal and shear) of the slice are analyzed using mechanical equilibrium theory. The factor of safety against slope failure is computed, a new potential failure surface is iterated, and the process can be repeated until the surface with the lowest factor of safety is found. Dozens of variations have been developed over the years, each differing in the factor of safety equation, shape of the failure surface, and the assumptions used to render the problem determinate (e.g., placement of the loads and moments on the slices, shape of the slices). Some of the most commonly used applications of the method of slices in practice are Janbu's method (*Janbu 1954, Janbu 1957*), Bishop's simplified method (*Bishop 1955*), Morgernstern-Price's method (*Morgernstern and Price 1965*), and Spencer's method (*Spencer 1967*).

Subsequent to the development of the method of slices, approaches using the finite element method and computer software have been developed to analyze slope stability of various materials under complex load conditions and in three dimensions.

2.2.1 Seismic Slope Stability

Post-earthquake investigations play a critical role on improving understanding and further defining the seismically induced landslide hazard. A historical review by researchers in Italy concludes that documentation of landslides can be effectively done by having comprehensive post-earthquake studies in combination with acquiring extensive ground based field studies. Xinpo and Siming *(Xinpo and Siming* 2009*)* discuss various types of landslides along the highways after the Sichuan earthquake in 2008. They note that a large portion of damages and injuries from an earthquake are instigated by seismically-induced landslides . Espinosa et al. *(Espinosa et al. 1991)* studied effects of landslides on lifeline routes after earthquakes, including property loss, damaged utility services, delayed recovery, and structural failures.

Study of the correlation of contributing factors, such as slope, geology, seismic sources, and seismic hazard curves improve understanding of seismically induced landslides. By means of remote sensing techniques, geospatial analysis, and probabilistic seismic hazard data, the delineation of areas prone to seismically-induced landslides is feasible. Afterwards, public infrastructure vulnerable to landslides can be identified and prioritized for further site-specific

analyses or mitigation. Significant landslide hazards underscore the need for future work in improving the understanding of existing or historical landslides, and refining estimates of potential shaking due to future earthquakes (*Department of Conservation 2011*).

Various studies have been done in order to better understand the influence of magnitudes, distance, time, and erosion factors affecting landslides and will be discussed in the following sections. In addition, Ashford and Sitar *(Ashford and Sitar* 1997*)* analyzed topographic effects on the seismic response of steep slopes. Havenith et al. *(Havenith el al.* 2003*)* studied the influence of topographic and site amplification effects on seismic slope stability. These studies conclude that localized topography can contribute greatly to the likelihood of slope failure during an earthquake.

2.2.1.1 Newmark's Method

Because the serviceability of a slope is strongly correlated with deformation, predictions of slope displacement due to landslides (i.e., co-seismic slope displacement) provide a more useful indication of the effects of seismic slope stability than computations of the factor of safety against slope failure .

Newmark *(Newmark* 1965*)* proposed a simple method of analysis to estimate co-seismic slope displacement. The method models the material displaced by a landslide as a rigid, plastic, block resting on an inclined plane. To initiate sliding of the block down an inclined plane, a seismic acceleration is needed to overcome frictional resistance. The method assumes that whenever the seismic acceleration from an earthquake time history is high enough to overcome frictional resistance and initiate sliding of the block (i.e., the seismic acceleration is greater than the "critical acceleration"), displacements occur. The total displacement is then estimated by integrating twice the difference of the seismic acceleration and the critical acceleration with respect to time.

Newmark's method has been widely accepted and used frequently in earthquake engineering analysis (*Kramer 1996*). For example, Wilson and Keefer *(Wilson and Keefer 1983)* applied Newmark`s method to analyze a landslide triggered by the 1979 Coyote Creek, California earthquake. Bray and Rathje (*Bray and Rathje 1998*) and Jibson (*Jibson 1993*) have employed Newmark's method along with actual strong motion records to calculate co-seismic displacement. Saygili and Rathje, (*Saygili and Rathje 2008*) and Miles and Ho, (*Miles and Ho 1999*) have used Newmark's method empirically to assess the potential for a seismically induced landslide.

The assumptions of Newmark's method are clearly not applicable for some types of landslides, and can be problematic when applied universally for regional hazard mapping. First, Newmark's method may underestimate total displacements because the method assumes the sliding block remains perfectly plastic, which is not realistic during landslide deformations. As soils are strained with increased displacement, they lose shear strength, which in turn reduces the critical acceleration (*Cornforth 2005*). Second, the method requires the use of time histories, the application of which is computationally intensive to

apply at a regional scale. A generalized method is preferred to one that requires several parameters since detailed information is rarely available for an entire region.

2.2.1.2 Empirical methods

Several researchers have used a form of Newmark's method to develop empirical models for estimating the displacement of slopes and earth structures during seismically induced landslides. Generally, these empirical models were developed by multivariate regression analyses of compiled case histories of landslides. Table 2.4 lists several of the recently developed empirical models and their variables for predicting seismically induced landslide displacements. The predictor variables used in these models are defined below:

Predominant period of the sliding mass (T),

Spectral Acceleration (S_a), maximum acceleration that a ground motion will cause at any point with a specified period (T),

Peak Ground Acceleration (PGA), spectral acceleration of the ground when $T = 0$,

Peak Ground Velocity (PGV), spectral velocity of the ground when $T = 0$,

RMS acceleration, the effective acceleration over a given time,

Yield acceleration (a_y), the minimum acceleration that puts the slope on the verge of failure or critical acceleration,

Earthquake moment magnitude (M),

Arias intensity (I_a), a parameter representing amplitude, frequency content, and duration characteristics of a ground motion. (Note that this also requires that one develop a time history for the site, which is computationally intensive for a regional study),

Number of earthquake loading cycles (N_{eq}).

In some cases, these regression equations listed in Table 2.4 have a probabilistic form to calculate likelihood of exceeding a threshold displacement. Interestingly, Strenk and Wartman (*Strenk and Wartman 2011*) evaluated 16 seismically-induced landslide models published since 1965 against actual case history data and have shown that these newer models performed similar to Newmark's method. Hence, there still is much uncertainty in predicting slope displacements for seismically induced landslides.

Table 2.4: Several empirical models and their predictor variables for estimating seismically induced landslide displacements of slopes.

Method	Year	a_y	a_{max} (PGA)	I_a	M	T	S_a	N_{eq}	PGV
Makdisi & Seed	1978	●	●		●	●			
Ambraseys & Menu	1988	●	●						
Yegian et al.	1991	●	●			●		●	
Jibson	1993	●		●					
Jibson (Scalar)	2007	●	●						
Jibson (Vector)	2007	●	●	●	●				
Bray & Travasou	2007	●	●		●	●	●		
Saygili & Rathje (Scalar)	2008	●	●						
Saygili & Rathje (Vector)	2008	●	●	●		●			●
Rathje & Saygili (1)	2011	●	●						●
Rathje & Saygili (2)	2011	●	●			●			

2.3 CONCLUSIONS

From the review of literature on landslides seismic slope stability analysis and mapping procedures described, the following conclusions can be drawn:

1. While landslides are very common occurrences and frequently cause damage, they are incompletely understood. Due to the complexity of triggering mechanisms and soil variability, it can be difficult to analyze slope stability, particularly across a regional scale.

2. While many recognize that there are various factors contributing to seismic slope stability, there is little research on the relative contribution of each factor to the overall hazard. Further, there is a large disconnect between site-specific displacement models and the geomorphological factors studied in general landslide assessment. For example, the only topographic input to the displacement models presented in Table 2-4 is the slope angle used to calculate the yield acceleration. Many of the other factors discussed in section 2.1.3 are ignored in the models. Conversely, many of the geospatial-based analyses to be discussed in Chapter 4 do not include detailed seismic information.

3. New, and in some cases, more sophisticated empirical models perform no better than earlier models when compared to case history data. Hence, for regional analyses, it is advantageous to use a simpler model with fewer inputs if it performs similar to a complex model requiring specialized data, which are often not available for regional analyses.

3.0   OREGON LANDSLIDE AND EARTHQUAKE HAZARDS

Figure 3.1 shows the topography and lithology across the state of Oregon. Tectonic plates and volcanic activities formed the landscape. The western section, bounded by the highest topography receives heavy rainfall compared to the eastern section, which consists of high desert country of volcanic rocks. In between the Coast Range (sedimentary rock) and Cascades (volcanic rock), lies the Willamette Valley, which consists of sedimentary or surficial weak soil deposits such as alluvium.

The coast range itself is primarily made up of weak, weathered, sedimentary rock. The natural topography throughout the coast range typically consists of slopes between 19° to 31° and elevations spanning from 9 to 549 m (*Natural Resource Conservation Service 2009*). The Tyee formation spans much of the coast range. It consists of sandstone sediments with significant silt and clay interbedding that were deposited on a rigid fore-arc block during the upper Eocene and Oligocene period (*Van de Water et al. 2009 and* 2010*)*. These sediments tilted, folded, and faulted resulting in flexure slip along bedding planes (*Hammond* et al. *2009*). Subsequent tectonic uplift (*Kelsey et al. 1996*) destabilized many of the hillslopes, enabling the development of landslides due to erosion, rainfall, and the incising of drainages (Van de Water et al. 2009 and 2010). As such, sliding often occurs along these weak, slippery, interbedded seams. Figure 3.2 shows a landslide that occurred in the Tyee formation due to sliding on a cut section of the US20 reconstruction project. Rikli *(Rikli 2011*) analyzed several surficial slope failures that occurred in remolded fill material from the Tyee formation.
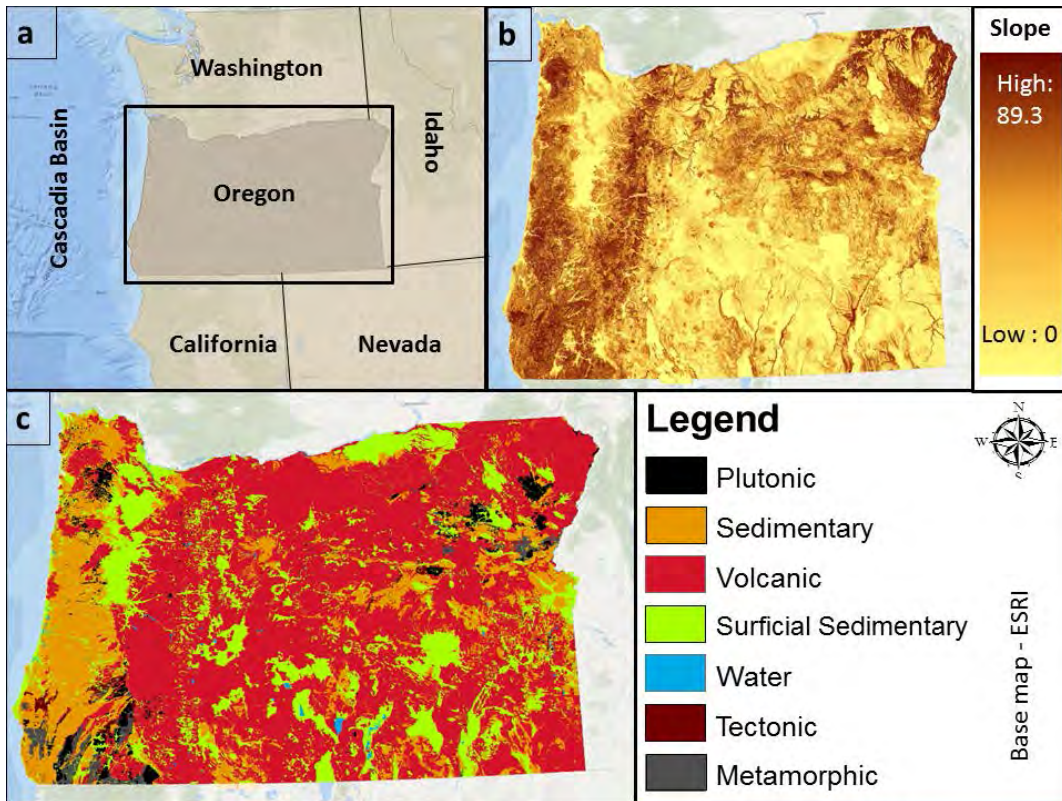
Figure 3.1: a) Extents of state of Oregon selected as the study area, b) Created slope map from hybrid DEM in the region, c) Lithology map within the ranges of state of Oregon

Figure 3.2: Example 3D laser scan of a landslide on the US 20 realignment project in the Tyee formation.

3.1   LANDSLIDE HAZARDS IN OREGON

Oregon's climate and soil conditions are well suited for the disturbing, yet natural, hazard of landslides. Landslides are observed across the entire coast range and Cascades, which contains

steep slopes of weak soils and rocks wetted by persistent rainfall during most of the year and abundant ground water. "Sunken grade" signs are a common feature along various highways. The pervasive storms and precipitation (including snow melt) weather the rock and can generate debris flows.

The Statewide Landslide Information Database of Oregon (SLIDO) represented in Figure 3.3 is an accumulation of reported and identified landslides in Oregon *(Burns et al. 2012a)*. Each point on that figure represents an inventoried landslide. SLIDO will be discussed in more detail in Chapter 5. Table 3.1 lists several media articles highlighting landslides that have blocked highways in recent years. In particular, many landslides occurred during heavy rainfall in 2011, leading to life safety concerns, traffic delays, detours, and necessary repairs. These serve as a stark reminder of how vital lifeline corridors are during emergency events.

Landslide damage to infrastructure and homes results in significant costs throughout Oregon. For example, a large storm event in February 1996 individually led to $4 million damage to the Portland urban area. Landslides that were triggered during storms occurring during 1996-97 caused $280 million in damages and resulted in five deaths. Overall, landslides are estimated to cause $10 million damage annually in Oregon *(*Wang *et al.* 2002*)*.

The Coast Range in Western Oregon is very susceptible to landslides because of the geological, topographical (steep slopes), and hydrological (heavy rainfall) conditions (*Burns et al. 1998*). The Oregon Department of Geology and Mineral Industries (DOGAMI) studied this relationship from west of the Cascades to the ocean beaches. Oregon experienced unusual amounts of rainfall during four storms from February 1996 to January 1997, resulting in numerous debris flows. When comparing rainfall data from weather stations with failure locations, DOGAMI found that slides tended to occur in western Oregon when (A) 8 inches (20 cm) of rain had fallen since the end of September 1996 and (B) the 24-hour rainfall exceeds 40 percent of the mean December rainfall (*Wiley 2000*).
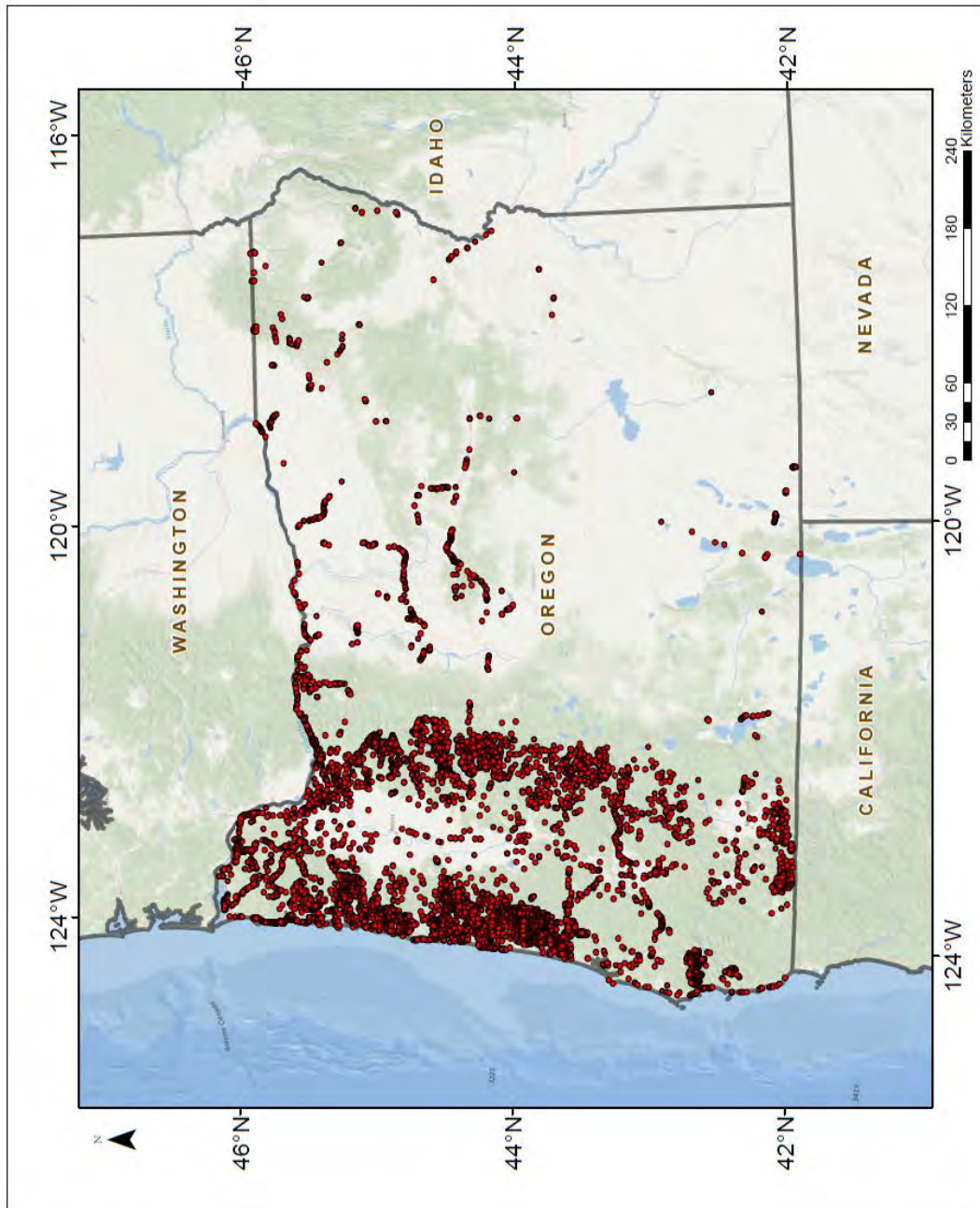
Figure 3.3: Historical landslide database (SLIDO) provided by DOGAMI.

Table 3.1: Examples of media coverage of recent road closures from landslides.

Report Date	Highway	Location affected	Size	Composition	Impacts	Trigger	Link
11/6/2006	Ore 6	Several landslides MP33-34			$5 million reapirs	Rainfall	http://www.oregonlive.com/news/index.ssf/2009/03/wilson_river_high way_will_get.html
12/12/2007	US 30	west of Clatskanie	5 acres	mud, trees, debris	Highway closed (prior to landslide occurence due to monitoring), damaged homes	Rainfall	http://www.nbcnews.com/id/22216397/ns/weather/t/landslide-covers- oregon-highway/#.Uctp8Zzgd3c
1/6/2008	Ore 126	10 miles east of Mapleton	-	mud, rocks, & large trees	Road closed	Heavy Snow	http://blog.oregonlive.com/breakingnews/2008/01/landslide_blocks_hig hway_to_or.html
1/1/2009	US 26	MP 34 and 35, nrear Alder Crrek	2 ft deep, 100 yards wide	mud, trees, other debris	Road closure	Rainfall	http://www.oregonlive.com/news/index.ssf/2009/01/landslide_blocks_ us_26_near_al.html
7/18/2010	US 101	Four lanes in North Bend (MP 236)	8 ft deep of debris,	-	4 lanes and shoulders closed.	Fire	http://www.oregonlive.com/pacific-northwest-news/index.ssf/2010/07/landslide_closes_four_lanes_of_highway_101_i n_north_bend.html http://www.katu.com/news/local/98716104.html
1/6/2011	US 20	US20	-	-	Project delays,	Rainfall	http://www.oregonlive.com/paci

Report Date	Highway	Location affected	Size	Composition	Impacts	Trigger	Link
		Realignment project			Damaged bridge columns, > $100 Million dollars in damages		fic-northwest-news/index.ssf/2011/01/landslides_causing_further_delays_to_star-crossed_us_20_improvement_project.html
1/13/2011	Ore 47	10 miles south of Mist	-	-	road closed	Rainfall	http://www.oregonlive.com/roadreport/index.ssf/2011/01/landslide_clo ses_all_lanes_of.html
1/17/2011	Ore 6	4 miles east of HW 35 Junction, MP6, and MP49	100 ft wide	thick mud, trees, large rocks	Partial Closure of roadway	Rainfall	http://www.kgw.com/news/local/Landslides-standing-water-close- Oregon-roads-113843679.html
1/17/2011	Ore 6	Just east of Tillamock	-	-	Road closed	Rainfall	http://www.kgw.com/news/local/Landslides-standing-water-close- Oregon-roads-113843679.html
1/17/2011	US 101	South of Rocakway Beach (16 miles north of Florence)	-		Road closed	Rainfall	http://www.kgw.com/news/local/Landslides-standing-water-close- Oregon-roads-113843679.html
1/17/2011	US 20	Santiam Highway (MP 44)	150 yd^3	mud, rock, and debris. 12 large trees	Closed near Cascadia	Rainfall	http://www.kgw.com/news/local/Landslides-standing-water-close- Oregon-roads-113843679.html http://www.oregonlive.com/pacific-northwest-news/index.ssf/2011/01/landslid

Report Date	Highway	Location affected	Size	Composition	Impacts	Trigger	Link
							e_closes_us_20_near_cascadia_in_centr al_oregon.html
2/15/2011	NW Cornell Road	Portland	-	debris, trees	Road Closed	Rainfall	http://www.oregonlive.com/portland/index.ssf/2011/02/landslide_close s_stretch_of_po.html
2/28/2011	US 30	2 miles east of Goble	-	debris, trees	Partial closure, accident	Rainfall	http://www.oregonlive.com/news/index.ssf/2011/02/landslide_blamed_in_accident_a.html
3/20/2011	Ore 224	Westbound landes west of Eagle Creek (MP 10.3)	-	Debris	Closed westbound lanes	Rainfall	http://www.oregonlive.com/clackamascounty/index.ssf/2011/03/landslide_closes_westbound_la n.html

3.2 SEISMICITY IN OREGON

Adding to these already precarious conditions, Oregon also experiences high seismicity. As an example, the Scott Mills (M 5.6) earthquake, a shallow, crustal earthquake, resulted in $30 million in damages. However, the most severe earthquakes in Oregon are derived from Cascadia subduction zone (CSZ), which is a convergent plate boundary extending from Vancouver Island to northern California (*James et al.* 2000*)*. The CSZ has resulted in powerful earthquakes, which have occurred at least 40 times over the last 10,000 years, ranging from magnitude ~8 to ~9 . Geologists estimate that the probability that a CSZ earthquake will occur in the next 50 years ranges from about 7 – 15% for a magnitude 8.7 to 9.3 earthquake affecting the entire Pacific Northwest to about 37% for a magnitude 8.3 to 8.6 earthquake affecting southern Oregon (*OSSPAC 2013*). Table 3.2 provides a summary of significant earthquakes that have occurred in Oregon (*EM-DAT 2013*). The most recent, documented CSZ earthquake occurred on January 26, 1700, with an estimated moment magnitude of 9.0.

A current subject of investigation is the potential of the CSZ to initiate new landslides or reactivate existing landslides throughout the Oregon Coast Range. For example, Schulz et al. *(Schulz et al. 2012*) studied several active landslides along the coast and discovered that these landslides were likely triggered by the 1700 Cascadia Earthquake. However, insufficient information exists to isolate the triggering mechanisms of all the landslides that cover Oregon's coast range.

Table 3.2: Large, historical earthquakes in Oregon (EM-DAT 2013)

Date	Time UTC	Latitude	Longitude	Magnitude	Intensity
1700 01 26	13:00	-	-	8.7 to 9.2	
1910 08 05	01:31:36	42.0 N	127.0 W	6.8	Felt
1993 09 21	03:28:55.4	42.314N	122.012W	6.0	VII

3.3 HAZARD MAPPING AND LANDSLIDE INVENTORY EFFORTS IN OREGON

The Oregon Department of Geology and Mineral Industries (DOGAMI) is the state agency charged with aiding Oregonians to understand and prepare for a variety of hazards including earthquakes, tsunamis, landslides, and coastal erosion. This section will focus on landslide and earthquake mapping efforts in Oregon.

3.3.1 Landslides

Many hazard maps have been produced by DOGAMI based on geologic, topographic, and hydrologic conditions for many communities in Oregon. Harvey and Peterson *(Harvey and Peterson* 1998 and 2000*)* and Beaulieu *(Beaulieu* 1973*),* Waters (Waters *1973*), and Wang et al. *(Wang et al.* 2002*)*, provide more information regarding specific landslide hazard maps produced by DOGAMI. Wang et al. *(Wang el al.* 2002*)* provides an overview of various agencies that have

mapped landslide hazards in the state of Oregon. For example, Burns et al. *(Burns et al.* 2008*)* and Niewendorp and Neuhaus *(Niewendorp and Neuhaus* 2003*)* discuss specific landslide studies for the state of Oregon. A few of these maps will be highlighted in this section.

DOGAMI developed the SLIDO *(Burns et al. 2008 and 2012a),* which integrates previous landslide mapping efforts in Oregon into a seamless, web-based viewer. Recent LIDAR technology, which has enabled detailed topography to be obtained for the ground beneath forest covered areas, improves mapping and delineation of landslides. As such, DOGAMI continues to update SLIDO with new landslides that have been inventoried in a consistent fashion. Burns and Madin *(Burns and Madin* 2009) present the standardized methodology used to map and inventory landslides using LIDAR topographic information.

Within Oregon DOT, an Unstable Slopes Program has been established to inventory and rate landslides, rockfalls, unstable slopes, etc., that impact Oregon's highway infrastructure. This information is important to determining priorities for repairs and maintenance. However, inventory systems are time-consuming (years) to complete and generally only provide basic information after a collapse has occurred. As such, it is a daunting task to maintain a current, comprehensive database.

In addition to inventory mapping, Hofmeister et al. *(Hofmeister et al.* 2002*)* provide a series of GIS overview maps (IMS -22) showing the potential for rapidly moving landslide hazards in western Oregon. For these maps, they established slope thresholds determined from evaluating slopes at landslide locations. They then categorized these thresholds based on four regions: Background, High Cascades, Columbia River Gorge, and the Coast Range. However, these maps were created prior to the availability of LIDAR data and have subsequently been deemed inaccurate based on LIDAR-based findings.

A GIS-based landslide hazard mapping technique developed for Benton County entitled "Water-Induced Landslide Hazard for Benton County" incorporates landslide inventory, slope, and soil properties with infinite-slope type of modeling. Using this technique, Bela *(Bela 1979)* mapped landslide deposits for eastern Benton County, and Walker and Duncan *(Walker and Duncan 1989*) produced landslide hazard maps for Salem.

3.3.2 Earthquakes

Because of the hazards earthquakes pose to infrastructure development, DOGAMI has diligently published maps and papers related to earthquakes and seismicity in Oregon, including maps showing potential liquefaction and soil amplification (*Hofmeister et al. 2003*). Common examples of maps and information include:

Fact sheets produced by DOGAMI help the public understand the need for the study of seismic activity in Oregon. For example, Clark *(Clark 1999)* provides evidence of earthquake related reports specific to Oregon.

The USGS maintains the website where the agency publishes information regarding earthquakes around the world (*USGS 2012a*).

Mabey et al. *(Mabey et al. 1993 and 1997)* completed the earliest earthquake hazard mapping in Oregon for the Relative Earthquake Hazard Mapping (REHM) project in the Portland Metro area. This mapping provides details about site amplification, liquefaction potential, and slope stability. Earthquake scenario and probabilistic ground shaking maps of the Portland Metro area by Wong et al. *(Wong 2000)* followed in the form of IMS-16. DOGAMI extended the REHM to urban areas throughout western Oregon (e.g*., Madin and Wang* 1999*)*. Such maps are for land-use planning, lifeline management, emergency mitigation etc., in addition to raising public awareness of earthquake hazards. *(Wang and Leonard 1996)*

Wang and Clark *(Wang and Clark 1999)* used HAZUS97, a software package developed by Federal Emergency Management Agency *(*http://www.fema.gov/hazus) for to assess the seismic risk in Benton County. They found that a M8.5 Cascadian subduction zone earthquake could result in $630 million in building losses.

Barnett et al. *(Barnett et al. 2004*) mapped potential effect of earthquake hazards on the Pacific Northwest section of the I-5 corridor.

Petersen et al. *(Petersen et al. 2008)* updated the national seismic hazard maps to include the best available science and Next Generation Attenuation relationships. These maps provide earthquake ground-motion levels and probabilities across the United States and are a compilation of the latest scientific consensus of potential earthquake hazards.

Despite all of the previous studies that have utilized the most current information, updates to these maps are sometimes needed. Considering the importance of slope angle to landslide studies on the western coast, it becomes essential to generate new maps incorporating more accurate geospatial technology such as LIDAR (*OLC 2013*). Further, our understanding of seismic mechanisms and impacts has improved as more case histories are compiled. For example, the Geo-Extreme Engineering Reconnaissance (GEER) group records information related to the degree of damage observed at sites following earthquake events (*GEER 2013*).

3.3.3 Recent Resilience Efforts

The importance of lifelines to withstand impacts from hazards has been a focus in Oregon, which faces multiple hazards including landslides, earthquake (shaking, landsliding, liquefaction, etc.), tsunami, volcanic activity, flooding, coastal erosion, etc.

Recently, Oregon DOT completed a seismic lifeline route-identification project for a CSZ event. Routes were classified as Tier 1, 2, and 3 (highest to lowest priority). This project identified the following corridors as Tier 1 (most critical) for the Coast Range:

OR 30 from Portland to Astoria

OR 18 from the Valley to US 101 and north and south on US 101 from Tillamook to Newport

OR 38 from I-5 to US 101 and north and south on US 101 from Florence to Coos Bay

The Oregon Seismic Safety Policy Advisory Commission (OSSPAC) has recently released the Oregon Resilience Plan to provide policy recommendations to prepare for a Cascadia Earthquake

and Tsunami (*OSSPAC 2013*). In this effort, several ground failure maps, including landslides, were generated using HAZUS. This plan provides detailed recommendations for various types of infrastructure. Amongst several transportation related recommendations (including mitigation efforts and additional studies), the committee recommended enhancement of the Highway Lifeline Maps to consider local routes and critical facilities.

4.0   LANDSLIDE HAZARD MAPPING

The objective of this chapter is to study the strengths and weaknesses of various methodologies available to map potential seismically induced landslides. This review will cover general landslide mapping methodologies as well as methods developed for seismically induced landslides. Both deterministic and probabilistic methodologies will be summarized.

Landslide hazard mapping provides an important service to society by distinguishing areas of different landslide risk. These maps are a useful tool for land-use planners, lifeline facility managers and personnel, local government building codes, and property owners. Most maps usually combine surface geology with slope (topographic gradient) to determine the perceived level of hazard (*Cornforth 2005*). Hazard may be defined as probability of occurrence within a reference time period and is a function of both the spatial probability and the temporal probability, related indirectly to some static environmental factors such as slope angle, and hydraulic conductivity and directly to dynamic factors like rain input and drainage (*Van Westen et al. 2006*). Most typical mapping consists of deterministic methodologies; however, advanced methodologies are being developed for probabilistic mapping. Spatial analyses used to generate maps are usually performed in a Geographic Information System (GIS). Appendix B of USGS Circular 1325 "The Landslide Handbook" (*Highland and Bobrowksy 2008*) discusses several mapping and remote sensing techniques to evaluate and monitor landslides.

It should be noted that several end products exist for landslide mapping, including:

- **Inventory** – mapping and documentation of existing landslides, both historic and pre-historic based on geologic evidence,

- **Susceptibility** – Mapping based on soil and site conditions that indicate areas susceptible to landsliding, and

- **Potential** – Mapping and evaluating the potential for damage, incorporating external effects. This differs from susceptibility in that the triggering sources are included in the analysis. In some literature, these are referred to generically as hazard maps. Further, potential mapping methodologies can be classified into deterministic and probabilistic.

4.1 DETERMINISTIC MODELS

Numerous published landslide hazard-mapping methodologies are deterministic, but require comprehensive datasets with detailed input information. Deterministic models are based on the physical laws of mass, energy or momentum to determine a factor of safety (i.e., ratio of resisting forces to driving forces) against slope failure, calculate predicted displacements, or an index (e.g., *Fabbri et al. 2003*)) of failure potential or magnitude.

Deterministic models will produce a particular result from a given input scenario; however, they cannot consider uncertainty or randomness in the input variables or the resulting outputs. Information at each point analyzed (e.g., pixel) such as the presence of pore water pressure, failure surface depth, strength parameters and limiting equilibrium slope stability information are essential for a deterministic analysis yet are difficult to obtain for large areas, leading to lower credibility when estimates are applied over large regions that do not account for spatial variability. Hence, a deterministic model is best applied over small areas where this information is available.

This section describes common geologic and hydrodynamic parameters needed for detailed, deterministic analyses that are difficult, if not impossible, to obtain for a regional scale.

Sub-surface geology. While slope values and surficial geology for a large study area are generally available, it is unlikely to acquire subsurface information such as soil thickness, interbedding, or dipping information for a regional scale (*Lee et al. 2008*). These parameters can have significant variability across the study area and require thorough geotechnical and geological investigations.

Hydrodynamic conditions. Cornforth *(Cornforth 2005)* discusses the difficulties in modeling fluctuations in groundwater on a regional scale. For example, many authors (e.g., *Densham et al. 1991, Stuart and Stocks 1993*) have coupled a hydrological model that simulates the time variance of pore water pressures with a slope stability analysis, which depicts the pore pressure threshold and can be further integrated into GIS for hazard mapping.

4.2 PROBABILISTIC LANDSLIDE HAZARD MAPPING

Although deterministic methodologies are the most common in typical hazard mapping, spatial analyses and advanced procedures are more recently being developed to generate probabilistic landslide hazard maps. Probabilistic methods are meant to capture the uncertainty associated with the inputs (e.g., geotechnical, geological and geomorphological data) and the resulting outputs. Van Westen et al. (*Van Westen el al. 2006*) describes a hazard assessment approach determining the probability of occurrence within a time period as a function of both the spatial likelihood and temporal probability influenced by static environmental factors (e.g., slope angle) and dynamic factors (e.g., precipitation and drainage characteristics). Probabilistic models take numerous variables such as slope, acceleration, strength parameters, pore pressure, distance and magnitude as random variables . Occasionally, geologic maps can be supplemented by geotechnical parameters gathered from laboratory tests. Unfortunately, the stratigraphic units depicted on geologic maps, don't correspond to geotechnical properties. This can cause poor positional accuracy in defining the spatial distribution of geotechnical properties. Advanced

versions of these methodologies can incorporate seismic induced landslides, which will be discussed a subsequent section. Several probabilistic techniques have been used in landslide hazard mapping (*Miles 2000*), including:

- Monte Carlo Simulation

- Bayesian theory

- Fuzzy gamma techniques

- Artificial Neural Networks

- Multivariate method

This section will provide background information on these techniques and discuss how they have been applied to landslide mapping.

4.2.1 Monte Carlo Simulation

Monte Carlo techniques account for the distribution or uncertainty of each variable in the model by simulation. Monte Carlo simulations follow a general pattern: (1) define the probability distribution of the inputs of the model; (2) for each input, randomly select a value from its probability distribution; (3) perform computations using the randomly selected values; and (4) repeat simulations numerous times until the distribution of outputs is defined.

This technique has been used in hazard mapping to produce a spatial slope-failure probability map. Soeters and Westen (*Soeters and Westen 1996*) described the application of Monte Carlo simulations for landslide hazard mapping in the following steps:

Generate probability distributions of the input strength parameters: 'φ', the effective friction angle of the soil; and, c', the effective cohesion of the soil.

Begin a simulation by randomly selecting values from the probability distributions of the strength parameters and computing the slope safety factor for each grid cell of a map. Repeat the simulations numerous times until a probabilistic distribution curve of the slope's factor of safety against failure is determined.

Integrate the distribution curve of the slope's factor of safety against failure from -8 to 1 (i.e. domain of unsafe values) to determine the slope failure probability for each grid cell of the map (*Graham 1984*).

Repeat these steps for all grid cells to produce a slope-failure probability map.

In addition to Soeters and Westen *(Soeters and Westen 1996)*, the Monte Carlo method has been applied for landslide hazard mapping by Luzi et al. (*Luzi et al. 2000*), Refice and Capolongo (*Refice and Capolongo 2002*), Capolongo et al. (*Capolongo et al. 2002*), and Zhou et al. (*Zhou et al. 2003*).

4.2.2 Bayesian Theory

Bayesian theory can be used to improve decision making under conditions of uncertainty or limited knowledge. Bruyninckx *(Bruyninckx 2002*) states that the Bayesian model is consistent, unique, and plausible, irrespective of the form or order of the input parameters. Probabilities are assigned based on the amount of available information.

Pradhan *(Pradhan 2010)* implemented Bayesian theory to produce a landslide susceptibility map for the landslide-prone Cameron Highlands in Malaysia. Previous studies by Mohamed et al. *(Mohamed et al. 2009)* determined that rainfall is the triggering factor for the common occurrence of landslides. With the help of aerial photographs, high-resolution satellite imagery and field surveys, a landslide inventory map was developed, showing the geographical distribution of past and recent landslides. This map is used to study the frequency and distribution of landslides, and was central to classifying *(Varnes 2004)* the landslides based on the mode of occurrence. Analysis, however, was only performed for rotational failures. For susceptibility analysis, a spatial database was created with conditioning factors such as soil, location, land cover, lineament, and topography. A weights-of-evidence model was used to calculate the relevant factors, enabling the derivation of a relationship between the landslide prone areas and factors contributing to those landslides. Weights-of-evidence models use a log-linear form to consider prior and posterior probability of the relative importance of a variable based on evidence and statistics *(Bonham-Carter 1994)*. However, it can only be applied when sufficient data are available.

Finally, the factors used for landslide mapping were tested for conditional independence after performing overlay analysis. This analysis is an important GIS spatial operation which combines information of one GIS layer with another GIS layer to derive and infer the attributes related to the spatial data. It also applies common scale of index to diverse input values *(ESRI 2011)*. A landslide susceptibility index (LSI) is then calculated by summing all the factors (weighted-based on previous studies), performing a test of independence between each factors and nine combinations of factors were derived for the final landslide susceptibility mapping.

4.2.3 Fuzzy Gamma Techniques

Introduced by Zadeh (*Zadeh 1965*), Fuzzy set theory is used to solve many complex, real-time, and/or multi-variable problems. The spatial objects in the map comprise the members of the set. In classical set theory, an object is a member if the value is 1 and not a member if the value is 0. In Fuzzy set theory, in contrast, membership is determined based on the attribute of interest and can be assigned any value between 0 and 1 (*Lee and Sambath 2006*).

Fuzzy logic is easy to understand and implement. The weighing-of-evidence is controlled by experience and judgment, and the model accepts data from any scale of measurement. It is very compatible to GIS modeling languages and allows the processing of weighted maps. The five operators commonly used for landslide hazard mapping are "Fuzzy algebraic sum," "Fuzzy and", "Fuzzy or," "Fuzzy algebraic product," and "Fuzzy gamma operator" (*Bonham-Carter 1994, Lee and Sambath 2006*).

Vaibhava et al. (*Vaibhava et al. 2010*) applied Fuzzy techniques for probabilistic landslide hazard mapping in a part of the Tons river valley, Northwest Himalaya, India. Their objective was to zone the landslide hazard areas spatially using factors such as slope, aspect, weathering, erosion and land-use (or cover). Data used for this study include:

- Satellite data from SPOT-1, HRV-2, Landsat-5, TM, IRS-1B, LISS-II, IRS 1C, LISS III, and IRS-1C PAN

- Aerial Photographs of scale 1:60,000 with 80 % overlap

- Topo-sheets from the Survey of India.

The spatial datasets have been integrated, and the interaction between them is analyzed to generate landslide hazard maps based on the information of existing landslides in the region. The model is based on both statistical data (quantitative approach) and expert knowledge (qualitative approach). This project used the combination of both the techniques by using bivariate techniques discussed by Yin and Yan (*Yin and Yan 1988*), which were then followed by fuzzy-based techniques. The weights were then calculated using a probabilistic approach.

The fuzzy values in this project were assigned based on the information value (e.g. landslide occurrence) since most of those values were supported by strong field evidence. All of the thematic information has been classified and their information values were re-scaled to a fuzzy scale of 0 to 1. For the case of no landslide information, such pixels have been given a value of 0.000001 in order to avoid complete negligence. Fuzzy operators such as:

- Fuzzy AND, (used when all of the inputs must have a high value to produce a output with high value)

- Fuzzy OR, (used when any of the inputs can have high value, to produce a output with high value)

- Fuzzy Algebraic Product (FAP) (used when overall evidence is less important than single evidence)

- Fuzzy Algebraic Sum (FAS) (used when overall evidences are important than single evidence)

- Fuzzy Gamma Operator is a combination of the previous conditions created by Zimmermann (*Zimmermann* 1985) and An et al. *(An et al. 1991)*

were used to generate the landslide hazard maps. The resultant maps were validated by calculating the quantity of active landslides falling in each of the hazard zones. It is assumed that landslide falling under a high hazard zone could have an impact on its neighboring zone also because of the magnitude and number of the landslides occurring in the high hazard zone.

4.2.4 Artificial Neural Networks

Garrett *(Garrett 1994)* defines Artificial Neural Networks (ANN) as "computational mechanism able to acquire, represent, and complete mapping from one multivariate space of information to another given a set of data representing that mapping." Artificial Neural Networks (ANN) is used to obtain outputs that have not been achieved previously from the inputs by building a model of the data used to generate the process. A simple processing element (a node) forms the Neural Network, which responds to the weighted inputs from other nodes. Back propagation is one of the methodologies used in artificial neural networks, which consist of three layers, namely, input, hidden, and output layers *(Young et al. 2003)*.

The errors between the actual output values and targeted values are used to adjust the weights between the neuron to produce a model that yields a target value from the input value. Until minimal error is achieved between targeted output and actual output, the back propagation algorithm trains the network. Upon completion of the network, the back propagation algorithm becomes the feed-forward structure that gives a classification for the entire data set *(Lee 2005)*.

Pradhan and Lee *(Lee 2010)* mapped landslide susceptible areas in Penang Island by applying landslide hazard analysis and verification using ANN. To perform risk analysis, a landslide map was produced using aerial photographs and field survey, which become the input for GIS analysis where the frequency and distribution of shallow landslides are predicted in that area. Topography, lithology, lineament, land-cover, and vegetation index were used for analysis. Topography, lithology, and other factors were derived from Landsat satellite image analysis using ARC/INFO and converted into a 10m by 10m grid, where ANN was applied to generate a landslide risk map. The output was verified quantitatively using the known landslide locations. Training locations included sites that were landslide prone and areas not prone to landslides. Random cells (training cells) were selected from each of the classes. MATLAB was used to implement the feed-forward network for input, hidden, and output layers. The back propagation algorithm was then implemented to calculate the weights between the hidden and input layers and the hidden and output layers, where modifications on hidden nodes and learning rates are performed.

4.2.5 Multivariate Methods

The multivariate method is a quantitative approach for higher degree of prediction of the landslide hazard. The distribution of landslides, spatial data layers of causative factors, and relationship to past landslides are the input parameters for analyses using this model. Hence, the approach is highly data driven and object-oriented. The accuracy results from the functionality, which uses forward parameter selection and backward removal *(Carrara 1983)*. When the multivariate method is coupled with a logistic regression method, likelihood-ratio analysis is performed and variables of least value in terms of contribution to trigger landslides are removed *(Qiu 2007)*.

Tetsuro and Esaki *(Tetsuro and Esaki 2007)* used the multivariate method to produce landslide hazard mapping by obtaining variables from thematic maps. Factors responsible for slope failures and landslide inventory map were integrated into a GIS analysis. The inventory maps

were used to determine the relationship for individual landslide and its causative factors. With this information, the strength of an individual factor can be obtained (*Erener 2008*)

Erener (*Erener 2008*) extended ordinary logistic regression (OLR) to spatial regression to produce a susceptibility map by assigning weights to the causative factors through spatial correlation and least square methods.

4.3 SEISMICALLY-INDUCED LANDSLIDE HAZARD MAPPING

Damage caused by seismically induced landslides has drawn attention for more research in recent years. This involves studying the inter-relationship of the earthquake and landslide from factors such as slope, geology, distance from fault, source parameters, and shaking patterns. Advancement in remote sensing techniques, geospatial analysis (e.g. GIS) and seismic network density have contributed to the detection of landslide prone areas triggered by earthquakes (*Harp et al. 2011*). A hazard map is generated by integrating the susceptibility map and causative factors. Susceptibility calculations are made using the past landslide records and factors such as slope angle, lithology, geomorphology, land-use, slope profile, and slope plan.

Sloping terrain and weak soils are more susceptible to landslides. Steep slopes made up of weak material tend to fail when shaken by earthquake and can be problematic when they intersect public infrastructure. This process includes understanding the potential shaking from the future earthquakes combined with evaluating evidence of existing landslides and the strength of soil (*Department of Conservation 2011*).

The California Geological Survey (CGS) recommends the following data and methodologies to assist in mapping the seismically induced landslide (*CGS 2004*):

- Landslides triggered due to earthquakes from the record of historic earthquake disasters.

- Areas showing the evidence of landslide deposits and sources for mass movements from past landslide movements.

- Indications from CGS`s analyses of geologic and geotechnical data which are susceptible to earthquake triggered landslide.

- Newmark's method, a multivariate method, and a probabilistic slope stability method are a few methods effectively used to map potential zones of landslides triggered by earthquakes.

- Deterministic and probabilistic approaches are both applicable to seismically induced landslides, and GIS can produce interactive maps using either of these methods. Deterministic models require modifying and updating input parameters to produce the maps based on subjective input. Probabilistic model integrate several variables such as distance magnitude, acceleration, duration, strength parameters, pore pressure, material characteristics as random variables (*Khazai and Sitar 2000*).

4.3.1 Deterministic Models for Mapping Seismically-Induced Landslide

Three factors (*Khazai and Sitar 2000*) coupled to analyze seismic slope stability under a GIS framework for deterministic models are:

1. The intensity of shaking at the site, obtained through attenuation relationships

2. The strength of the slope determined through traditional slope stability analyses using pseudo-static earthquake loading

3. The level of deformation along the potential slip surface at the time of shaking, usually estimated using Newmark`s displacement method *(Newmark 1965)*.

Jibson *(Jibson 1993)* suggests that on a regional basis, the Newmark method could be effectively applied in order to capture permanent ground deformation by either a double integration of the area under the accelerogram record that exceeds the critical acceleration or by deriving a regression equation from the ground motion to determine displacement. A possible downside to the second approach is that displacement at a particular location will not be calculated accurately with a mean displacement curve, and furthermore, local site responses are not accounted in analyses .

Khazai and Sitar *(Khazai and Sitar 2000)* integrated three factors to analyze seismic slope stability in GIS environment: (1) the concentration of shaking at the site from attenuation relationships; (2) yield strength of the slope through traditional slope stability analyses by pseudo-static approach; and (3) deformation calculated from the Newmark displacement method (*Newmark 1965*).

Khazai and Sitar (*Khazai and Sitar 2000*) created a program that enables a user to interact, modify and update input parameters like slope map and estimated site response in order to produce a seismically-induced landslide susceptibility map for an area. The landslide inventory map, soil map and topography were analyzed within a pseudo-static analysis approach in combination with Newmark`s displacement model.

Lee et al. (*Lee et al. 2008*) introduced a Landslide Susceptibility Index (LSI) for each pixel using a summation of factors weighted linearly. In this study, which was done in Taiwan, event based landslide inventory maps were created in addition to triggering elements. They calculated the correlation of the factors in susceptible and not susceptible regions to landslides in various terrain types by statistically testing of factors and analyzing their weights using discriminant analysis.

Important notes related to implementing deterministic models for seismically induced landslides mapping (*Lee et al. 2008*) include:

*   At every point of study pore water pressure, failure surface depth, strength parameters, and limit –equilibrium slope stability are needed. This can be problematic for data collection and may reduce credibility in spatial variability, which is not needed for a statistical model (*Jibson 1993*).

- Deterministic models could be applied anywhere if parameters needed are available

- The deterministic model can be used to analyze scenario event when the intensity of earthquake and Newmark's displacement are known.

- Deterministic models are well suited when potential failure depth, ground water parameters, and material strengths are known since this model is fully physically based.

4.3.2 Probabilistic Method to Map Seismically-Induced Hazard Mapping

A probabilistic method considers the spatial variability of geological, geomorphological, seismological, and geotechnical parameters. Geotechnical parameters are obtained from laboratory tests and combined with geologic maps to extrapolate their spatial variability (*Refice and Capolongo 2002*). Miles *(Miles 2000)* mentions that distinct lithological factors are generally not available in geologic maps, which leads to poor positional accuracy in determining the spatial distribution of such factors. Hence, probabilistic values provide improved results over single, deterministic values. Bray and Travasou (*Bray and Travasou 2007*) discuss the methodologies used to develop a probabilistic model:

- Determine the slope displacement anticipated from seismic activity, which is governed by variables related to ground motion and slope (soil and topographic) properties,

- Calculate the impact of ground motion variables on slope failure,

- Integrate the above steps to produce the output.

Jibson et al. (*Jibson et al. 1998*) produced an earthquake triggering landslide susceptibility map for Northern San Fernando Valley and Santa Susana Mountains. The Northridge earthquake in 1994 had all the datasets needed to conduct the regional analysis. Harp and Jibson (*Harp and Jibson 1996*) used 200 strong motion records all over the region, DEMs, geologic maps and engineering properties of geologic units to analyze seismically triggered landslides. They introduced a dynamic model based on Newmark`s deformation analysis to calculate the landslide displacement in each pixel. The digital inventory of landslides triggered by the earthquake was compared with the model displacement to construct a probability curve relating to the predicted displacement to failure. This probability function could be used in any case that involves ground shaking because the function can predict the spatial variability of failure probability. The authors suggest that maps produced with this method could be used for lifeline siting, maintenance, land use planning, and emergency preparedness planning. However, it cannot be compared to the sophisticated published regulatory maps like seismic hazard zonation maps issued by California Division of Mines and Geology.

Capolongo et al. (*Capolongo et al. 2002*) introduced a simplified Newmark slope stability model on a pixel by pixel basis. They used a Monte Carlo technique to simulate necessary samples from probability density function in all stages of the work. They developed a series of function in Matlab to read the raster matrices and tabulated numerical values containing the statistical

parameters of involved variables. The combination of the latter with the Monte Carlo simulation and Newmark method generated the probabilistic map. The output was quite valuable in areas with common seismic activity.

4.3.3 Combination Approaches

Ferentinou et al. (*Ferentinou et al. 2006*) discuss the use of GIS to estimate seismically-induced slope failures using applying a Newmark displacement model in conjunction with ANN. The stability of the slope is analyzed under both static and dynamic conditions. Governing factors are introduced in ANN and other estimated factors were given as input for the GIS model. Subsequently, a tool was developed to enable the user to produce hazard maps for different load conditions.

Analysis with deterministic modeling for circular landslides and plane landslides was then performed. This modeling was for the wedge failure and input parameters were basic geotechnical parameters used for slope stability analysis. Deterministic FS and S (Stability) data were then exported to Matlab to determine the FS through Neural Networks. These were then transferred back to the GIS environment. Rock fall analysis were performed and visualized within GIS using a 3D rock fall simulation model (*Charalambous 2006*).

Ferentinou et al. (*Ferentinou et al. 2006*) also discuss rainfall-induced slope failures, considering positive and negative pore pressures. Slidev5.0 and Face2 v6.0 by Rockslides have been used to estimate the FS. CHASM (Combined Hydrology and Stability Model, *Lateh et al. 2008*) is an integrated slope hydrology/slope stability software package that is meant to support the estimation of controls on slope stability, pre site investigations, and evaluations related to effects of bioengineering on slope stability. It was used to study the precipitation effect.

Advantages of this methodology include:

- 2D hill slope and hydrology models are coupled directly to a 2D slope stability model.

- Positive and negative pore pressures are calculated during each iteration, considering the change due to precipitation.

- These models can be applied for regional or medium scale areas to estimate landslide potential in a deterministic mode.

- The FS is calculated for every single terrain unit (e.g. there is no need to extrapolate the FS value), effectively overcoming the limitations from infinite slope model.

4.4 LIDAR USE IN LANDSLIDE STUDIES

Topographic information is critical to landslide hazard investigation. Conventional topographic maps are limited in areas with difficult access, visibility constraints, or heavy vegetation. These maps typically have resolutions greater than 10 m, which removes important details for analyzing smaller, surficial landslides. LIDAR (Light Detection and Ranging) offers an

excellent way to overcome these problems by providing high-resolution topographic data. LIDAR sensors are often mounted to planes, termed airborne laser scanning (ALS), airborne laser swath mapping (ALSM) or laser altimetry. Jaboyedoff et al. (*Jaboyedoff et al. 2012*), provide a comprehensive review of various applications of LIDAR to produce High Resolution Digital Elevation Models (HRDEM) as a new platform to improve landslide analysis. LIDAR enables the production of high resolution DEMs and maps products, which are used for accurate topographic mapping in areas with dense vegetation (*Haneberg et al. 2009*). Projects based on using LIDAR to map landslide hazards have been completed throughout the world, including Belgium (*Van Den Eeckhaut et al. 2006*), Japan (*Sato 2007*), North Carolina (*Wooten 2007*), Oregon (*McKean & Roering 2004, Burns and Madin 2009*). Particularly, Burns and Madin (*Burns and Madin 2009*) provide a standard protocol for interpreting LIDAR data to map landslide deposits.

Haneberg et al. (*Haneberg et al. 2009*) provide an example of how landslide hazard mapping can be done with high-resolution airborne LIDAR data for the Paranuss Campus of the University of California, San Francisco, which is heavily forested. The work began with the collection of high-resolution LIDAR data pertaining to the area of study. Afterword, the data were processed to generate DEMs and other maps. Though the project was intended to assist geotechnical investigations and campus-wide emergency planning, emphasis was placed on the factors contributing to landslides by identifying the geomorphic features.

The processing workflow consisted of the following steps:

- LIDAR data was collected from a private vendor who covered an area of 400 m with the flying height of 900m following National Standard for Spatial Data Accuracy (NSSDA) norms for vertical accuracy and Federal Emergency Management Agency (FEMA) norms for high-resolution data.

- ASCII text files of the coordinates were converted to California State Plane Coordinate System from the original WGS84 coordinates.

- The vendor produced a bare earth data set by removing vegetation and cultural features.

- Using interpolation algorithms such as inverse distance squared and regularized splines with tension, a trial and error process was carried out to produce an optimally interpolated DEM from the bare earth point data given by the vendor. Based on the ground strike data, the grid spacing for the DEM was selected. Based on MFWorks, which is a commercial GIS software package, DEM was interpolated to 0.6m horizontal grid by regularizing splines with tension.

Based on Haneberg et al. (*Haneberg et al. 2007*), Haneberg (*Haneberg 2006, Keaton 1996Madin*

), and Troost et al. (*Troost et al. 2006*), a series of geographic derivative maps were created which included contour maps, maps showing slope angle and terrain ruggedness, and relief images with variety of simulated illumination directions. Data for these derivative maps were then used to generate a probabilistic hazard map using software called PISA-m.

This analysis resulted in three interpretative maps created for the purpose of analysis:

- Using the Unified Engineering Geologic Mapping System (*Keaton et al. 1996; Troost et al. 2006*), a standard engineering geologic map was produced.

- The modified natural slope due to human activity was shown in a cut and fill slope map.

- Quantitative interpretations were used to produce slope stability hazard map.

4.5 REQUIREMENTS FOR A NEW METHODOLOGY

While previous work takes significant steps towards the improvement of landslide mapping, the available methods do not achieve all of the objectives desired for this study. It is desirable that the methodology be:

- **Fully Probabilistic:** The method should include the whole probability chain from strong ground motion, physical characteristics of the type of landslide, its mode of deformation, and native soil strength.

- **Consistent:** The method can be implemented throughout other regions and across a wide range of scales without requiring significant modification. Results from one location should be able to be directly compared with results of a second location.

- **Simple:** The method should be based on readily available data while being interactive and user-friendly.

- **Scalable:** The method can be applied across a large area without problems. Hence, it cannot be reliant on detailed time histories or other site-specific factors.

- **Rigorous:** The method can combine as much of the rigor of a site-specific analysis to a regional scale, as is possible.

- **Reliable:** The method can be verified by using an existing and available landslide inventory database.

- **Cost-efficient:** The method must not rely on limited, expensive data like boreholes and in-situ or laboratory testing of soils, which are not available for a large region.

- **Compatible:** This method can be integrated with other datasets and analysis (e.g., lateral spreading, flooding, and settlement) for a complete multi-hazard analysis.

- **Updatable:** The living maps can easily be updated when new information and data are available.

An additional focus of this effort that may not normally be considered in traditional landslide hazard mapping and analysis is to examine the influence of landslides on highway corridors, particularly those designated as lifeline corridors. Conversely, the influence of the roadway on

the landslide susceptibility is also an important consideration. Hence, some deterministic methodologies include a factor for distance to roadways (e.g*., Belsius and Weirich 2005*) as part of the overall landslide susceptibility. As previously discussed, it is crucial that these corridors remain open following an earthquake and/or tsunami on the Oregon Coast.

5.0   COMPILATION OF RELEVANT GIS DATA

5.1   OVERVIEW

As previously discussed, there are several important factors that need to be considered in seismically induced landslide hazard analyses and mapping. For this project, data for these factors were collected from several sources and organized into a geodatabase structure within ArcGIS 10. A geodatabase (Figure 5.1) is an efficient format for storing and compiling geospatial data into a single folder and file structure. Geodatabases support tabular data, vector data (e.g., points, lines, polygons), raster datasets (e.g., images, DEMs), and relationships between the datasets. Table 5.1 summarizes the primary data sources used in this project. Table 5.2 summarizes processing software used to prepare the data.

Properties of the primary coordinate system used are listed below:

- Name: NAD 1983 UTM Zone 10 N

- Projection: Universal Transverse Mercator

- Datum: North American 1983

- Units: Meters

Most raster grids were resampled to a cell size of 30 m to be consistent with the DEM used for the study.
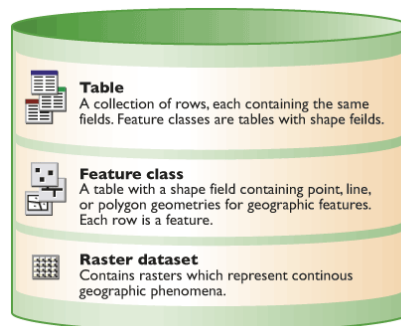
Figure 5.1: File geodatabase contents (ESRI model)

Table 5.1: Summary of primary data sources

Classes	Layers	Source	Data format
Topography	Digital Elevation Model (DEM)	NASA	Raster- Continuous (degrees)
	Slope	Functions of the DEM	
	Aspect		
	Slope roughness		
	Terrain ruggedness		
Geology	Lithology	OGDC	Vector(polygon)-Categorical
	Fault pattern		Polyline feature
Land cover	Land use	OGDC	Vector(polygon)-Categorical
	NDVI	NASA	Raster-Continuous
Hydrography	Streams	OGDC	Polyline feature
	Precipitation	PRISM	Raster-Continuous(inches)
Geomorphology	Landslide distribution	NASA	Vector(polygon)-Categorical

Table 5.2: Summary of the parameters used and the processing methodology.

Parameters	Calculation Techniques	Software Used
Slope	uses DEM and built-in slope tool	3D analyst in ArcGIS 10
Aspect	uses DEM and built-in aspect tool	
Slope roughness	uses slope map and focal statistics tool	Spatial analyst in ArcGIS 10
Terrain roughness	uses DEM and focal statistics tool	
NDVI	uses LANDSAT ETM+ and model maker	ERDAS Imagine 2010
PGA	uses online data source and ASCII to Raster tool	
Precipitation	uses online data source and ASCII to Raster tool	conversion tool in ArcGIS 10

5.2 TOPOGRAPHY

Several DEM sources were used in this study, including DEMs from NASA's ASTER program (*USGS 2012c*), USGS National Elevation Dataset (NED) (*USGS 2012b*), and LIDAR topographic data. Because the LIDAR dataset was not available until over halfway into the project, initial results in Chapter 6 were derived using the ASTER or NED DEMs since they were readily available. However, the output maps and analyses in Chapter 7-10 use the LIDAR\NED hybrid DEM. Appendix B compares results derived using each of the DEMs. Overall, trends are very similar regardless of the DEM used; however, the results from the hybrid DEM appear to have less uncertainty.

5.2.1 Aster

The initial topographic base map was generated by processing the Advanced Space-borne Thermal Emission and Reflection Radiometer Global Digital Elevation Map (ASTER GDEM) photographic datasets freely obtained from the USGS website (*USGS 2012c*). The ASTER satellites were built by the Ministry of Economy, Trade, and Industry (METI) of Japan and launched by NASA. The following paragraph explains the specifications of the satellite images

and why this imagery is reliable compared to other imageries. ASTER GDEM V2 was made available on October 17, 2011 (*Tachikawa et al. 2011a and 2011b*).

ASTER has fourteen spectral bands with resolutions ranging between 15 and 90 meters. (Table 5.3).

Elevation data are available at 30 m resolution.

It has three sensors, each covering a swath of 60 kilometers

The along track scanner uses the NIR and stereo images acquired by the nadir viewing and backward viewing telescopes.

The data are provided in GeoTIFF format in either geographic coordinates (1 arc second) or projected into Universal Transverse Mercator (UTM) coordinates.

The coverage extends between 83 degrees in latitude north to south and covers 99% of the earth's land mass.

The ASTER GDEM V2 has an estimated vertical accuracy of 8.68 m (RMS) for the continental US. It is a known fact that any GDEM will include residual anomalies and artifacts.

The ASTER data were downloaded in 1 x 1 degree tiles, were mosaicked in ERDAS IMAGINE 2010, a computer software program, re-projected into UTM Zone 10 North coordinates and resampled using cubic convolution interpolation techniques.

Table 5.3: Specifications of ASTER sensors

	VNIR	SWIR	TIR
Bands	4	6	5
Resolution	15 m	30m	90m

5.2.2 USGS National Elevation Dataset

The USGS National Elevation Dataset (NED)(*USGS 2012b*) seamlessly integrates elevation data for the entire US from a variety of sources derived through several techniques (typically photogrammetric). As new data are made available, the seamless map is continually updated with the improved elevation data. Characteristics of the data include:

- The data are provided in geographic coordinates (decimal degrees)

- Horizontal coordinates are referenced to the horizontal North American Datum of 1983 (NAD 83).

- Elevation values in meters are referenced to the North American Vertical Datum of 1988 (NAVD 88).

- NED data are available nationally (except for Alaska) at resolutions of 1 arc-second (about 30 meters) and 1/3 arc-second (about 10 meters)

- In some locations (typically metropolitan locations), data are available at 1/9 arc-second (about three meters).

- Nationally, this dataset has a determined vertical accuracy of 2.44 meters (*USGS 2012d*). However, given that the elevation data comes from a variety of sources, accuracy can vary substantially depending on the location.

- This dataset represents the most commonly used data source in the US.

5.2.3 HYBRID LIDAR and USGS Dataset

As part of the development of the Oregon Resilience Plan, DOGAMI created a 30 m DEM for the state of Oregon by combining resampled LIDAR data, where available, with the USGS NED (*USGS 2012b*) to create a topographic map across the entire state at 30 m resolution.

The LIDAR data has high vertical accuracy (5-15 cm RMSZ) and native resolution (typically 8 points/m^2 processed into a 1 m grid) compared to ASTER and NED and has shown improved capabilities for landslide detection (*Burns and Madin 2009*).

However, using the data at the highest resolution (1m) creates several challenges, including:

Data are typically divided into 10 km x 10km tiles to limit file size so that computers are able to process them efficiently. Using a 1m grid across the entire state of Oregon (~250,000 km^2) would require at least 1TB of memory to be able to process (assuming a 4-byte floating-point value per grid cell).

Using too high of a resolution DEM will contain very steep slopes on relatively small, localized features such as drainage ditches. This may result in over-prediction of landslide hazard at those locations. For this type of regional assessment, an overall, general terrain slope grid, where the terrain elevation is averaged over a larger cell size (e.g.*,* 30 m), may perform better in some situations.

As a result, a 30 m pixel size was used for this study. This resolution balances level of detail, file size, and slopes that would contribute to landslide hazard. Appendix B evaluates the influence of cell size and DEM type on this mapping effort.

5.2.4 Derivative Topographic Datasets

5.2.4.1 Slope

Slope can be defined as the rate of change in elevation values, usually expressed in degrees ranging from 0 to 90 degrees. There are a variety of GIS-based techniques to calculate slopes using a grid-based DEM. (Figure 5.2) The approach employed by

ArcGIS uses the following process to determine slopes considering adjacent cells in all directions:

a	b	c
d	e	f
g	h	i

Figure 5.2: Process used to calculate slope based on neighboring pixels.

Using the z values from the adjacent grid cells (Figure 5.2), the slope is calculated as follows:

$$\frac{dz}{dx} = \frac{(a+2d+g)-(c+2f+i)}{8\times x\,\mathrm{dim}}$$

$$\frac{dz}{dy} = \frac{(g+2h+i)-(a+2b+c)}{8\times y\,\mathrm{dim}}$$

$$\frac{rise}{run} = \sqrt{\left(\frac{dz}{dx}\right)^2+\left(\frac{dz}{dy}\right)^2} \qquad \deg=\tan^{-1}(\frac{rise}{run})$$

(5-1)

Figure 5.3 shows the derived slope map for the study area.
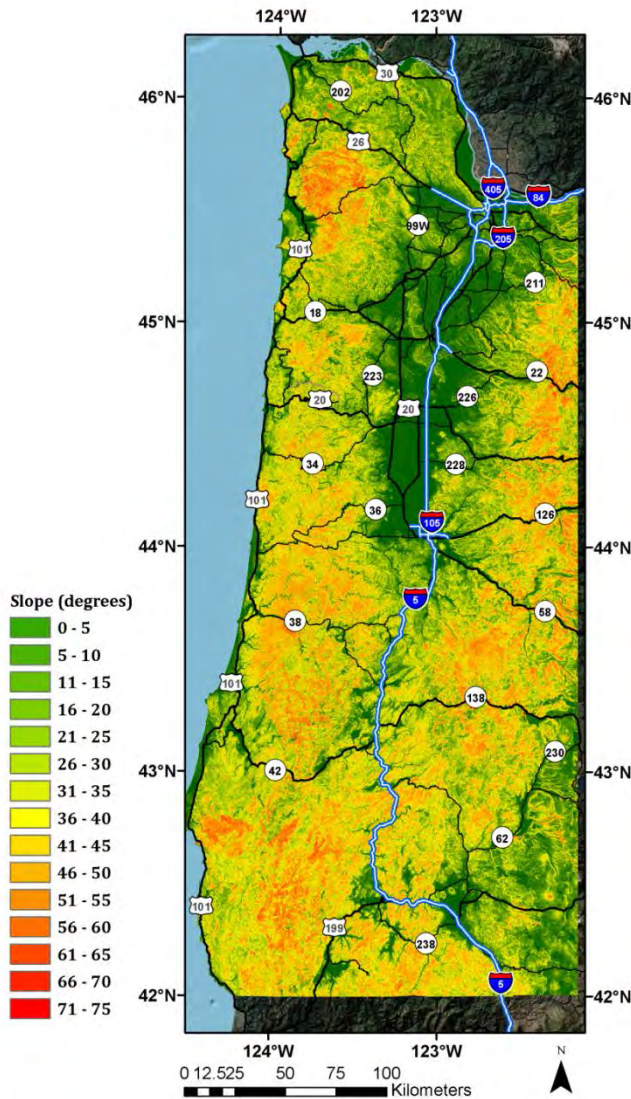
Figure 5.3: Slope map for the study area.

5.2.4.2 Slope roughness

Slope roughness can be defined as the variation of slope throughout a local neighborhood. This is achieved by using the focal statistics tool in ArcGIS 10.0 with a kernel of 3 by 3 to calculate the standard deviation of slope within the kernel as the slope roughness value for each cell. Note that there is a wide variety of other slope-based roughness metrics.

5.2.4.3 Terrain (elevation) ruggedness

Terrain (elevation) ruggedness can be defined as the variation of elevation throughout a local neighborhood. This is also calculated using the focal statistics tool in ArcGIS 10.0 with a kernel of 3 by 3 to calculate the standard deviation of elevation values within the

kernel as the terrain ruggedness value for each cell. Note that there is a wide variety of other elevation-based ruggedness metrics.

5.2.4.4 Aspect

The primary direction of change of a DEM is represented as the Aspect, expressed in degrees ranging from 0 to 359.9 in clockwise direction from north. The aspect map (Figure 5.4) is grouped into classes, as shown below (Table 5.4).

Table 5.4: Classifications used in the aspect map (*ESRI 2011*)

Classes	Range
Flat	-1
North	0-22.5
North east	22.5-67.5
East	67.5-112.5
South east	112.5-157.5
South	157.5-202.5
South west	202.5-247.5
West	247.5-292.5
North west	292.5-337.5
North	337.5-360

'
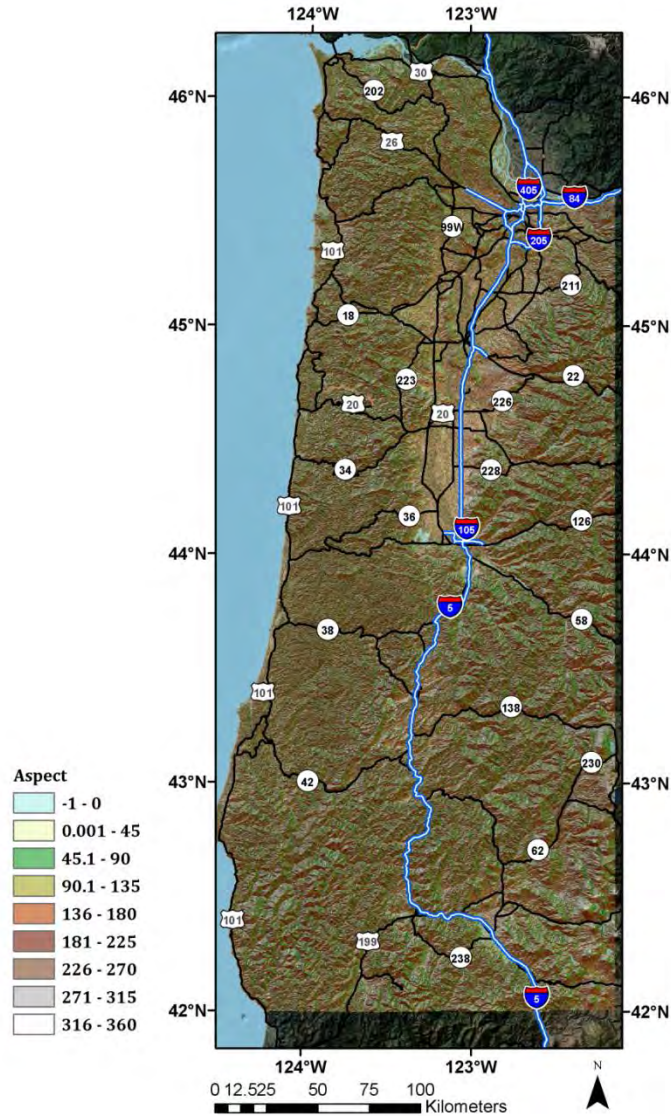
Figure 5.4: Aspect map for the study area.

5.3   GEOLOGY

5.3.1 Geology

The Oregon Geologic Data Compilation (OGDC V5, http://www.oregongeology.org/sub/ogdc/) is an effort to integrate the best available geologic mapping (consisting of parts or all of 345 separate reference maps with scales ranging from 1:12,000 to 1:500,000) available across the state into a single GIS database.

Given the wide range of geologic units across the entire state, the geologic database was simplified into six lithologic categories: metamorphic, plutonic, sedimentary, surficial sedimentary, tectonic, and volcanic. This was necessary since it was not possible to statistically quantify strength parameters for each geologic unit.

The OGDC database also contains mapped fault locations throughout Oregon. Figure 5.5 depicts the lithology and Figure 5.6 depicts the spatial distribution of the faults in the study area.
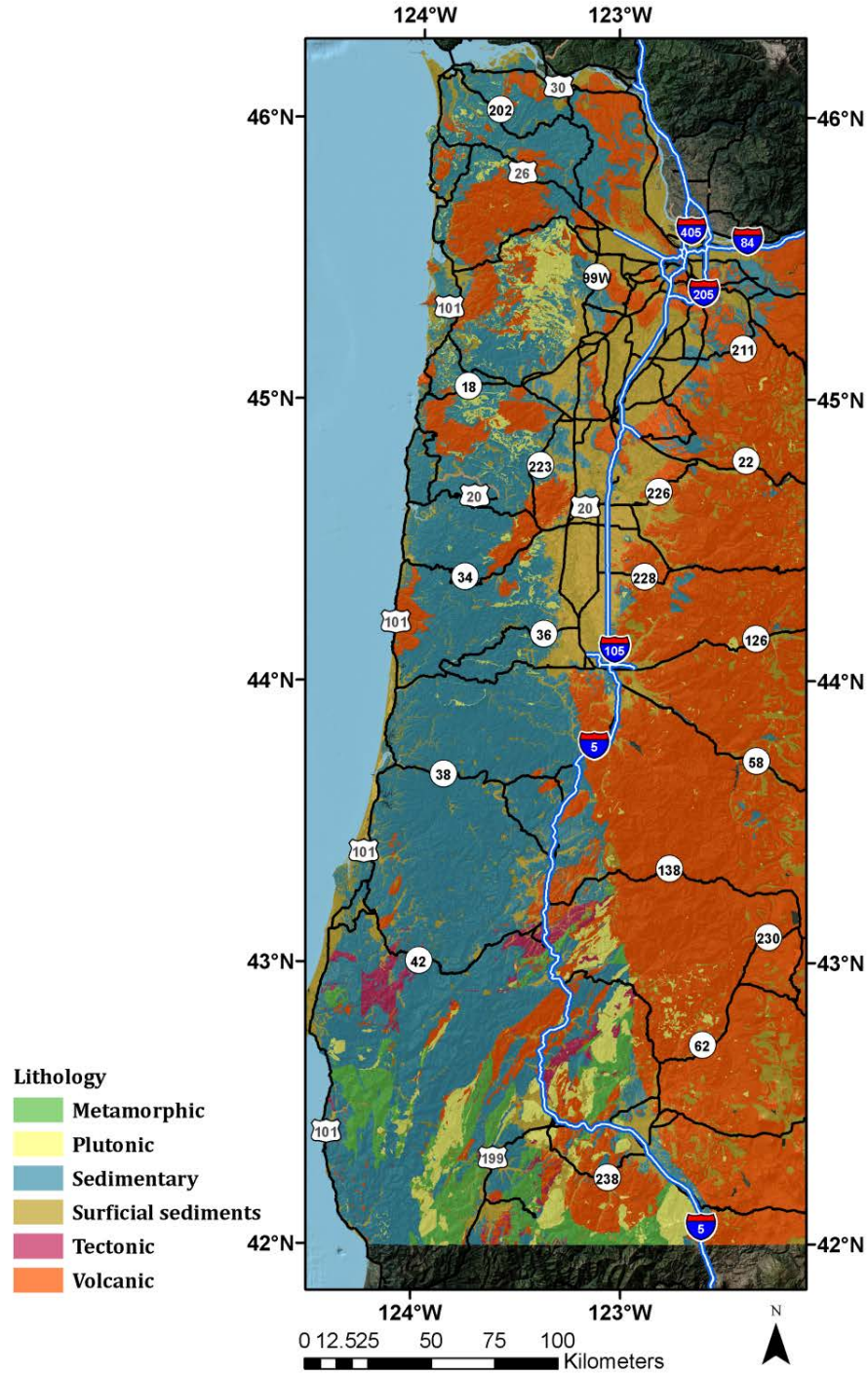
Figure 5.5: Lithology units throughout the study area
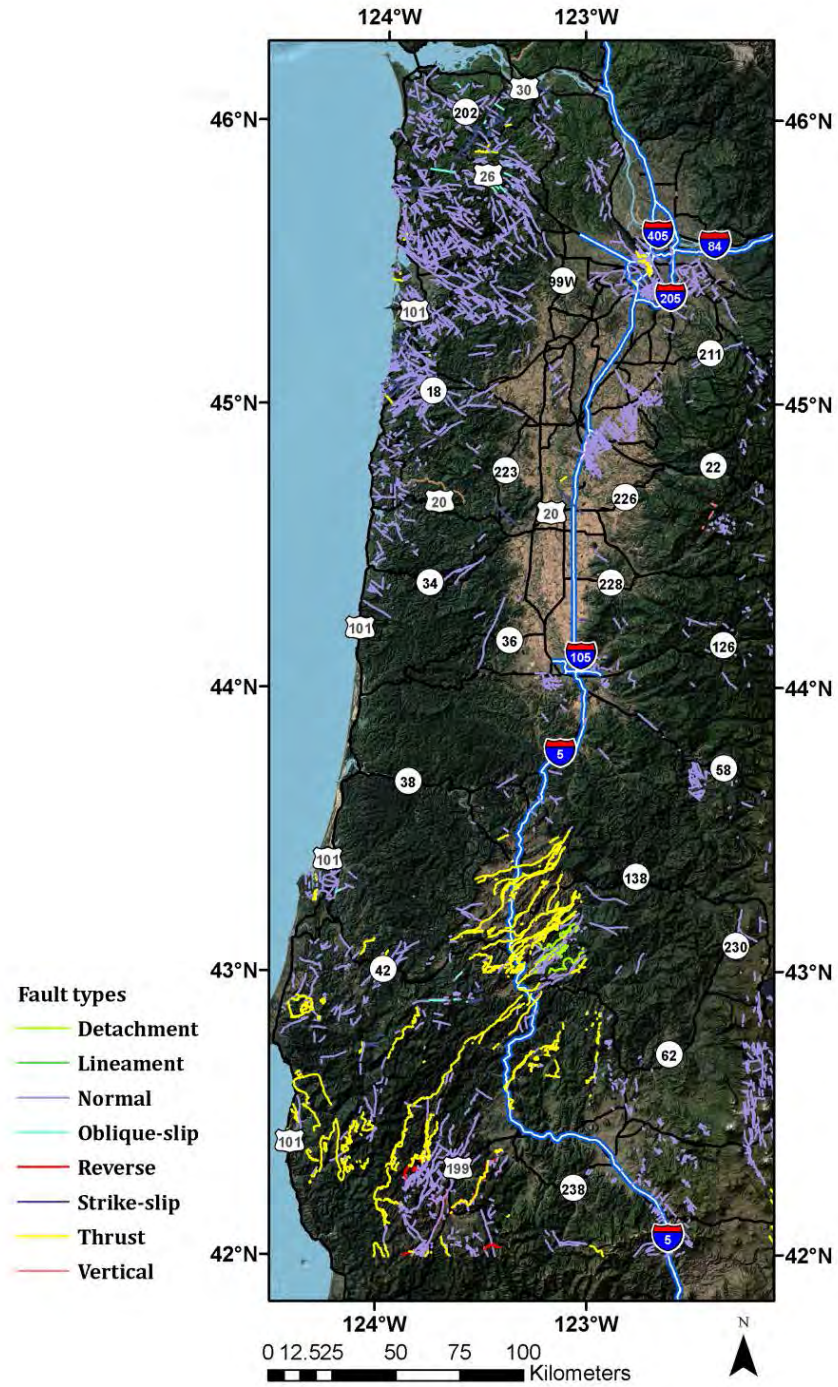
Figure 5.6: Spatial distribution of faults in the study area

5.3.2 Landslides

Landslide data were acquired from two sources: The Statewide Landslide Information Database of Oregon (SLIDO) and the ODOT Unstable Slopes database. This section will discuss these two datasets.

5.3.2.1 SLIDO

The project team obtained SLIDO Release 2 from DOGAMI in digital, vector format (Figure 5.7). This database is a collection of the most current landslide data available and includes point, line, and polygon feature classes created in ArcGIS 10.0 with Oregon Statewide Lambert NAD 1983 HARN as the coordinate system. As previously discussed, DOGAMI is very active in using LIDAR datasets for landslide inventory mapping. LIDR provides improved resolution to determine landslide locations compared to previous techniques. As such, future releases will include many more landslides than those cataloged in SLIDO Release 2.

The point feature dataset includes historic landslides, grouped in four-year intervals since 1931. The attributes include date, landslide-mapping method, name of the landslide, adjacent slope angle, factors responsible for the movement, type of slide material, size, volume, length, and width in feet.

The polygon feature dataset represents the visible spatial extent of the landslides. The attributes include age, movement classification, material type, confidence of map identification, geologic unit, and the change in elevation from bottom to the top of head scarp and from top to toe of the fan. Also included are the horizontal distances between the head scarp and various internal scarps, the calculated horizontal distance between the internal scarps, and the size and volume of the landslide deposits.

The polyline feature dataset is used to represent the scarp features. The attributes include a description of the geometry type, length of the shape, and unique code assigned to each original reference map. Further metadata details can be found in the webpage:
http://www.oregongeology.org/sub/slido/metadata.htm
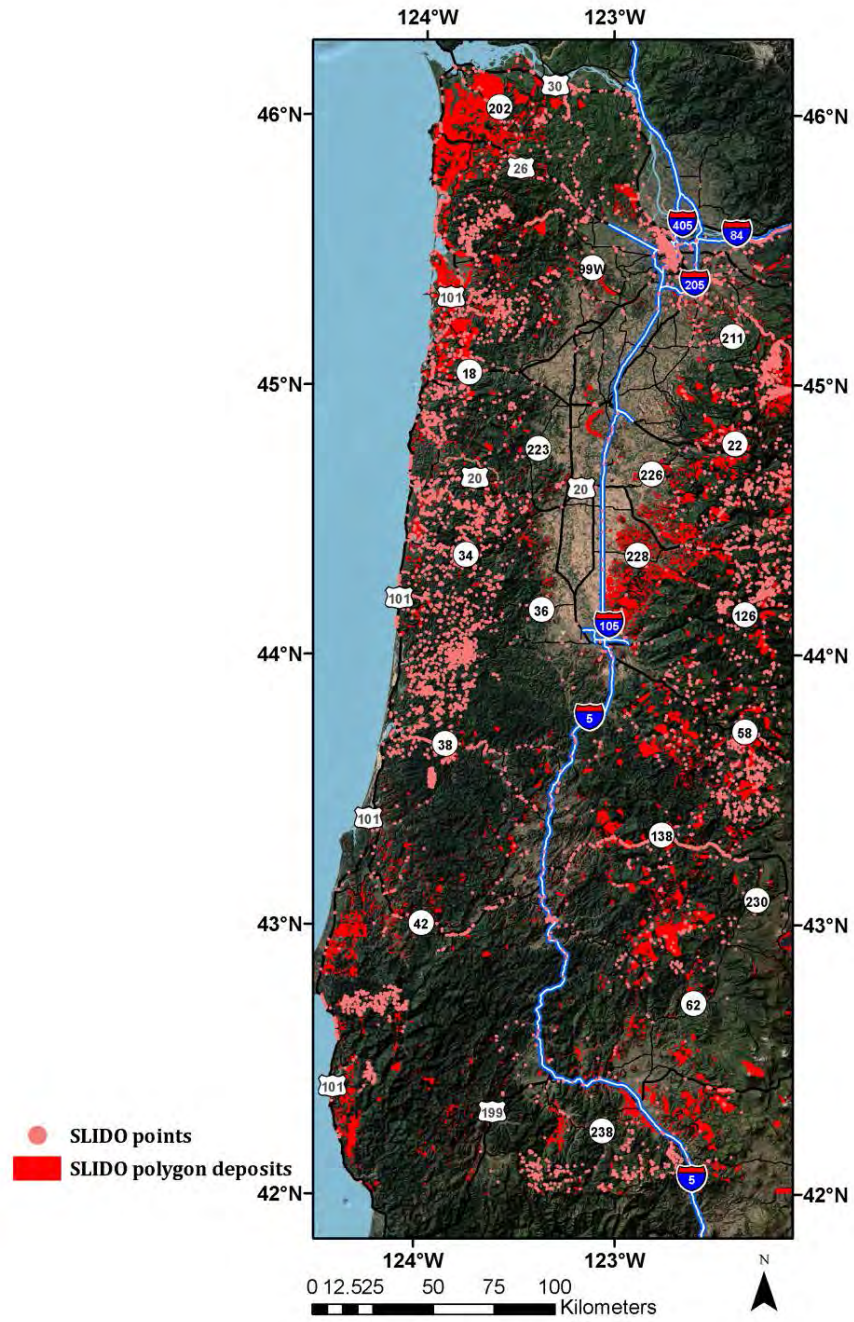
Figure 5.7: Study extents showing locations of previously mapped landslides in the SLIDO database. Base map from LandSat.

5.3.2.2 Unstable Slopes

In addition to the SLIDO 2 database, data from the ODOT Unstable Slopes database (http://www.oregon.gov/ODOT/HWY/GEOENVIRONMENTAL/pages/unstable_slope.aspx) was collected. This database locates landslides affecting the highway system in Oregon. Attributes include the name of the adjacent highway, identification number, geographical coordinates, elevation, and type of landslide hazard. Some features have detailed benefit-cost ratio information for repair. The emphasis of this database is in rating the overall risk from each of the landslides, rock falls, and other types of slope failures causing damage to the highway infrastructure. This data was of primary importance, since this study is focused on the impacts of landslides to the lifeline corridors. Note that there is considerable overlap between the landslides recorded in the SLIDO and Unstable Slopes database. Refer to Figure 5.8 for depiction of the inventoried landslides from the SLIDO and Unstable Slope databases.
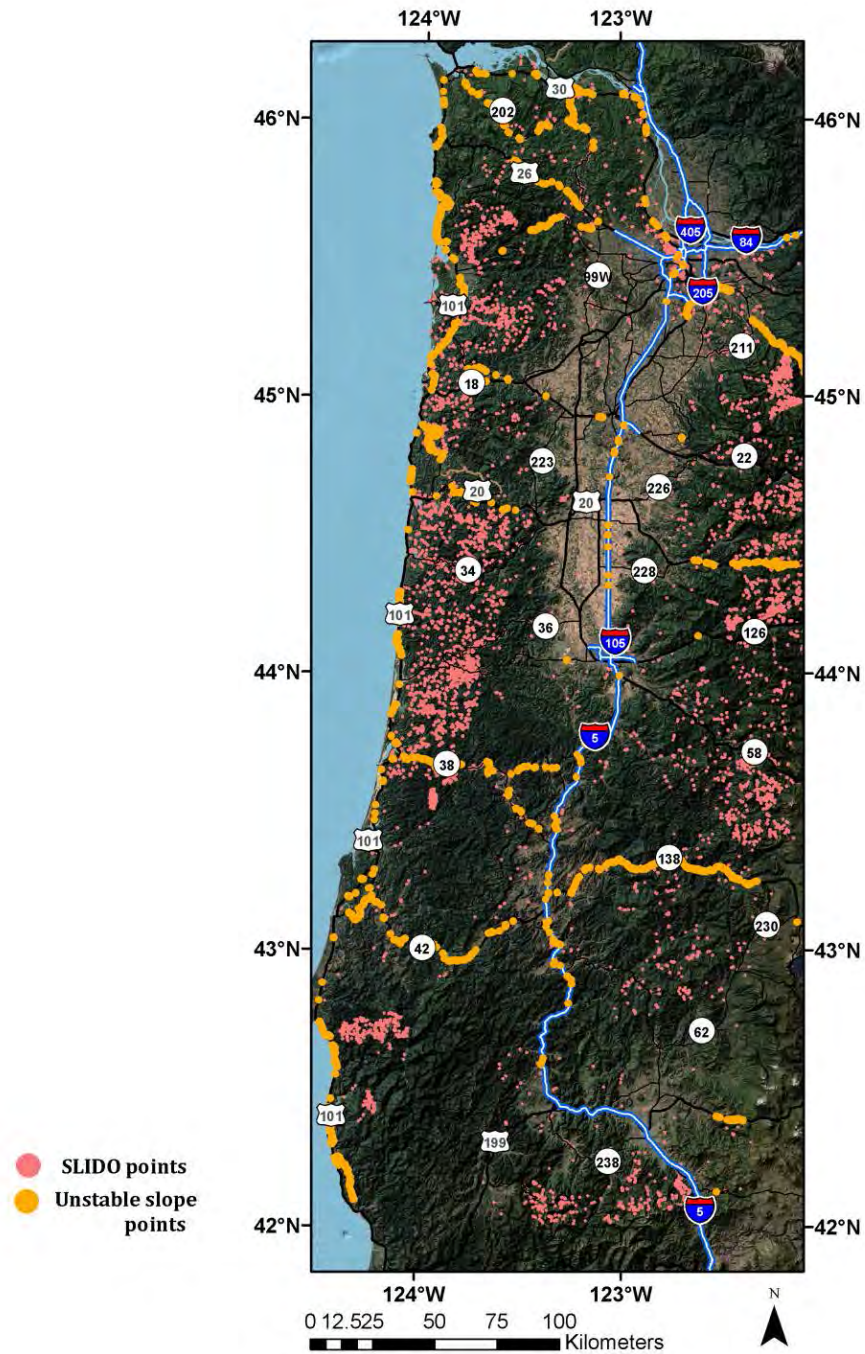
Figure 5.8: Spatial distribution of landslide points from SLIDO and the ODOT Unstable Slopes database

5.3.3 Seismic

This section describes the sources of seismic hazard information used for this study.

5.3.3.1 USGS Seismic Hazard Curves

To study seismically-induced landslides, peak ground acceleration (PGA), in conjunction with mass, is commonly used to define the lateral forces from an earthquake and is often represented as equivalent static forces in seismic codes. Seismic hazard curve data were acquired from the National Seismic Hazard Map (NSHM) program of the USGS (*2008*).

In addition to PGA estimates, spectral accelerations at various periods are available at this website, gridded at 0.05 degree increments across the entire US . PGA values (in %g) with a 2% probability of exceedance in 50 years were used.

A series of complete Next Generation Attenuation (NGA) (*Petersen et al. 2008*) seismic hazard curves with mean annual rates of exceedance for 19 PGA bins based on average shear wave velocities in the upper 30 meters of the soil profile (VS30), equal to 180, 259, 360, 537, and 1,150 m/s. These data will be discussed in more detail in Chapter 10.

Because the data are available as text files that cannot be immediately input into GIS, the PGA files were converted in to grid format using the 'Bin N Grid' software program (*Olsen 2011*). A separate C++ program was developed to convert the seismic hazard curve data into a series of floating point grids (flt) organized by VS30 and PGA bins.

Using information from recent earthquakes (e.g.*,* Chile and Japan) and new scientific findings, the USGS (*2012a*) is currently updating the seismic hazard data and models, scheduled for release in 2014. These new seismic hazard data will include new models for the CSZ based on rupture geometries and rates using recent turbidite studies (*Goldfinger et al. 2012*). These efforts will include new ground motion prediction equations, directivity, directionality of ground motions, and new site amplification recommendations

5.3.3.2 Oregon Resilience Plan

Peak Ground Acceleration (PGA) and Peak Ground Velocity (PGV) estimates for a scenario event of the CSZ M9.0 earthquake of the coast of Oregon were obtained from a recent analysis completed as part of the Oregon Resilience Plan (*Madin and Burns 2013*).

To create the PGA map (Figure 5.9), the following steps were completed by Madin and Burns (*Madin and Burns 2013*). First, the USGS provided PGA estimates gridded at 0.02 degree spacing for bedrock conditions (VS30= 760 m/sec). Next, a map of estimated shear-wave velocities (VS30) was created by combining geologic information with shear-wave velocity measurements. Site amplification factors were calculated across the entire study area using the Boore and Atkinson (*Boore and Atkinson 2008*) procedure. This site classification is described in section 5.3.4 of the report. Finally, the bedrock PGA map was multiplied by the site amplification factor map to create the PGA map for the state of Oregon.

Madin and Burns (*Madin and Burns 2013*) then created the PGV map (Figure 5.10) with the following steps. First, the USGS Cascadia M9.0 ShakeMap was used to calculate bedrock 1-second period spectral acceleration (SA01) values for each pixel. Next, site amplification factors were applied. Finally, the Newmark and Hall *(Newmark and Hall 1982)* equation was used to estimate PGV from the SA01 values.

Figure 5.9: PGA estimates for a M9.0 CSZ earthquake scenario event

Figure 5.10: PGV estimates for a M9.0 CSZ earthquake scenario event

64

5.3.4 NEHRP Site Classification

As part of the Oregon resilience plan, Madin and Burns *(Madin and Burns 2013)* created a statewide National Earthquake Hazard Reduction Program (NEHRP) site classification map based on evaluating VS30 measurements within generalized geologic units. The NEHRP site classifications are presented in Table 5.5 and the map is presented in Figure 5.11.

Table 5.5: NEHRP site classifications and corresponding VS30 values.

Site Class	Soil/Rock type	VS30 (m/s, NEHRP)	VS30 (m/s, ORP)
A	Hard Rock	$V_s > 1500$	-
B	Rock	$760 < V_s \leq 1500$	686
C	Very dense soil and soft rock	$360 < V_s \leq 760$	464
D	Stiff soil	$180 < V_s \leq 360$	301
E	Soft soil	$V_s < 180$	163
F	Soils susceptible to potential failure under seismic loading (e.g. landslide deposits)	-	98
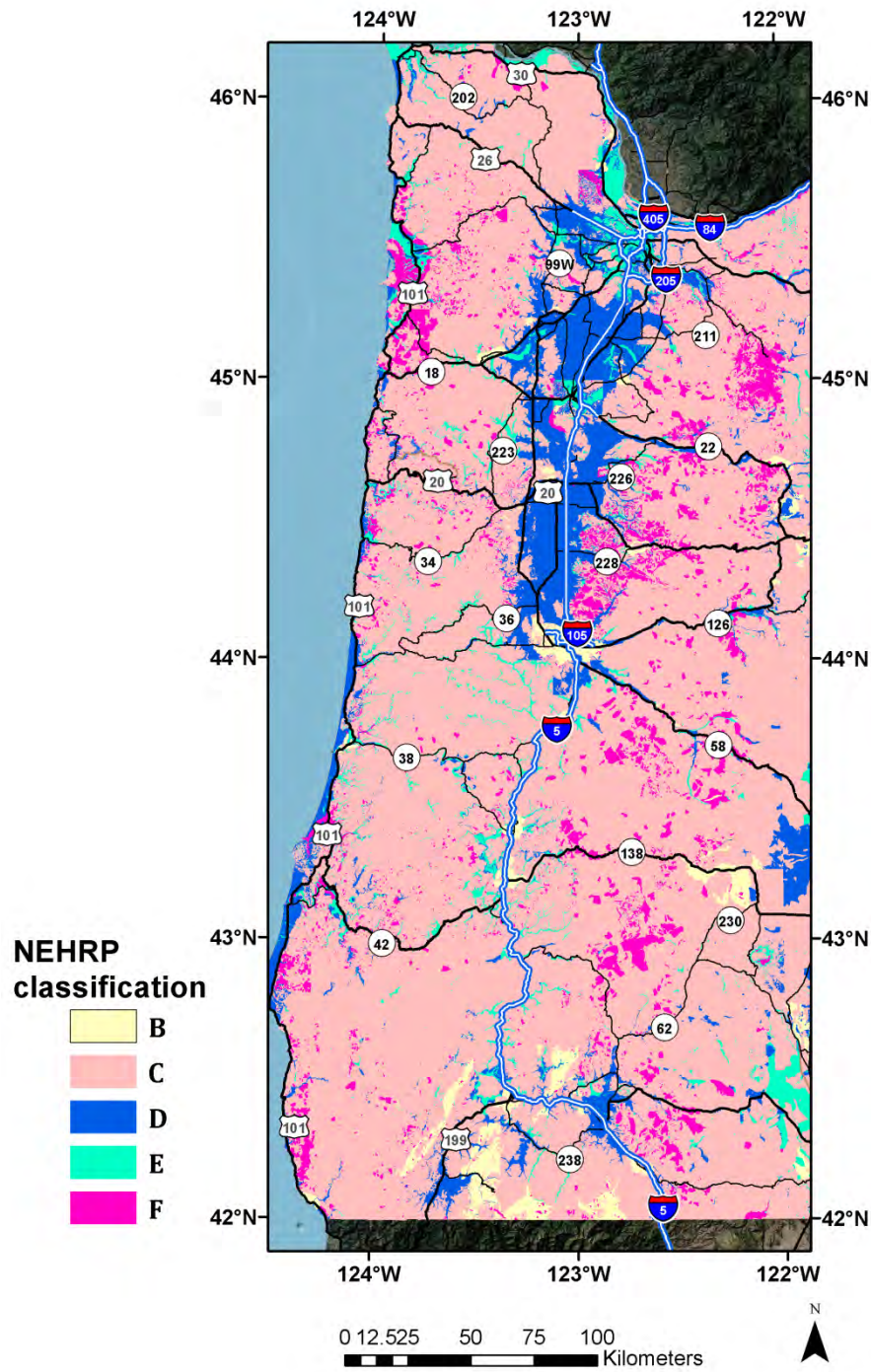
Figure 5.11: ORP NEHRP site classifications for the study area

5.3.5 Geotechnical Reports

Initially, it was hoped to find geotechnical investigations to quantify soil properties in the coast range in an approach similar to Olsen *(Olsen 2005*) for liquefaction hazard mapping. However, given the scarcity of available data in the coast range and difficulty in acquiring such data for the entire study area, the research team decided to pursue an alternate approach to estimating soil strength to ensure timely completion of the project. DOGAMI is currently compiling geotechnical data throughout the Portland area in a 3D database that may prove valuable to quantifying soil strength and other properties of geologic units. However, it will be some time before that database is available. In particular, the necessary soil information for this study must be manually populated from boring logs, which are only available as pdfs.

5.4   LAND COVER

5.4.1 Land Use

The land use and land cover shapefile available from the Oregon Geospatial Data Enterprise (http://www.oregon.gov/DAS/CIO/GEO/Pages/sdlibrary.aspx) was used in this study. This shapefile was grouped in to six major categories: Vegetation, Coastal, Non-resources, Rural commercial and residential, Urban commercial and residential, and water.

5.4.2 NDVI

The Normalized Difference Vegetation Index (NDVI) is used to represent the relative amount of biomass and provides an indication of vegetation type. NDVI is based on the red band of the electromagnetic spectrum being absorbed by the chlorophyll pigment while near infrared (NIR) is reflected. The Landsat Enhanced Thematic Mapper (ETM)+ satellite has seven multi spectral bands. The NIR band with a spectral range of 0.75-0.90 micrometers and the red band (0.63-0.69 micrometers) are used   to calculate NDVI at a resolution of 30 m. The Landsat data was downloaded from the satellite imagery repository operated by the USGS *(USGS 2011)*. Figure 5.12 shows the processing and calculation procedure to find NDVI. This process also includes a haze correction. Figure 5.13 depicts NDVI for the study area. Low vegetation will have an NDVI = -1, whereas high vegetation will have an NDVI = +1.
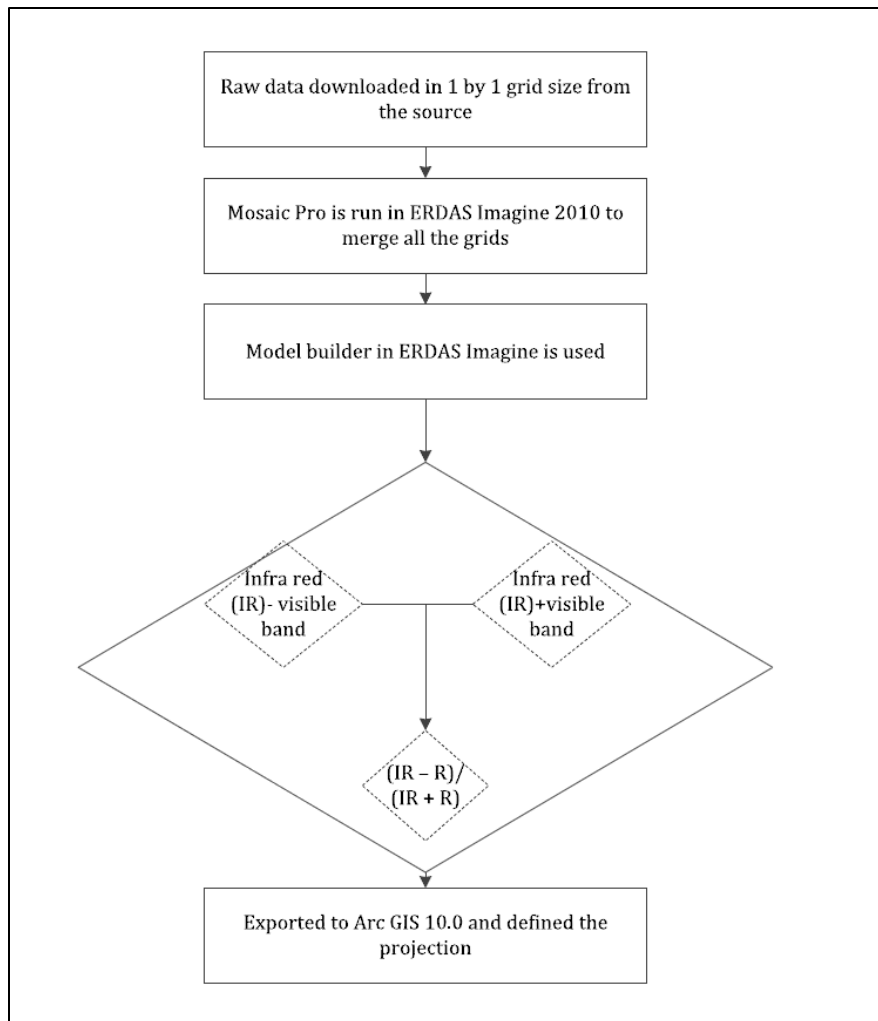
Figure 5.12: : Logistics applied to generate NDVI map
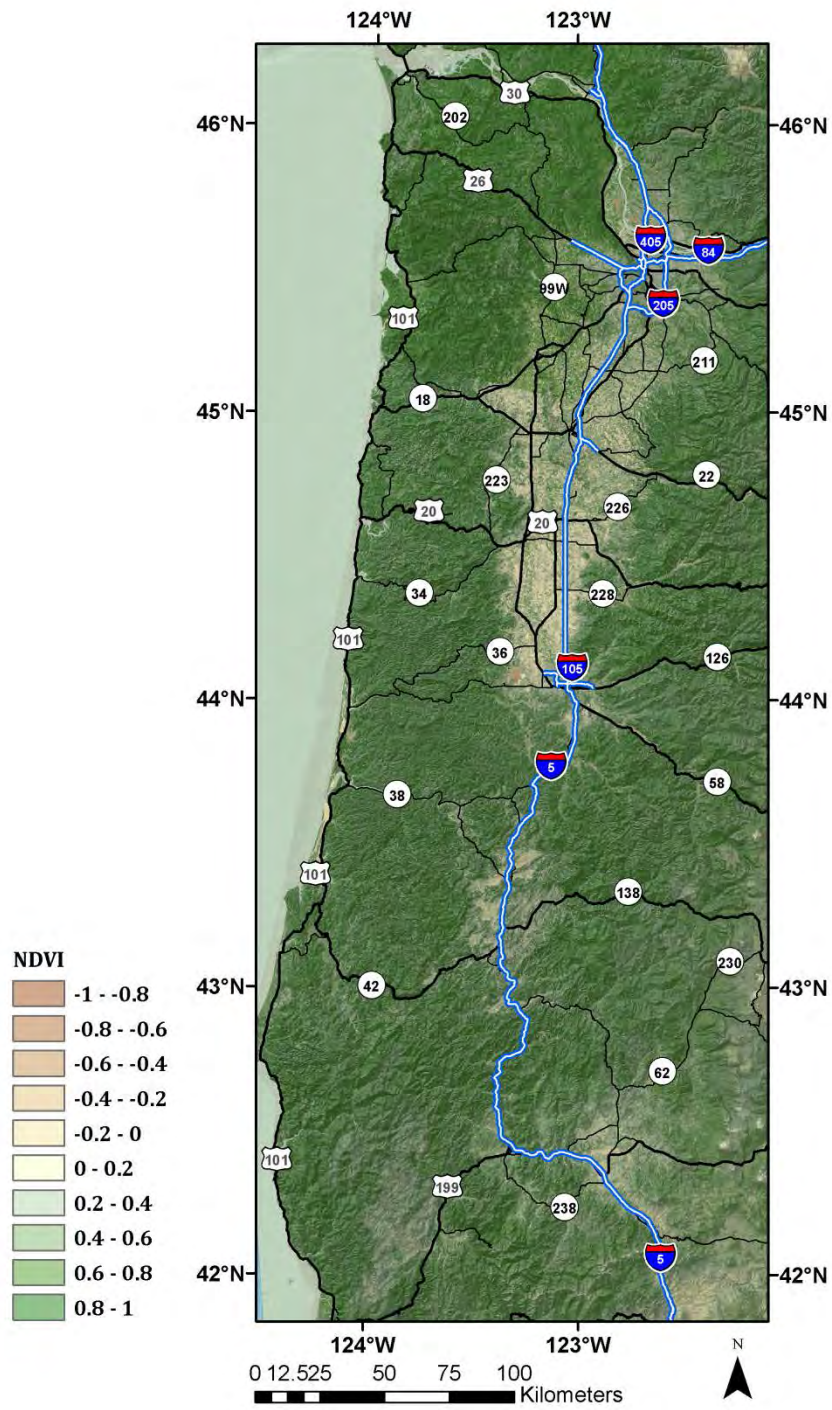
Figure 5.13: NDVI map created for the study area

5.5   HYDROGRAPHY

5.5.1 Rivers and Streams

The Oregon rivers and stream dataset available from the Oregon Geospatial Data Enterprise (http://www.oregon.gov/DAS/CIO/GEO/Pages/sdlibrary.aspx) was used in this study. These rivers have been mapped to a scale of 1:100,000. Figure 5.14 shows the spatial distribution of major rivers and streams.

5.5.2 Precipitation

The Parameter elevation Regressions on Independent Slopes Model (PRISM) precipitation model, developed by researchers at Oregon State University, provided the average (1971-2010) annual precipitation dataset. To create a continuous grid,   PRISM combines point data (e.g. discrete precipitation measurements) with DEM, and expert knowledge of complex climatic extremes rather than standard interpolation techniques. The precipitation values obtained from PRISM are in units of millimeters times hundred . Figure 5.15 depicts the average rainfall from 1980-2010 for the study area.

5.6   HIGHWAYS

The Highway Network 2011 dataset, available from the Oregon Geospatial Data Enterprise (http://www.oregon.gov/DAS/CIO/GEO/Pages/sdlibrary.aspx), was used in this study. This dataset includes all state owned\maintained highways, connections, frontage roads, temporary traveled routes, and lines. It has been mapped to a scale of 1:24,000. The database is maintained by the Geographic Information Services Unit, Oregon DOT. The major routes are identified in each of the maps in this section.
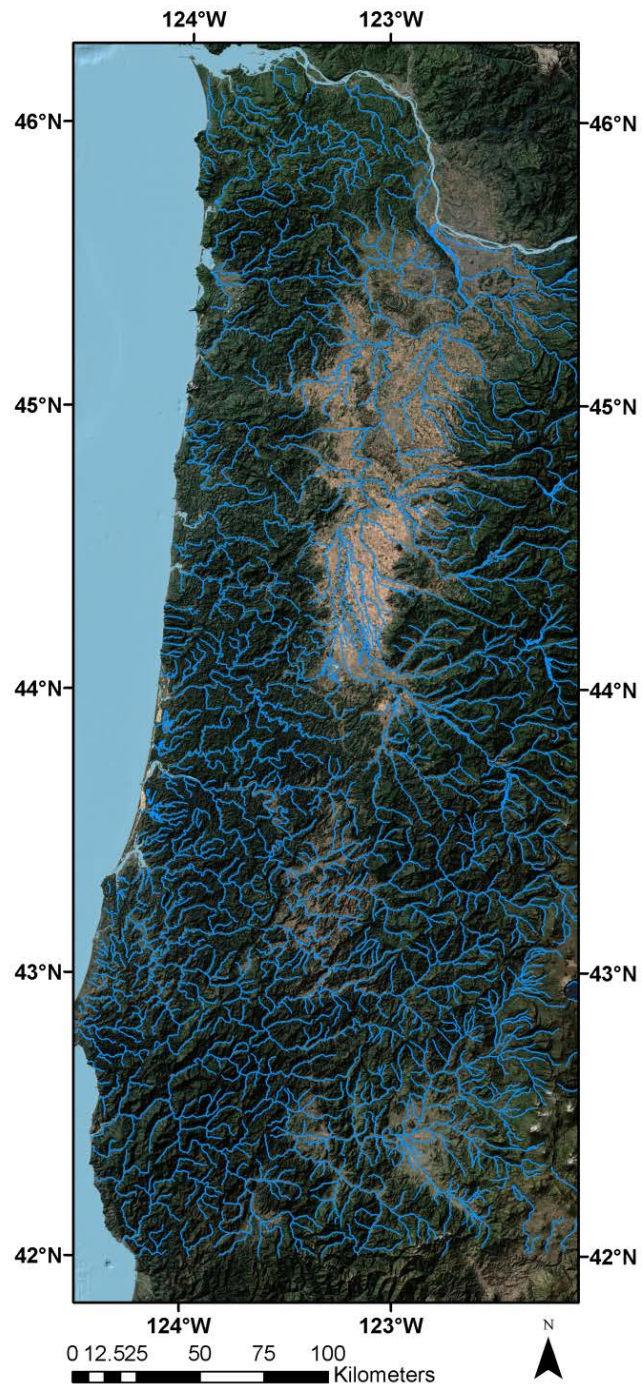
Figure 5.14: Rivers and Streams map for the study area.
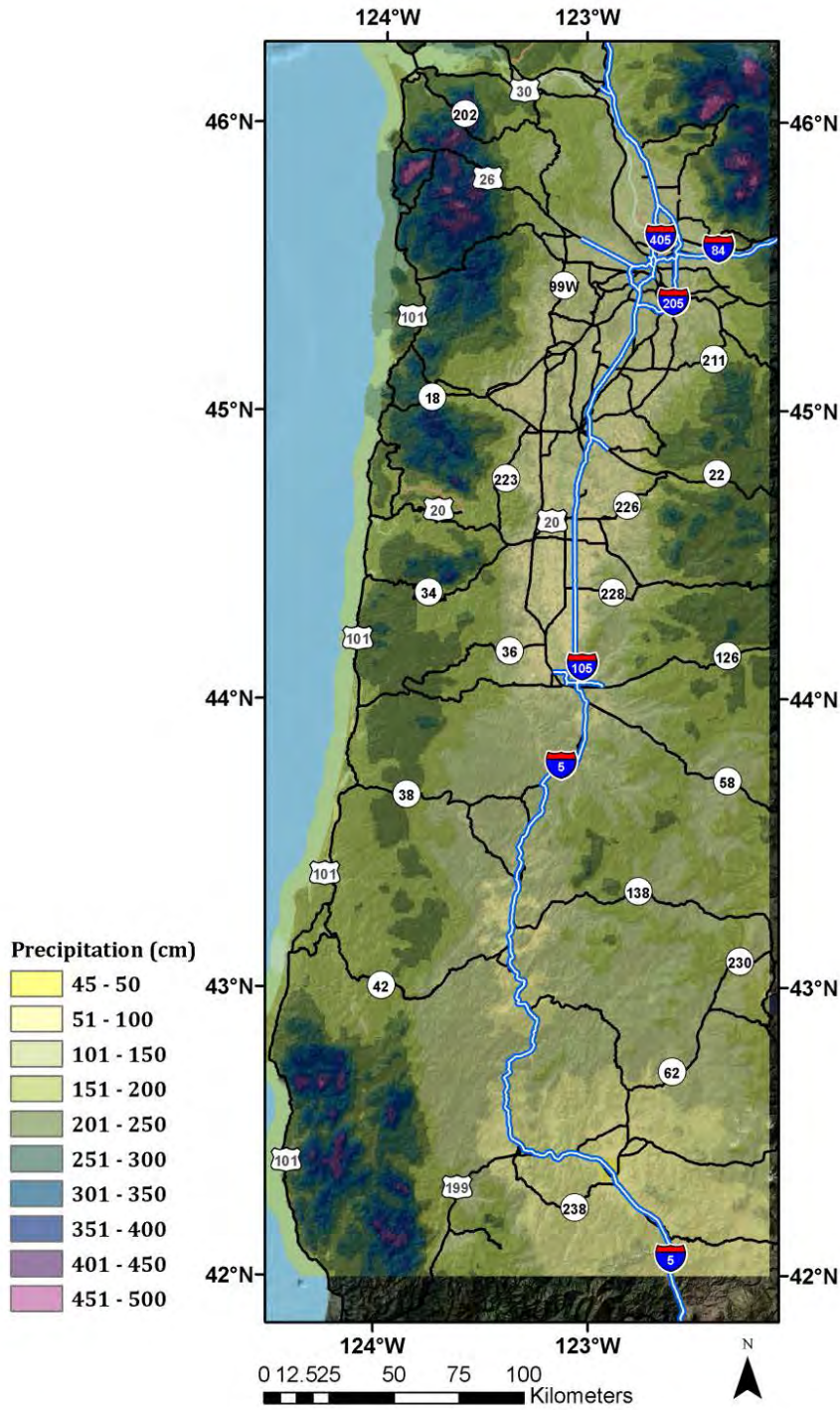
Figure 5.15: Average annual rainfall from 1980-2010 for the study area. Precipitation data provided by OSU PRISM climate group.

6.0   CORRELATION OF CAUSATIVE FACTORS

6.1   CHAPTER SUMMARY

The Oregon coast range is highly prone to landslides, which create a significant maintenance problem for ODOT. Many causative factors contribute to the failure of these slopes including slope angle, slope and terrain ruggedness, weak soils, significant precipitation, and high groundwater levels. These unstable slopes are further threatened by future seismic hazards, such as the Cascadia Subduction Zone. These coast range landslides are capable of isolating communities by blocking the limited number of lifeline highway corridors, critical for evacuation and/or supply transport during emergencies. This chapter presents statistical evaluations that geospatially characterize the influence of these causative factors on the potential for landslides. A methodology in a GIS environment for querying and analyzing the wide variety of data sources needed to characterize each major lithological unit for these evaluations is also presented. This work lays the foundation for performing regional seismic slope stability analysis and mapping to determine the vulnerability of these lifeline corridors during the next major earthquake event.

6.2   INTRODUCTION

Conditions are near perfect for triggering landslides (e.g.*,* slope angle, rough terrain, weak soils, significant precipitation, and high groundwater levels) in the Oregon coast range. A significant portion of the Oregon coast range is covered with weak soil and rock in which large mass movements commonly occur (Figure 6.1). Steep slopes, wet soils due to heavy rainfall and human activities, such as highway construction (i.e.*,* embankments, cut slopes, etc.) exacerbate the landslide hazard in Oregon. For example, Burns et al. *(Burns et al. 2008)* estimated as many as 9,500 landslides occurred in Oregon from a large winter storm in 1996-1997, most of which were located in western Oregon. In addition to these factors, landslides can also be triggered by earthquakes, such as those from the Cascadia subduction zone (*Schulz et al. 2012*).

Both existing and potential new landslides threaten public safety and create economic problems. For example, many lifeline routes connecting coastal areas to the Willamette valley are threatened by landslides. Wang et al. (*Wang et al. 2002*) estimated an average cost of approximately $10 million in damages from landslides in a typical year in Oregon. This shows the importance of developing landslide susceptibility maps for planning and preparation. A key part to creating these maps and performing triggering analyses is to understand the correlation among contributing factors and characterize lithological properties.

Although landslides are unique in each region and have site-specific considerations, it is vital to understand the spatial relationships between the various triggering factors. Detailed, site-specific analysis would not be feasible at large scales. By using geospatial characterization and analyzing parameters statistically, the correlation among the causative factors to landslide generation can be determined *(van Western and van Asch 2006)*. Multi-temporal landslide

inventory maps are very efficient tools to find the suitable relationships towards assessing this hazard *(Guzzetti et al. 2005)*. The Department of Geology and Mineral Industries (DOGAMI) for Oregon has been actively publishing landslide inventory and susceptibility maps for the state.

Numerous factors such as slope (topographic gradient), aspect, Normalized Differential Vegetation Index (NDVI), lithological units, slope roughness, precipitation and land cover/land use play a significant role in landslide susceptibility (*Wilson and Gallant 2000*). For seismic slope stability, an estimate of ground motion intensity such as Peak Ground Acceleration (PGA) is important. Lee et al. *(Lee et al. 2008)* have proposed and tested a method for assessing the contribution of various parameters responsible for landslides using a historical database.
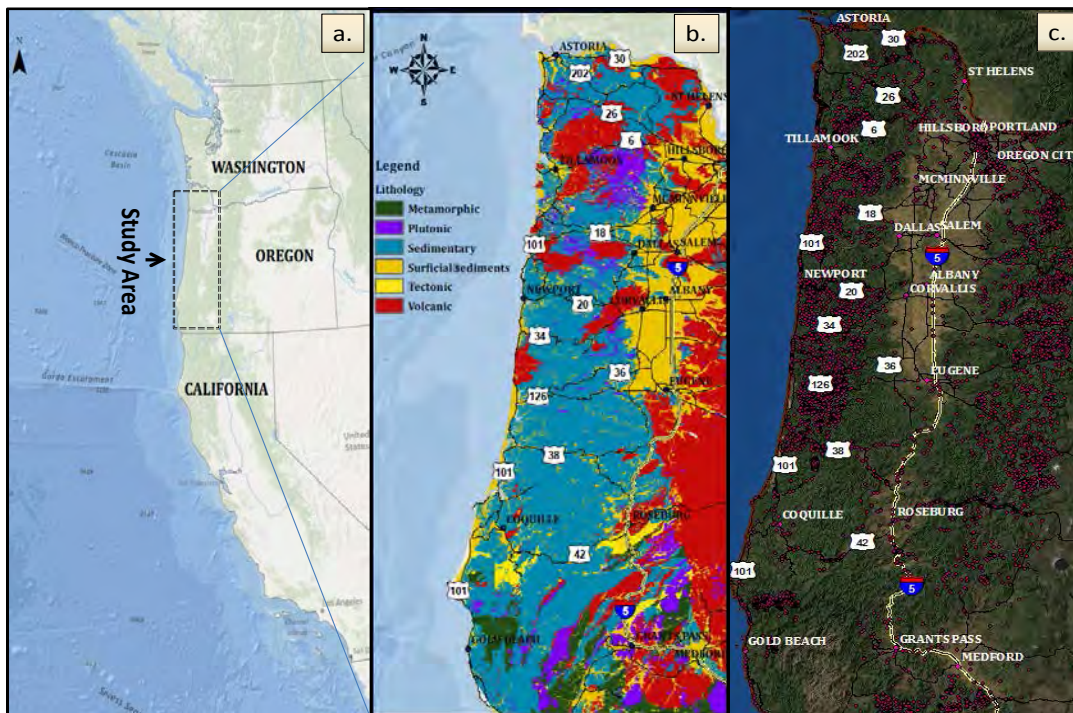
Figure 6.1: a. Study area b. Lithology map in Oregon coast c. Landslide inventory map.

6.3   METHODOLOGY

This study statistically analyzes the relationship between causative factors and landslide occurrence by comparing a detailed landslide inventory map (*Burns et al. 2008 and 2012a*) to several datasets characterizing susceptibility factors including slope, NDVI, aspect, precipitation, land cover, and lithology. The logic behind the methodology used in this paper is adapted from Lee et al. *(Lee et al. 2008)*: Similar landforms (e.g.*,* slope and lithology) where historical landslides have previously been reported are most likely to experience future landslides.

Comparisons of causative factors to historical landslides were made in two ways. First, historical landslides were analyzed together regardless of lithology, similar to Lee et al. *(Lee et al. 2008)* to evaluate the hazard frequency. Second, as a deviation from previous work,

landslides were discretized by lithology to characterize each lithological unit separately to enable comparisons. In previous work, lithology is solely treated as another causative factor and handled in the same manner as other factors, such as slope. However, lithological units will have varying strengths and properties. This being the case, they are expected to have different potentials for landsliding. Hence, the other parameters are dependent on lithological units.

6.3.1 Data Collection and Processing

Data were acquired from several sources. Six raster datasets were processed in ERDAS Imagine 2010 and Arc GIS 10.0 for the respective analysis. Table 6-1 provides a summary of the source of raw data and the information of how they were acquired. For simplicity, all datasets were resampled to a consistent cell size of 26.7 meters using the UTM NAD83 Z10 N coordinate system. Digital elevation models (DEMs) were created through ASTER images from satellites *(NASA 2011)* and then processed into derivative datasets such as slope maps, aspect, and terrain ruggedness.

The DOGAMI Statewide Landslide Information Database for Oregon (SLIDO-2, *Burns et al. 2012a)* was used as the input landslide map. This database includes polygons delineating landslide deposits and related features from 313 published studies as well as 10,636 point features representing landslide locations compiled for the past 10 decades. These are referred as LS points in this study. For simplicity, the centroid of each polygon was considered as a single landslide point.

Equally important to knowing the location of where landslides occur is where landslides do not tend to occur. To model this, a number of random samples representing non-landslide (NLS) points were created inside the study area where landslides have not been mapped. Two constraints were applied in the selection of NLS points: (1) a 2 km buffer was used between the LS and NLS points, and (2) NLS points were at least 30 m apart.

Table 6.1: Summary of raster datasets used in this chapter

Dataset	Source	Provider	Native Resolution
Slope	Aster GDEM V2	NASA	26.7 (m)
Aspect	Aster GDEM V2	NASA	26.7 (m)
NDVI	Landsat ETM+	USGS	14.25 (m)
Land cover	Raster Conversion	OGDC	26.7 (m)
Precipitation	Rain gauges	OSU (PRISM)	4630 (m)
Lithology	Raster Conversion	DOGAMI	26.7 (m)

6.3.2 Workflow

Figure 6.2 illustrates the geospatial processing workflow to determine characteristics of LS and NLS in each raster dataset using ArcGIS. First, the points (both LS & NLS) were classified by lithological units. Next, the causative factor values from the raster datasets were obtained for each landslide location using the "Zonal Statistics" tool in ArcGIS. Bin intervals were selected for each parameter, and the data were reclassified to determine the frequency of LS & NLS in each individual bin, producing histograms for each dataset.

The Landslide Ratio (LSR), comparing the number of landslides (LS) in a bin to the total number (LS+NLS) within that bin, was then calculated by:

$$\text{LSR} = (\#\text{LS} \times 100\%)/(\#\text{LS} + \#\text{NLS}) \qquad \text{(6-1)}$$

LSR represents a pseudo-probability for each factor. It can vary from 0 (the pixel is not landslide prone) to 1 (the pixel is highly prone to landslide). However, this parameter may not be reliable in bins with small numbers of LS and NLS samples.
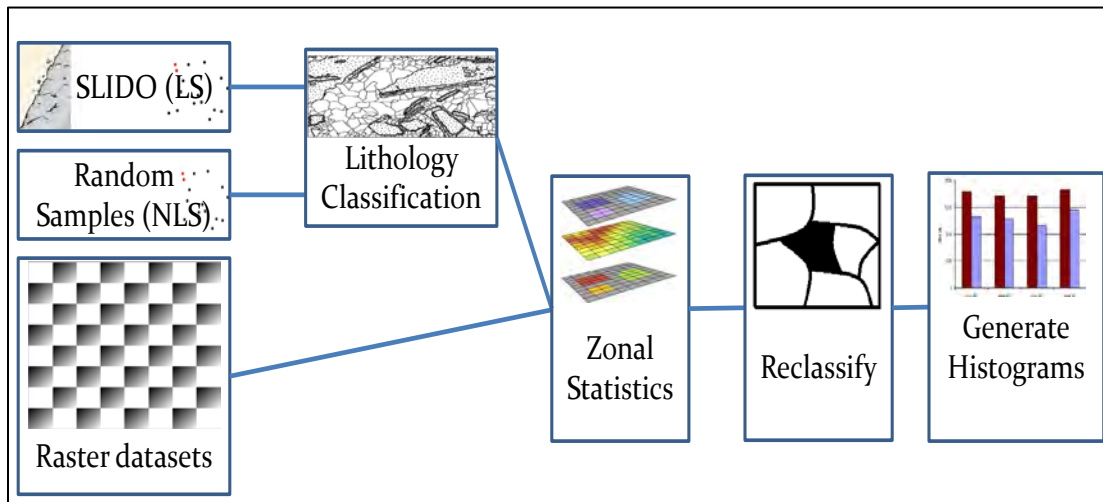
Figure 6.2: Workflow chart showing the methodology used to create histograms

6.4   RESULTS

The analysis results are presented in Figures 6.3 through 6.8. Table 6.2 presents the frequency and density of landslides in each lithological unit, which provides an indication of their susceptibility. LSR is plotted on a secondary axis, except for those factors that were discontinuous (e.g., land use and lithology).

Table 6.2: Frequency and density of landslides in each lithological unit.

Lithological Unit	# LS	Coverage (km^2)	LS Density (#LS/ km^2)
Volcanic	8837	30855	0.286
Sedimentary	6890	24109	0.286
Surficial Sedimentary	3969	14192	0.280
Tectonic	249	948	0.263
Plutonic	649	3651	0.178
Metamorphic	133	2632	0.051
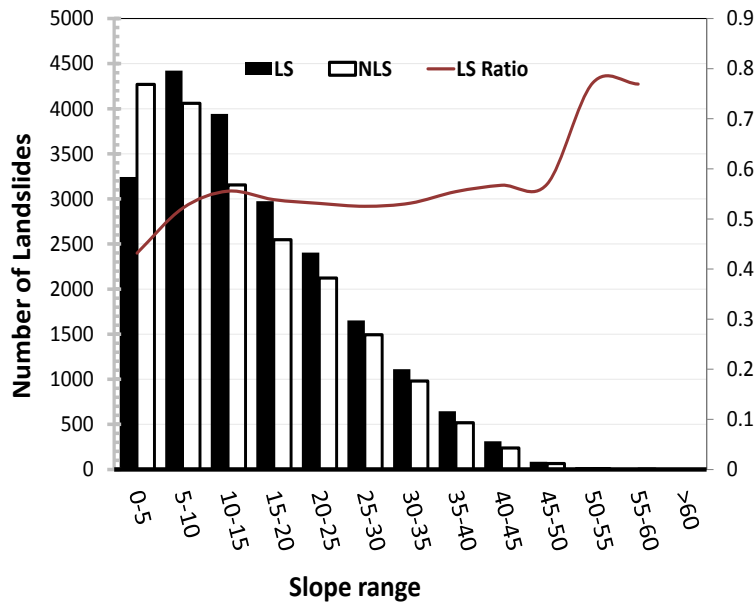
Figure 6.3: Slope histogram study area
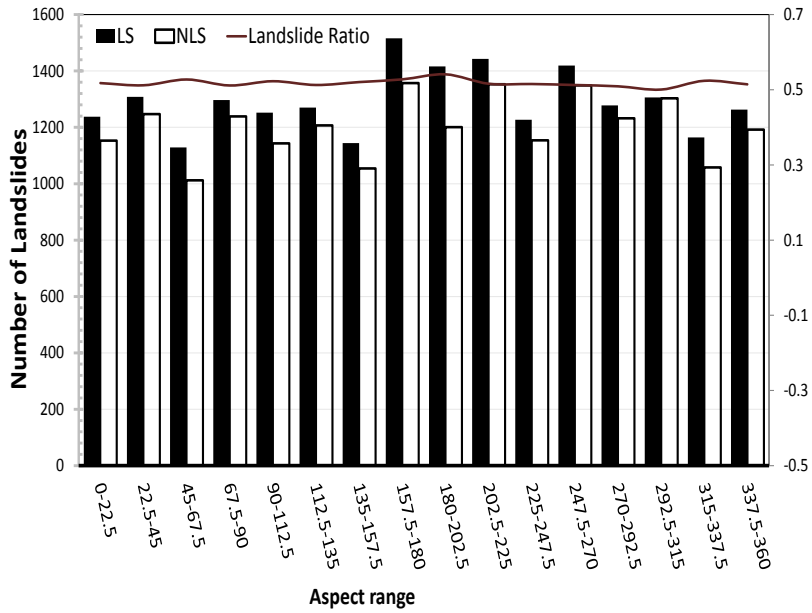
Figure 6.4: Aspect histogram for study area.
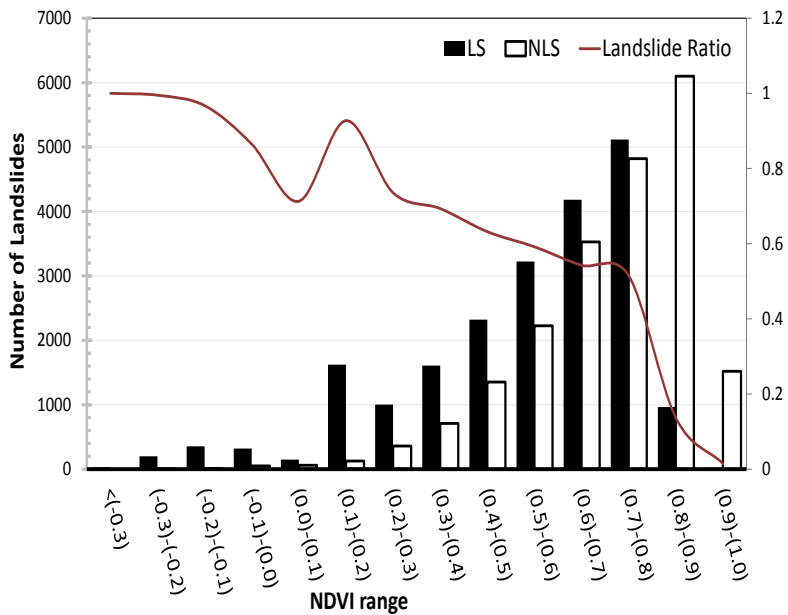
Figure 6.5: NDVI histogram for study area.
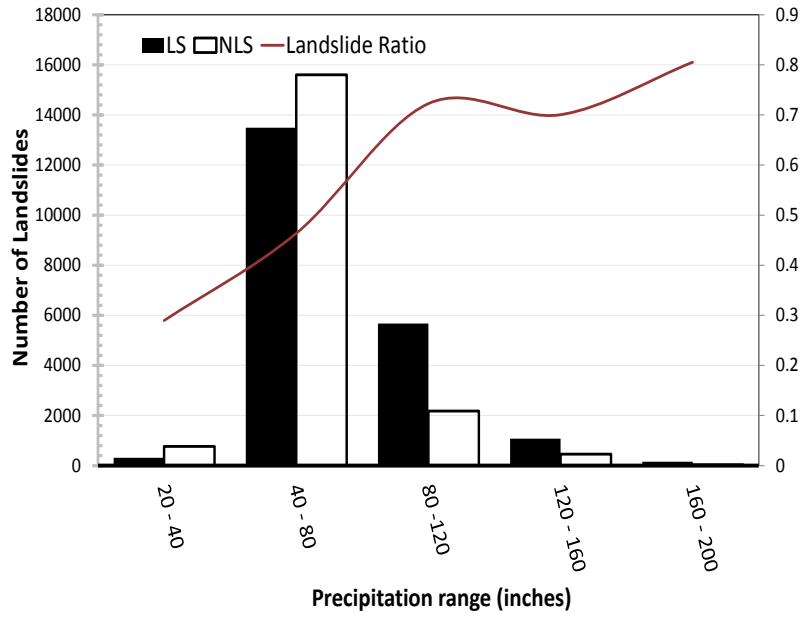
Figure 6.6: Precipitation histogram for study area.
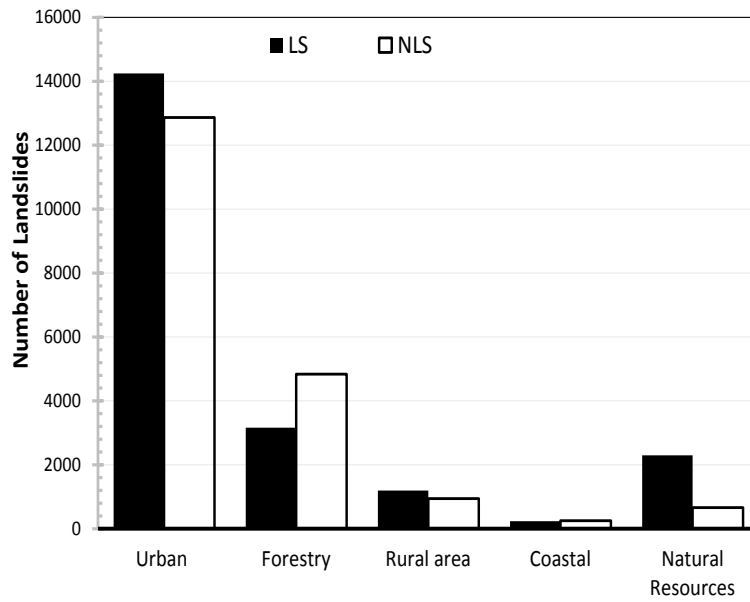
Figure 6.7: Distribution of various land covers within study area.
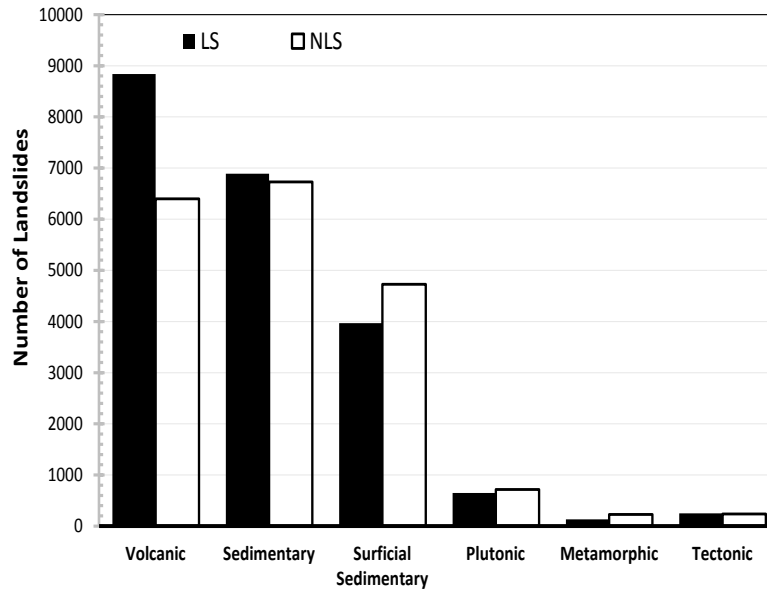
Figure 6.8: Distribution of various lithological units within study area.

The following histograms highlight various contributing factors within specific lithology.

Figures 6.9 to 6.14 display the number of landslides occurring in different lithological units within various intervals of slope, in degrees. In addition, the quantity of non-landslide samples is given for the same slope intervals. On the second axis, the landslide ratio is plotted.

Figures 6.15 to 6.20 show the number of landslides and non-landslides in primary axis and landslide ratio in secondary axis for various lithological units with respect to bins of aspect values.

Lastly, Figures 6.21 to 6.26 exhibit the landslide points and non-landslide points for bins of NDVI in each lithological unit in the study area. In the same plot landslide ratio was plotted as a secondary axis.
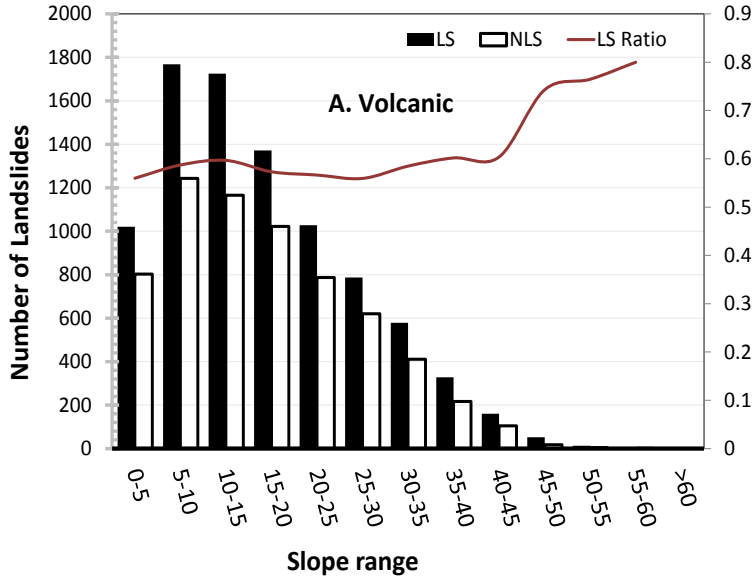
Figure 6.9: Generated slope histogram within volcanic lithology.
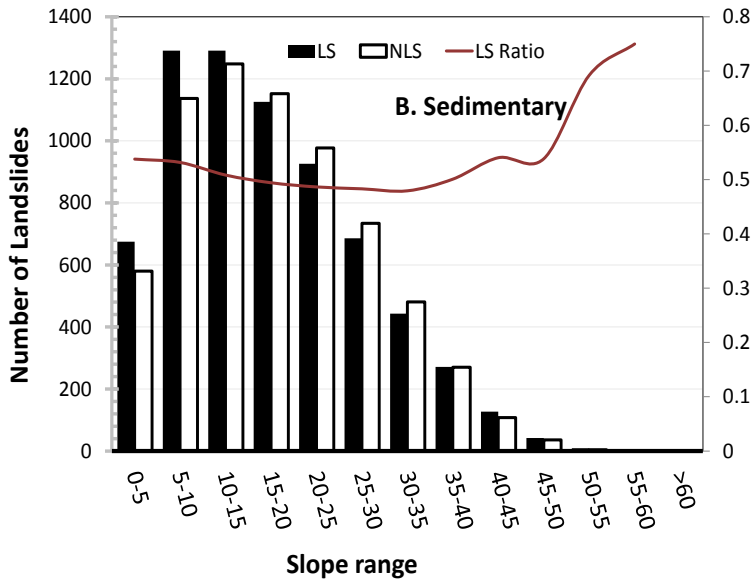
Figure 6.10: Generated slope histogram within sedimentary lithology.
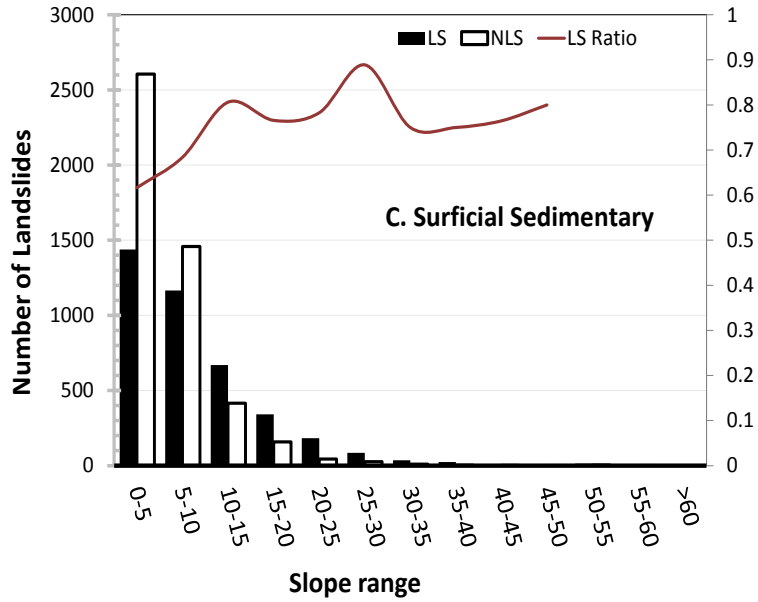
Figure 6.11: Generated slope histogram within surficial sedimentary lithology.
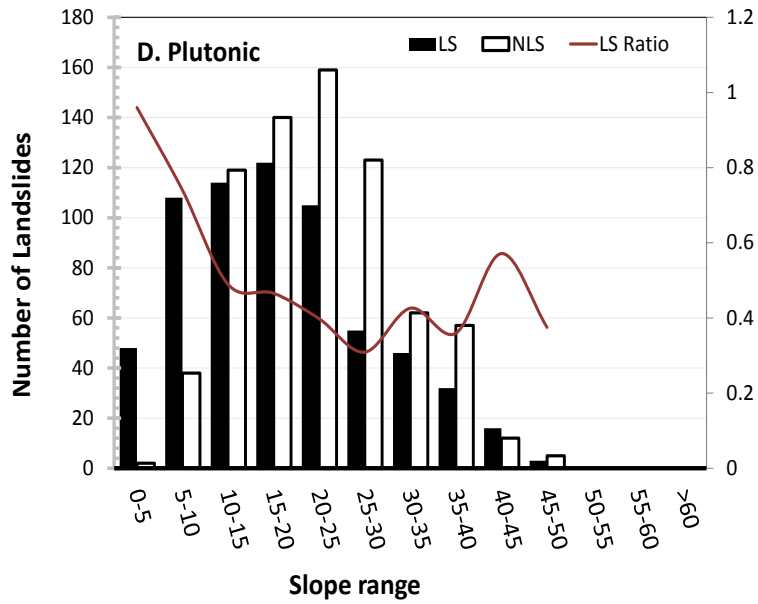
Figure 6.12: Generated slope histogram within plutonic lithology.
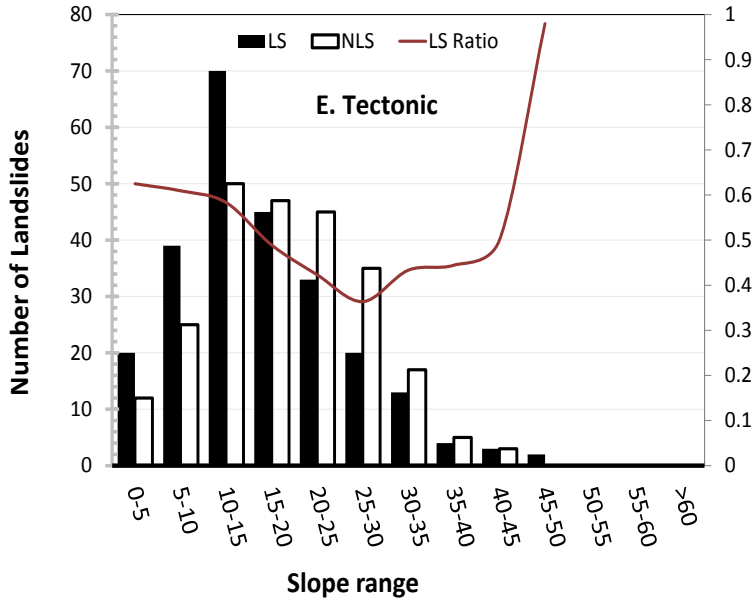
Figure 6.13: Generated slope histogram within tectonic lithology.
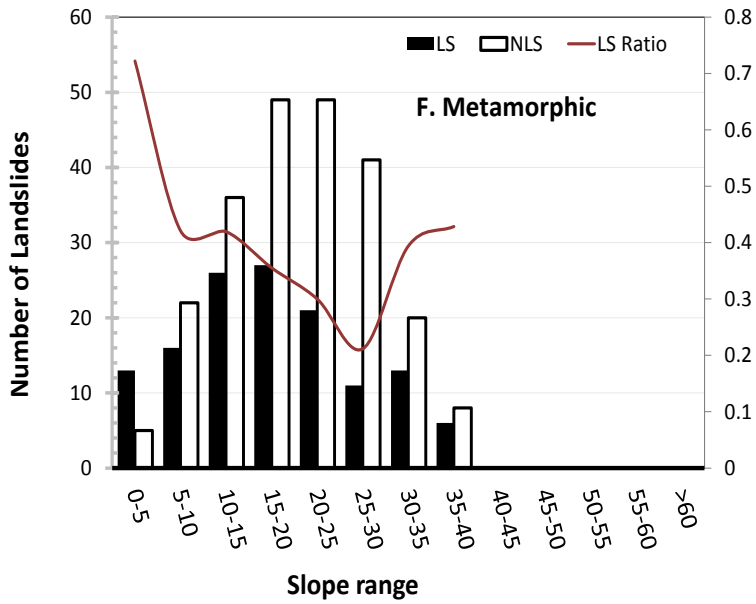
Figure 6.14: Generated slope histogram within metamorphic lithology.
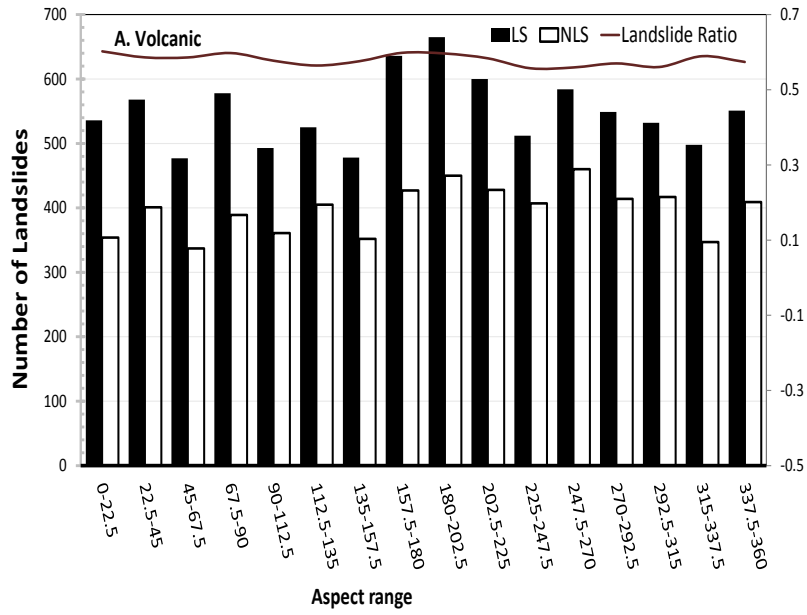
Figure 6.15: Generated aspect histogram within volcanic lithology.
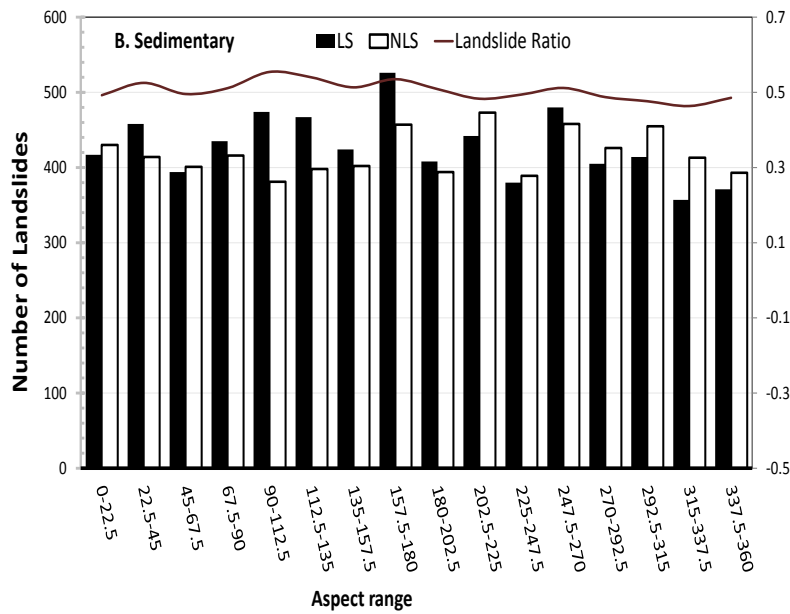
Figure 6.16: Generated aspect histogram within sedimentary lithology.
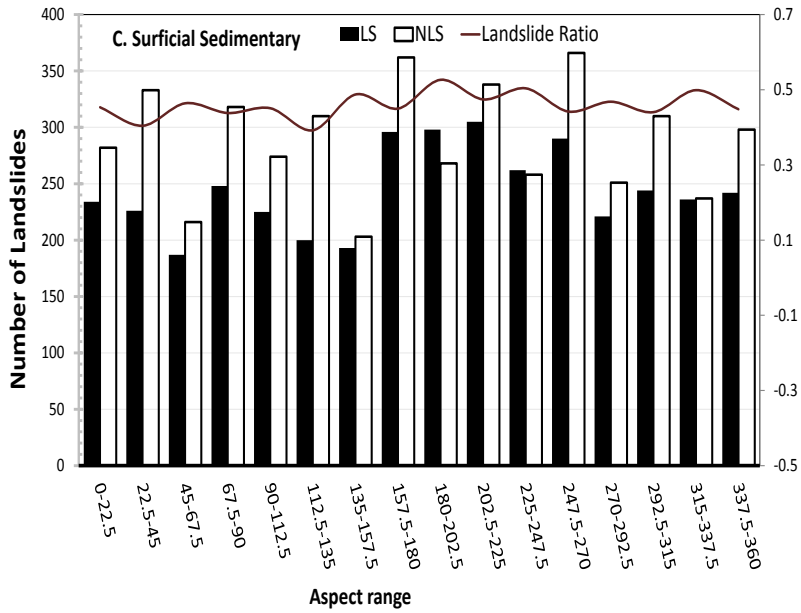
Figure 6.17: Generated aspect histogram within surficial sedimentary lithology.
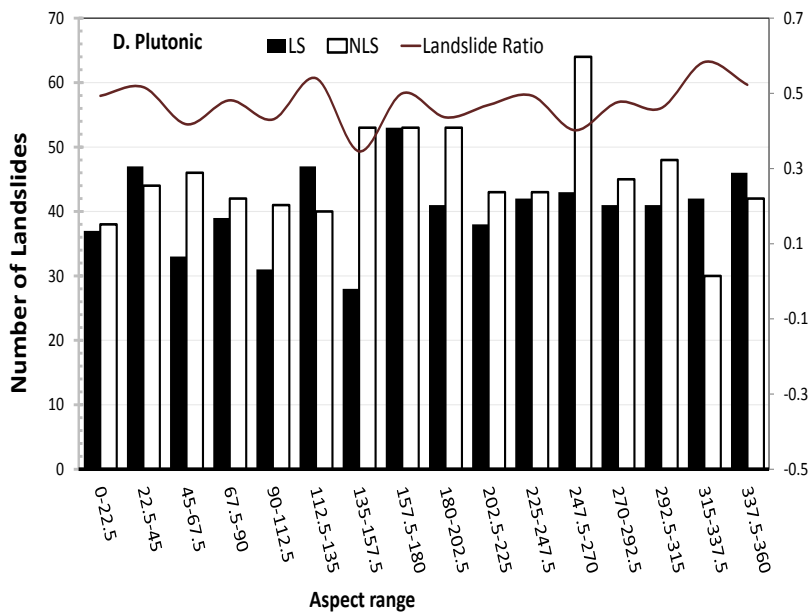
Figure 6.18: Generated aspect histogram within plutonic lithology.
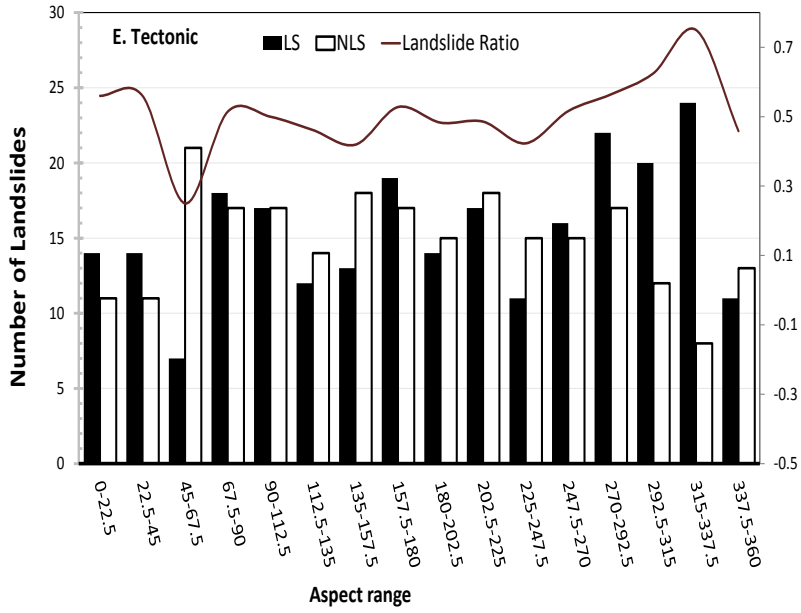
Figure 6.19: Generated aspect histogram within tectonic lithology.
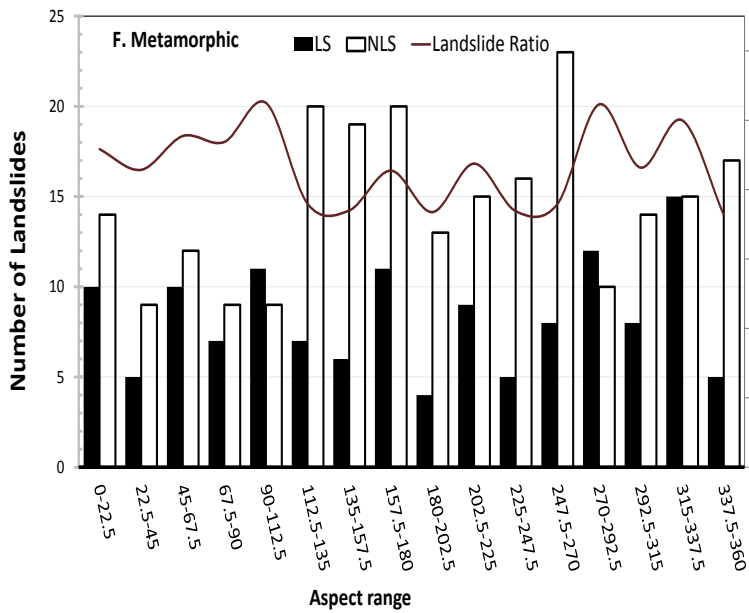
Figure 6.20: Generated aspect histogram within metamorphic lithology.
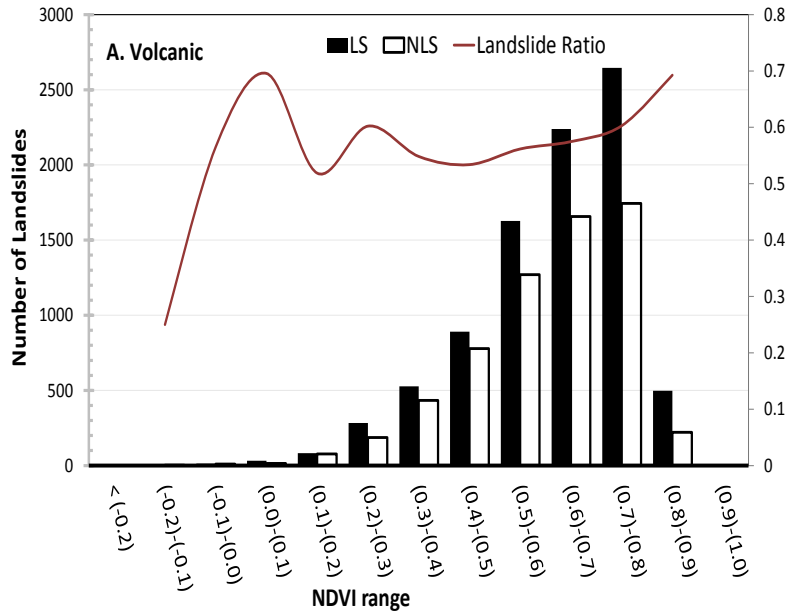
Figure 6.21: Generated NDVI histogram within volcanic lithology.
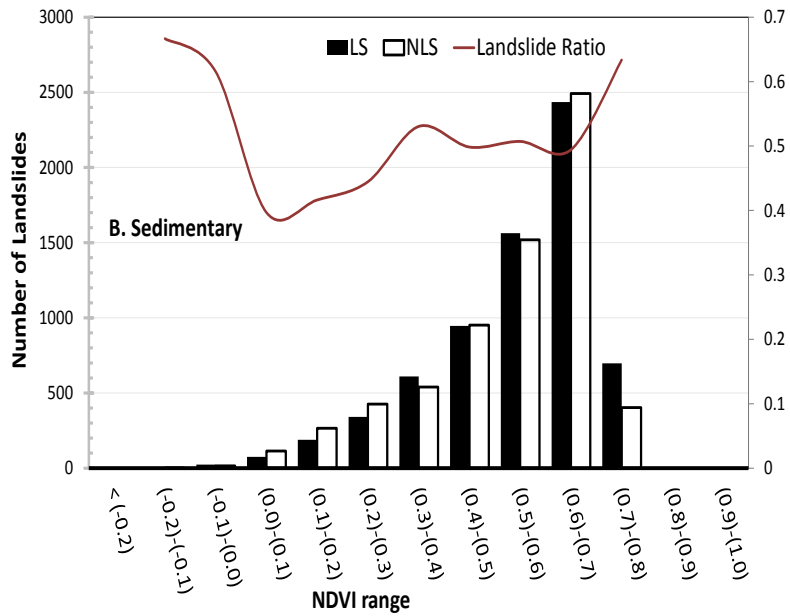
Figure 6.22: Generated NDVI histogram within sedimentary lithology.
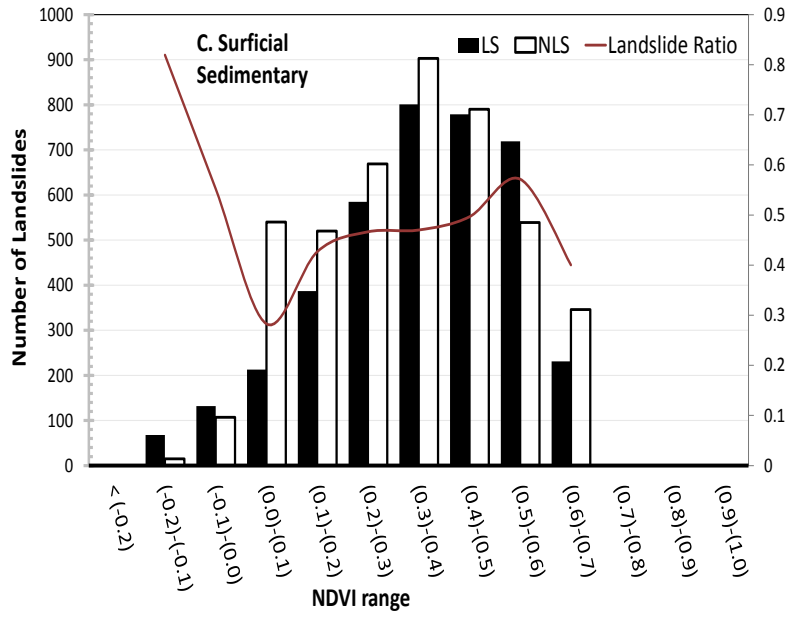
Figure 6.23: Generated NDVI histogram within surficial sedimentary lithology.
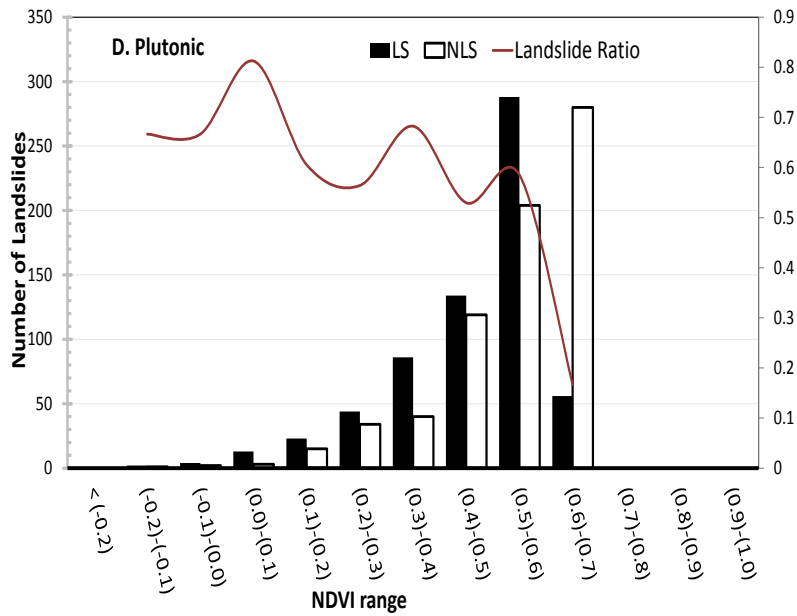
Figure 6.24: Generated NDVI histogram within plutonic lithology.
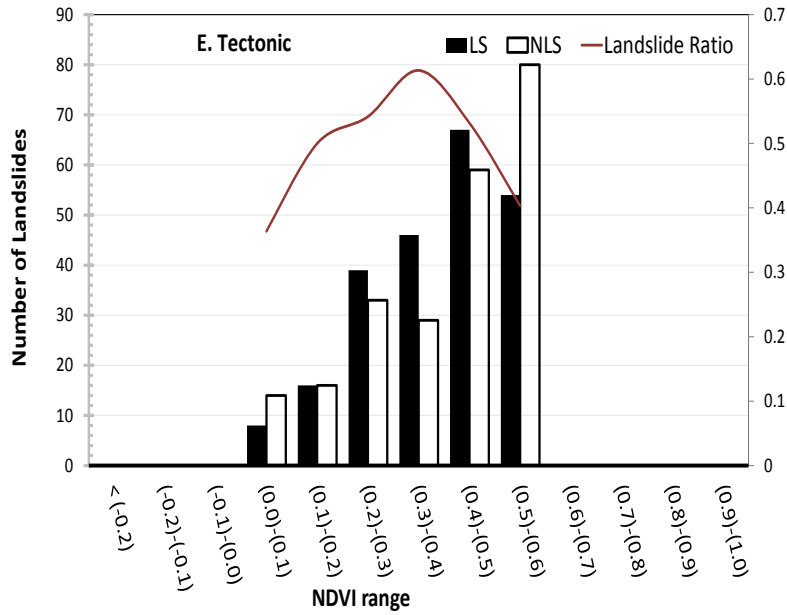
Figure 6.25: Generated NDVI histogram within tectonic lithology.
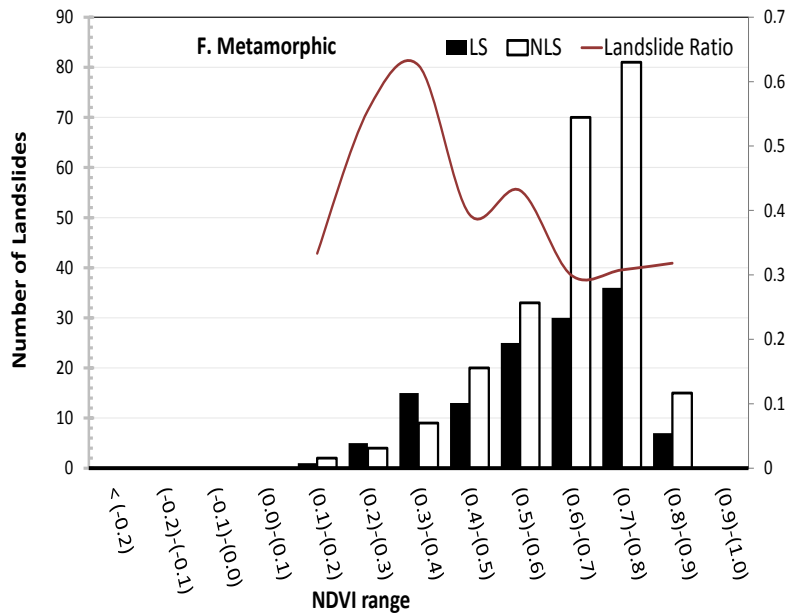
Figure 6.26: Generated NDVI histogram within metamorphic lithology.

6.5   DISCUSSION

Various trends can be observed in the histograms for each of the parameters:

- **Slope** – Relating soil strength to slope angle at failure is not possible without a better understanding of geologic structure of slopes, yet in absence of such data, the slope at failure can provide a reasonable estimate of the soil's shear strength and ability to resist landsliding. Hence, the slope histograms represent a distribution of likely soil strength for each lithological unit. Considering the slopes for all landslides, not distinguished by lithology, a LS peak is observed around 5° to 10° compared to 0° to 5° for NLS points. The LSR trend indicates an increase in landslide hazard with the rise of slope, which makes physical sense. In volcanic, most of the landslides fall within the span of 5° to 15°, with a peak between 10° to 15°. The LSR trend observed in surficial sedimentary signifies the fact that there are actually not many steep slopes of this unit. The surficial sedimentary lithology is common in valley areas and LSR characterizes this earth structure as a very weak unit with generally shallow slopes. However, the steepest slopes are not always the most likely to fail. Many shallow slopes are shallow because they have weak material and many steep slopes can remain steep because they have a stronger material.

- **Aspect** – Given the climate of Oregon where storms approach from the north-west, one would expect more landslides on north-west facing slopes (e.g., 300°). Further, because of the NW regional dip of the Tyee formation, one would also expect an increased number of landslides on the NW slopes, as has been observed on the US20 Highway Realignment Project. However, the plots show minimal variance in LSR based on aspect. Using a more generalized aspect from a lower resolution DEM may produce improved results compared to the results from the 30 m DEM used in this study since it will highlight the more general trend and include less surface variability.

- **Rainfall** – A strong, increasing LSR trend with precipitation is observed. However, nearly the entire study area experiences heavy rainfall relative to most regions in the US and the eastern part of the state of Oregon. Further, because many landslides in the database occurred as a result of the 1996-1997 storms, the samples are heavily biased towards precipitation-induced landslides.

- **Land Cover** – Western Oregon is dominated by forested terrain. There are two reasons behind the high value of NLS points in forested regions: First, the high vegetation index factor can provide stability to slopes; second, most of the study area is covered by this type of land cover. Urban areas and agriculture regions also show significant landslide potential, presenting importance of human effect on landslide threat besides other discussed factors.

- **Lithology** – Histograms for each of the lithology units correlate well with the LS density given in Table 6.2. From the table, it can be noted that volcanic and sedimentary units appear more susceptible to landslide hazard. The Oregon coast range lithology consists mostly of volcanic, sedimentary, and surficial sedimentary material. Distinct trends can be observed in the aforementioned parameters between lithological units.

- **NDVI –** The NDVI histograms for the individual lithological units vary significantly, particularly when compared to the whole dataset. In some lithological units, certain types of vegetation can stabilize the slope, while it may have little effect in other units. Most of the NLS points fall within regions with high NDVI values.

6.6   CONCLUSIONS

Lithology is commonly treated in a similar fashion to other parameters in landslide analysis and mapping. However, many of the other parameters are actually functions of the lithology; hence, improved results may be obtained by creating different models for each lithological unit. For example, slope angle at landslide failure (estimating shear strength) varies with lithology when comparing histograms for entire dataset and the individual lithological units, revealing a shift in peaks.

This study characterizes slope stability properties of the principal lithological units in western Oregon. Future research will utilize higher resolution LIDAR DEMs in place of the ASTER DEMs to improve characterization of the terrain. Finally, this data will be combined with seismic parameters for regional slope stability analyses in the following chapters.

7.0   ASSESSMENT OF SOIL EROSION

7.1   INTRODUCTION

Western Oregon has a fault-riddled topography, mixed rock types, steep mountains, rapidly flowing, enormous streams, and high precipitation that all contribute to high erosion rates, thereby triggering shallow landslides. Soil erosion is sometimes considered a silent hazard, indirectly contributing to other, larger problems. Larsen *(Larsen 2000)* showed that many shallow landslides in the western Cascade Range of Oregon resulted from soil erosion. Oftentimes, these more frequent, shallow landslides can be highly destructive to life and property, just as are less frequent, deep-seated landslides.

A detailed discussion on the influence of soil erosion in generating and destabilizing landslides in western Oregon is discussed by (*Swanson and Dyrness 1975*). This study showed that there was an increase in the number of landslides due to highway cuts and storms. The State of Oregon recently created a "Criterion 4 Indicator 18" project to perform soil erosion analysis and mapping across the state (*Oregon Department of Forestry 2013*).

The objectives of this chapter are to:

1. Determine a model suitable to produce a satisfactory soil erosion map for the study area

2. Assess the vulnerability of slopes to soil erosion due to natural and man- made hazards within 2 km of the lifeline routes

3. Compare soil erosion to existing landslides in the study area

The intent of this chapter is not to perform a detailed soil erosion analysis for western Oregon; rather the erosion map is meant to highlight sites that would be expected to erode. Hence, one should not use this map for other purposes.

7.2   SOIL EROSION MODELING BACKGROUND

Modeling of susceptibility to, and quantities of, soil erosion can be complicated because of the interactions among the various contributing factors, such as soil, topography (slope, elevation, aspect, roughness, ruggedness , and curvature), land use, land cover, and climatic conditions (*Wischmeier 1978*). To calculate the potential for soil erosion, models are often developed considering the relationship of such factors to observed occurrences and the physics involved. The three major types of models (*Acharya et al. 2011*) are empirical, conceptual and physically derived models, which are summarized in Table 7.1. Models are chosen based on the objective of the study, scale of the study and the type of data sets available.

Table 7.1: Comparison and description of soil erosion model types (summarized from Theimann (*Theimann 2006*) and other sources)

Model Type	Notes
Empirical	- Simplest of the three models - Often based on field experiments or measurements - Derives relationships using statistical correlations. - Should only be used within the range of conditions for which it was derived. - Demands high temporal aggregation. - Can be used to determine the source of sediments (*Bartsch et al. 2002*)
Physical	- Based on the physics of the erosion and sediment transfer processes (e.g., gravity, resisting forces, and fluid-soil interaction) - A mathematical representation is used to describe the fundamental hydrological and erosion processes (*Nearing 1998*) - Requires high spatial and temporal resolution - Accounts for spatial variability of input factors
Conceptual	-Combination of empirical and physically based models - Includes a general description of the catchment process, but does not incorporate details about the process interaction - Does not require large amount of temporarily distributed data - Can provide qualitative or quantitative results (*Acharya et al. 2011*)

The Revised Universal Soil Loss Equation (RUSLE) is the most widely used empirical model for soil erosion due to its simplicity and widespread applicability. However, these models are not capable of measuring the deposition along steep slopes, depressions, and valleys because of its

capability is limited to estimating only the gross erosion (*Acharya et al. 2011*). For a landscape with hilly topography containing a mixture of such elements, such as Oregon, this model may have limitations in assessing the vulnerability of soil erosion.

Another common alternative, SHETRAN (Système Hydrologique Européen Transport) is a widely used physical based model, which simulates rain drop impact, leaf drip and sheet overland flow. This model can be used for a catchment scale analysis; however, it cannot be used for evaluating a single hill slope profile (Bathurst et al. 2005, Floris et al. 2004). Unfortunately, this model requires too many detailed inputs that are not available for the study area.

T.Pawar (*T. Pawar 2011*) applied a conceptual model using an index based approach considering four principal factors controlling the quantity of soil erosion: slope, NDVI, precipitation and land use. This model was termed the Watershed Erosion Response Model (WERM) and is a process-based model based on the fundamentals of hydrology, plant science, hydraulics and erosion (J.M., 1991).

Fortunately, GIS has proven to be a powerful tool for use in the above models to estimate soil erosion across a region *(Aleotti*

et al. 1999, Kertész 1993, Swanson and Dyrness 1975, Wischmeier 1978). However, when modeling soil erosion within GIS, it is very important to understand the resolution of the inputs. Coarse resolution might compromise on the representation of the information and high resolution requires significant lab or fieldwork. Hence, it important to prioritize in defining the sensitivity of the modeling approaches.

7.2.1 Methodology

In this study, the WERM model was modified to eliminate land use in the model since 70 % of the study area is covered by forest and vegetation. Aspect, the direction of the slope, was added to the model because of typical weather patterns with storms arriving from the northwest. Additionally distance to streams and lithology were considered in other versions of the map, but were not incorporated because the maps did not perform as well. Figure 7.1 is a conceptual depiction of the modified WERM model used for this study.

The map was created as follows:

Each raster was reclassified to values of 0 to 9, where 0 indicates little contribution to erosion and 9 = high contribution to erosion. Table 7.2 shows the reclassified values for each category. Figure 7.2 shows the distribution of values in the study area. Erosion is positively correlated with slope and precipitation. All slopes greater than 20 degrees were considered to have the same weight following (*Panhalkar and Pawar 2011*). For precipitation, once a critical precipitation value was exceeded, the erosivity would not increase. This value was estimated considering trends observed in Figure 6.6. Erosion would be negatively correlated with distance from rivers or streams and NDVI. Areas in close proximity to streams would likely erode more. Areas with high NDVI contain a significant amount of vegetation, which can strengthen surficial sediments with roots and trap sediment, reducing erosion. Further, the State of Oregon (*2012*)

website reports that areas east of the Cascades have high soil erosion because of sparse vegetation and fire frequency. For aspect, highest weight was given to slopes facing the west and northwest (the direction of approaching storms) and was lowered the greater the deviation from the northwest. For the lithology, weaker sediments were given higher weights and stronger sediments lower weights. The landslide density results were also considered for determining these weights; however, surficial sediments were given a high weight for erosion, despite their low landslide density, because they would be expected to be looser and more erodible. It has a low landslide density primarily because they are only found in areas of shallow slopes.

Each factor was assigned a category weight (influence factor) based on its relative expected contribution and summed in a weighted overlay analysis.

$$E = \frac{\sum_{i=1}^{n} w_i x_i}{10}$$

(7-1)

Where E = the relative susceptibility to erosion (erosivity), ranging from 0-100, i = an identifier for the factor, w = the weight of factor i, x = the value of influence factor i, and n = the number of factors.

The final map was reclassified into sections of Low (10-33), Medium (33-66), and High (66-100) erosivity.

The model was visually inspected and compared to the landslide-mapped polygons in the SLIDO database. It is seen that a considerable number of landslide-mapped polygons from SLIDO database were located adjacent to the highly erodible regions from the map. This supports a supposition that such landslide deposits might have been triggered due to erosion.
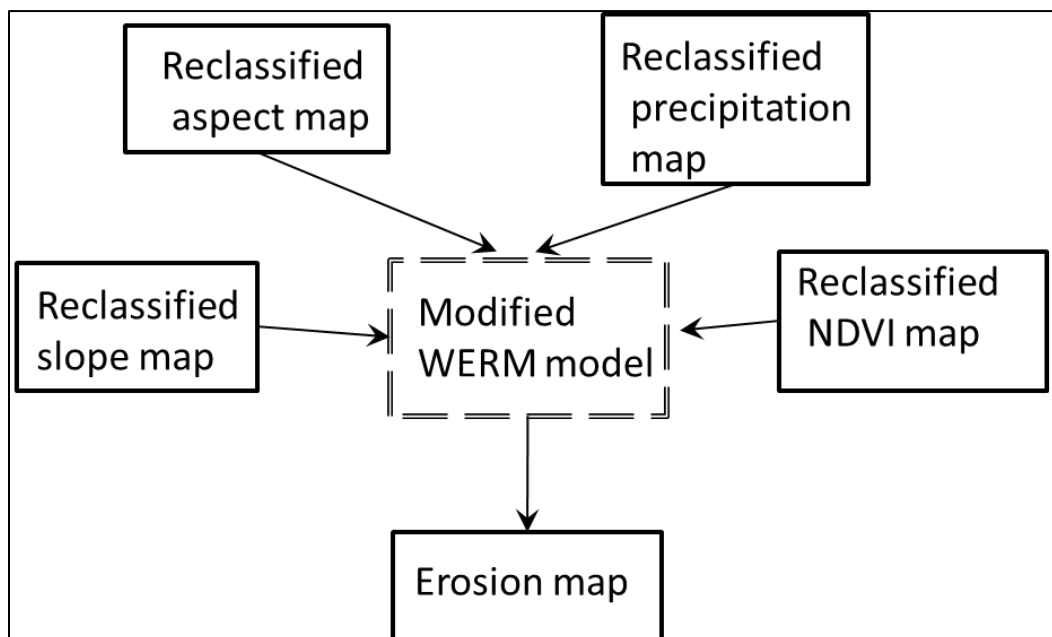
Figure 7.1: Combination of factors to calculate erosivity.
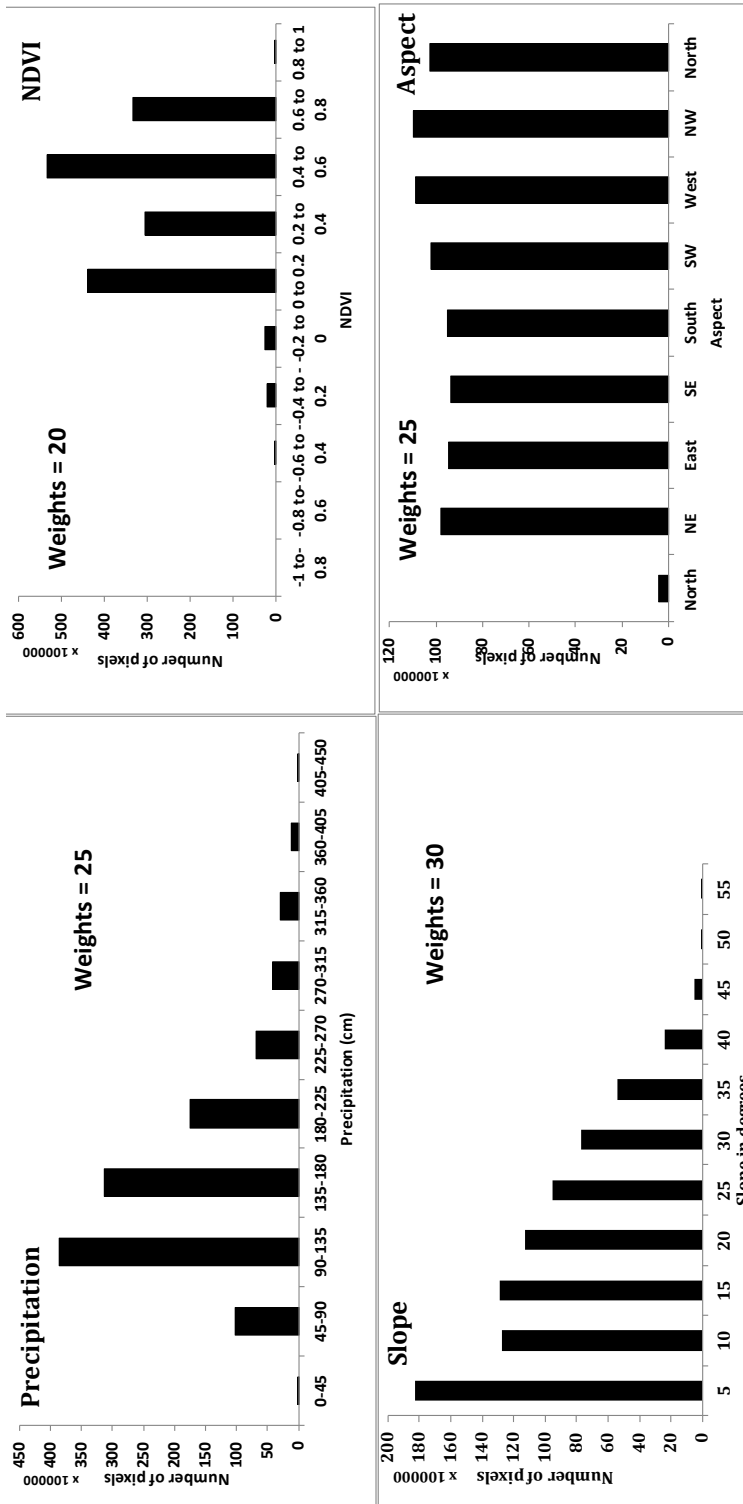
Figure 7.2: Histograms of input parameters for the entire study area (based on pixels).

Table 7.2:Reclassification (Weights) used for each input parameter.

Weights for precipitation			Weights for NDVI	
Intervals	Weights		Intervals	Weights
0-20	1		-1 to -0.8	9
20-40	2		-0.8 to -0.6	8
40-60	3		-0.6 to -0.4	7
60-80	4		-0.4 to -0.2	6
80-100	5		-0.2 to 0.0	5
100-120	6		0.0 to 0.2	4
120-140	7		0.2 to 0.4	3
140-160	8		0.4 to 0.6	2
160-180	9		0.6 to 0.8	1
180 >	9		0.8 to 1.0	1

Weights for Slope			Weights for Aspect	
Intervals	Weights		Intervals	Weights
0 to 2	1		North	8
2 to 4	2		Northeast	5
4 to 6	3		East	2
6 to 8	4		Southeast	3
8 to 10	5		South	3
10 to 12	6		Southwest	4
12 to 14	7		West	9
14 to 16	8		Northwest	9
18 to 20	9			
20 >	9			

7.2.2 Results and Discussion

Figure 7.3 presents the erosivity map for the study area. The highly erodible area is 13,925 sq. km, roughly 70% of the total study area. The output maps show high erosivity close to streams and along the coast. There is a significant level of vulnerability along the bank of the streams. A correlation of erosivity towards the coast and towards the valley with stream order is observed. The lithology (surficial sedimentary) in the valley region may be another reason for high level of erosivity in that section. Precipitation by itself does not dominate the degree of soil erosion in the study area, because it is seen that precipitation is high in the North West area but the erosivity is lower in that section. In addition, rainfall is relatively high throughout the entire study area, which is another reason for precipitation not being a standalone influence.

Depressions near lower NDVI values also tend to show a high erosivity. There is also a relationship with proximity to streams. Cut slopes near highways, which also show significant number of landslides, also tended to have a high erosivity index, likely indicating that human-induced disturbances could have generated some of these landslides.

When comparing the data to mapped landslides from the SLIDO polygons (Figures 7.4 and 7.7), many of the landslides occur in, or near, highly erodible sections. Further, in the example areas shown, erosion appears to be very high in the upslope direction from mapped landslides that extend into river valley below. Hence, it is likely that erosion was a contributing factor to these slope failures.
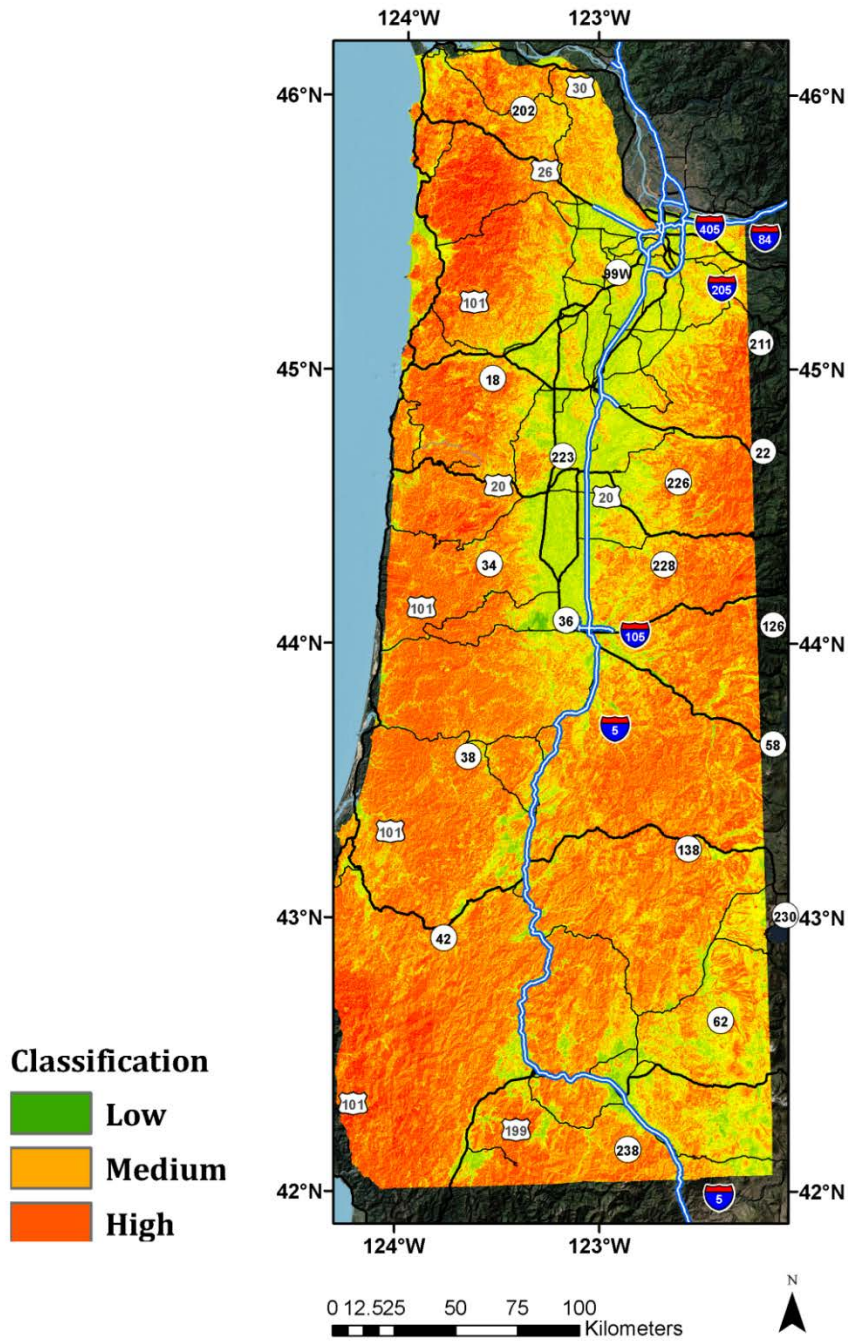
Figure 7.3: Soil erosion susceptibility map.

100
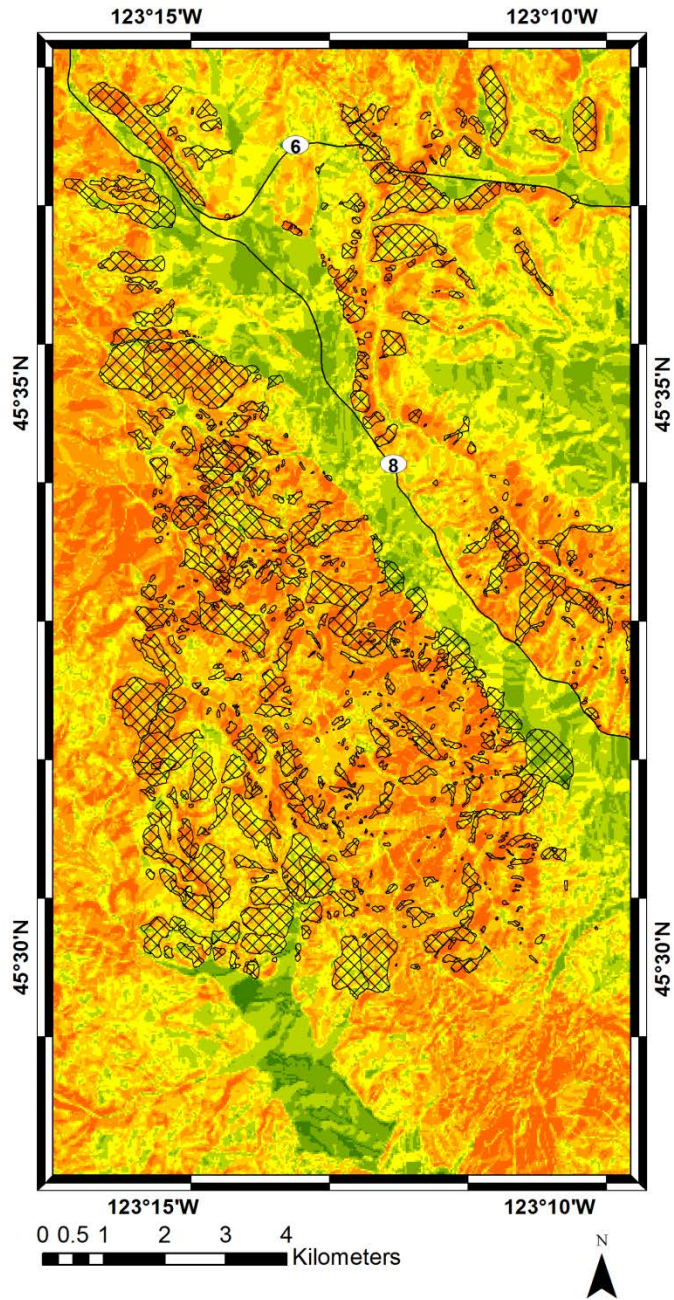
Figure 7.4: Mapped landslides (hatched polygons) plotted over an erosivity map near Highway 8. Note the high erosivity near the highway and the frequency of landslides within the high erosivity areas.
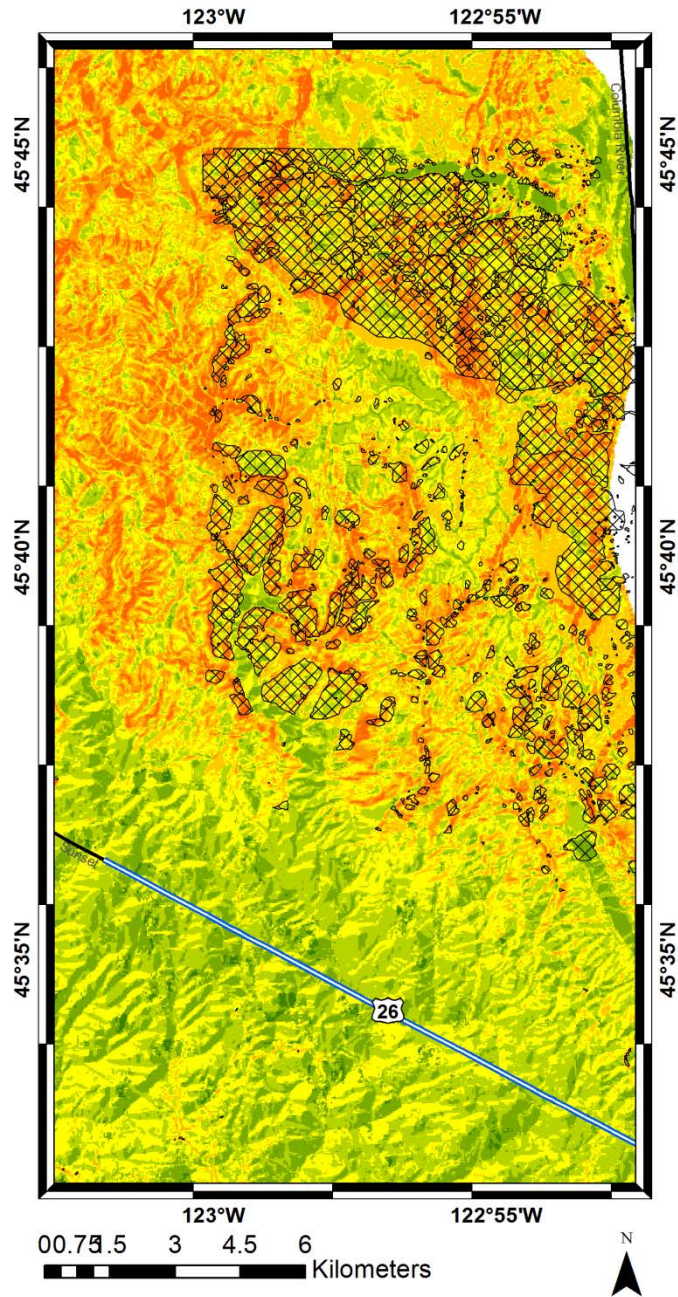
Figure 7.5: Mapped landslides (hatched polygons) plotted over an erosivity map near Highway 26. Note the high erosivity near the highway and the frequency of landslides within the high erosivity areas.
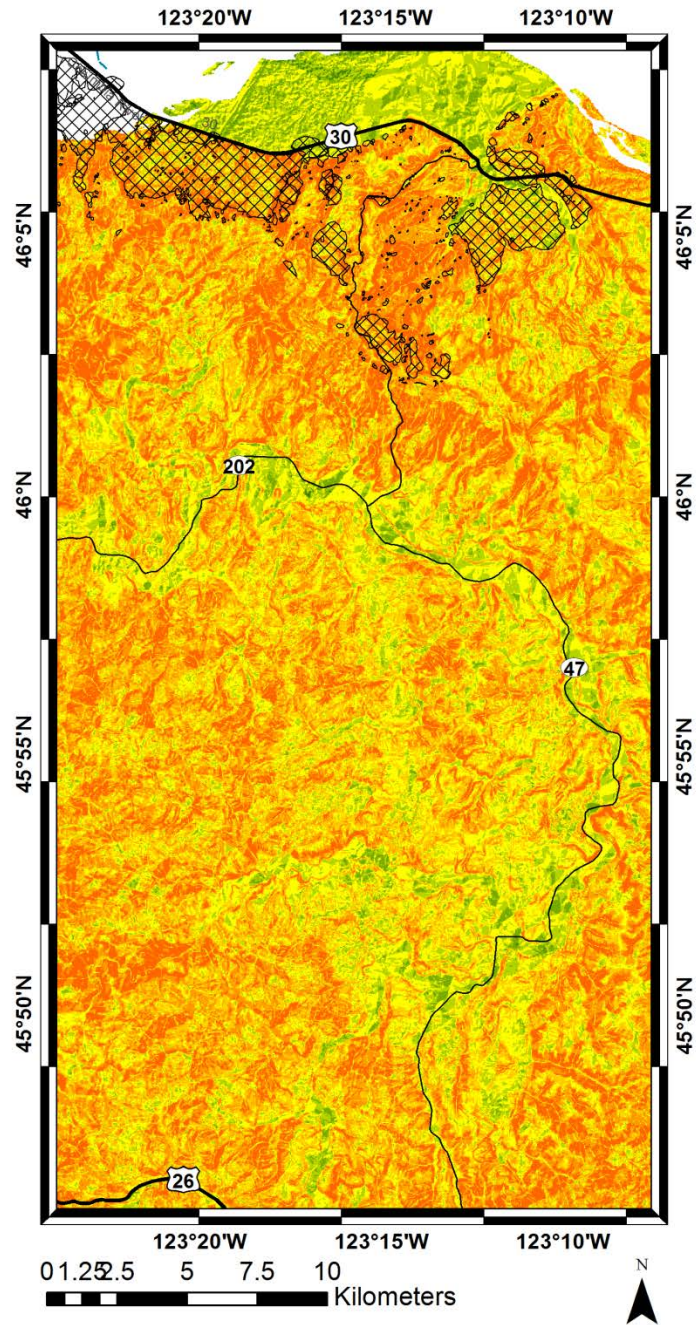
Figure 7.6: Mapped landslides (hatched polygons) plotted over an erosivity map near Highway 30. Note the high erosivity near the highway and the frequency of landslides within the high erosivity areas.
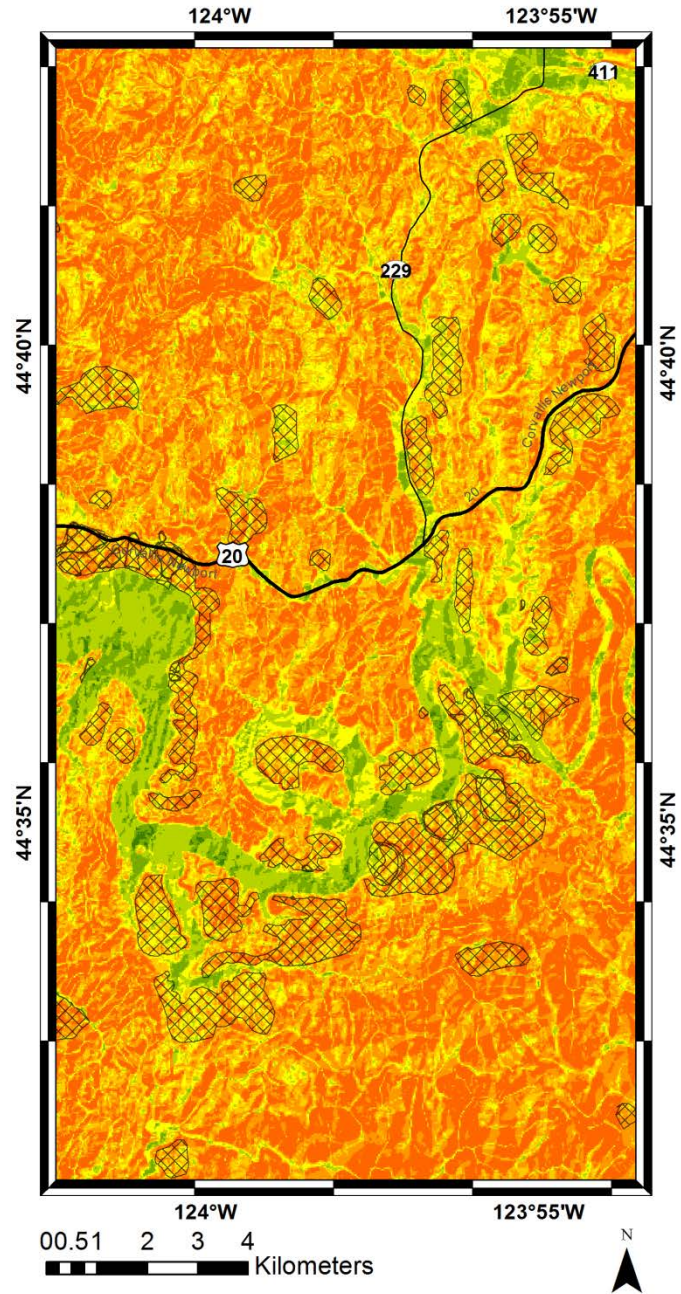
Figure 7.7: Mapped landslides (hatched polygons) plotted over an erosivity map near Highway 20. Note the high erosivity near the highway and the frequency of landslides within the high erosivity areas.

8.0 INITIAL REGIONAL SEISIC SLOPE STABILITY ANALYSES USING MULTIVARIATE REGRESSION MODELS

8.1 INTRODUCTION

Coastal communities in Oregon are highly dependent on only a few highway and utility corridors routed across the coast range, connecting them with the cities in the Willamette Valley and the Interstate 5 corridor. Unfortunately, these routes are constantly threatened by landslides, which can damage the roadway, block traffic, and threaten life safety. Understanding how landslides can affect these routes is important for planning, preparation, and resilience purposes. To this end, we analyzed the contribution of numerous factors to landslide triggering by using multiple linear regression analysis. During the analysis, factors were evaluated for their level of correlation with previously mapped landslides by developing automated, batch processing tools in a Geographic Information System (GIS) domain. Several factors were evaluated from: (1) vector datasets, such as highway locations, faults, folds, geology/lithology, streams, and land use; and (2) raster datasets, such as slope, aspect, slope roughness, terrain (elevation) ruggedness, peak ground acceleration (PGA) and peak ground velocity (PGV) from a Cascadia subduction zone scenario earthquake, and annual precipitation averaged over the past 30 years.

Afterwards, a single regression equation to estimate the probability of a landslide triggering in the study area was selected from several models created from factors identified as most influential to predicting previously mapped landslides in the coastal region of Oregon. The factors in this equation are slope, PGA and PGV from a Cascadia subduction zone scenario earthquake, and precipitation. The influence of other factors was generally minimal, in comparison; hence, they were left out of the final equation. The new equation was then applied to generate probabilistic landslide triggering maps of the study area.

Given the wide variety of parameters, data accuracies, and variability across the study area, we used several techniques to validate the map, including a validity index, which compares the percentage area of occurrence of landslides, from the inventory maps derived from lidar data, to the susceptibility map.

Finally, using tools in GIS, the raster data sets from the maps were generalized along lifeline corridors to improve visualization of the potential landslide hazard. To provide context to the potential impact of the landslide on the highway, the "fuzzy AND" technique was used to classify each pixel based on its relative position to the highway and within the susceptibility map.

8.2 PURPOSE

The primary objectives of this initial analysis were to:

1. Compile the available geospatial data for landslide studies in to a Geographic Information System (GIS) in order to identify vulnerable segments of lifeline routes.

2. Analyze the influence of different factors contributing to the landslide hazard using multivariate techniques.

3. Create automated tools for efficiency such that maps can be easily updated when improved data becomes available.

4. Provide a series of probabilistic landslide triggering maps for the study area. The maps must be validated using the methodology presented in Chapter 10.

5. Support transportation professionals by depicting the landslide hazard on the maps along critical transportation routes and corridors.

8.3 BACKGROUND

Knowledge of the geographic and geologic conditions of the study area is necessary to understand the instability factors responsible for landslides. This study uses instability factors including locations of faults, folds, geology/lithology, stream proximity, land use, slope, aspect, slope roughness, terrain (elevation) ruggedness, precipitation, and peak ground acceleration and peak ground velocity from a Cascadia scenario event (*Madin and Burns 2013*). Landslide inventory maps including the Statewide Landslide Inventory Database for Oregon (SLIDO-2, *Burns et al. 2012a*) and the ODOT unstable slopes databases (unpublished database obtained in 2011) were incorporated as both training and validation datasets. Although there are many ways to map susceptible zones, this study has adopted a multivariate approach, which is a type of indirect, quantitative method, to use the available parameters for regional mapping and to analyze the parameters' relative contributions. It should be noted that each of the data layers used in the multivariate analysis have variable levels of accuracy, resolution, consistency, and completeness. Sometimes, the magnitude of these factors varies widely within a single layer. Hence, there may be regional variations in the multivariate analysis resulting from data quality issues.

Quantifying the landslide susceptibility of highway routes with limited information has always been a challenge for agencies which directly or indirectly work for the safety of the community (*Aleotti and Chowdhury 1999*). Generally, there are multiple methods used to map the vulnerable routes based on zoning of the susceptible regions. The primary goal is to evaluate the relative contribution of numerous available factors, including: locations of faults, folds, geology/lithology, proximity to streams, land use, vegetation, slope, aspect, slope roughness, terrain ruggedness, precipitation, and peak ground acceleration (PGA) and peak ground velocity (PGV) from a Cascadia subduction zone scenario earthquake (*OSSPAC 2013*). Using ordinary least squares (OLS) regression analysis, these multiple factors were analyzed as predictor variables of previously mapped landslides from existing landslide inventory maps, including the

Statewide Landslide Inventory Database of Oregon (SLIDO) from the Oregon Department of Geology and Mineral Industries (DOGAMI) and the Oregon DOT Unstable Slopes databases. Afterwards, an empirical model can be developed using the best predictor variables to predict and map the probability of the triggering of landslides in susceptible areas (*Van Westen 1993*). The resulting mapped probabilities can then be classified into different categories from very low, low, medium, high, and very high. As discussed in Chapter 3, there are multiple ways to map landslide susceptible zones Table 8.1 summarizes common approaches.

Table 8.1: Summary of common techniques for landslide susceptibility analysis and mapping (modified from *(Roa 2007)*)

Types	Approach	Ideas	Authors and Year
Direct method	Heuristic approach	Landslide density factors	DeGraff et al. (*DeGraff 1998*)
	Geomorphic analysis	Geomorphology maps	Leroy (*Leroy 1996*)
	Map combinations	Terrain maps reclassification	Van Western (*Van Western 1993*)
Indirect method	Qualitative map combinations	Multi Criteria Evaluation	Roa (*Roa 2007*)
	Statistical approach	Point based data with descriptive details	Yang et al. (*Yang et al. 2007*) Carrara et al. (*Carrara et al. 1977*)
	Bivariate approach	Susceptibility mapping	Yin and Yan (*Yin and Yan 1988*)
		Weight of evidence modelling	Bonham-Carter (*Bonham-Carter 1994*)
		Likelihood ratio	Carrara et al. (*Carrara et al. 1978*)
		Information value approach	Chung and Fabbri (*Chung and Fabbri 1999*)
	Multivariate approach	Ordinary least squares	Gorsevski et al. (*Gorsevski et al. 2000*)
		Discriminant function analysis	Lee et al. (*Lee et al. 2008*)
		Artificial neural network	Aleotti et al. (*Aleotti et al. 1996*)
Deterministic method	Static, pseudo static and dymanic conditions	Integration of geotechnical and geometrical data to ascertain stability conditions	Bishop (*Bishop 1955*), Newmark (*Newmark 1965*), Sarma (*Sarma 1979*)

A disadvantage to the direct methods is that they require expert opinion about the area of interest. This can lead to unacceptable outputs and have shown problems in subjectivity of the weighting of parameters. It also is problematic for application across a very large study area where it can be difficult to have the appropriate depth of knowledge. Deterministic methods determine safety factors of the variable over the study area using slope stability approaches (see Chapter 2). Hence, they are well suited for the areas where fundamental properties are homogenous. However, two main drawbacks of these methods are that complete data availability is prohibitive and the over simplification of the data when it is incomplete (*Turner and Schuster 1996, Yilmaz 2009*). The indirect or statistical techniques, in contrast, tend to overcome the deficits to certain extent, but still require large amounts of systematic data to give steadfast results. Often, this method uses sample data, and generates its relationship with the parameters inducing the events, thereby helping to understand characteristics that contribute to the presence and absence of a landslide. As such, this study has adopted the multivariate approach (logistic regression) which is a type of indirect quantitative method that can be readily implemented with the data available for regional mapping.

A wide spectrum of literature on approaches as well as strengths, and weakness of multivariate and other mapping techniques can be found in previous works (*Carrara et al. 1990, Chung and Fabbri 2003, Guzzetti et al. 1999, Guzzetti et al. 2005*). According to Dai and other (*Densham 2001*), the quantitative multivariate technique of susceptibility analysis has been applied and tested in many works (*Carrara 1983, Guzzetti et al. 1999, Jibson et al. 2000, Lee et al. 2008*). The multivariate technique can be defined as a statistical method which involves simultaneous observation and investigation of more than one outcome variable (*Zar and Breen 1986*). Multivariate techniques are both robust and flexible, which is important when working with a wide variety of data sources of varying quality (*Lee and Min 2001, Lee and Sambath 2006*) However, as with any technique, results obtained with multivariate techniques are dependent on the quality, quantity, and availability of the data.

Logistic regression is a type of multivariate regression that is suited for a dichotomous dependent variable for the outcome (e.g., either there is a landslide, or there is not a landslide). It is similar to ordinary least squares (OLS); however, OLS assumes a normal distribution and that the dependent variable is continuous. The objective of OLS is minimizing the sum of the square of errors; the objective of logistic regression is to maximize likelihood. Both methods determine statistically significant parameters, perform diagnostics to verify assumptions, and can provide a coefficient and standard error for each of the predictor variables.

8.4 DATA

The landslide hazard depends on many factors, which can be integrated into a GIS environment. Chapter 5 provides details on the datasets used for the entire project. For the analysis in this chapter, the following data were considered:

- Slope (topographic gradient), slope roughness, terrain (elevation) ruggedness, and slope aspect data: derivatives of a digital elevation model (DEM) created by combining the U.S. Geological Survey National Elevation Dataset *(USGS 2012b)*

with available LIDAR data *(OLC 2013),* down sampled to a cell size resolution of 30 m (*Gesch et al. 2002, Gesch 2007, Madin and Burns 2013*).

- Normalized Difference Vegetation Index (NDVI) map: generated from Landsat7 ETM + using the near-infrared and red bands *(Huete et al. 2002)*; this resulted in indices varying from –0.8 to 1.0. The predominance of NDVI values in the range of 0.7 to 1.0 indicates that the vegetation is dense in most parts of the study zone.

- Landslide inventory data (*SLIDO-2; Burns et al. 2012a):* over 30,000 mapped landslides in Oregon. It should be noted that the parts of this database not mapped with LIDAR may be capturing as little as 12% of existing landslides. Additionally, the vast majority of those points represent relatively small debris flow or road cut/culvert failures that occurred during a few severe storms in 1996 and 1997,

- Unstable slope data *(ODOT, 2011).*

- 30-year annual average precipitation data: obtained from Parameter-elevation Regressions on Independent Slopes Model *(PRISM 2011)* for the climatological period 1981-2011. As the entire study area received a similar level of high rainfall, this dataset did not correlate well with landslide locations within the study area. However, if a study were completed across the entire state of Oregon, this data would be vital to analyze.

- PGA and PGV estimates: from magnitude 9.0 Cascadia earthquake scenario maps (*Madin and Burns 2013*).

- Lithology data from the Oregon Geologic Data Compilation (OGDC- V5; *Ma et al. 2009*). Note that the scale, scope, accuracy, and purpose of the geologic maps in OGDC vary widely across the state. This dataset enabled correlations of all of the other parameters to be developed within each lithological unit (*Sharifi-Mood et al. 2013*). Given the large number of geologic units (thousands), it was not possible to develop correlations for each geologic unit. Hence, generalized lithology was used for the study.

The soil erosion map was discussed in Chapter 7.

The following feature datasets, all accessible at the Oregon Geospatial Data Enterprise:
- Highways plotted at 1:24,000 provided by Oregon DOT (*ODOT 2011),*

- Rivers and streams plotted at 1:100,000, provided by WDFW, IDFG, and ODFW (2001), and

- Faults and folds (*OGDC- V5; Ma et al. 2009).*

8.5   METHODOLOGY

With the landslide inventory data and several other data sets provided in a spatial domain, a multivariate approach is well-suited for this type of study (*Lee et al. 2008*). Ordinary least squares (OLS) analysis, a type of multivariate discriminant analysis, is a flexible approach that can simultaneously analyze a variety of predictive variables (factors triggering landslides) without requiring them to be normally distributed (*Lee and Sambath 2006*). In this study, a hybrid approach was implemented where factors derived from an OLS analysis to predict a continuous variable Z, were incorporated into a logit function equation. Pure logistic regression was conducted; however, OLS produced superior results. Following the generation of a logit function using coefficients from the OLS analysis, it is possible to classify landslide susceptibility into different categories: very low, low, medium, high, and very high (*Guzzetti et al. 1999, Lee and Min 2001, Nandi and Shakoor 2010*). The working procedure for landslide susceptibility mapping (LM) is illustrated in Figure 8.1.

The approach first considers the previously mapped landslide events (or landslide samples, LS) as well as samples in areas without landslides (non-landslide samples, NLS) for use in the analysis (Figure 8.2). A defined protocol is needed to mark the occurrence and non-occurrence. Since this will have an impact in the regression relation and accuracy of the estimates *(Atkinson and Massari 1998)*. NLS points are taken from areas that are not mapped as landslides in SLIDO or the ODOT database within the study area. Given that many landslides were mapped as point features rather than as polygons delineating landslide extents, 2-km buffers were applied to both landslide points and landslide polygons. NLS points were chosen from areas outside the buffered areas to reduce the influence of landslides. The intent of this approach is to create a spatial database from which locations with and without landslides can be correlated to each of the aforementioned parameters to identify their contribution to the triggering of landslides. For example, it would be expected that the landslide samples should generally occur on steep slopes and that non-landslide samples should typically occur on shallower slopes. Given the wide variability of other contributing factors, there are still a significant number of landslides that have occurred on relatively shallow slopes *(Sharifi-Mood et al. 2013)*.
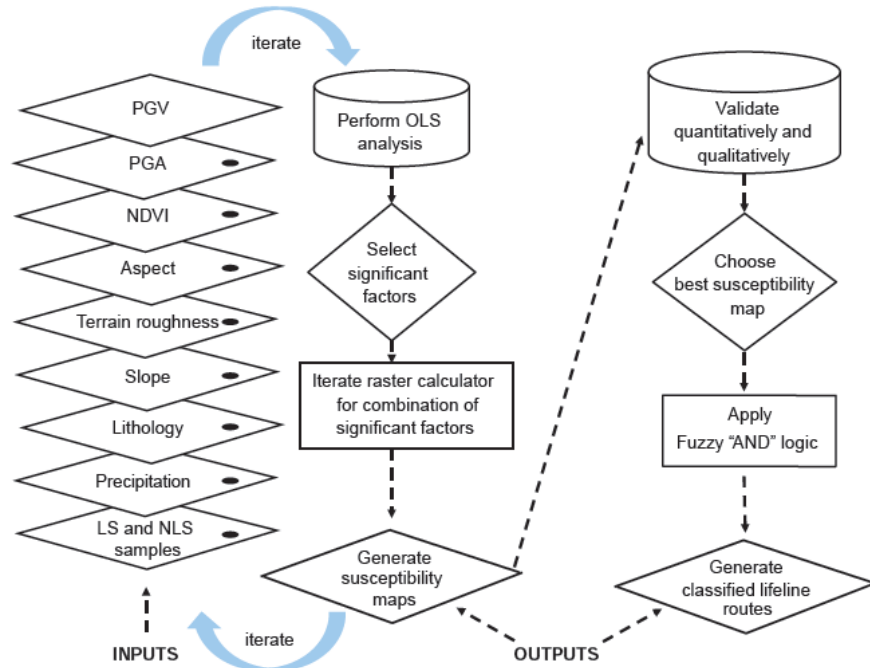
Figure 8.1: Work flow for automated map generation, validation, and output lifeline route susceptibility to landslides.

In this study, the sample set included a total of 42,000 point features (21,000 LS and 21,000 NLS points), each occupying a pixel and given a dichotomous value of 1 (LS) or 0 (NLS). Note that this is less than the total number found in the DOGAMI database because (1) the present study is for western Oregon only and (2) several (approximately 9,000) point landslide features fell within the polygons, so only the point features were used to avoid redundancy.
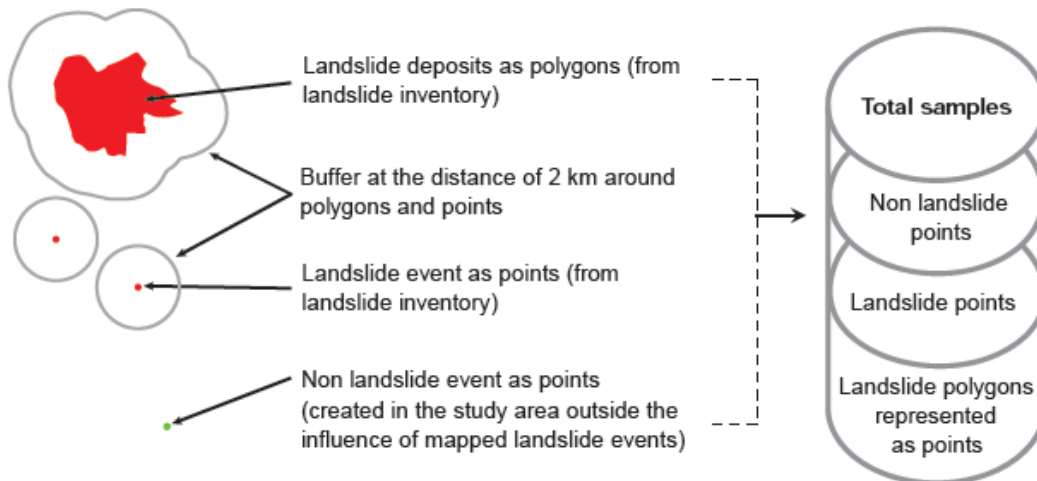
Figure 8.2: Non-landslide sample points generation protocol.

The independent variables from the other data sources were used as predictors (*Yesilnacar and Topal 2005*), and values for each of the variables were extracted or calculated at each LS and NLS location. This resulted in a table consisting of the sample ID, corresponding dichotomous value (P = 0 or 1), slope, slope roughness, aspect, precipitation value, NDVI, PGA, PGV, and the various measured distances from the polyline features. The table was then input into an OLS scripting module, which compared the values for each parameter with the dichotomous value to determine the contribution of each parameter to landslide susceptibility. This analysis was then placed in a probabilistic equation of the form:

$$P = \frac{1}{1 + e^{-Z}} \qquad\qquad (8\text{-}1)$$

where:
$Z = B_0 + B_1X_1 + B_2X_2 + \ldots B_nX_n$, the dependent or predicted variable (representing the dichotomous cases), and where:

$X_1, X_2 \ldots X_n$ are the independent variables (factors triggering landslides),

$B_1, B_2 \ldots B_n$ are the regression coefficients, and

B_0 is an intercept for the model.

This equation was then applied using a raster calculator operation in GIS to perform a stability analysis across the study area, resulting in a probability map of landslide susceptibility with a 30 m pixel size. A focal statistics operator in GIS was used to calculate the average probability across a 300 m × 300 m window to account for the potential for landslides in neighboring pixels. The resulting map is shown in Figure 8.3. The raster was then clipped to a 1-km buffer from the highway, shown in Figure 8.4. Finally, to improve readability of the final map the probabilities (expressed as floating point values from 0 to 1.0) were reclassified into five bins: very low (0-0.2), low (0.2-0.4), medium (0.4-0.6), high (0.6-0.8) and very high (0.8-1.0) *(Irigaray et al. 2007, Jiménez-Perálvarez et al. 2009)*.

In order to limit over prediction of landslide potential in flat areas (such as parts of the valley), that may experience high levels of ground motion, we used a filter similar to the focal relief filter in Burns et al. (*Burns et al. 2012b,c,d*); however, the filter has been adapted for the spatial scale and DEM resolution. This filter limits the maximum value of landslide probability to 0.1 if the following conditions are met:

- The pixel is not within 300 m of a SLIDO polygon

- The elevation range is no more than 5 m within a 300m by 300m window, centered at the pixel

- The slope range is no more than 2 degrees within a 300m by 300m window, centered at the pixel

- The slope at that pixel is less than 2 degrees.

114

Note that these locations may still be susceptible to lateral spreading or other hazards. They also may be impacted by neighboring steep slopes. Aside from a few coastal valleys, most of the area modified by this procedure was in the Willamette Valley. These areas were already in the low bin.

Because this study was focused on impact to highways, especially those routes designated as lifeline corridors (*CH2M-HILL 2012*), a fuzzy overlay ("AND") technique (*ESRI 2011*) was used to find locations along highways particularly vulnerable to landslides. The raster was clipped to a 1km buffer from the highway. To enable use by a variety of people, the final map was exported as a keyhole markup language (KML) file, which can be viewed within Google Earth or other software capable of reading KML.

8.6 RESULTS

Based on focused groups of factors to analyze (Table 8.2), s series of regression equations (Table 8.3), and maps were generated from combinations of the evaluated factors. The map provided in this paper was generated using model D5, which showed the highest degree of accuracy in the validation process (discussed in the next section):

$$Z = -3.6379 - 20.7068 * PGA + 0.2023 * PGV$$
$$+ 0.02862 * SLOPE * + 0.01646 * PRECIPITATION \quad \text{(8-2)}$$

where slope is expressed in degrees, PGA is in percent of gravity, PGV is in centimeters per second, and precipitation is in centimeters per year. (Figure 8.3 and Figure 8.4) This model was determined to be statistically significant at the 0.05 level. Note that while all variables except PGA are positively correlated, this does not indicate that there is a negative correlation of PGA with landslide potential. Both PGA and PGV are correlated variables and, when considered jointly, they still produce a positive correlation. When PGA is considered without PGV or PGV without PGA, the models produced unsatisfactory results because they eliminated the contribution of slope. Addition of other factors tended to produce very similar results compared to this model and hardly improved predictions. Hence, in favor of a simplistic model requiring fewer inputs, without compromising reliability, these factors were considered extra and were eliminated from the model.

Table 8.2: Foci of model groups analyzed.

Model Group	Primary Factors Analyzed
A	Individual Topographic or Geographic Factors
B	Combinations of Factors
C	PGA with 2% exceedance in 50 years
D	PGA PGV ORP
E	Precipitation
F	Erosion

Table 8.3: Coefficients for several models created for landslide prediction.

Model Group	Model Number	Intercept	Slope (Deg)	Aspect (Deg)	NDVI	Distance to roads (km)	Distance to rivers (km)	Distance to faults (km)	PGA (2% in 50 years) (%g)	ORP PGA (%g)	ORP PGV (%g)	Precipitation (cm/year)	Soil Erosion Factor	CLS	CNLS	MVI
A	A1	0.740812	0.040448					-0.273150						0.8407	0.0107	0.0090
	A2	-0.323442	0.026592				0.038000							0.2491	0.0000	0.0000
	A3	0.290620	0.044360			-0.024000								0.9009	0.0000	0.0000
	A4	-1.345419	0.016787		2.763421									0.4995	0.1612	0.0805
	A5	-0.140333	0.025822	0.000117										0.3112	0.0000	0.0000
	A6	-0.119487	0.025831											0.3119	0.0000	0.0000
B	B1	0.109090	0.036830	-0.000093	2.592525	-0.023000	0.007000	-0.081000						**0.9835**	0.0009	0.0009
	B2	-0.167119	0.019168	-0.000078	2.448146			-0.083000						0.9450	0.0032	0.0030
	B3	-0.167119	0.019168	-0.000078			0.021000	-0.083000						0.0922	0.0147	0.0014
	B4	-1.011594	0.035364	0.000109	2.919998	-0.025000								0.8422	0.0659	0.0555
	B5	0.109090	0.036830	-0.000093	2.592525	-0.023000	0.007000	-0.081000						**0.9835**	0.0009	0.0009
C	C1	-0.558978	0.033177	-0.000104	2.388257	-0.020000	0.007000	-0.078000	1.554994					0.9806	0.0007	0.0007
	C2	-2.445197	0.028538	0.000063	2.434672	-0.018000	0.026000		3.222326					0.6788	0.0930	0.0631
	C3	-1.521806	0.016454		2.056930			-0.076000	3.301950					0.8904	0.0049	0.0043
	C4	-2.384660	0.019700						5.210865					0.4227	0.2176	0.0920
D	D1	-3.591841	0.023623	-0.002093	1.217600		-0.033075			-20.968051	0.201868	0.016086		0.5018	**0.6145**	0.3084
	D2	-4.293667	0.011071	-0.002168	0.985444		0.019049				0.085996	0.012183		0.4953	0.4951	0.2453
	D3	-4.273344	0.010831	-0.002164	0.990792						0.085932	0.012248		0.4938	0.5240	0.2588
	D4	-3.192683	0.027306	-0.002302						-20.691589	0.201343	0.016616		0.5175	0.5796	0.2999
	D5	-3.637901	0.028621							-20.706807	0.202256	0.016459		0.5177	0.5985	**0.3099**
	D6	-3.629584	0.023989	-0.002099	1.207487					-20.888360	0.201538	0.015959		0.5188	0.5619	0.2915
	D7	-4.421304	0.044987							-20.626710	0.202401	0.016309	0.114137	0.5184	0.5960	0.3089
	D8	-3.568283	0.054738	-0.001550	1.211077		-0.089730	-0.217947		-21.550954	0.193384	0.014566	0.196651	0.6017	0.4154	0.2500
	D9	-2.364729	0.025250	-0.000660	1.215755		-0.088463	-0.218863		-21.618772	0.193724	0.014727		0.6017	0.4072	0.2450
E	E1	-1.346783	0.010779	0.000000				-0.248780				0.014770		0.6915	0.0388	0.0268
	E2	-1.824431	0.007190		1.308009			-0.247500				0.014040		0.7081	0.0690	0.0488
	E3	-1.805923	0.007101	0.000000	1.306004			-0.248057				0.013974		0.7114	0.0661	0.0470
	E4	-3.168048	0.003426		1.397829							0.016502		0.4817	0.3632	0.1749
	E5	-2.863754	0.000823									0.018784		0.4888	0.3874	0.1893
F	F1	-2.761166	0.027273	0.000000	1.349193			-0.247381				0.013857	0.134744	0.7128	0.0751	0.0535
	F2	-4.342217	0.028489		1.450080							0.016301	0.167784	0.4869	0.3614	0.1759
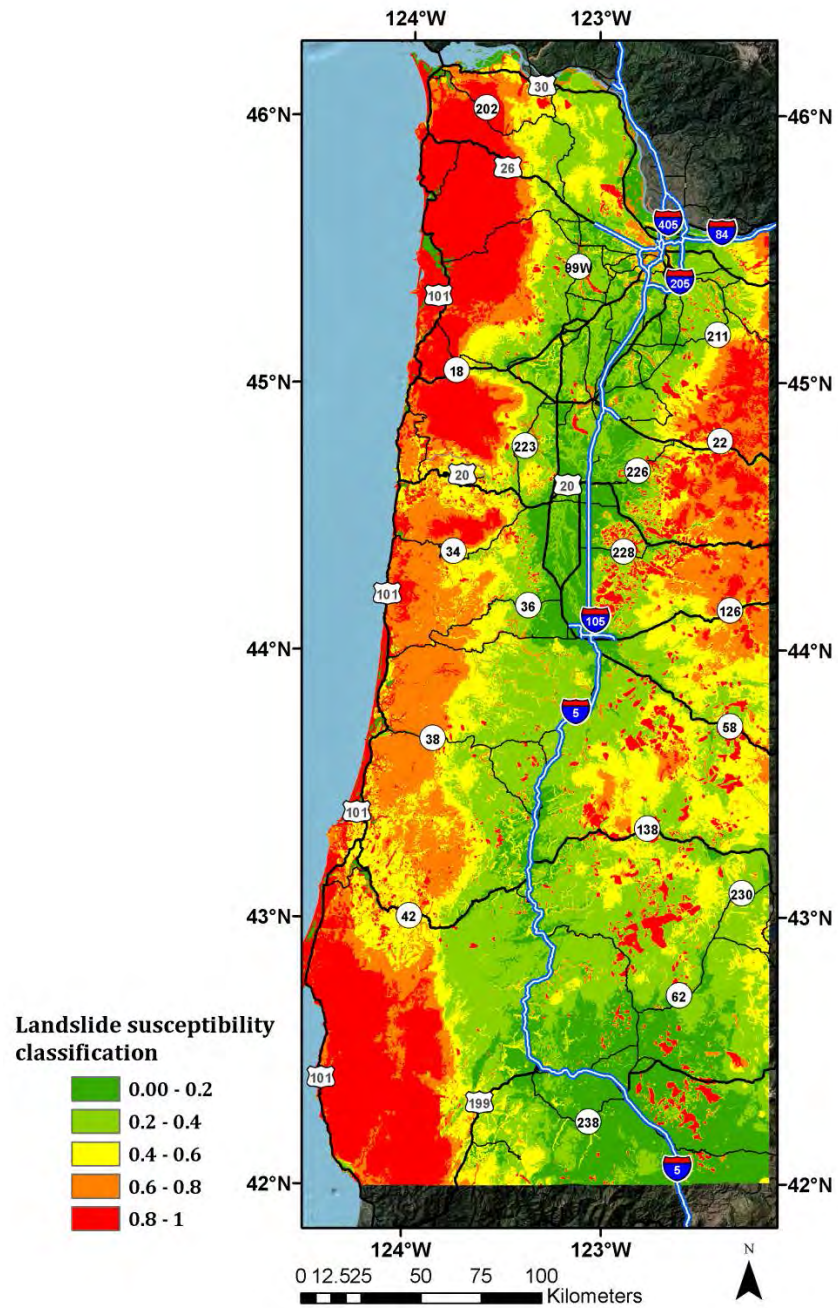
Figure 8.3: Landslide susceptibility map using multivariate techniques considering slope, PGA, PGV, and precipitation for a CSZ scenario event.
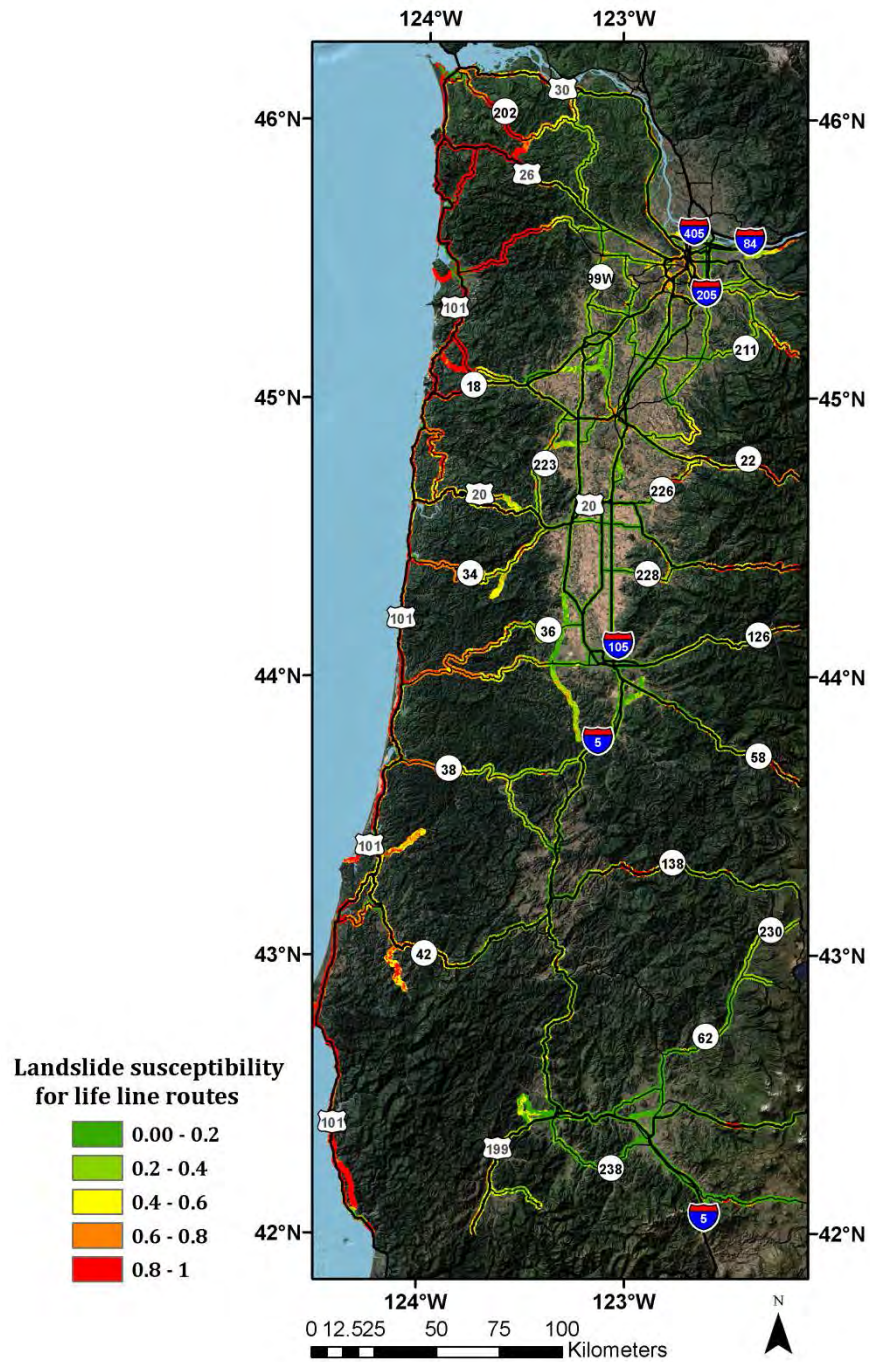
Figure 8.4: Landslide susceptibility map (focused on highways) using multivariate techniques considering slope, PGA, PGV, and precipitation in a CSZ scenario event.

8.6.1 Models for automatic mapping

To automate the generation of susceptibility maps and influence of parameters, tools were generated using the model builder® in ArcGIS. Jiménez-Perálvarez et al. *(Jimenez-Peralvarez 2009)* developed similar models for landslide susceptibility analysis based on GIS matrix methods. These models are available for GIS users to develop landslide susceptibility maps. There are three models namely, "array," "architect" and "authentication" placed inside a toolbox called "Automatic mapping.tbx." Each model requires the input of the data from the user and stores the output in the default database unless otherwise directed by the user.

The *"Array"* module generates the distribution of LS and NLS samples in each raster dataset with the flexibility of deciding the bin sizes by the user (e.g., 1 degree versus 5 degrees for slope). This tool can be used to obtain results similar to those in Chapter 6.

The "Architect" module extracts values at each of the LS and NLS points from each of the raster datasets and performs the regression. The output table (Table 8.3) provides the coefficients for each variable, which are fed in raster calculator, thus producing the potential map in the range between the probability values of 0 and 1.

The "Authentication" module uses the subset of LS and NLS that did not participate in the calculation for purposes of validation.

8.7   VALIDATION:

Validation of the hazard maps can be ascertained by two different techniques: (1) using the same data samples used to find the significant factors, and (2) using a different "training set" of data which was not employed in the process (*Guzzetti et al. 2005*). There are multiple methods for using the data for validation (*Irigaray et al. 2007*). For example,

1. The primary historical dataset can be divided in to two groups: one of which could be used for analysis and another one for validation.

2. The study area can be divided in to two sectors: one part where analysis is done and the other part where landslides are known to exist.

3. The landslide events with in certain time period are used for analysis and the remaining is reserved for validation

In this study, existing landslides delineated by LIDAR were used to check the accuracy of the output (*Madin and Burns 2006a and 2006b, Lewis 2006*).

8.7.1 Histogram Analysis

The landslide susceptibility category at the location of each LS and NLS point from the maps created using each model was extracted. From this, histograms were generated to show the number of LS and NLS points inside each category bin. The histograms were based on the landslide samples used for the input in to regression model. Intuitively, a model that performs well will show a significant portion of the landslides plotting in the higher susceptibility bins.

Conversely, a satisfactory model will also show a significant portion of the non-landslide points plotting in the lower susceptibility bins. Figure 8.5 provides examples of validation histograms for four of the models. This will determine the capacity of the model to discriminate the between the two groups.
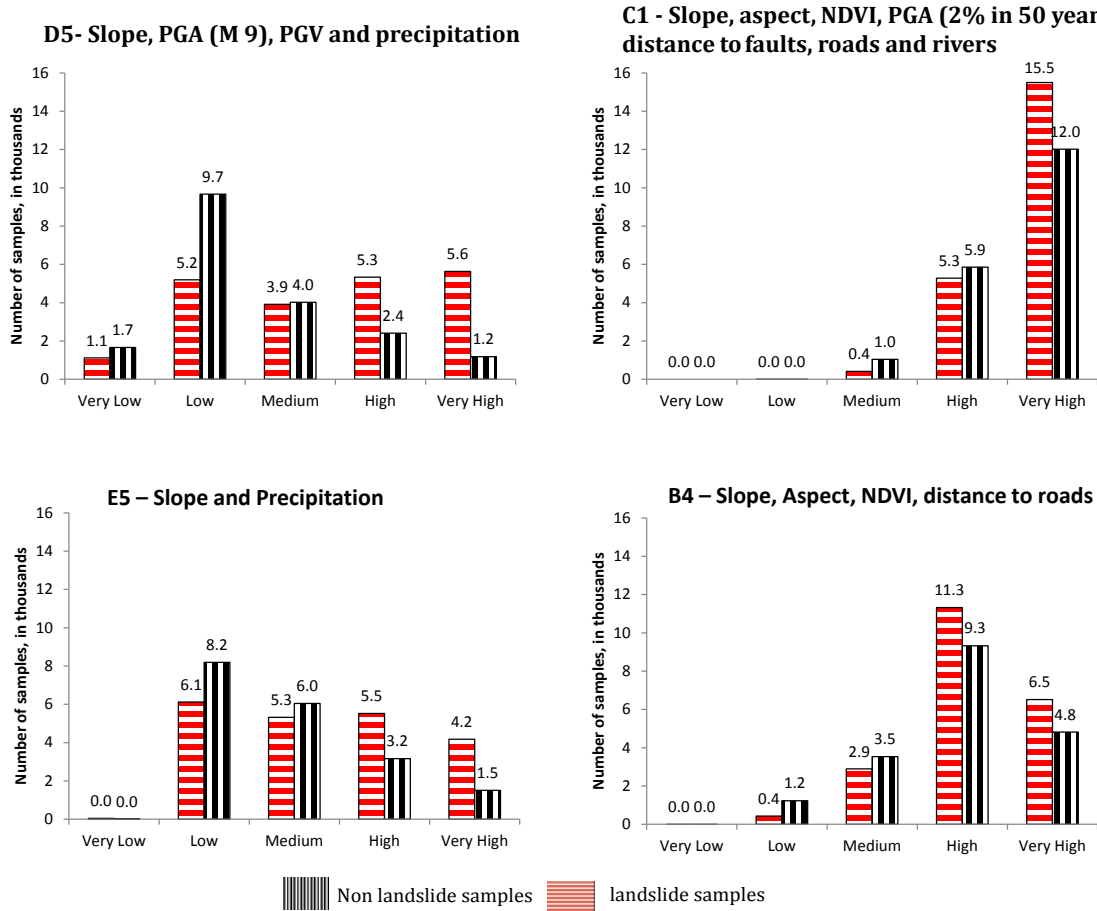
Figure 8.5: Example histograms used for validation.

8.7.2 Modified Validation Index

Dai and Lee (*Dai and Lee 2002*) defined a common validation index with the number of landslides falling under the category of high and very high divided by the total number of landslide samples. However, this approach does not consider the non-landslide sample and hence fails to answer for the overall fitness of the model. A second validation technique was completed to calculate the frequency ratio of landslide sample points occurring in the high and very high bins compared to the landslide samples occurring in the low to very low bins. The higher the frequency ratio, the better the model performed. This determines the overall fitness of the model. The modified validation index is calculated as:

$$MVI = C_{LS} \times C_{NLS} = \frac{\#LS_{H+VH}}{\#LS} \times \frac{\#NLS_{L+VL}}{\#NLS}$$

<div align="right">(8-3)</div>

By calculating the correctly categorized landslides and non-landslides separately before combining into the MVI, one can see if a model is over-predicting the hazard for the NLS samples or under-predicting the hazard for the LS samples. The MVI was useful to distinguish the value added by parameters. For example, Model A had the highest MVI of 0.31. Other models, such as C and D, which included additional parameters, had similar MVIs of 0.3. Hence, they were insignificant to the model based on the currently available data. However, in the future with improved LIDAR mapping of landslides, one should verify that this is still true. Note that while many of the models properly categorized the landslide points, they failed to categorize the non-landslide points properly.

Interestingly, the models incorporating the PGA and PGV from the ORP tended to perform better than those without those parameters and considering precipitation alone. This may suggest that many of those landslides were triggered by earthquakes; however, a more detailed analysis would be required to confirm this.

8.7.3 Area Under the Receiver Operating Characteristic Curve (AUC)

A critical component of judging the relative validity of models is the area under the receiver operating characteristic curve (AUC). AUC is calculated using the receiver operator characteristic curve, which plots the percentage of predicted occurrences that match actual occurrence samples versus the percentage of predicted occurrences that do not match. More specifically, the AUC compares the likelihood that the probability of landslide occurrence predicted by the model will be higher in a location shared by an actual landslide occurrence than a random location with no landslide occurrence (*Convertino et al. 2013*). The AUC of the selected model was 0.7, the highest of any of the models with seismic factors.

8.7.4 Landslide Ratio Analysis

A critical component of judging the relative validity of models is the area under the receiver operating characteristic curve (AUC). AUC is calculated using the receiver operator characteristic curve, which plots the percentage of predicted occurrences that match actual occurrence samples versus the percentage of predicted occurrences that do not match. More specifically, the AUC compares the likelihood that the probability of landslide occurrence predicted by the model will be higher in a location shared by an actual landslide occurrence than a random location with no landslide occurrence (*Convertino et al. 2013*). The AUC of the selected model was 0.7, the highest of any of the models with seismic factors. (Figure 8.6)
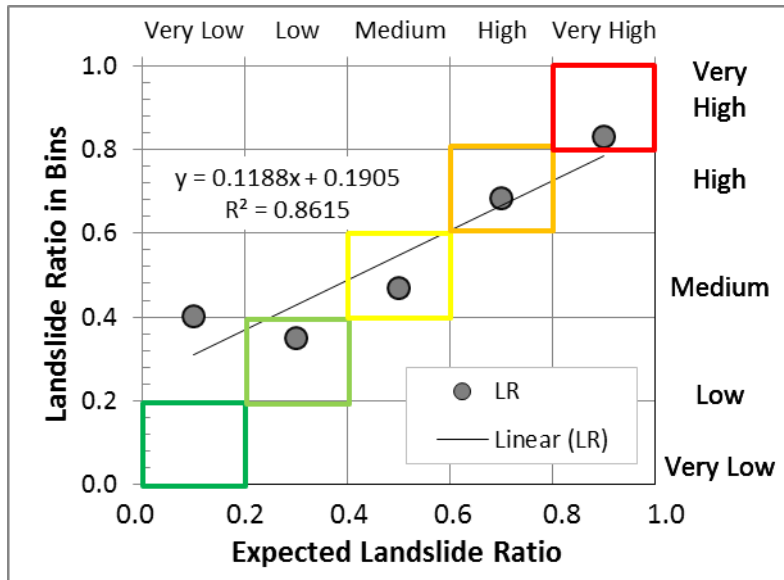
Figure 8.6: Landslide Ratio Validation for selected model. Ideally, each point would be in the centroid of each of the colored boxes.

8.7.5 LIDAR-Derived Landslide Polygons

In order to validate the model using sample sets that were not included in the regression analysis, LIDAR-derived landslide polygons were used to check the accuracy of the map. There were 2,067 polygon features, covering 82 sq. km, masked with the susceptibility map. Landslide polygons smaller than 0.1 sq. km. (300 m x 300 m) were excluded because they are smaller than the smoothing and other filters applied previously in the creation of the map. The resultant shapes were reclassified, and it was found that 58 of the 82 sq. km were classified under high and very high level of susceptibility, representing an accuracy of 70%. However, it should be noted that the landslides mapped using LIDAR could have been triggered by other factors than seismic activity. Further, after a landslide occurs it will likely be in a more stable condition compared to its condition prior to the landslide. When visually validating the map with the LIDAR polygons, it was observed that many of the polygons that showed a lower level of hazard were adjacent to areas with a higher hazard, suggesting that the landslide deposit would be more stable than the uphill scarp. Thus, a model is validated by checking the goodness of the fit and the discrimination on a different set of data that was not included in the numerical calculation.

8.8   DISCUSSION AND CONCLUSIONS

The chronic, widespread nature of landslide movements within the state of Oregon is of extreme concern, particularly when land sliding is exacerbated by seismic activity. Although the landslide susceptibility maps in this study may be conservative, they agree well with recent LIDAR-based map analyses by DOGAMI (*Burns et al. 2010, 2012b, 2012c, 2012d, and 2013a, 2013b*). LIDAR-based mapping, which can identify 3 to 200 times more landslides than other techniques and can accurately portray the spatial extent of existing landslides (*Burns, 2007*), has

led to the discovery of many new landslides. This is revealing that landslides are a problem not only in the Coast Range, but also throughout the state. Continued LIDAR-based mapping will help overcome shortcomings of the current non-LIDAR-based landslide inventories. Replacing the non-LIDAR-based inventories used for the initial calculations in this study would improve quantification of the various parameters analyzed as well as improve selection of non-landslide points. In many cases, it is likely that the NLS points used in this study fall within locations that are actually landslides but have not yet been mapped.

With the potential of Cascadia subduction zone and other seismic sources in Oregon to create large-magnitude earthquakes, which can result in additional landslides, it is essential to mitigate the potential for damage at vital structures, utilities, and lifeline corridors that fall within high and very high probability landslide hazard areas. One limitation in applying this method for regional seismic slope stability analysis in Oregon is that there are no databases providing information regarding seismically induced landslides versus landslides triggered by other sources. Although Oregon is densely vegetated with high NDVI, the landslide samples and NDVI trend did not help in understanding the pattern of occurrence. Hence, choosing the right parameters for a prediction model is important for an efficient overall fitness of the model.

At the regional scale, the results are very similar to the Oregon Resilience Plan *(Madin and Burns 2013)* landslide probability maps. Note that because of the differences in methodology, the ORP maps are scaled to a maximum of 30% probability, compared to 100% in this study. Nonetheless, when comparing the relative hazard, both maps predominately show high hazards in the coast range and cascades, with lower probabilities in the Willamette Valley. In particular, the NW and SW sections of the coast range show the highest level of hazard. The SE section, in both maps, shows a lower level of hazard. The ORP maps tend to show a higher hazard in the western portion of the Valley. However, when evaluating the displacement maps produced in the ORP, the western portion of the Valley tends to show less hazard.

When the "fuzzy AND" overlay technique is adopted to determine which lifeline routes are most vulnerable, it shows that 14% (958 km) of the entire road system inside the study area is classified under very high and 13.8% (947 km) under high probability of landslides. A similar technique can also be used to categorize other features of interest (e.g., cities) that lie within susceptible zones, for additional uses in planning and development.

9.0   FULLY PROBABILISTIC ANALYSIS TECHNIQUE

9.1   CHAPTER SUMMARY

Seismically induced landslides can be detrimental to urban communities due to high damage and repair costs, disruption of lifeline connection routes and utilities, environmental impacts, and potential for loss of life. A consistent, reliable hazard map can assist agencies in allocating limited resources to prepare for these events. This chapter presents a methodology for determining probabilities of exceeding displacement thresholds (e.g. 0.1, 0.3, 1.0 m) which relate to anticipated damage for regional, seismically induced landslide hazard mapping. This approach scales site-specific techniques to a regional scale evaluation by combining generally available data, including: previous landslide inventories, LIDAR and photogrammetric topographic data, geologic mapping, NEHRP site classification, and seismic hazard curves for the analysis. Maps were generated for the state of Oregon, which contains weak, wet soils, which already have a high potential for landslides even without seismic activity. These results can then be integrated with an analysis of other hazards for probability based hazard evaluation and risk assessment.

Chapter 8 presented the results from the commonly used multivariate approach to landslide hazard mapping. However, there are several shortcomings to this approach:

- They do not physically model the effects of the earthquake, but merely treat parameters statistically to develop correlations. As such, they tend to perform very poorly when seismic parameters are considered.

- They are not capable of considering multiple seismic sources.

- When the training landslide database does not include displacements, the method cannot be used to evaluate landslide displacement (or probabilities of exceeding displacements), but solely susceptibility.

9.2   DATA SOURCES

In landslide studies, there are several geospatial, geologic, and geotechnical data sources which need to be considered to determine hazard levels, including: topographic information (e.g. slope angle, land-cover), sub-surface data, ground water levels, soil properties, intensity and probability of triggering sources such as earthquake and rainfall (*Soeters and Van Westen 1996*). For this project, the necessary datasets were acquired from numerous sources, which are summarized in this section (Table 9.1).

Table 9.1: Datasets used for the landslide analysis and their source, provider and resolution.

Dataset	Source	Provider	Native Resolution	Algorithm Resolution
Hybrid Slope	National Elevation	USGS	26.88 (m)	30 (m)
	LIDAR DEM	DOGAMI	1 (m)	
PGA Exceedance probabilities	De-aggregated Seismic Hazard Curves	USGS	0.05 (deg)	Bilinear Interpolation
NEHRP Site Class	The Oregon Resilience Plan	DOGAMI	Polygons 1:20,000	100 (m)
Lithology	OGDC v 5.0	DOGAMI	Polygons 1:20,000	100 (m)

These datasets include:

9.2.1 Digital Elevation Model (DEM)

The DEM consisted of LIDAR data, where available from the Oregon LIDAR consortium, DOGAMI *(DOGAMI 2012),* and the USGS National Elevation Dataset (NED)*(USGS 2012b),* for the remainder of the state. The original resolution for LIDAR DEMs was 1 meter, which was then resampled to a pixel size of 26.7 meters to match the USGS NED DEM. Slope, was derived from the DEM for a 30 m pixel size.

9.2.2 Lithology Map

The lithology map was obtained from the Oregon Geologic Data Compilation (OGDC v 5.0)(*Ma el al. 2009*), which provides the most current geologic and lithological mapping in the study area. Because the numerous geologic units were difficult to statistically quantify (e.g., soil properties) for such a large area given the limited number of landslides, lithological units were used to simplify the mapping procedure. However, should one be able to characterize individual geologic units, improved results can be obtained.

9.2.3 SLIDO Database

Historical landslides in the Statewide Landslide inventory Database of Oregon (SLIDO) (*Burns et al, 2012a*) that contains approximately 10,000 landslides. While the database includes many polygons indicating the extent of landslides, most consist of only a single point to represent the location of the landslide.

9.2.4 NEHRP Site Class

NEHRP site classification, which is based on the soil shear wave velocity in the upper 30 meter (Vs 30) and average properties of soil in the upper 30 meters, provided by the Oregon Resilience Plan (*OSSPAC 2013*).

Both the NEHRP site classification and lithology datasets were polygon vector files mapped at a scale of 1:20,000. They were converted into a grid format (with 100 meter pixel size) to improve computation speed at the expense of requiring additional disk storage space.

9.2.5 Seismic Hazard Curves

The USGS (*2008*) de-aggregated seismic hazard curves plot the mean annual rate of exceedance (λ) versus peak ground acceleration (PGA) for various VS_{30} measurements (180, 259, 360, 537 and 1150) NEHRP site classifications were provided at 0.05 degree increments throughout the entire study area. An example of these curves is shown in Figure 9.1. C++ routines were written to convert the available gridded text file to a GIS floating point grid format and separate various PGA intervals within the study area for efficient computation. During the probabilistic landslide analysis, bilinear interpolation is used for the finer cell increments.
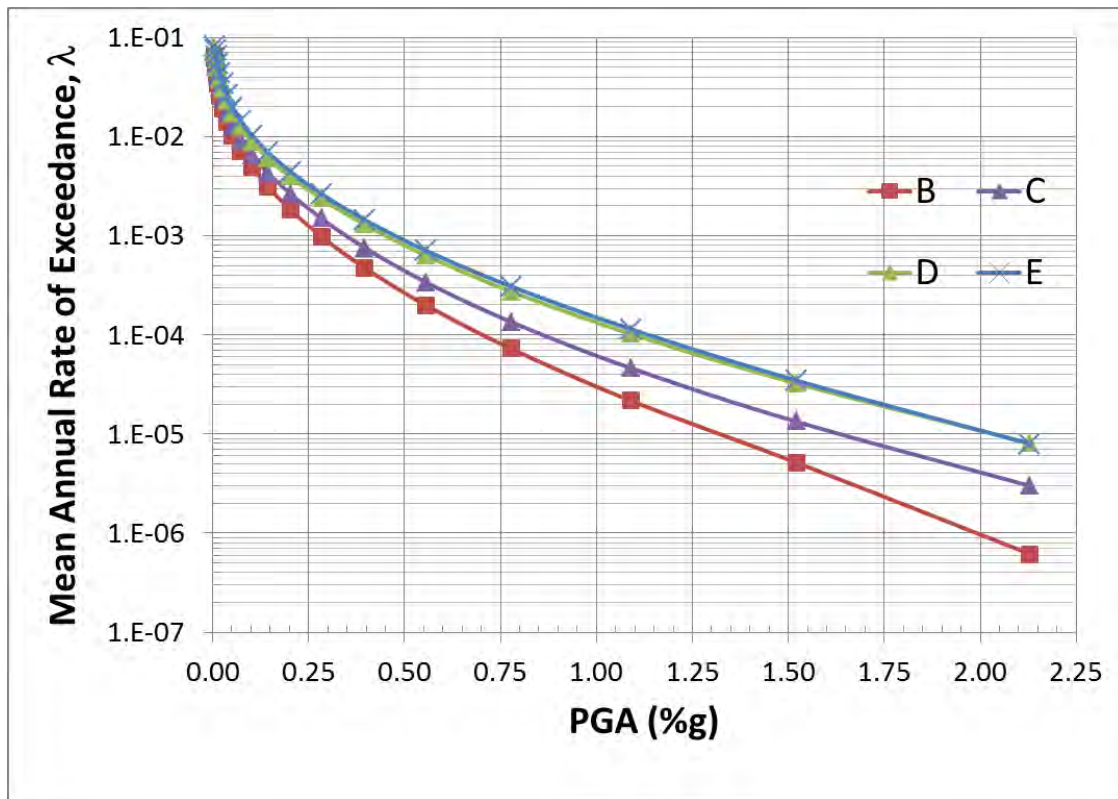
Figure 9.1: Example of seismic hazard curves for NEHRP site classifications B, C, D and E for a site in Corvallis, Oregon.

9.2.6 Friction Angle Histograms

Because the extents of the study area are too large to obtain necessary geotechnical information such as soil strength, the soil strength was estimated by determining the slopes at each of the landslides in the SLIDO database categorized by each lithological unit (Chapter 2). This correlation results in an estimated soil strength distribution (normalized by the total number of landslides in each unit) for each lithological unit based on the assumption that the slope at each of the failure sites gives an indication of the maximum soil strength (φ), such as the curve shown in Figure 9.2 for the sedimentary lithological unit. Shear strength values are generally low compared to what would be expected for these materials (*Montgomery 2001, Schmidt and Montgomery 1995*). However, substantial weathering from heavy precipitation combined with the effects of inter-bedding of weak clay seams leads to significantly reduced strength in these units. In areas where lithological units have been characterized through detailed testing, the actual soil strength distribution curves obtained from the testing can be used.
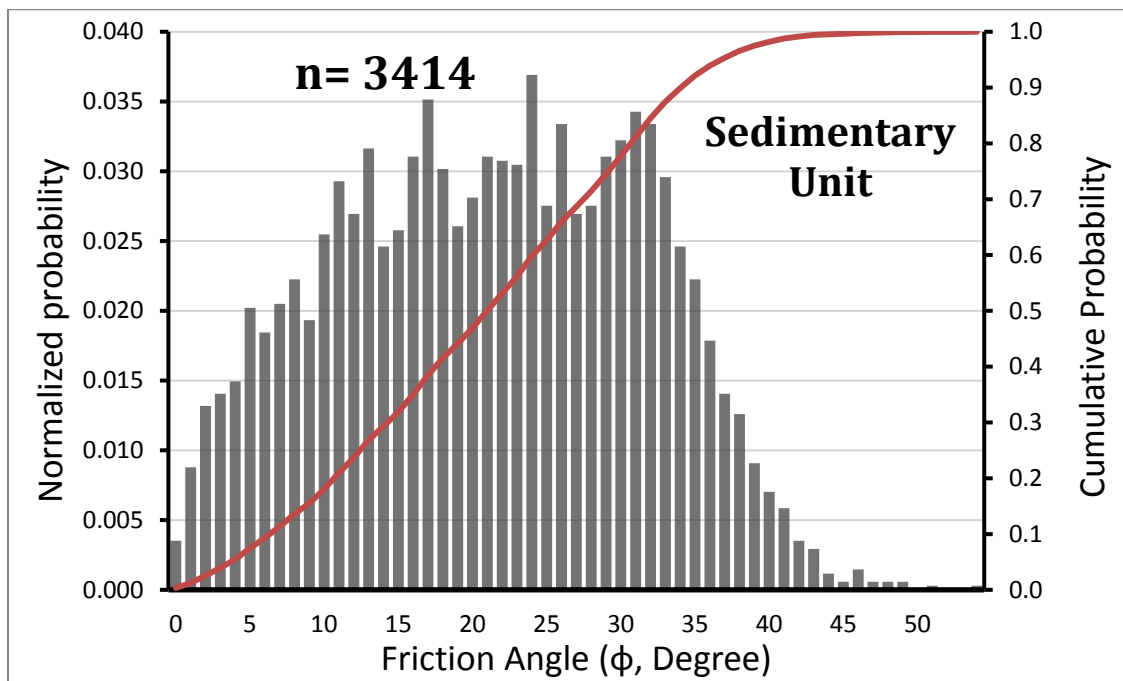
Figure 9.2: Example estimated friction angle distribution in sedimentary lithological unit with 1 degree bins.

9.3   METHODOLOGY

The primary goal of this chapter is to present a new methodology to quantify the likelihood of seismically induced landslide occurrence and the probability of exceeding certain thresholds of ground displacement given all possible earthquakes in the study area. To facilitate the ability to create new maps quickly when new data are available (e.g., updates to the seismic hazard curves), code was developed in C++ to process the probabilistic calculations efficiently for such a large area. This enables the code to be flexible such that one can run it for fully probabilistic

calculations or for scenario events. Following creation of the maps from the analysis, they can be brought into a GIS platform for further analysis and visualization.

There are three main factors contributing to the landslide hazard, including slope, friction angle and peak ground acceleration. According to the chain rule in probability theory, conditional probabilities are used over all possible members of a joint distribution of a set of random variables (slope, PGA and friction angle) to calculate the aggregated probability of a landslide. The following expression can be used to calculate the probability of a landslide at a given location:

$$P(LS)_{x,y} = \sum_{j=0}^{90^\circ} \sum_{i=0}^{n} P(PGA_i > a_y | \beta_{x,y}, \varphi_j) \times P(\varphi_j) \times P(PGA_i) \qquad (9\text{-}1)$$

Where:

i is a counter variable for the current PGA bin

n is the number of PGA bins,

P(LS) is the probability of a seismically induced landslide happening at   a location xy,

$\beta_{x,y}$ is the slope angle at location x, y

PGA$_i$ is the average peak ground acceleration for bin i from corresponding seismic hazard curve (based on site classification) at a location x,y

a_y is the minimum pseudo-static acceleration required to produce instability the sliding block (yield acceleration), calculated using Newmark's method (downhill equation),

$$a_y = \tan(\varphi_j - \beta_{x,y}) \times g \qquad (9\text{-}1a)$$

g is the acceleration due to gravity of Earth, equal to 9.81 m/s^2

$P(PGA_i > a_y | \beta_{x,y}, \varphi_j)$ is the probability of having an earthquake with peak ground acceleration exceeding yield acceleration given the condition representing pixel located at x,y with slope of β degree and friction angle of φ from corresponding histogram. (Could be 1 or 0),

P(φ$_j$) is the probability of the soil having a given strength (friction angle ranging from j = 0 to 90 degrees), obtained from the histograms such as that shown in Figure 9.2,

P(PGA$_i$) is the annual interval probability for bin i of having an earthquake producing a peak ground acceleration from seismic hazard curve (based on site classification) for the location x,y calculated from the mean annual rate of exceedance (λ) by:

$$P(PGA_i) = P(PGA_2) - P(PGA_1) = (1 - e^{-\lambda_2}) - (1 - e^{-\lambda_1}) = e^{-\lambda_1} - e^{-\lambda_2} \qquad (9\text{-}1b)$$

Calculations were done for each 30 m x 30 m pixel (representing 900 m^2) in the state of Oregon. A related approach was used for liquefaction and lateral spread hazard mapping in Utah, Olsen *(Olsen 2005)*, Erickson (*Erickson 2006*) and Gillins (*Gillins 2012*). Figure 9.3 depicts the methodology in a flowchart format.
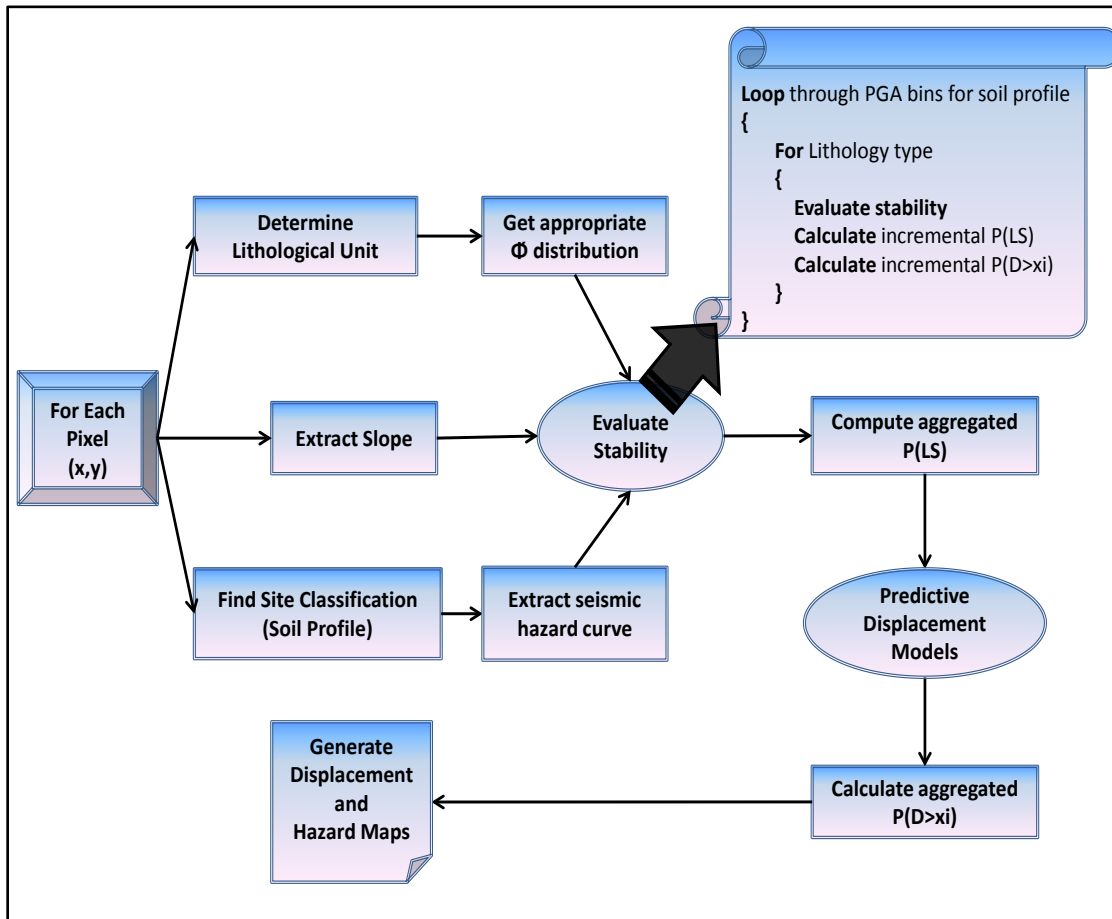
Figure 9.3: The methodology displayed as flowchart with simplified pseudo-code for stability evaluation.

Simultaneous with the landslide triggering analysis, probabilities of exceeding displacement thresholds of (0.1, 0.3, 1.0, 10, and 100 m) are determined since they provide a better indicator of damage potential. The first threshold was selected as 0.1 m, which represents the lower threshold of the Saygili and Rathje (*Saygili and Rathje 2008*) regression model describing the initiation of landslide producing minimal damage, which is likely to be easily repairable. The next threshold is 0.3 m, which is where significant damage may occur to structures (*Olsen et al. 2007*). Exceeding 1-meter threshold will create serious damage that would bring considerable consequences and extensive problems for lifeline utilities. The next two thresholds represent larger displacements, of 10 and 100 meters. These displacements have impacts that are more serious when they are close to lifeline corridors but with extremely low chances of happening.

Exceeding a 10 or 100 meter threshold is a catastrophic situation, likely produced by a large moment magnitude earthquake from Cascadia subduction zone.

When performing regional analysis over a large area, a simple displacement approach is needed since parameters such as number of cycles, predominant period, and arias intensity are not easily obtained for such a large area or require significant assumptions and computations to acquire, reducing their reliability. Hence, Ambraseys and Menu (*Ambraseys and Menu 1988)* and Saygili and Rathje *(Saygili and Rathje 2008)* were two selected methods among the available models discussed previously because they required only critical acceleration (ay) and peak ground acceleration (amax) to calculate permanent displacement (see Table 2.4).

Ambraseys and Menu *(Ambraseys and Menu 1988)* showed that if upslope movements are not considered (landslide case), for smaller values of a_y/PGA the shape of input motion will be influenced and strong ground motion will produce permanent displacement (in centimeters) calculated from following expression:

$$\text{Log } D_L = 0.9 + \log [(1- (a_y/PGA))^{2.53} \times (a_y/PGA)^{-1.09}] \quad \sigma_{logDL} = 0.30 \quad (9\text{-}2)$$

Where:

D_L is the amount of permanent displacement, in centimeters,

a_y is the Newmark's yield acceleration defined as the minimum pseudo-static acceleration to create instability in sliding block, in g,

PGA is the peak ground acceleration of the input motion, in g,

σ_{logDL} is the standard error for the above regression equation, where D_L is in centimeters.

Rathje and Saygili (*Rathje and Saygili 2011*) created various scalar and vector models through the years from 2008 to 2011. Scalar displacement models are regression over a single ground motion parameter whereas vector models need multiple motion parameters. The scalar model developed by Saygili and Rathje (*Saygili and Rathje 2008*) was chosen in order to estimate the permanent displacement from the landslide for the same second displacement map:

$$\ln D_L = 5.52 - 4.43 (a_y / PGA) - 20.39 (a_y / PGA)^2 +$$

$$42.61 (a_y / PGA)^3 - 28.74 (a_y /PGA)^4 + 0.72 \ln(PGA) \quad \sigma_{lnDL} = 1.13 \quad (9\text{-}3)$$

Where:

D_L is the amount of permanent displacement, in centimeters,

a_y is the yield acceleration, in g,

PGA is the peak ground acceleration of the input motion, in g,

σ_{lnDL} is the standard error for aforementioned regression equation,

When the yield acceleration from Newmark's sliding block analysis was determined to be a negative value, indicating that the estimated strength was less than the existing slope angle, there is no effect on calculating the landslide probability (since 0 g, just like a negative value, is always less than the PGA at the midpoint of any of the seismic hazard curve bin). However, this presents problems with the stability of the displacement regression equations. Hence, a lower bound of zero was used for ay based on the assumption that at the time of DEM acquisition, the slope was not instantaneously failing (the failure either happened before or after) and would have a strength equal to or greater than its current slope angle.

Conversely, for an upper bound, the Saygili and Rathje (*Saygili and Rathje 2008*) equation automatically converges to 0 cm displacement for large (a_y/PGA) ratios. For the Ambraseys and Menu (*Ambraseys and Menu 1988*) equation, an upper bound of a_y/PGA equal to 0.9999 (approximately 0 cm displacement) and a lower bound of a_y/PGA of 0.01 was used (equivalent to 1172 cm of displacement) for computational stability. When placed in the exceedance probability context discussed below, this has little effect. Further, such large displacements are well outside of the predictive capabilities of the model.

The probability of displacement exceeding a threshold value $P [D_L > t]$ is computed within each cell by looping through possible acceleration intervals from the seismic hazard curve for that location and critical acceleration. The standard errors of the regression models of Ambraseys and Menu (*Ambraseys and Menu 1988*) and Saygili and Rathje (*Saygili and Rathje 2008*) were used to calculate the probability of exceedance for given values of a_y and PGA. Equations 2 and 3 were used to estimate D_L and exceedance probabilities were calculated from equation 4:

$$P [(D_L>t) \mid a_y, PGA_i] = 1 - F_z(z) \qquad (9\text{-}4)$$

Where:

t is a threshold value, equal to one of five different values, 0.1, 0.3, 1.0, 10, and 100 m, discussed below,

$F_z(z)$ is cumulative density function (CDF) for the standard normal variant, z, which can be calculated or taken from a CDF table of standard normal distribution in either general statistics textbooks or Table C-1 in Kramer 1996, p. 593)

z can be computed from equation 5a or 5b depending on the selected regression model:

$$z = \frac{\overline{\log(D_L = t)} - \log(D_L)}{\sigma_{\log(D_L)}} \qquad (9\text{-}5a)$$

$$z = \frac{\overline{\ln(D_L = t)} - \ln(D_L)}{\sigma_{\ln(D_L)}} \qquad (9\text{-}5b)$$

Where:

$log(D_L)$ is the logarithm of the estimated displacement by the Ambraseys and Menu (*Ambraseys and Menu 1988)* model,

$ln(D_L)$ is the natural logarithm of the estimated displacement by Saygili and Rathje (*Saygili and Rathje 2008*) model,

$log(D_L = t)$ is the log of the selected threshold displacement, t,

$ln(D_L = t)$ is the natural log of the selected threshold displacement, t,

$\sigma_{log(DL)} = 0.30$, the standard error for the Ambraseys and Menu (*Ambraseys and Menu 1988*) regression model,

$\sigma_{ln(DL)} = 1.13$, the standard error for the Saygili and Rathje (*Saygili and Rathje 2008*) regression model.

In order to calculate the exceedance probabilities equations 9-1 and 9-4 can be merged to calculate the full probability:

$$P(DL > t)_{x,y} = \sum_{j=0}^{90°} \sum_{i=0}^{n} P\left[DL > t \,|ay, PGAi\,\right] \times P(PGA_i > a_y | \beta_{x,y}, \varphi_j) \times P(\varphi_j)$$
$$\times (PGA_i)$$

(9-6)

A similar equation was developed in Rathje and Saygili *(Rathje and Saygili 2011)* for a site specific analysis. The probability that D_L exceeds a given threshold can be calculated with equation 9-5, which is a summation of PGA and friction angle with given slope and computed yield acceleration in a particular cell. After the aggregation of all PGA values on the seismic hazard curve, the mean annual rate of exceedance of several displacement thresholds will be produced, resulting in the creation of a series of hazard maps, which will be discussed in the following section.

10.0 FINAL, FULLY PROBABILISTIC ANALYSIS MAPS

The landslide-susceptibility map, generated using equation 9-1 is presented in Figure 10.1. Figures 10.2 through 10.6 show maps for the five displacement threshold exceedance probabilities using the Saygili and Rathje (*Saygili and Rathje 2008*) model (SR) The upper and lower extents of the legends on the maps corresponding to red and green are varying according to the type of map, exceedance threshold and the method. Appendix D contains the maps of displacement threshold exceedance probabilities using the Ambraseys and Menu *(Ambraseys and Menu 1988*) model (AM).

The landslide hazard map in Figure 10.1 provides detailed information regarding western Oregon and delineates domains extremely susceptible to landslide. While the hazard is very high, this map shows reasonable probability results when it is compared with landslide inventory datasets (SLIDO) (Figure 10.1). Note that SLIDO database has some limitations including that it does not address all landslides that actually happened in Oregon. On the other hand, most of the reported landslides in SLIDO were triggered by rainfall rather than earthquake. Most of the regions where it is estimated to have a high level of hazard, already frequently experience landslides without significant seismic activity. In most cases, the high hazard level prediction inside the map is in accordance with active landslides and some are dormant steep slopes, which have historically failed. The displacement maps in Figures 10.2 to 10.6, calculated using the method of Saygili and Rathje (*Saygili and Rathje 2008*), show a rational, decreasing order of likelihood of failure with increasingly large deformations.

The results may be over conservative in eastern Oregon (not shown) because the soil strength estimates were determined in western Oregon (where most of the landslides were documented and more rigorous mapping has been completed), which experiences significantly more weathering due to increased rainfall. However, such an approach is a conservative approach. If appropriate information were available to compare lithological units between eastern and western Oregon, one could develop and apply a scale factor for soil strength in eastern Oregon.

Figures 10.4 and 10.5 represent larger displacement thresholds, indicating significant damage. Such displacements could likely only be triggered by large earthquakes; hence, the areas of higher probabilities are in close proximity to the Cascadia Subduction Zone and there is less influence from local faults. However, these exceedance probabilities are extremely low because these thresholds can only be met once a catastrophic earthquake happens, which has a lower probability of occurrence. The 10 and 100-meter threshold maps (Figures 10.5 and 10.7) were created in order to provide reference validation. Caution needs to be exercised when using these maps since the 10 and 100-meter thresholds are outside the bounds of data used to develop and calibrate the empirical regression models.

The maps presented in Appendix D using the displacement regression model of Ambraseys and Menu (*Ambraseys and Menu 1988*), all follow the same trend of decreasing chance of exceeding higher displacement thresholds. However, the Ambraseys and Menu (*Ambraseys and Menu 1988*) model predicted much higher probabilities of exceeding a given displacement compared to

Saygili and Rathje (*Saygili and Rathje 2008*) model, particularly at small thresholds. Although the color trend shown by Ambraseys and Menu (*Ambraseys and Menu 1988*) model maps is reasonable and similar to what Saygili and Rathje model maps represent, the probability values are much higher. Table 10.1 presents statistical parameters for the difference of between the two models, showing that the results of two models converge to similar amounts within large thresholds of displacement, while the most discrepancy is witnessed below the 1-meter displacement threshold.

Overall, both methodologies tend to have lower discrepancy in high seismic regions (the Oregon coast range, in particular). In such regions, at higher displacement minimal differences were observed. On the other hand, eastern Oregon depicts the largest differences between the approaches and these discrepancies tend to increase in higher distance threshold maps.

Fully Probabilistic

Displacements were calculated using the Saygili and Rathje (2008) displacement model

Note that the return period of a landslide displacement exceeding a threshold can be calculated as 1/P (e.g. a 1% probability has a return period of 100 years)

Legend

Landslide Susceptibility

- 0.0 - 0.1
- 0.1 - 0.2
- 0.2 - 0.3
- 0.3 - 0.4
- 0.4 - 0.5
- 0.5 - 0.6
- 0.6 - 0.7
- 0.7 - 0.8
- 0.8 - 0.9
- 0.9 - 1.0
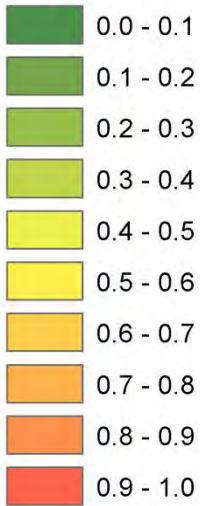
Note that the last bin Increment is larger than the other bins.
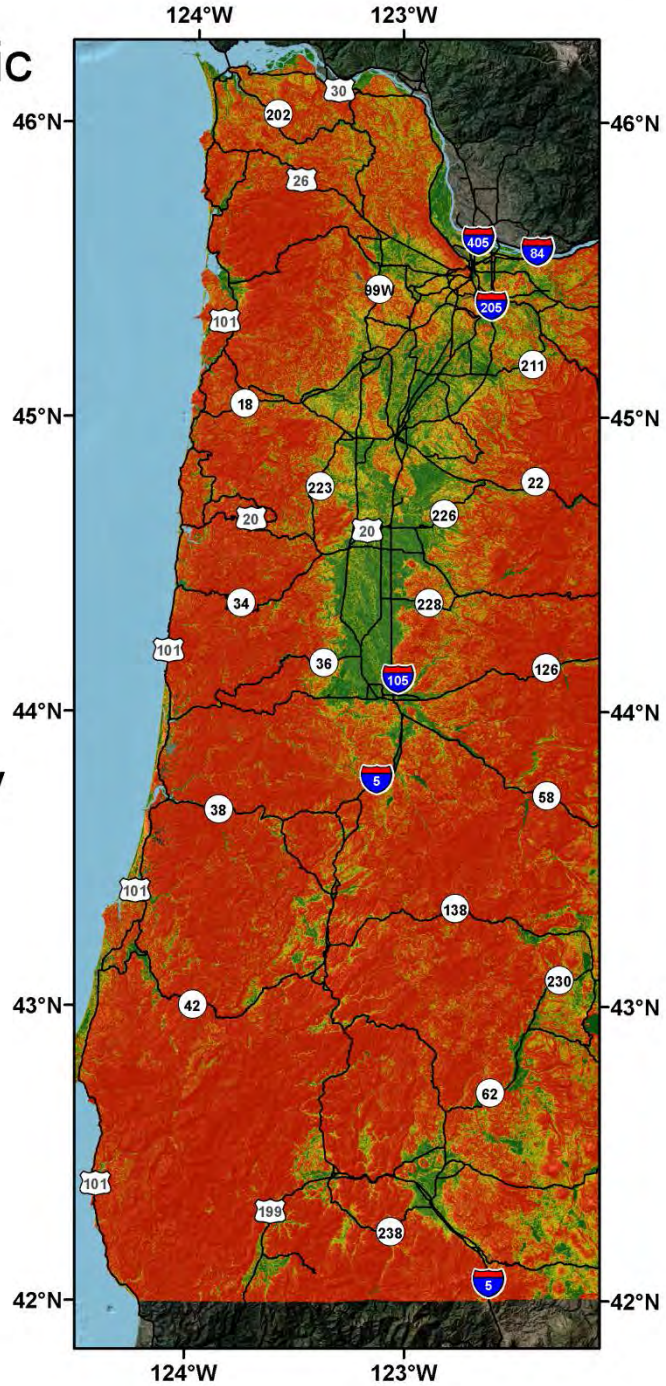
Figure 10.1: Fully probabilistic landslide hazard map for western Oregon.

138
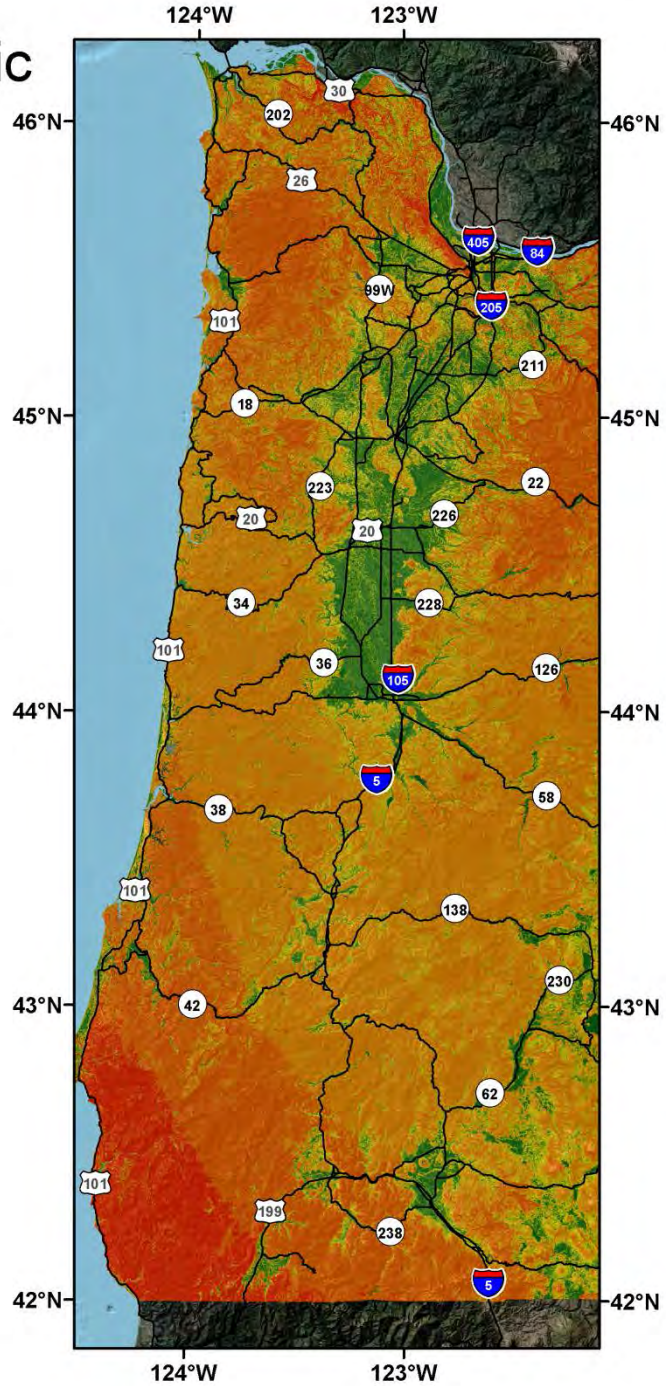
Figure 10.2: Map of the probability of exceeding 10 cm displacement for western Oregon.
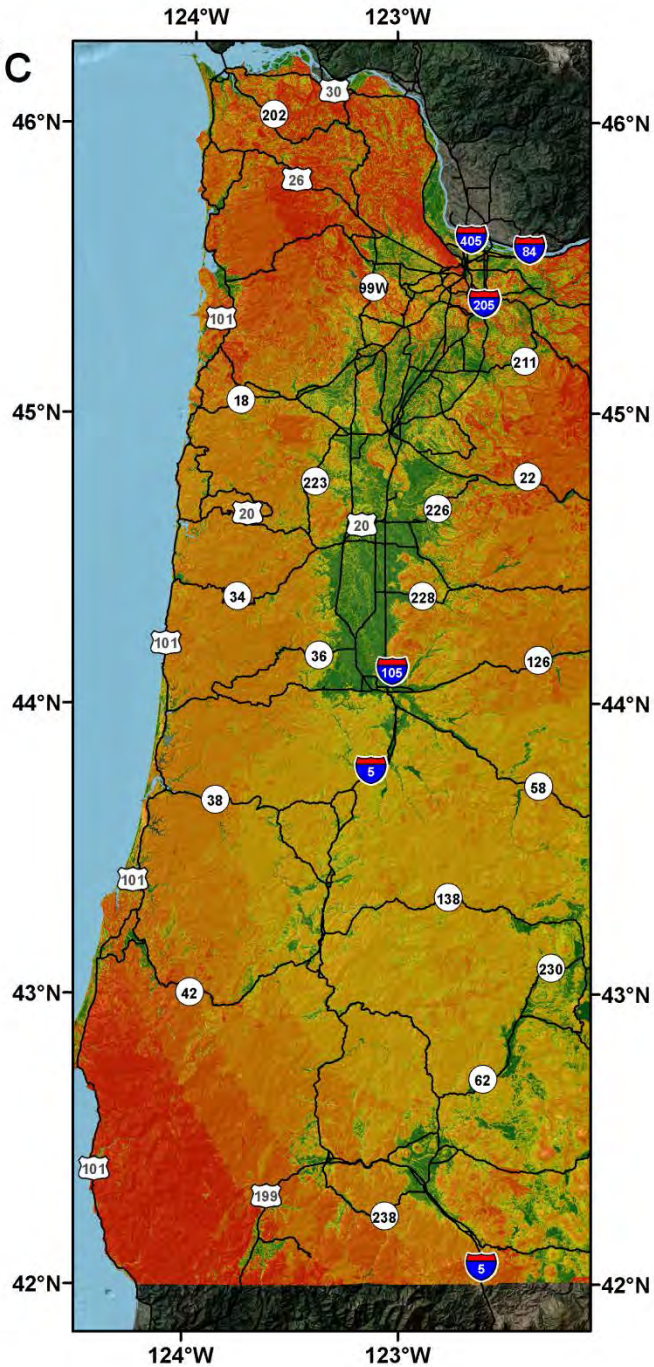
Figure 10.3: Map of the probability of exceeding 30 cm displacement for western Oregon.

Fully Probabilistic

Displacements were calculated using the Saygili and Rathje (2008) displacement model

Note that the return period of a landslide displacement exceeding a threshold can be calculated as 1/P (e.g. a 1% probability has a return period of 100 years)

0 12.5 25   50   75   100
Kilometers

Legend

P(DL>1 m)

	0.000 - 0.001
	0.001 - 0.002
	0.002 - 0.003
	0.003 - 0.004
	0.004 - 0.005
	0.005 - 0.006
	0.006 - 0.007
	0.007 - 0.008
	0.008 - 0.009
	0.009 - 0.023

Note that the last bin Incriment is larger than the other bins.

Figure 10.4: Map of the probability of exceeding 1 meter displacement for western Oregon.

141

Fully Probabilistic

Displacements were calculated using the Saygili and Rathje (2008) displacement model

Note that the return period of a landslide displacement exceeding a threshold can be calculated as 1/P (e.g. a 1% probability has a return period of 100 years)

0 12.5 25   50   75   100
Kilometers

Legend

P(DL>10 m)

	0.00000 - 0.00002
	0.00002 - 0.00004
	0.00004 - 0.00006
	0.00006 - 0.00008
	0.00008 - 0.00010
	0.00010 - 0.00012
	0.00012 - 0.00014
	0.00014 - 0.00016
	0.00016 - 0.00018
	0.00018 - 0.00036
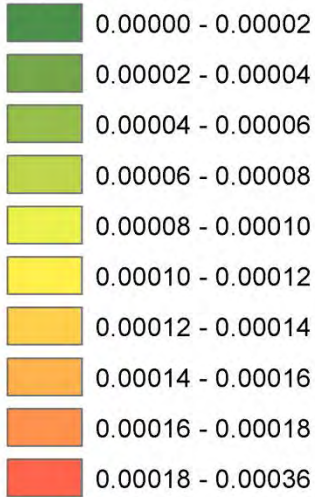
Note that the last bin Increment may be larger than the other bins.
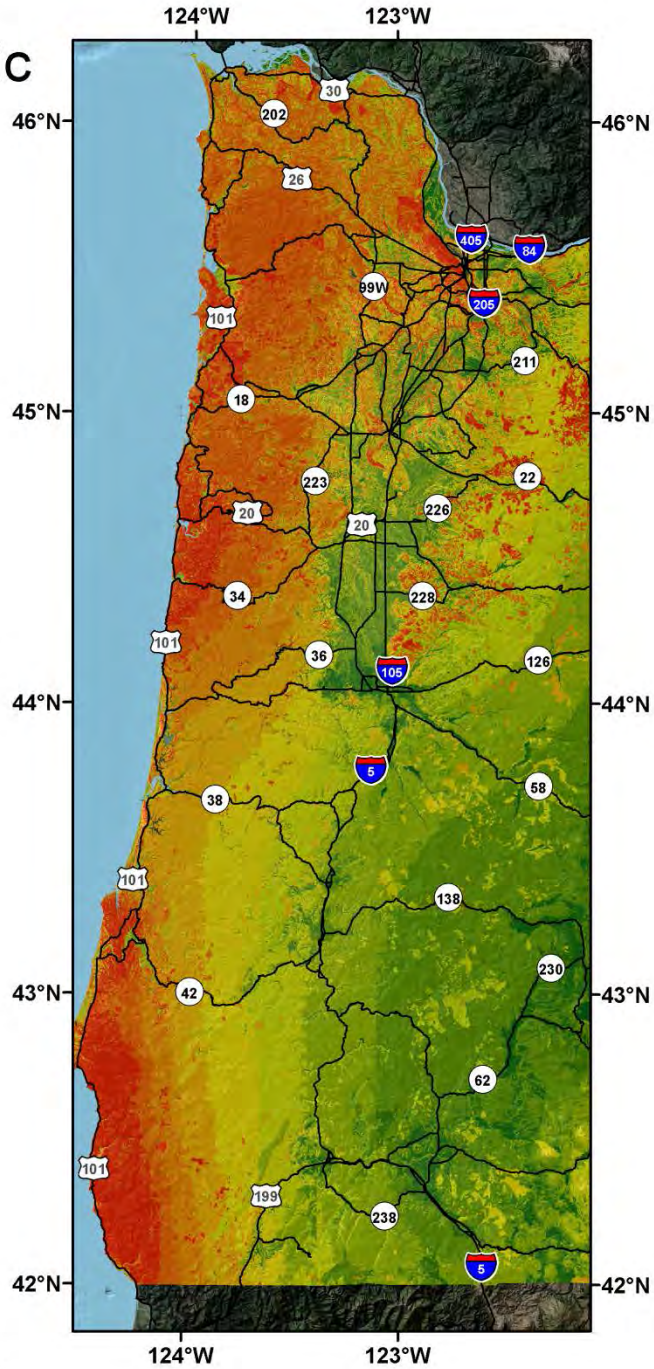
Figure 10.5: Map of the probability of exceeding 10 m displacement for western Oregon. (Note-for model validation purposes only. This is outside the bounds of the displacement regression equations).

Fully Probabilistic

Displacements were calculated using the Saygili and Rathje (2008) displacement model

Note that the return period of a landslide displacement exceeding a threshold can be calculated as 1/P (e.g. a 1% probability has a return period of 100 years)

Legend

P(DL>100 m)

	0.0e00 - 4.0e-8
	4.1e-8 - 8.0e-8
	8.1e-8 - 1.2e-7
	1.3e-7 - 1.6e-7
	1.7e-7 - 2.0e-7
	2.1e-7 - 2.4e-7
	2.5e-7 - 2.8e-7
	2.9e-7 - 3.2e-7
	3.3e-7 - 3.6e-7
	3.7e-7 - 1.0e-6
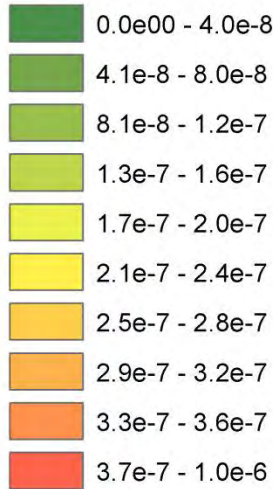
Note that the last bin Increment may be larger than the other bins.
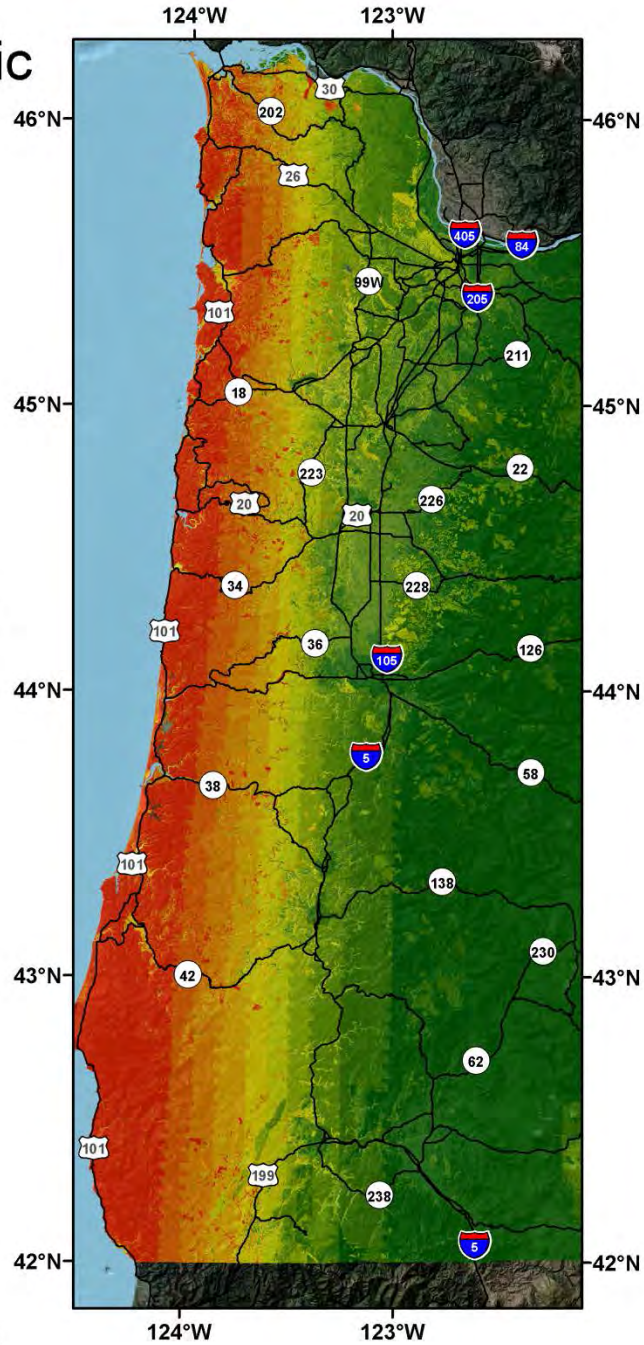
Figure 10.6: Map of the probability of exceeding 100 m displacement for western Oregon. (Note-for model validation purposes only. This is outside the bounds of the displacement regression equations).

143
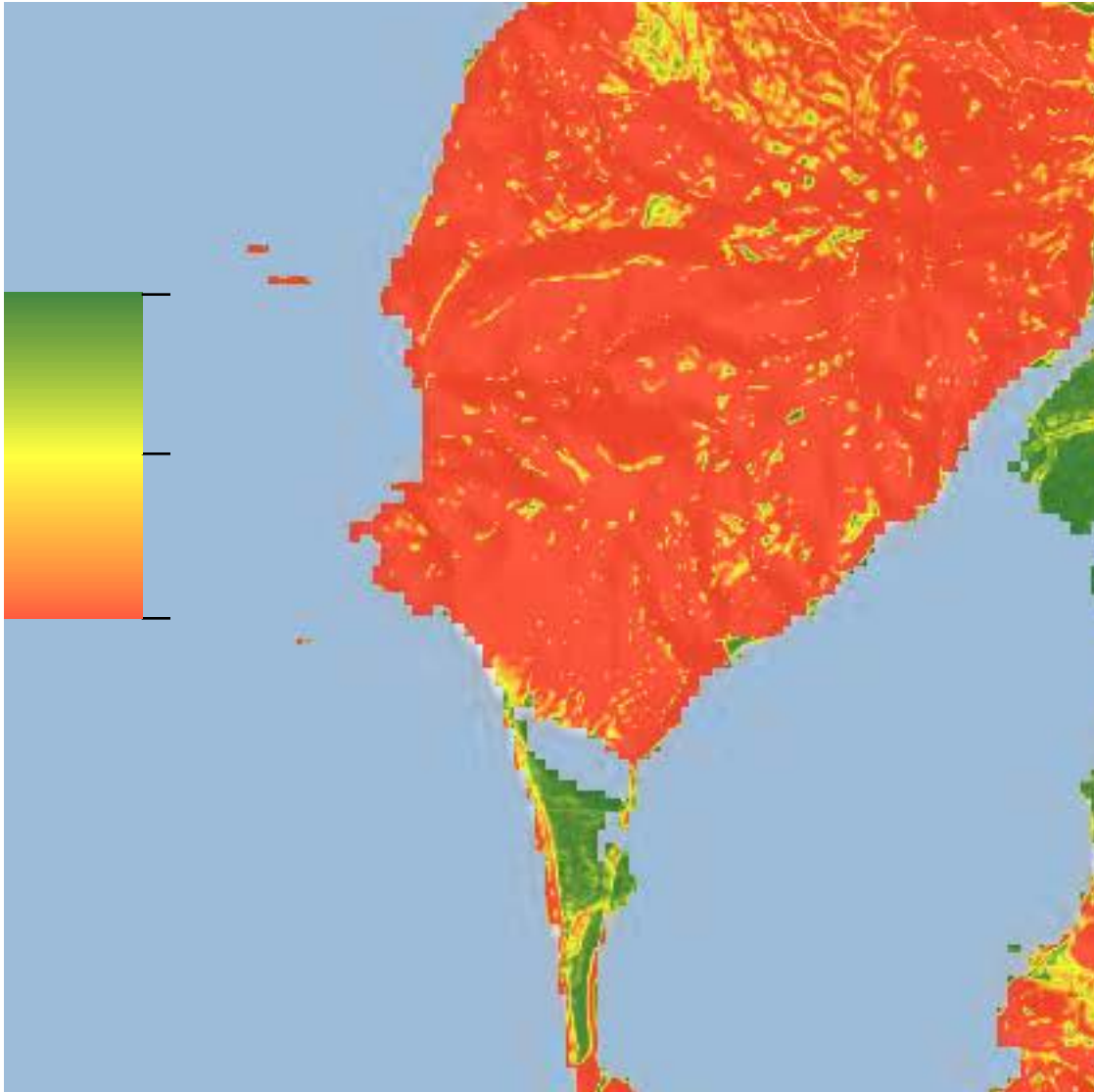
Figure 10.7: Close up maps of the Tillamook area. Note the change in symbology coloring compared to the previous maps.

Table 10.1: . Statistical parameters for displacement differences between maps based on the Ambraseys and Menu (1988) model and maps based on the Saygili and Rathje (2008) model at different thresholds.

Displacement threshold (m)	0.1	0.3	1.0	10	100
Mean	0.45	0.56	0.60	0.30	0.00027
Min	0.00	0.00	0.00	0.00	0.00000
Max	0.77	0.95	0.99	0.50	0.00045
Std.Dev	0.29	0.37	0.39	0.20	0.00018

10.1 VALIDATION

The SLIDO was used for validation of the created landslide probability map. While these landslides do not represent seismically induced landslides, they provide an indication of where landslides would be expected to occur (i.e., seismic loading will re-activate existing landslides). An ArcGIS Zonal Statistics function was used to extract the landslide triggering probability value at the locations of all landslides in SLIDO, which were classified into 5 different landslide hazard level of very low, low, medium, high and very high (Table 10.2). Almost all the reported landslides fall in the very high category. This result suggests that future landslides that would have similar characteristics within this region will be well predicted by presented hazard map. In addition, none of the landslides from the database falls in very low or low hazard level, also indicating a high accuracy for the map. The lowest calculated mean annual rate of exceedance for previously reported landslides was 0.56, which is within the medium level.

Table 10.2: Validation information of produced landslide probability map with SLIDO database.

Hazard Level	Annual Probability	#LS	Percentage
Very Low	0.0 - 0.2	0	0%
Low	0.2 - 0.4	0	0%
Medium	0.4 - 0.6	11	0.1%
High	0.6 - 0.8	4	0.04%
Very High	0.8 - 1.0	10,317	99.85%

11.0 CASCADIA SUBDUCTION ZONE SCENARIO EVENT MAPS

The code and methodology described in Chapter 9 were modified to enable the production of maps based on scenario events in addition to the fully probabilistic analysis. For these maps, the PGA estimates for a Cascadia Subduction Zone (CSZ) scenario event from the Oregon Resilience Plan (ORP) were used as input. From these, two types of maps can be created:

A deterministic map of expected displacements from a CSZ M=9.0 scenario event. For this case, the seismic hazard curve is not needed and the PGA value is simply read from the input grid, greatly simplifying the calculations. Because the deterministic process cannot incorporate a probabilistic distribution for slope strength estimates, the mean strength values were used. As such, expected displacements can be calculated by determining a_y from equation 10-1a and then displacements using a seismically induced displacement model such as the Saygili and Rathje (*Saygili and Rathje 2008*) model (equation 10-3).

Probabilistic maps of exceeding displacement thresholds given that the scenario event has occurred are another scenario option. In this case, the probability of the earthquake event (or others) are not considered (i.e., given a value of 1) and the seismic hazard curve is not used. The PGA value for each pixel is read from the input grid for the scenario event. However, the remainder of the analysis is conducted similar to the fully probabilistic maps by evaluating the probabilistic distribution of strength parameters for the lithological unit and then calculating the probabilities of exceedance.

One should note that the maps described here differ from the maps in Chapter 10 because: 1) They do not consider all known events and hazards in the analysis, just the scenario event, and 2) They do not consider the probability of the event occurring, but rather assume the event will happen. Hence, they will produce much higher values when compared to the fully probabilistic maps in Chapter 10. The maps in Chapter 10 are important to relate the seismically induced landslide hazard in context with other hazards within a given time window; whereas, the maps in this chapter are useful to evaluate the damage potential assuming the scenario earthquake happens.

A similar process can be used for other types of scenario events provide that a PGA grid incorporating site effects for the scenario has been created. For example, one could run additional events based on 2% in 50 year or 10% in 50 year events.

11.1 OUTPUT MAPS AND DISCUSSION

Figure 11.1 presents the estimated displacement map produced by this study, given a CSZ scenario event. Note that the general map patterns are similar to the results of the Oregon Resilience Plan map created in HAZUS. The map in this study shows higher amounts of displacement in the Willamette Valley and the cascades in the Eastern portion of the study area.

For the displacement bins used in Figure 11.1, the map for this study is showing banding due to ground motions. The ORP map also shows this banding, if different displacement bins are used

Figures 11.2 to 11.7 show the probabilities of exceeding 0.1, 0.3, 1.0, 10.0, and 100.0 m given a CSZ M9.0 scenario event. Note that a progression of decreasing probabilities is observed. The 10m and 100 m models are provided for validation purposes only and are outside the bounds of the Saygili and Rathje model regression equations.

Note that for display purposes, the map values are categorized into bins. However, within each bin, there is a continuous set of values in the computed results.
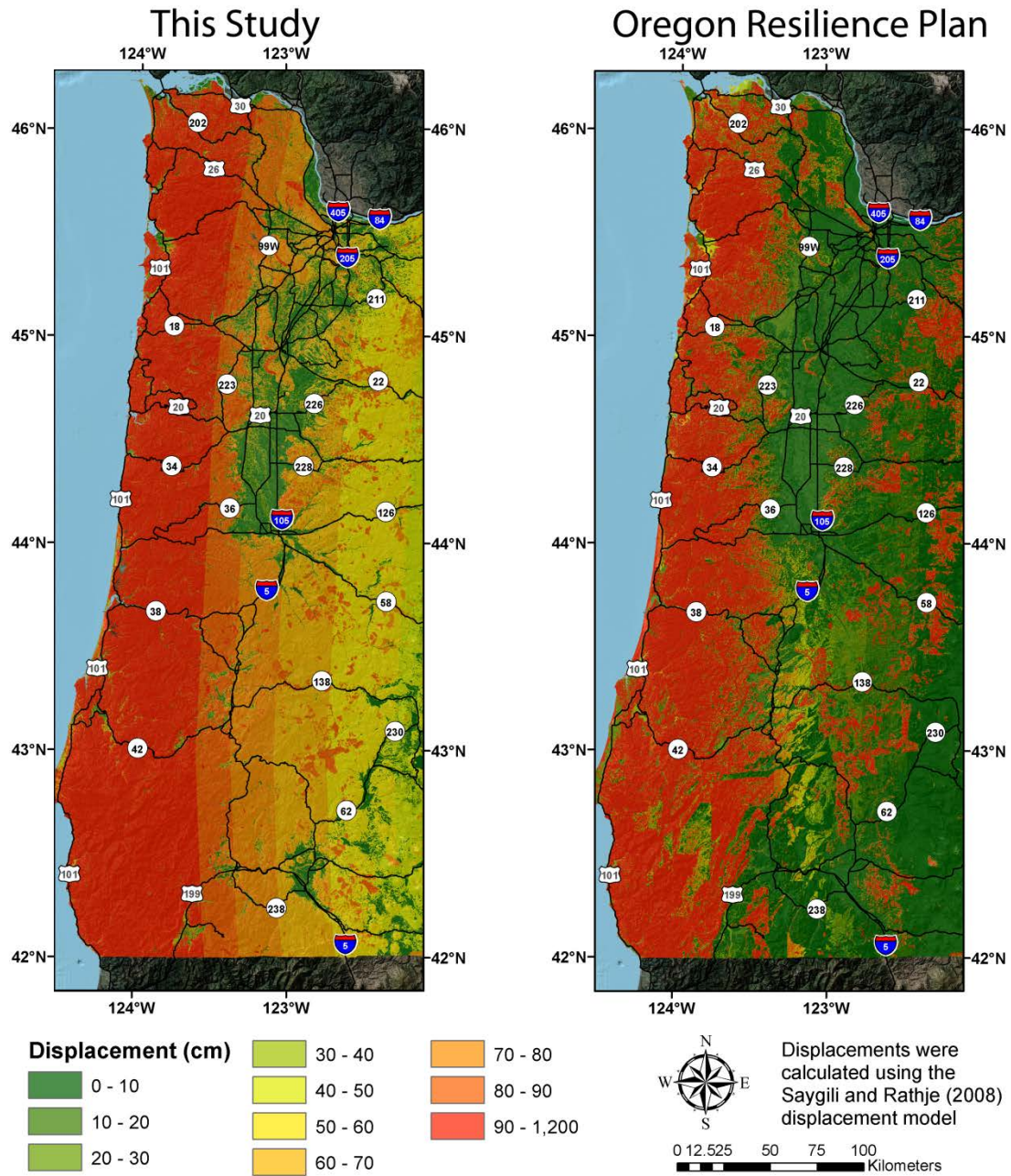
Figure 11.1: Estimated slope displacements for a M9.0 CSZ scenario event from (Left) this analysis and (Right) from the Oregon Resilience Plan

CSZ M9.0 Scenario Probabilistic

Displacements were calculated using the Saygili and Rathje (2008) displacement model

Note this map calculates the probability of exceeding a threshold displacement given a M9.0 CSZ scenario event.

0 12.5 25   50   75   100
Kilometers

Legend

Landslide Susceptibility

- 0.0 - 0.1
- 0.1 - 0.2
- 0.2 - 0.3
- 0.3 - 0.4
- 0.4 - 0.5
- 0.5 - 0.6
- 0.6 - 0.7
- 0.7 - 0.8
- 0.8 - 0.9
- 0.9 - 1.0
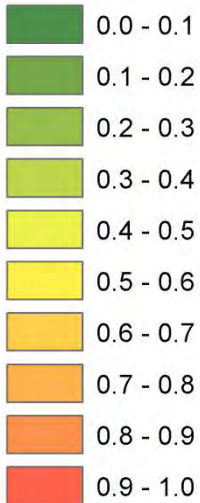
Note that the last bin Increment may be larger than the other bins.
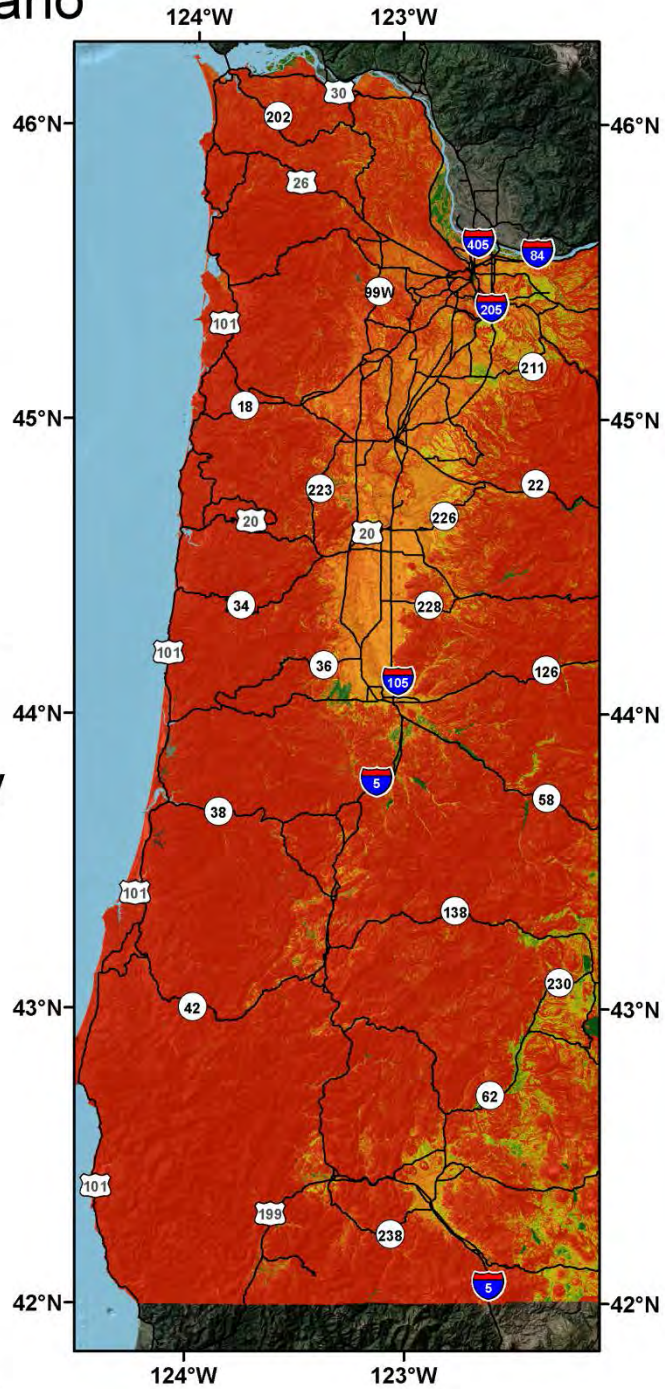
Figure 11.2: Probability of landslide occurrence for a M9.0 CSZ scenario event.

149

CSZ M9.0 Scenario Probabilistic

Displacements were calculated using the Saygili and Rathje (2008) displacement model

Note this map calculates the probability of exceeding a threshold displacement given a M9.0 CSZ scenario event.

0 12.5 25   50   75   100
Kilometers

Legend

P(DL>0.1 m)

- 0.0 - 0.1
- 0.1 - 0.2
- 0.2 - 0.3
- 0.3 - 0.4
- 0.4 - 0.5
- 0.5 - 0.6
- 0.6 - 0.7
- 0.7 - 0.8
- 0.8 - 0.9
- 0.9 - 1.0
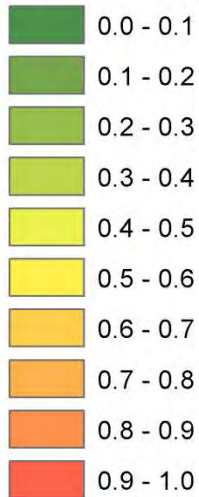
Note that the last bin Increment may be larger than the other bins.
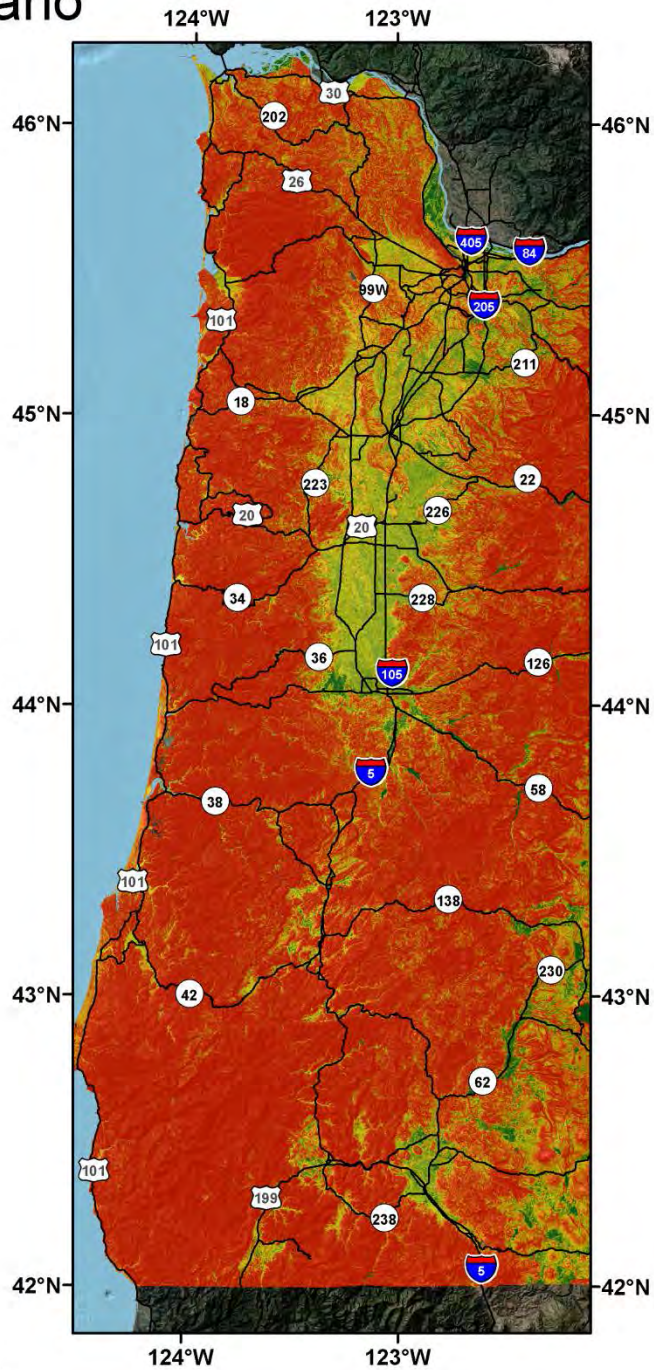
Figure 11.3: Probability of slope displacement exceeding 10 cm for a M9.0 CSZ scenario event.

150

CSZ M9.0 Scenario Probabilistic

Displacements were calculated using the Saygili and Rathje (2008) displacement model

Note this map calculates the probability of exceeding a threshold displacement given a M9.0 CSZ scenario event.

0 12.5 25   50   75   100
Kilometers

Legend

P(DL>0.3 m)

	0.0 - 0.1
	0.1 - 0.2
	0.2 - 0.3
	0.3 - 0.4
	0.4 - 0.5
	0.5 - 0.6
	0.6 - 0.7
	0.7 - 0.8
	0.8 - 0.9
	0.9 - 1.0
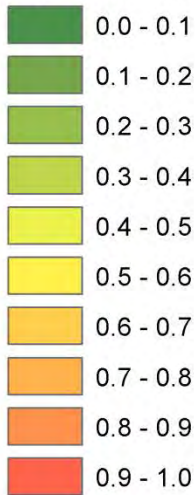
Note that the last bin Increment may be larger than the other bins.
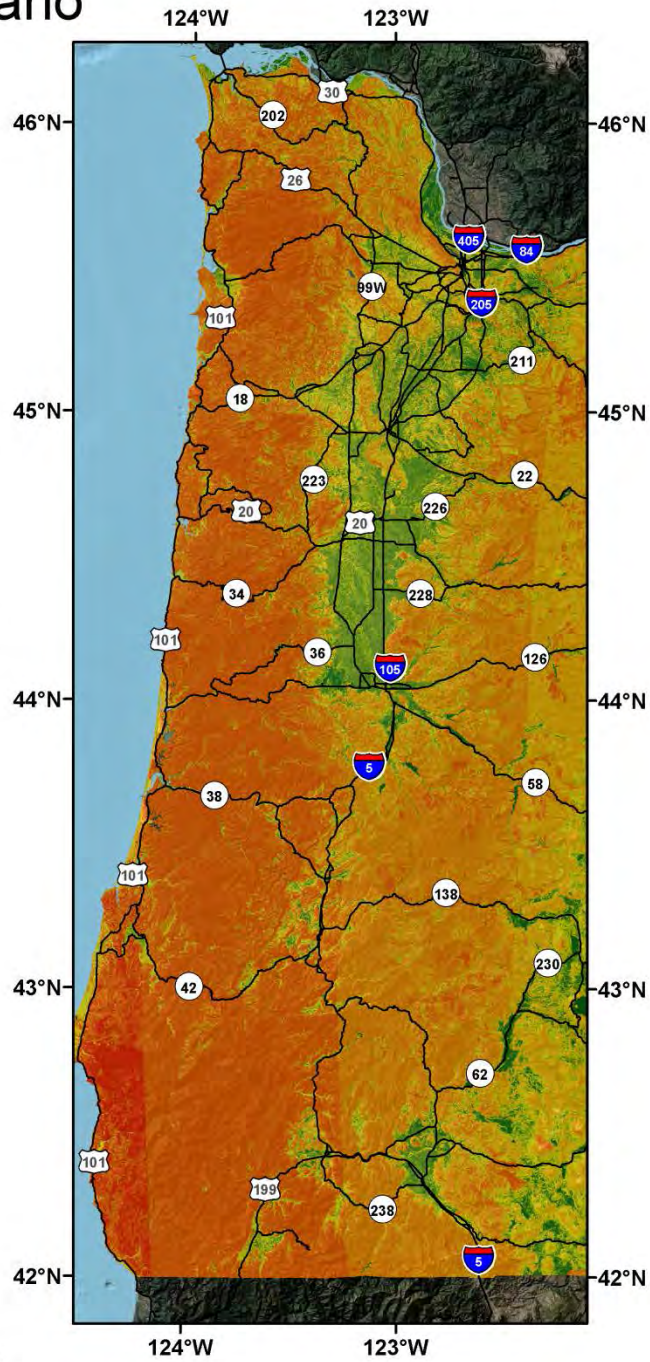
Figure 11.4: Probability of slope displacement exceeding 30 cm for a M9.0 CSZ scenario event.

Figure 11.5: Probability of slope displacement exceeding 1 m for a M9.0 CSZ scenario event.

CSZ M9.0 Scenario Probabilistic

Displacements were calculated using the Saygili and Rathje (2008) displacement model

Note this map calculates the probability of exceeding a threshold displacement given a M9.0 CSZ scenario event.

0 12.5 25   50   75   100
Kilometers

Legend

P(DL>10 m)

- 0.0000 - 0.0030
- 0.0031 - 0.0060
- 0.0061 - 0.0090
- 0.0091 - 0.0120
- 0.0121 - 0.0150
- 0.0151 - 0.0180
- 0.0181 - 0.0210
- 0.0211 - 0.0240
- 0.0241 - 0.0270
- 0.0271 - 0.0427
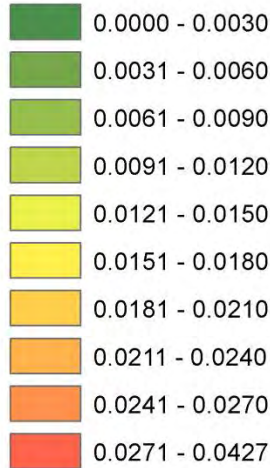
Note that the last bin Increment may be larger than the other bins.
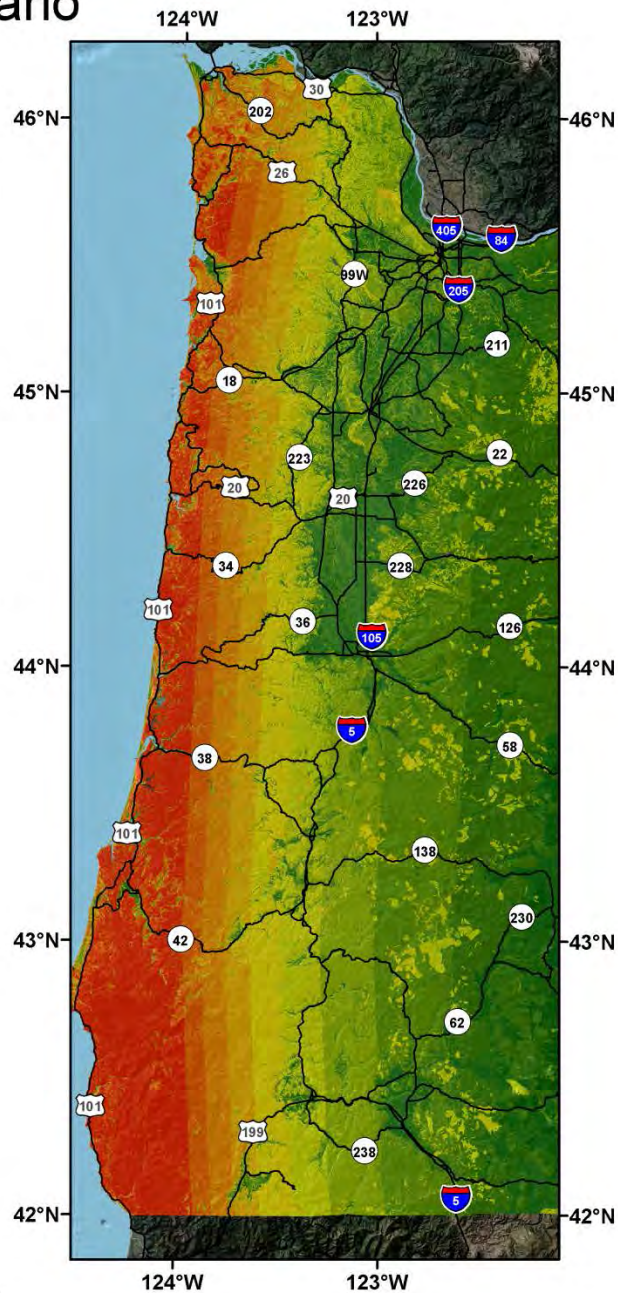
Figure 11.6: Probability of slope displacement exceeding 10 m for a M9.0 CSZ scenario event. (Note the change in scale from 0 to 0.1 compared to the previous figures. Also, this map is provided for validation purposes only and is outside the bounds of the SR regression equation).

153
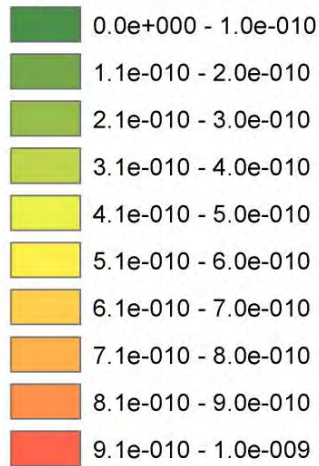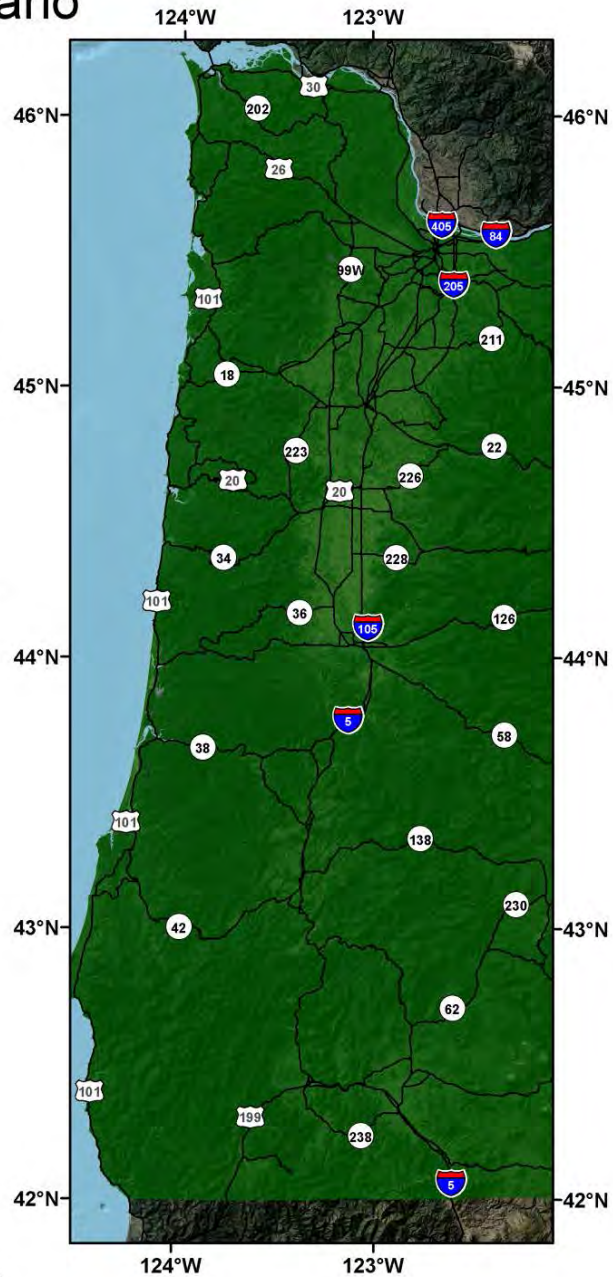
Figure 11.7: . Probability of slope displacement exceeding 100 m for a M9.0 CSZ scenario event. Also, this map is provided for validation purposes only and is outside the bounds of the SR regression equation).

12.0 CONCLUSIONS

12.1 RECOMMENDED MAPS

Several maps were created for this study using a variety of methodologies (multivariate, frequency ratio, MAXENT, and fully probabilistic) and show significant similarities. However, the recommend maps for general use by ODOT are the fully probabilistic maps using Saygili and Rathje's (*Saygili and Rathje 2008*) displacement methodology presented in Chapter 10 for 0.1 m, 0.3m, and 1.0 m displacements. When it is desired to consider a CSZ scenario event, the maps in Chapter 11 for the same displacement thresholds should be used. The other maps are presented in this report solely for validation purpose. Note that these displacements are predicted displacements for the slope itself and are not intended to represent dislodged material, which can spread over a much larger distance affecting a greater area.

12.2 OREGON'S SITUATION

The chronic, widespread nature of landslide movements within the state of Oregon is of extreme concern, particularly when exacerbated by seismic activity. While the soil strength estimate approach may be conservative (e.g. slope after failure will be less than slope prior to failure when FS = 1), it agrees well with recent map analyses by DOGAMI using LIDAR technology, which has led to the discovery of many new landslides (*Madin and Burns 2006a and 2006b*). Similar findings of significant slope displacements were found in the Oregon Resilience Plan.

The Cascadia subduction zone plate boundary is located within approximately 90 km of the coast and is capable of creating large magnitude earthquakes with return period of 300 to 500 years. Given that the last occurrence of such an earthquake was in January of 1700, it is essential to prepare and reinforce vital structures, utilities, and lifeline corridors in high probability landslide hazard areas.

12.3 METHODOLOGY FINDINGS

Overall, the multivariate techniques did not perform well for the study area and had a substantial amount of uncertainty. However, the multivariate techniques were useful to fine-tune the most significant parameters.

LIDAR data proved very helpful when determining slopes at landslide locations for estimates of strength parameters. The Hybrid DEM, which contained a significant amount of LIDAR data, resulted in histograms that were closer to a normal distribution, had less variance, and typically estimated slightly higher friction angles compared to ASTER and NED DEMs.

A very significant limitation of performing a regional landslide assessment is the collection of accurate, detailed data. It is quite challenging to use available data and systematically evaluate stability analysis and incorporate site-specific displacement regression models into regional analyses. Regional assessments often require simplifying assumptions and procedures for analysis due to limitations in available data compared to site investigations, which can be much more rigorous, detailed and account for a wide range of factors. The methodology presented herein takes analyses (e.g. using the full seismic hazard curve, Saygili and Rathje (*Saygili and Rathje 2008*)) displacement model) that are typically only done for local site investigations and applies them to a regional scale.

12.4 APPROPRIATE USE OF METHODOLOGY AND MAPS

It is critical to note that at the time of application, values from these maps should not be used for engineering design in site-specific projects, but rather as a relative screening criterion for when more detailed site investigations and design analyses should be completed. Further, earthquake-shaking characteristics (e.g. peak ground accleeration and arias intensity or predominant period) are important parameters. The actual motions in Oregon might differ from the input motions used in empirical predictive displacement models, which will result in aleatory variability. Finally, the methodology was shown to produce results consistent with the best available landslide inventories for comparison.

The developed map series can be used in disaster management to minimize damages from the landslide hazard in the State of Oregon. For example, Oregon DOT will use the results of this study, in conjunction with consideration of other variables, to determine priority lifeline corridors for resource allocation. The probabilistic nature of these maps enables them to be combined with other hazards for a more complete hazard analysis.

12.5 FUTURE WORK

This project has created the groundwork for additional research that will lead to additional insights regarding seismically induced landslides in Oregon. Several improvements can be made to the methodology, which was designed to be expandable. One can include other factors (e.g., probability of increased groundwater levels leading to instability, probability of rainfall intensity or duration exceeding thresholds, etc.). In addition, some geologic units could be quantified separately from the general lithological units. Further analysis of appropriate DEM cell size (as well as other data sources) would also help refine the results.

New data are continually available for use in the analysis. Because the approach is modular, as these new data are available, new maps can be readily generated. In particular, the maps should be updated periodically to include:

1. Updated landslide inventories. In particular, in addition to knowing the location of landslides, it would be most helpful to have recorded displacements to correlate with the parameters analyzed in this study.

2. Newly acquired LIDAR topographic data that are continually being collected throughout the state.

3. The USGS will release new seismic hazard curves that incorporate results from recent earthquakes (Chile and Japan) for improved subduction zone modeling as well as insights on the CSZ from recent scientific research. These efforts will include new ground motion prediction equations, directivity, directionality of ground motions, and new site amplification recommendations.

4. New displacement prediction models, particularly ones developed using landslide databases (e.g., *Wartman et al. 2013*) from recent subduction zone earthquakes.

5. Improved strength estimation for lithological units achieved through repeating the process over a larger landslide database containing landslides reported all over the state rather than solely in the western Oregon. Further, field-testing to obtain in-situ strength parameters on sliding planes would help reduce uncertainty.

6. As more data are available to quantify parameters for more generalized geologic units rather than the lithological units, the maps can be improved. This will improve the strength estimation discussed in (5).

The probabilistic seismic hazard routines written in C++ can be also implemented consistently in other locales where similar datasets are available. (Note that most of the required input datasets are available, albeit with varying data quality, across the US). The code also has the capability to run any number of scenario events (e.g. CSZ M9.0, PGA with 2% probability of exceedance in 50 years, PGA with 10% probability of exceedance in 50 years, etc.).

The regional mapping approach could also be scaled down to evaluate a corridor in more detail using technologies such as mobile LIDAR. Future research can evaluate change detection capabilities of ODOT's mobile LIDAR system to begin to quantify the magnitudes of displacements observed near roadways with landslides.

This methodology and the results can also be integrated into a multi-hazard probabilistic framework that considers all likely ground deformation together. For example, Olsen *(Olsen 2005)* and Gillins (*Gillins 2012*) describe a related procedure for probabilistic liquefaction and lateral spread analysis and mapping.

Future work should test the methodology in areas with historic seismic-induced landslides where inventories have been compiled to see how well it compares with landslides that are known to be co-seismic for a more thorough evaluation. For example, Wartman et al. (*Wartman et al. 2013*) recently released a landslide inventory for Japan.

Finally, to-date, few studies exist to determine whether these existing landslides in Oregon are predominately triggered from earthquake or precipitation events. Limited information are available to know whether these large, deep-seated landslides will be reactivated by earthquakes, erosion, or precipitation. Research is needed to isolate the relative contribution of seismic, erosion, and precipitation sources to triggering existing and potential landslides in western Oregon.

13.0 REFERENCES

Acharya, G., T. Cochrane, T. Davies, and E. Bowman. Quantifying and Modeling Post-Failure Sediment Yields from Laboratory-Scale Soil Erosion and Shallow Landslide Experiments with Silty Loess. *Geomorphology*, Vol. 129, No. 1, 2011, pp. 49-58.

Adinarayana, J., K. Gopal Rao, N. Rama Krishna, P. Venkatachalam, and J. Suri. A Rule-Based Soil Erosion Model for a Hilly Catchment. *Catena*, Vol. 37, No. 3, 1999, pp. 309-318.

Aleotti, P., P. Baldelli, and G. Polloni. Landsliding and Flooding Event Triggered by Heavy Rains in the Tanaro Basin (Italy). In. Procedures International Symposium Interpraevent, 1996.

Aleotti, P., and R. Chowdhury. Landslide Hazard Assessment: Summary Review and New Perspectives. *Bulletin of Engineering Geology and the Environment*, Vol. 58, No. 1, 1999, pp. 21-44.

Ambraseys, N., and J. Menu. Earthquake-Induced Ground Ddisplacements. *Earthquake Engineering & Structural Dynamics*, Vol. 16, No. 7, 1988, pp. 985-1006.

An, P., W.M. Moon, and A. Rencz. Application of Fuzzy Settheory for Integration of Geological, Geophysical and Remote Sensing Data, *Canadian Journal of Exploration Geophysics*, Vol. 27, No. 1, 1991, pp. 1–11.

Ashford, S. A., and N. Sitar. Analysis of Topographic Amplification of Inclined Shear Waves in a Steep Coastal Bluff. *Bulletin of the Seismological Society of America*, Vol. 87, No. 3, 1997, pp. 692-700.

Atkinson, P., and R. Massari. Generalised Linear Modelling of Susceptibility to Landsliding in the Central Apennines, Italy. *Computers & Geosciences*, Vol. 24, No. 4, 1998, pp. 373-385.

Barnett, E., C. Weaver, K. Meagher, Z. Wang, I. Madin, M. Wang, R.A. Haugerud, R.E. Wells, D.B. Ballantyne, M. Darienzo, and S.W.V.W. Group. *Lifelines and Earthquake Hazards along the Interstate 5 Urban Corridor: Cottage Grove to Woodburn, Oregon*. USGS Open File Report 2001-1052, 2004.

Bartsch, K., H. Van Miegroet, J. Boettinger, and J. Dobrowolski. Using Empirical Erosion Models and GIS to Determine Erosion Risk at Camp Williams, Utah. *Journal of Soil and Water Conservation*, Vol. 57, No. 1, 2002, pp. 29-37.

Bathurst, J., G. Moretti, A. El-Hames, A. Moaven-Hashemi, and A. Burton. Scenario Modelling of Basin-Scale, Shallow Landslide Sediment Yield, Valsassina, Italian Southern Alps. *Natural Hazards and Earth System Science*, Vol. 5, No. 2, 2005, pp. 189-202.

Bela, J.L. Geologic Hazards of Eastern Benton County, Oregon. *DOGAMI Bulletin - State of Oregon,* Vol. 98, 1979. p. 122.

Belsius, L. and F. Weirich. The Use of the Minnaert Correction for Land Cover Classification in Mountainous Terrain. *International Journal of Remote Sensing*, Vol. 26, 2005. pp. 3831-3851.

Bishop, A.W. The Use of the Slip Circle in the Stability Analysis of Slopes. *Geotechnique*, Vol. 5, No. 1, 1955, pp. 79-79.

Bishop, D.M., and M.E. Stevens. *Landslides on Logged Areas in Southeast Alaska*. Northern Forest Experiment Station, Juneau, Alaska, Forest Service, US Department of Agriculture, 1964.

Bonham-Carter, G.F. *Geographical Information Systems for Geoscientists: Modeling with GIS*. Pergamon Press, Tarrytown, NY 1994.

Boore, D.M., and G.M. Atkinson. Ground Motion Prediction Equations for the Average Horizontal Component of PGA, PGV, and 5%-Damped PSA at Spectral Periods between 0.01s and 10.0s. *Earthquake Spectra*, Vol. 24, No. 1, 2008, pp. 99-138.

Borchardt, G. *Preparation and Use of Earthquake Planning Scenarios*. California Department of Mining and Geology, 1998.

Boston.com. *Landslides strike Zhouqu County, China*. 2010 http://www.boston.com/bigpicture/2010/08/landslides_strike_zhouqu_count.html. August 13, 2010.

Bray, J.D., and E.M. Rathje. Earthquake-Induced Displacements of Solid-Waste Landfills. *Journal of Geotechnical and Geoenvironmental Engineering*, Vol. 124, No. 3, 1998, pp. 242-253.

Bray, J.D., and T. Travasarou. Simplified Procedure for Estimating Earthquake-Induced Deviatoric Slope Displacements. *Journal of Geotechnical and Geoenvironmental Engineering*, Vol. 133, No. 4, 2007, pp. 381-392.

Bruyninckx, H. *Bayesian Probability*. 2002, p. 36. www.**stats**.org.uk/**bayesian**/**Bruyninckx**2002.pdf. Accessed 2013

Burns, S.F., W.J. Burns, D.H. James, and J.C. Hinkle. *Landslides in the Portland, Oregon Metropolitan Area Resulting from the Storm of February 1996: Inventory Map, Database and Evaluation*. Report prepared as fulfillment of Metro contract, Vol. 905828, 1998.

Burns, W.J. Comparison of Mapping Techniques in the Portland Hills Pilot Study Area. In 2007 Landslide Symposium Proceedings and Field Trip Guide, Oregon Department of Geology and Mineral Industries, Open File Report O-07-04. 2007.

Burns, W.J., K.A. Mickelson, and E.C. Saint- Pierre. Landslide Inventory Maps of the Southern Half of the Pittsburg Quadrangle, Columbia County, Oregon IMS-55, 2013.

Burns, W.J., K.A. Mickelson, and E.C. Saint- Pierre. Landslide Inventory Maps of the Northern Half of the Vernonia Quadrangle, Columbia County, Oregon Interpretive Map Series-54, 2013.

Burns, W.J., K.A. Mickelson, and E.C. Saint-Pierre. *Statewide Landslide Information Database for Oregon Release 2 (SLIDO-2), Scale 1: 750,000*. Department of Geology and Mineral Industries, 2012.

Burns, W.J., K.A. Mickelson, S. Duplantis, and K. Williams, Landslide Inventory Maps of the Forest Grove Quadrangle, Washington County, Oregon., Interpretive Map Series-39, 2012, 4 Plates.

Burns, W.J., S. Duplantis, K.A. Mickelson, J.M. Spritzer, and R.E. Wells, Landslide Inventory Maps of the Gales Creek Quadrangle, Washington County, Oregon. Oregon Department of Geology and Mineral Industries, Portland, Oregon, Interpretive Map Series-46, Scale 1:8000, 2012.

Burns, W.J., K.A. Mickelson, S. Duplantis, and I.P. Madin. Landslide Inventory Maps of the Dixie Mountain Quadrangle, Washington, Multnomah, and Columbia Counties. Oregon Department of Geology and Mineral Industries, Portland, Oregon, Interpretive Map Series-44, Scale 1:8000, 2012.

Burns, W.J. and K.A. Mickelson, Landslide Inventory Maps of the Astoria Quadrangle, Clatsop County, Oregon. Interpretive Map Series-31, 2010,

Burns, W.J., I.P. Madin, and L. Ma. Statewide Landslide Information Database of Oregon (SLIDO)-Release 1. In 2008 Joint Meeting of The Geological Society of America, Soil Science Society of America, American Society of Agronomy, Crop Science Society of America, Gulf Coast Association of Geological Societies with the Gulf Coast Section of SEPM, 2008.

Burns, W.J., and I.P. Madin. *Protocol for Inventory Mapping of Landslide Deposits from Light Detection and Ranging (Lidar) Imagery*. DOGAMI, Special Paper 42, 2009.

Capolongo, D., A. Refice, and J. Mankelow. Evaluating Earthquake-Triggered Landslide Hazard at the Basin Scale through GIS in the Upper Sele River Valley. *Surveys in Geophysics*, Vol. 23, No. 6, 2002, pp. 595-625.

Carrara, A. Multivariate Models for Landslide Hazard *Evaluation. Journal of the International Association for Mathematical Geology*, Vol. 15, No. 3, 1983, pp. 403-426.

Carrara, A., M. Cardinali, R. Detti, F. GuzzettI, V. Pasqui, and P. Reichenbach. Geographical Information Systems and Multivariate Models in Landslide Hazard Evaluation. *Alps*, Vol. 90, 1990, pp. 17-28.

162

Carrara, A. Digital Terrain Analysis for Land Evaluation. *Geologia Applicata e Idrogeologia*, Vol. 13, 1978, pp. 69-127.

Carrara, A. Landslide Morphometry and Typology in Two Zones, Calabria, Italy. *Bulletin of the International Association of Engineering Geology-Bulletin de l'Association Internationale de Géologie de l'Ingénieur*, Vol. 16, No. 1, 1977, pp. 8-13.

CGS. California Geological Survey. Recommended Criteria for Delineating Seismic Hazard Zones in California, Special Publication 118, *California Geological Survey*, Vol. 118, 2004, 12 pages.

CH2M-Hill. Seismic Lifelines Evaluation, Vulnerability Synthesis, and Identification. *Lifeline Selection Summary Report*, 2012.

Charalambous, S. *Programming the Wedge Failure Mode and Rock Fall in a GIS Environment*. Master's of Science Thesis, National Technical University of Athens, 2006.

Chung, C.J.F., and A.G. Fabbri. Validation of Spatial Prediction Models for Landslide Hazard Mapping. *Natural Hazards*, Vol. 30, No. 3, 2003, pp. 451-472.

Chung, C.J.F., and A.G. Fabbri. Probabilistic Prediction Models for Landslide Hazard Mapping. *Photogrammetric Engineering and Remote Sensing,* Vol. 65, No.12, 1999, pp. 1389-1399.

Convertino, M., A. Troccoli, and F. Catani. Detecting Fingerprints of Landslide Drivers: A Maxent Model. *Journal of Geophysical Research*, Vol. 118, 2013, pp. 1-20.

Cornforth, D. *Landslides in Practice: Investigations, Analysis, and Remedial/Preventive Options in Soils*. John Wiley and Sons, 2005.

Craig, R.F. *Craig's Soil Mechanics*. Spon Press, Taylor and Francis, London, UK, 1997.

Crespo, E., K.J. Nyman, and T.D. O'Rourke. Ecuador Earthquakes of March 5, 1987. *EERI Special Report* No. 4., 1987.

Cruden, D. M., and D. J. Varnes. Landslide Types and Processes. *Landslides: Investigation and Mitigation,* Vol. 247, 1996, pp. 36-75.

Dai, F., and C. Lee. Landslide Characteristics and Slope Instability Modeling Using GIS, Lantau Island, Hong Kong. *Geomorphology*, Vol. 42, No. 3, 2002, pp. 213-228.

Dai, F., C. Lee, and X. Zhang. GIS-Based Geo-Environmental Evaluation for Urban Land-Use Planning: A Case Study. *Engineering Geology*, Vol. 61, No. 4, 2001, pp. 257-271.

DeGraff, J.V., and P. Canuti. Using Isopleth Mapping to Evaluate Landslide Activity in Relation to Agricultural Practices. *Bulletin of the International Association of Engineering Geology-Bulletin de l'Association Internationale de Géologie de l'Ingénieur*, Vol.38, No.1, 1998, pp. 61-71.

Densham, P.J. Spatial Decision Support Systems. *Geographical Information Systems: Principles and Applications*, Vol. 1, 1991, pp. 403-412.

Clark, L., How Many Earthquakes Occur in Oregon Over a Year, and Where? Oregon Geology, *Oregon Department of Geology and Mineral Industries*, Vol. 61, No. 5, 1999, pp. 127.

EM-DAT. *Em-dat: The Ofda\Cred International Disaster Database*. Université catholique de Louvain – Brussels – Belgium. 2013. www.emdat.be. Accessed 2013.

Endo, T., and T. Tsuruta. *The Effect of the Tree's Roots upon the Shear Strength of Soil*. 1968 Annual Report of the Hokkaido Branch, Forest Exp. Sta., 1969. pp. 157-182.

Erener, A., and H.S.B. Düzgün. Analysis of Landslide Hazard Mapping Methods: Regression Models versus Weight Rating. XXIst ISPRS Congress 2008; 3–11 July. Beijing, China. Commission VIII papers, Vol. 21, No. B8, 2008, pp. 1682-1750.

Erickson, G.L. *Probabilistic Liquefaction Potential Mapping of Salt Lake Valley, Utah*. In Civil and Environmental Engineering, Masters of Science Thesis, University of Utah, 2006.

Espinosa, A., J. Egred, M. Garcla-Lopez, and E. Crespo. Intensity and Damage Distribution. *The March 5, 1987, Ecuador Earthquakes: Mass Wasting and Socioeconomic Effects*, Vol. 5, 1991, p. 42.

ESRI. *ArcGIS Release 10 Desktop Help*. New York Street, Redlands, California, USA. 2011.

Fabbri, A.G., C.-J.F. Chung, A. Cendrero, and J. Remondo. Is Prediction of Future Landslides Possible with a GIS? *Natural Hazards*, Vol. 30, No. 3, 2003, pp. 487-503.

Ferentinou, M., M. Sakellariou, V. Matziaris, and S. Charalambous. An Introduced Methodology for Estimating Landslide Hazard for Seismic and Rainfall Induced Landslides in a Geographical Information System Environment. Proceedings of Geohazards, Engineering Conferences International, Paper 40, 2006, p. 9.

Fernandes, N.F., R.F. Guimarães, R.A.T. Gomes, B.C. Vieira, D.R. Montgomery, and H. Greenberg. Topographic Controls of Landslides in Rio de Janeiro: Field Evidence and Modeling. *Catena*, Vol. 55, No. 2, 2004, pp. 163-181.

Floris, M., M. Mari, R.W. Romeo, and U. Gori. *Modelling of Landslide-Triggering Factors-A Case Study in the Northern Apennines, Italy*. Engineering Geology for Infrastructure Planning in Europe, Springer, 2004. pp. 745-753.

Fujiwara, K. A Study on the Landslides by Aerial Photographs. *Research Bulletin of the College Experimental Forests*, College of Agriculture, Hokkaido University, Vol. 27, No. 2, 1970, pp. 297-345.

Garrett, J. Where and Why Artificial Neural Networks are Applicable in Civil Engineering. *Journal of Computing In Civil Engineering*, Vol. 8, No. 2, 1994, pp. 129-130.

GEER. *Geotechnical Extreme Events Reconnaissance: Turning Disaster into Knowledge.* 2013. http://www.geerassociation.org/. Accessed 2013

Gesch, D., M. Oimoen, S.reenlee, C. Nelson, M. Steuck, and D. Tyle. The National Elevation Dataset. *Photogrammetric Engineering and Remote Sensing*, Vol. 68, No. 1, 2002, pp. 5-11.

Gesch, D.B. Digital Elevation Model Technologies and Applications: The Dem Users Manual. *American Society for Photogrammetry and Remote Sensing*, Vol. 2, 2007, pp. 99-118.

Gillins, D.T. Mapping the Proability and Uncertainty of Liquefaction-Induced Ground Failure. PhD Dissertation *Civil and Environmental Engineering*, University of Utah, 2012.

Goldfinger, C., C.H. Nelson, A.E. Morey, J.E. Johnson, J. Patton, E. Karabonov, J. Gutierrez-Pastor, and A.T. Eriksson. *Turbidite Event History: Methods and Implications for Holocene Paleoseismicity of the Cascadia Subduction Zone*. USGS, Open File Report 1661-F, 2012. p. 170.

Gordon, P., J.E. Moore II, H.W. Richardson, M. Shinozuka, D, An, and S. Cho. *Earthquake Disaster Mitigation for Urban Tranportation Systems: An Integrated Methodology that Builds on the Kobe and Northridge Experiences*. Modeling Spatial and Economic Impacts of Disasters, Y. Okuyama and S.E. Chang. Editors, 2004, pp 205-232

Gorsevski, P.V., P. Gessler, and R.B. Foltz. Spatial Prediction of Landslide Hazard using Logistic Regression and GIS. 4th International Conference on Integrating GIS and Environmental Modeling (GIS/EM4). 2000.

Graham, J. Methods of Stability Analysis. *Slope Instability*, D. Brunsden and D.B. Prior, Editors., New York, Wiley & Sons, 1984, pp. 171-215.

Greenwood, J.R., J.E. Norris, and J. Wint. Assessing the Contribution of Vegetation to Slope Stability. *ICE - Geotechnical Engineering*, No. 157, 2004. pp. 199-207.

Guzzetti, F., A. Carrara, M. Cardinali, and P. Reichenbach. Landslide Hazard Evaluation: A Review of Current Techniques and Their Application in a Multi-Scale Study, Central Italy. *Geomorphology*, Vol. 31, No. 1, 1999, pp. 181-216.

Guzzetti, F., P. Reichenbach, M. Cardinali, M. Galli, and F. Ardizzone. Probabilistic Landslide Hazard Assessment at the Basin Scale. *Geomorphology,* Vol. 72, No. 1, 2005, pp. 272-299.

Hammond, C.M., P. Reichenback, M. Cardinali, M. Galli, and F. Ardizzone. Paleo-Landslides in the Tyee Formation and Highway Construction, Central Oregon Coast Range. *Guides*, 2009, pp. 481-494.

Haneberg, W.C. Effects of Digital Elevation Model Errors on Spatially Distributed Seismic Slope Stability Calculations: An Example from Seattle Washington. *Environmental & Engineering Geoscience*, Vol. 12, 2006, pp. 247-260.

Haneberg, W.C., R.L. Burk, D.P. Findley, and N.I. Norrish. Virtual Structural Mapping using 3-D Digital Rock Slope Models, I-90 near Snoqualmie Pass Washington. *Geological Society of America Abstract Program*, No. 39, Geological Society of America, 2007. p. 24.

Haneberg, W.C., W.F. Cole, and G. Kasali. High-Resolution Lidar-Based Landslide Hazard Mapping and Modeling, UCSF Parnassus Campus, San Francisco, USA. *Bulletin of Engineering Geology and the Environment*, Vol. 68, No. 2, 2009, pp. 263-276.

Harp, E.L., and R.W. Jibson. Landslides Triggered by the 1994 Northridge, California, Earthquake. *Bulletin of the Seismological Society of America*, Vol. 86, No. 1B, 1996, pp. S319-S332.

Harp, E.L., D.K. Keefer, H.P. Sato, and H. Yagi. Landslide Inventories: The Essential Part of Seismic Landslide Hazard Analyses. *Engineering Geology*, Vol. 122, No. 1, 2011, pp. 9-21.

Harvey, A., and G. Peterson. Water-Induced Landslide Hazards: Western Portion of the Salem Hills. Marion County, Oregon, Oregon Department of Geology and Mineral Industries Interpretive Map Series IMS-6, 1998.

Harvey, A.F., and G.L. Peterson. Eastern Portion of the Eola hills, Polk County, Oregon. 2000.

Havenith, H.B., M. Vanini, D. Jongmans, and E. Faccioli. Initiation of Earthquake-Induced Slope Failure: Influence of Topographical and Other Site Specific Amplification Effects. *Journal of Seismology*, Vol. 7, No. 3, 2003, pp. 397-412.

Heynekamp, M.R., L.B. Goodwin, P.S. Mozley, and W.C. Haneberg. Controls on Fault-Zone Architecture in Poorly Lithified Sediments, Rio Grande Rift, New Mexico: Implications for Fault-Zone Permeability and Fluid Flow. *Geophysical Monograph*, Vol. 113, 1999, pp. 27-50.

Highland, L., and P.T. Bobrowsky. The Landslide Handbook: A Guide to Understanding Landslides. *USGS Circular* 1325, USGS, Reston, VA, USA, 2008. p. 129.

Hofmeister, R.J., C.S. Hasenberg, I.P. Madin, and W. Yumei. *Relative Earthquake and Landslide Hazards in Clackamas County*. DOGAMI Open File Report O-03-10, 2003.

Hofmeister, R.J., D.J. Miller, K.A. Mills, J.C. Hinkle, and A.E. and Beie. *GIS Overview of Potentially Moving Landslides in Western Oregon*. DOGAMI IMS-22, 2002.

Holzer, T.L., T.C. Hanks, and T.L. Youd. Dynamics of Liquefaction During the 1987 Superstition Hills, California, Earthquake. *Science*, Vol. 244, No. 4900, 1989, pp. 56-59.

Huete, A., K. Didan, T. Miura, E.P. Rodriguez, X. Gao, and L.G. Ferreira. Overview of the Radiometric and Biophysical Performance of the Modis Vegetation Indices. *Remote Sensing of Environment,* Vol. 83, No. 1, 2002, pp. 195-213.

Irigaray, C., T. Fernandez, R. El Hamdouni, and J. Chacón. Evaluation and Validation of Landslide-Susceptibility Maps Obtained by a GIS Matrix Method: Examples from the Betic Cordillera (Southern Spain). *Natural Hazards*, Vol. 41, No. 1, 2007, pp. 61-79.

Jaboyedoff, M., T. Oppikofer, A. Abellán, M.-H. Derron, A. Loye, R. Metzger, and A. Pedrazzini. Use of Lidar in Landslide Investigations: A Review. *Natural Hazards*, Vol. 61, No. 1, 2012, pp. 5-28.

James, T.S., J.J. Clague, K. Wang, and I. Hutchinson. Postglacial Rebound at the Northern Cascadia Subduction Zone. *Quaternary Science Reviews*, Vol. 19, No. 14, 2000, pp. 1527-1541.

Janbu, N. Stability Analysis of Slopes with Dimensionless Parameters. *Harvard Soil Mechanics Series*, Vol. 46, 1954, p. 811.

Janbu, N. Earth Pressure and Bearing Capacity Calculations by Generalized Procedure of Slices. In 4th International Conference on Soil Mechanics and Foundation Engineering, No. 2, London, UK, 1957. pp. 207-212.

Jibson, R.W. Predicting Earthquake-Induced Landslide Displacements using Newmark's Sliding Block Analysis. *Transportation Research Record*, Issue 1411, 1993, pp. 9-17.

Jibson, R.W. Regression Models for Estimating Coseismic Landslide Displacement. *Engineering Geology*, Vol. 91, No. 2, 2007, pp. 209-218.

Jibson, R.W., E.L. Harp, and J.A. Michael. A Method for Producing Digital Probabilistic Seismic Landslide Hazard Maps: An Example from the Los Angeles, California, Area. US Department of the Interior, *US Geological Survey*, 1998.

Jibson, R.W., E.L. Harp, and J.A. Michael. A Method for Producing Digital Probabilistic Seismic Landslide Hazard Maps. *Engineering Geology*, Vol. 58, No. 3, 2000, pp. 271-289.

Jiménez-Perálvarez, J., C. Irigaray, R. El Hamdouni, and J. Chacón. Building Models for Automatic Landslide-Susceptibility Analysis, Mapping and Validation in Arcgis. *Natural Hazards*, Vol. 50, No. 3, 2009, pp. 571-590.

Keaton, J.R., and J.V. DeGraff. Surface Observation and Geologic Mapping, In Landslides, Investigation and Mitigation, *Transportation Research Board*, National Research Council Special Report 247, 1996.

Kelsey, H.M., R.L. Ticknor, J.G. Bockheim, and E. Mitchell. Quaternary Upper Plate Deformation in Coastal Oregon. *Geological Society of America Bulletin*, 1996, pp. 843-860.

Kertész, Á. Application of GIS Methods in Soil Erosion Modelling. *Computers, Environment and Urban Systems*, Vol. 17, No. 3, 1993, pp. 233-238.

Khazai, B., and N. Sitar. Assessment of Seismic Slope Stability using GIS Modeling. *Geographic Information Sciences*, Vol. 6, No. 2, 2000, pp. 121-128.

Kramer, S.L. *Geotechnical Earthquake Engineering*. Prentice-Hall Civil Engineering and Engineering Mechanics Series, Upper Saddle River, NJ: Prentice Hall, 1996, Vol. 1, 1996.

Lambe, T.W., and R.V. Whitman. *Soil Mechanics*. Wiley & Sons, New York, 1969, 553 pages.

Larsen, M.C., G.F. Wieczorek, L.S. Eaton, H.T. Torres-Sierra. The Venezuela Landslide and Flash Flood Disaster of December 1999. In The Proceedings of the Second Plinius Conference on Mediterranean Storms., European Geophysical Society, Siena, Italy, 2000. pp. 519–529.

Lateh, H., M.G. Anderson, and F. Ahmad. CHASM—The Model to Predict Stability of Gully Walls Along the East–West Highway in Malaysia: A Case Study. In Proceedings of the First World Landslide Forum. ISDR, Tokyo, Japan. 2008.

Lee, C.T., C.C. Huang, J.F. Lee, K.L. Pan, M.L. Lin, and J.J. Dong. Statistical Approach to Earthquake-Induced Landslide Susceptibility. *Engineering Geology*, Vol. 100, No. 1, 2008, pp. 43-58.

Lee, S., and K. Min. Statistical Analysis of Landslide Susceptibility at Yongin, Korea. *Environmental Geology*, Vol. 40, No. 9, 2001, pp. 1095-1113.

Lee, S. Application of Logistic Regression Model and Its Validation for Landslide Susceptibility Mapping using GIS and Remote Sensing Data. *International Journal of Remote Sensing*, Vol. 26, No. 7, 2005, pp. 1477-1491.

Lee, S., and T. Sambath. Landslide Susceptibility Mapping in the Damrei Romel Area, Cambodia using Frequency Ratio and Logistic Regression Models. *Environmental Geology*, Vol. 50, No. 6, 2006, pp. 847-855.

Leiba, M. Impact of Landslides in Australia to June 1999. *Australian Journal of Emergency Management*, Vol. 14, No. 3, 1999, p. 30.

Lewis, D. *Technology Dramatically Improves Hazard Mitigation Mapping -Seeing Landslides with Lidar*. DOGAMI, 2006.

Luzi L, F. Pergalani, M.T.J. Terlien. Slope Vulnerability to Earthquakes at Sub Regional Scale: using Probabilistic Techniques and Geographic Information Systems. *Engineering Geology*, Vol. 58, 2000, pp. 313-336.

Ma, L., I.P. Madin, K.V. Olson, R.J. Watzig, R.E. Wells, A.R. Niem, and G.R. Priest. *OGDC-5: Statewide Coverage of the Oregon Geologic Data Compilation*. Oregon Department of Geology and Mineral Industries, 2009.

Mabey, M.A., I.P. Madin, T.L. Youd, and C.F. Jones. *Earthquake Hazard Maps of the Portland Quadrangle, Multnomah and Washington Counties, Oregon, and Clark County, Washington.* Oregon Department of Geology and Mineral Industries, GMS-79, 3 plates, 1993, 104 pages.

Mabey, M.A., G.L. Black, I.P. Madin, D.B. Meier, T.L. Youd, C.F. Jones, J.B. Rice. *Relative Earthquake Hazard Map of the Portland Metro Region, Clackamas, Multnomah, and Washington Counties, Oregon, Oregon*. Department of Geology and Mineral Industries, IMS-1, 1 plate. (Also published as a CD and in Metro Area Disaster (MAD) GIS), 1997.

Madin, I.P. and W.J. Burns. *Pilot Study, Mapping Portland Landslides with LIDAR*. Cascadia from the Oregon Department of Geology and Mineral Industries, Fall, 2006, Vol. 4, No. 2, 2006a.

Madin, I.P., and W.J. Burns. *Map of Landslide Geomorphology of Oregon City. Oregon and Vicinity Interpreted from LIDAR Imagery and Aerial Photographs.* Oregon Department of Geology and Mineral Industries Open File Report O-06-27, 2006b.

Madin, I. P., and W.J. Burns. *Ground Motion, Ground Deformation, Tsunami Inundation, Coseismic Subsidence, and Damage Potential Maps for the 2012 Oregon Resilience Plan for Cascadia Subduction Zone Earthquakes*. DOGAMI O-13-06, 2013. p. 41.

Madin, I.P., and Z. Wang. *Relative Earthquake Hazard Maps for Selected Urban Areas in Western Oregon*. DOGAMI IMS-8, 1999. p. 22.

Makdisi, F.I. and H.B. Seed. Simplified Procedure for Estimating Dam and Embankment Earthquake-Induced Deformations. *Journal Geotechnical Engineering Division*, ASCE, Vol. 104, No. 7, 1978, pp. 849-867.

McKean, J., and J. Roering. Objective Landslide Detection and Surface Morphology Mapping using High-Resolution Airborne Laser Altimetry. *Geomorphology*, Vol. 57, No. 3, 2004, pp. 331-351.

Miles, S., and C. Ho. Rigorous Landslide Hazard Zonation using Newmark's Method and Stochastic Ground Motion Simulation. *Soil Dynamics and Earthquake Engineering*, Vol. 18, No. 4, 1999, pp. 305-323.

Miles, S.B. *Seismic Landslide Hazard for the City of Berkeley, California*. USGS Miscellaneous Field Studies Map MF-2378, 2000.

Montgomery, D.R. Slope Distributions, Threshold Hillslopes, and Steady-State Topography. *American Journal of Science*, Vol. 301, No. 4-5, 2001, pp. 432-454.

Montgomery, D.R., W.E. Dietrich, R. Torres, S.P. Anderson, J.T. Heffner, and K. Loague. Hydrologic Response of a Steep, Unchanneled Valley to Natural and Applied Rainfall. *Water Resource Research*, Vol. 33, 1997.

MorgerNASANearnstern, N.R., and V.E. Price. The Analysis of the Stability of General Slip Surfaces. *Geotechnique*, Vol. 15, No. 1, 1965, pp. 79-93.

Nandi, A., and A. Shakoor. A GIS-Based Landslide Susceptibility Evaluation using Bivariate and Multivariate Statistical Analyses. *Engineering Geology*, Vol. 110, No. 1, 2010, pp. 11-20.

NASA. Aster Global Digital Elevation Map Announcement. 2011. http://asterweb.jpl.nasa.gov/gdem.asp. Accessed 2011.

Nearing, M. Why Soil Erosion Models Over-Predict Small Soil Losses and Under-Predict Large Soil Losses. *Catena*, Vol. 32, No. 1, 1998, pp. 15-22.

Newmark, N.M. Effects of Earthquakes on Dams and Embankments. *Geotechnique*, Vol. 15, 1965, pp. 139-160.

Newmark, N.M., and W.J. Hall. *Earthquake Spectra and Design. Engineering Monographs on Earthquake Criteria, Structural Design and Strong Motion Records*. Vol. 3. Berkeley, Calif., University of California, Earthquake Engineering Research Institute, 1982.

Niewendorp, C.A., and M.E. Neuhaus. *Map of Selected Earthquakes for Oregon, 1841 through 2002*. DOGAMI Open File Report 03-02, 2003.

ODOT. *Unstable Slopes Database*. 2011. http://www.oregon.gov/ODOT/HWY/GEOENVIRONMENTAL/pages/unstable_slope.aspx. Accessed 2011.

Olsen, M.J. *Lateral Spreading Hazard Mapping of Northern Salt Lake County for a Magnitude 7.0 Scenario Earthquake*. In Civil and Environmental Engineering, Masters of Science Thesis, University of Utah, 2005.

Olsen, M.J. Bin 'n' Grid: A Simple Program for Statistical Filtering of Point Cloud Data. *Lidar News,* Vol. 1, No. 10, 2011.

Olsen, M.J., S.F. Bartlett, and B.J. Solomon. Lateral Spread Hazard Mapping of the Northern Salt Lake Valley, Utah, for a m7. 0 Scenario Earthquake. *Earthquake Spectra*, Vol. 23, No. 1, 2007, pp. 95-113.

Oregon Department of Forestry. *Area and Percent of Forest Land with Significant Soil Erosion.* Oregon Department of Forestry. 2013. http://www.oregon.gov/odf/pages/state_forests/frp/ crt4ind18.aspx. Accessed 2013

Orr, E., and W. Orr. *Geology of Oregon*. 6th edition, Oregon State University Press, 2012, 304 pages.

Oregon Lidar Consortium (OLC).   DOGAMI. *Lidar Collection and Mapping*. 2013. http://www.oregongeology.org/sub/projects/olc/. Accessed 2013.

OSSPAC. *The Oregon Resilience Plan, Reducing Risk and Improving Recovery for the Next Cascadia Earthquake and Tsunami*. 2013.

Panhalkar, S., C.T. Pawar, S.P.a.C. Watershed Development Prioritization by Applying Werm Model and GIS Techniques in Vedganga Basin (India). *ARPN Journal of Agricultural and Biological Science,* Vol. 6, No. 10, 2011, pp. 38-44.

Petersen, M.D., A.D. Frankel, S.C. Harmsen, C.S. Mueller, K.M. Haller, R.L. Wheeler, R.L. Wesson, Y. Zeng, O.S. Boyd, D.M. Perkins, N. Luco, E.H. Fields, C.J. Wills, and K.S. Rukstales. *Documentation for the 2008 Update of the United States National Seismic Hazard Maps*. U.S.G.S. Open-File Report 2008–1128, 2008. p. 61.

Pradel, D., and G. Raad. Effect of Permeability on Surficial Stability of Homogeneous Slopes. *Journal of Geotechnical Engineering*, Vol. 119, No. 2, 1993, pp. 315-332.

Pradhan, B. Remote Sensing and GIS-Based Landslide Hazard Analysis and Cross-Validation using Multivariate Logistic Regression Model on Three Test Areas in Malaysia. *Advances in Space Research*, Vol. 45, No. 10, 2010, pp. 1244-1256.

Pradhan, B., and S. Lee. *Landslide Susceptibility Assessment and Factor Effect Analysis: Backpropagation Artificial Neural Networks and Their Comparison with Frequency Ratio and Bivariate Logistic Regression Modelling*. Environmental Modelling & Software, Vol. 25, No. 6, 2010, pp. 747-759.

PRISM Climate Group. *Parameter-Elevation Regressions on Independent Slopes Model*. 2011. http://prism.oregonstate.edu. Accessed 2011.

Qiu, C. Spatio-Temporal Estimation of Shallow Landslide Hazard Triggered by Rainfall using a Three-Dimensional Model. *Environmental Geology*, Vol. 52, No. 8, 2007, pp. 1569-1579.

Rahardjo, H., T.H. Ong, R.B. Rezaur, and E.C. Leong. Factors Controlling Instability of Homogeneous Soil Slopes Under Rainfall. *Journal of Geotechnical and Geoenvironmental Engineering,* Vol. 133, No. 12, 2007, pp. 1532-1543.

Rathje, E.M., and G. Saygili. Estimating Fully Probabilistic Seismic Sliding Displacements of Slopes from a Pseudoprobabilistic Approach. *Journal of Geotechnical and Geoenvironmental Engineering*, Vol. 137, No. 3, 2011, pp. 208-217.

Refice, A., and D. Capolongo. Probabilistic Modeling of Uncertainties in Earthquake-Induced Landslide Hazard Assessment. *Computers & Geosciences*, Vol. 28, No. 6, 2002, pp. 735-749.

Rikli, A.M. *Evaluation of Straw Wattle Placement and Surficial Slope Stability*. Masters Of Science, Oregon State University, 2011.

Roa Lobo, J.G. *Identifying Landslide Hazards in a Tropical Mountain Environment using Geomorphologic and Probabilistic Approaches*. PhD Dissertation, University of Maryland-College Park, 2007.

Sarma, S.K. Stability Analysis of Embankments and Slopes. *Journal of the Geotechnical Engineering Division,* Vol. 105, No. 12, 1979, pp. 1511-1524.

Saygili, G., and E.M. Rathje. Empirical Predictive Models for Earthquake-Induced Sliding Displacements of Slopes. *Journal of Geotechnical and Geoenvironmental Engineering*, Vol. 134, No. 6, 2008, pp. 790-803.

Schmidt, K.M., and D.R. Montgomery. Limits to Relief. *Science*, Vol. 270, No. 5236, 1995, pp. 617-620.

Schulz, W.H., S.L. Galloway, and J.D. Higgins. Evidence for Earthquake Triggering of Large Landslides in Coastal Oregon, USA. *Geomorphology*, Vol. 141, 2012, pp. 88-98.

Sharifi-Mood, M., R. Mahalingam, and M.J. Olsen. Geospatial Characterization of Causative Factors for Landslides in the Oregon Coast Range. Presented at ASCE GeoCongress San Diego, California, 2013, pp. 1595-1604.

Sidle, R. Shallow Groundwater Fluctuations in Unstable Hillslopes of Coastal Alaska. *Zeitschrift fur Gletscherkunde und Glazialgeol,* 1984, pp. 79-95

Sidle, R.C., and H. Ochiai. *Landslides: Processes, Prediction, and Land Use, Water Resources Monograph*, Vol. 18, American Geophysical Union, 2006, 312p.

Soeters, R. and C.J. van Westen. Slope Instability Recognition, Analysis and Zonation. Landslides, Investigation and Mitigation. *Transportation Research Board*, National Research Council, Special Report 247, Chapter 8, 1996, pp. 129-177.

Spencer, E. A Method of Analysis of the Stability of Embankments Assuming Parallel Inter-Slice Forces. *Geotechnique*, Vol. 17, No. 1, 1967, pp. 11-26.

Strenk, P.M., and J. Wartman. Uncertainty in Seismically Induced Slope Deformation Model Predictions. *Engineering Geology*, Vol. 122, 2011, pp. 61-72.

Stuart, N., and C. Stocks. *Hydrological Modelling within GIS: An Integrated Approach*. IAHS PUBLICATION, 1993, pp. 319-319.

Swanson, F.J., and C.T. Dyrness. Impact of Clear-Cutting and Road Construction on Soil Erosion by Landslides in the Western Cascade Range, Oregon. *Geology*, Vol. 3, No. 7, 1975, pp. 393-396.

Tachikawa, T., M. Hato, M. Kaku, and A. Iwasaki. The Characteristics of ASTER GDEM Version 2, *IGARSS*, IEEE, 2011a, pp. 3657 - 3660.

Tachikawa, T., M. Kaku, A. Iwasaki, D. Gesch, M. Oimoen, Z. Zhang, J. Danielson, T. Krieger, B. Curtis, J. Haase, M. Abrams, R. Crippen, and C. Carabajal. *ASTER Global Digital Elevation Model Version 2 – Summary of Validation Results*. NASA, 2011b, 26 pages.

Troost, K.G, D.B. Booth, and S.A. Shimel. *The Geologic Map of Seattle – A Progress Report*. US Geological Survey Open-File Report 2005-1252. http://pubs.usgs.gov/of/2005/1252/, Accessed 2005.

Tsuboyama, Y., R.C. Sidle, S. Noguchi, S. Murakami, and T. Shimizu. A Zero-Order Basin - Its Contribution to Catchment Hydrology and Internal Hydrological Processes. *Hydrol. Process*, Vol. 14, 2000, pp. 287-401.

Turner, A., and R. Schuster. Slope Stability Analysis, Landslides Investigation and mitigation. Chapter 13. *Transportation Research Board*, Special Report 247, 1996, pp. 337-371.

USGS. *2008 NSHM Gridded Data*. 2008. http://earthquake.usgs.gov/hazards/products/conterminous/2008/data/. Accessed 2012

USGS. *Earthquake Hazard Program*. 2012a. http://earthquake.usgs.gov/hazards/. Accessed 2012

USGS. *Landsat Missions*. 2011. http://landsat.usgs.gov/. Accessed 2011

USGS. *Landslide Types and Processes*, Fact Sheet 2004-3072. USGS, 4 p., 2004

USGS. *National Elevation Dataset*. 2012b. http://ned.usgs.gov. Accessed 2012.

USGS. *Routine ASTER Global Digital Elevation Model*. 2012c. https://lpdaac.usgs.gov/products/aster_products_table/astgtm. Accessed 2012.

USGS. *Vertical Accuracy of the National Elevation Dataset*. 2012d. http://ned.usgs.gov/documents/NED_Accuracy.pdf. Accessed 2012

US Earthquake Consortium. Earthquake Vulnerability of Transportation Systems in the Central United States. 2000.

US Search & Rescue Task Force. *Landslides*. 2011. http://www.ussartf.org/landslides.htm. 2011

Van de Water, P.K., S.W. Leavitt, I.P. Panyushkina, A.T. Jull, N.R. Testa, and J. Squire. Tree Trunks from MIS3 Revealed in Pacific Northwest Landslide Deposits. American Geophysical Union, Fall Meeting 2010, abstract #GC21A-0863

Van de Water, P.K., S.W. Leavitt, A.J.T. Jull, J. Squire, and N.R. Testa. Tree Boles Revealed in Pacific Northwest Landslide Deposits Provide Tree-Ring Record for Period Prior to Deglaciation, 2009 Portland GSA Annual Meeting (18-21 October 2009), Paper No. 247-13

Van den Eeckhaut, M., T. Vanwalleghem, J. Poesen, G. Govers, G. Verstraeten, and L. Vandekerckhove. Prediction of Landslide Susceptibility using Rare Events Logistic Regression: A Case-Study in the Flemish Ardennes (Belgium). *Geomorphology*, Vol. 76, No. 3, 2006, pp. 392-410.

Van Westen, C.J. Remote Sensing and Geographic Information Systems for Geologic Hazard Mitigation. *ITC Journal*, Vol. 4, 1993, pp. 393-399.

Van Westen, C., T.W. Van Asch, and R. Soeters. Landslide Hazard and Risk Zonation—Why is It Still So Difficult? *Bulletin of Engineering Geology and the Environment*, Vol. 65, No. 2, 2006, pp. 167-184.

Varnes, D. J. Slope Movement Types and Processes. National Academies of Sciences, *Transportation Research Board*, Special Report 176, 1978. pp. 11-33.

Walker, G.W., and R.A. Duncan. *Geologic Map of the Salem 1 by 2 Quadrangle, Western Oregon.* USGS Miscellaneous Investigations Series Map I-1893, scale 1:250000, 1989.

Wang, Y., and J.L. Clark. *Earthquake Damage in Oregon: Preliminary Estimates of Future Earthquake Losses.* DOGAMI Special Paper 29, 1999. p. 59.

Wang, Y., and W.J. Leonard. *Relative Earthquake Hazard Maps of the Salem East and Salem West Quadrangles, Marion and Polk Counties, Oregon.* DOGAMI GMS-105, 1996.

Wang, Y., R.D. Summers, and R.J. Hofmeister. *Landslide Loss Estimation Pilot Project in Oregon.* Department of Geology and Mineral Industries, 2002.

Wartman, J., L. Dunham, B. Tiwari, and D. Pradel. Landslides in Eastern Honshu Induced by the 2011 Tohoku Earthquake. *Bulletin of the Seismological Society of America,* Vol. 103, No. 28, 2013, pp. 1503-1521.

Waters, A. The Columbia River Gorge—Basalt Stratigraphy, Ancient Lava Dams, and Landslide Dams. Beaulieu, JD, Geologic Field Trips in Northern Oregon and Southern Washington. *Oregon Department of Geology and Mineral Industries Bulletin*, Vol. 77, 1973, pp. 133-162.

Wiley, T. J. Relationship Between Rainfall and Debris Flows in Western Oregon. *Oregon Geology*, 2000, pp. 27-47.

Wilson, J.P., and J.C. Gallant. *Terrain Analysis*. John Wiley & Sons, Inc., 2000. p. 479.

Wilson, R.C., and D.K. Keefer. Dynamic Analysis of a Slope Failure from the 6 August 1979 Coyote Lake, California, Earthquake. *Bulletin of the Seismological Society of America*, Vol. 73, No. 3, 1983, pp. 863-877.

Wilson, R.I., J.A. Treiman, M.A. Silvia, and T.P. McCrink. Multi-Hazard Demonstration Project-Seismically-Induced Landslide Hazard Analysis and Impacts at Areas of Lifeline Concentration, in *The ShakeOut Scenario*. USGS Open File Report 2008-1150, 2008.

Wischmeier W.H. S.D. Prediction Rainfall Erosion Losses: A Guide to Conservation Planning, *Agricultural Handbook*, United States Department of Agriculture, 1978, p. 67.

Wong, I., W. Silva, J. Bott, D. Wright, P. Thomas, N. Gregor, S. Li, M. Mabey, A. Sojourner, and Y. Wang. *Earthquake Scenario and Probabilistic Ground Shaking Maps for the Portland, Oregon, Metropolitan Area*. DOGAMI IMS-16, 2000.

Wooten, R.M., Landslide Hazard Mapping in North Carolina—Geology in the Interest of Public Safety and Informed Decision Making. *Geological Society of America*, Abstract Programs, Vol. 39, No. 2, 2007.

Xinpo, L., and H. Siming. Seismically Induced Slope Instabilities and the Corresponding Treatments: The Case of a Road in the Wenchuan Earthquake Hit Region. *Journal of Mountain Science*, Vol. 6, No. 1, 2009, pp. 96-100.

Yegian, M., E. Marciano, and V. Ghahraman. Earthquake-Induced Permanent Deformations: Probabilistic Approach. *Journal of Geotechnical Engineering*, Vol. 117, No. 1, 1991, pp. 35-50.

Yesilnacar, E., and T. Topal. Landslide Susceptibility Mapping: A Comparison of Logistic Regression and Neural Networks Methods in a Medium Scale Study, Hendek Region (Turkey). *Engineering Geology*, Vol. 79, No. 3, 2005, pp. 251-266.

Yilmaz, I. Landslide Susceptibility Mapping using Frequency Ratio, Logistic Regression, Artificial Neural Networks and Their Comparison: A Case Study from Kat Landslides (Tokat—Turkey). *Computers & Geosciences*, Vol. 35, No. 6, 2009, pp. 1125-1138.

Yin, K.L., and T.Z. Yan. Statistical Prediction Models for Slope Instability of Metamorphosed Rocks. Proceedings of the 5th International Symposium on Landslides, Lausanne, Switzerland, Vol. 2, 1988, pp. 1269-1272.

Young, O.C., K.J. Cheung, and C.U. Choi. The Comparative Research of Landslide Susceptibility Mapping Using FR, AHP, LR, ANN, ESRI User Conference Proceedings, 2003.

Yu, F.C., T.C. Chen, M.L. Lin, C.-Y. Chen, and W.H. Yu. Landslides and Rainfall Characteristics Analysis in Taipei City During the Typhoon Nari Event. *Natural Hazards*, Vol. 37, No. 1-2, 2006, pp. 153-167.

Zadeh, L.A. Fuzzy Sets. *Information and Control*, Vol. 8, 1965, pp. 338-353

Zar, J.H., and T. Breen. *Contemporary Textbooks on Multivariate Statistical Analysis: A Panoramic Appraisal and Critique*. American Statistical Association, 1986.

Zhou, G., T. Esaki, Y. Mitani, M. Xie, and J. Mori. Spatial Probabilistic Modeling of Slope Failure using an Integrated GIS Monte Carlo Simulation Approach. *Engineering Geology*, Vol. 68, No. 3, 2003, pp. 373-386.

Zimmermann, H.J. Applications of Fuzzy Set Theory to Mathematical Programming. *Information Sciences*, Vol. 36, No. 1, 1985, pp. 29-58.

APPENDIX A

LIST OF SYMBOLS

APPENDIX A – LIST OF SYMBOLS

Symbol/Abbreviations	Definition
a_y	Yield Acceleration
AM	Ambraseys and Menu displacement model (1988)
ASCE	American Society of Civil Engineering
ASTER	Advanced Spaceborne Thermal Emission and Reflection Radiometer
ANN	Artificial Neural Network
β	Slope Angle
DA	Discriminant Analysis
D_L	Permanent Displacement
DEM	Digital Elevation Model
DOGAMI	Department of Oregon Geology and Mineral Industries
DTM	Digital Terrain Model
ERDAS	Earth Resources Data Analysis System
ETM+	Enhanced Thematic Mapper Plus
FR	Frequency Ratio
g	Acceleration due to Gravity of Earth (9.81 m/s^2)
GDEM	Global Digital Elevation Map
GIS	Geographic Information Systems
I_a	Arias Intensity
LIDAR	Light Imaging Detection and Ranging
LS	Landslide
LSI	Landslide Susceptibility Index
LR/ LSR	Landslide Ratio
NAD	North American Datum
NASA	National Aeronautics and Space Administration
NDVI	Normalized Difference Vegetation Index

LIST OF SYMBOLS AND ABBREVIATIONS (CONTINUED)

Symbol/Abbreviations	Definition
NED	National Elevation Dataset
NEHRP	National Earthquake Hazards Reduction Program
NLS	Non Landslide
ODOT	Oregon Department of Transportation
OGDC	Oregon Geologic Data Compilation
OGEO	Oregon Geospatial Enterprise Office
OLS	Ordinary Least Squares
φ (Phi)	Friction Angle, component of soil shear strength
P(LS)	Probability of Landslide
PGA	Peak Ground Acceleration
PGV	Peak Ground Velocity
PGD	Peak Ground Displacement
RMS	Root Mean Square
σ	Standard Error
SR	Saygili and Rathje displacement model (2008)
SLIDO	Statewide Landslide Information Database for Oregon
SPR	Statewide Planning and Research
Std.Dev.	Standard Deviation
SVM	Support Vector Machine
T	Period of Sliding Mass
USGS	United States Geological Survey
UTM	Universal Transverse Mercator

APPENDIX B

**ANALYSIS OF DEM PIXEL SIZE AND DATA SOURCE AND
CONTRIBUTION TO LANDSLIDE DETECTION**

APPENDIX B – ANALYSIS OF DEM PIXEL SIZE AND DATA SOURCE AND CONTRIBUTION TO LANDSLIDE DETECTION

B.1 INTRODUCTION

The previous chapters discuss the vulnerability to landslides in Western Oregon and related works that have been done across the research world for landslide mapping. The common conclusion from the studies indicate that GIS is a powerful tool for predicting landslides and remote sensing techniques are the most effective way of collecting the dataset needed for such analysis.

As discussed in the previous chapters, a diverse range of factors such as slope, aspect, precipitation, seismic activity, total wetness index, soil thickness, lithology, NDVI, terrain, terrain ruggedness, land use, influence of stream and faults contribute for triggering a landslide. It should be noted that although terrain, terrain ruggedness, slope roughness and aspect are all important parameters for landslide mapping, these factors are second order products of DEMs compared to slope.

Slope angle and height are the primary parameters that influence the magnitude and spread of the scarp in landslide. These slope parameters are derived from Digital Elevation Models (DEMs). Although there are many ways to generate such models, the most common way of obtaining the model is from satellite images and aerial photographs. However, recent technology advancements have led to improved elevation modeling using remote sensing techniques. This chapter evaluates the efficiency and influence of different techniques and resolutions used for elevation mapping using a frequency ratio analysis. Three different elevation models are used to study its efficiency in developing a landslide susceptibility map.

B.2 DATASETS

Three DEMs (ASTER [30 m], NED [10 m], and Hybrid [30 m]) were used in the analysis for this chapter. Details on these datasets are provided in Chapter 5.

B.3 FREQUENCY RATIO APPROACH

As discussed in Chapter 3, there are multiple techniques available in predicting landslides but Frequency Ratio (FR) and conditional probability (CP) are the two techniques that primarily consider past landslide events. Other techniques like Artificial Neural Networks (ANN), Ordinary Least Squares (OLS), Discriminant Analysis (DA), Support Vector Machine (SVM), and Logistic Regression (LR), which are widely used, incorporate samples which are morphologically undisturbed by landslides. This can sometimes lead to false assumptions, substantially influencing the output. In particular, ANN, DA and SVM are valid for generalized planning but are less useful for site specific ,. In contrast, the FR technique can overcome these problems to be applied across a wide range of scales, from site specific to regional.

With the FR approach, landslides can be predicted by assuming that they are likely to occur under similar conditions as past landslides. It is also a simpler procedure, readily implemented in GIS, compared to the other approaches. For each bin, i, FR is calculated by:

$$FR_i = \frac{\# \, Landslide \, Pixels \, in \, Bin \, i \, / \, Total \, Landslide \, Pixels}{Total \, Pixels \, in \, Bin \, i \, / \, Total \, Pixels \, in \, Grid} \qquad (9\text{-}1)$$

A frequency ratio greater than 1 indicates the site is susceptible to landslides. In order to calculate the frequency ratio, the following preprocessing steps were performed:

The elevation and slope grids were reclassified in to suitable bins (100 m for elevation, 3° for slope).

Summary statistics of the number of pixels classified in each bin were calculated.

Zonal statistics were used to extract DEM and slope values at the locations of existing landslides

Summary statistics of the number of pixels occupied by landslides for each bin (a) were calculated.

The frequency ratio was computed for each bin as the number of landslide pixels in each bin from step (d)/ total number of pixels in each bin from step (b).

A resulting map can then be produced by applying the frequency ratios found in step (e) to the reclassified map in (a).

Table B-1 presents the frequency ratio calculations for slope and Table B-2 presents the frequency ratio calculations for elevation. The frequency ratios for slope and elevation are also plotted in Figures 9.1 and 9.2, respectively.

Several trends can be observed in the plots. For instance, the Hybrid Grid predicts a higher frequency ratio at higher slopes compared to a lower frequency ratio at lower slopes when compared with the ASTER (30 m) or NED (10m). This could indicate that lower accuracy elevation data over predicts landslides at low thresholds and under predicts landslide potential at higher thresholds.

With respect to resolution, the one would expect the higher resolution would enable us to quantify landslide potential better at steeper slopes since vertical surfaces are captured. When examining the NED (10m) DEM curve, we see a higher FR for shallow slopes. This is likely because as resolution improves the pixel size over which elevations are averaged is smaller. This then leads to slope estimates that are not representative of the overall terrain, but capture the finer scale details of steeper and flatter sections (Figure B.3).

Table B-13-1. Frequency ratio analysis for slope values at landslide locations

Bins(degree)	pixels in each bin (%)			Landslide pixels in each bin			Frequency ratio		
	10	hybrid	30	10m	hybrid	30m	10m	hybrid	30m
0-3	0.196687	0.214025	0.081562	0.07758	0.0729	0.037878	0.394435	0.340614	0.464405
3-6	0.099159	0.095316	0.125223	0.084016	0.0564	0.0795222	0.847287	0.591718	0.635043
6-9	0.098683	0.097337	0.123001	0.094547	0.075164	0.0948025	0.95809	0.772211	0.770746
9-12	0.094233	0.094326	0.112501	0.100164	0.079694	0.0989992	1.062938	0.844874	0.879989
12-15	0.0862	0.086542	0.101143	0.094781	0.09134	0.1010438	1.099556	1.055444	0.999019
15-18	0.077444	0.078647	0.092563	0.08542	0.092311	0.0988916	1.102986	1.173737	1.068376
18-21	0.068884	0.070767	0.080694	0.082261	0.093713	0.093296	1.194196	1.324239	1.156167
21-24	0.060502	0.063826	0.069463	0.078165	0.088968	0.0858711	1.291945	1.393904	1.23622
24-17	0.052477	0.056603	0.058952	0.075708	0.082929	0.0718821	1.442679	1.465105	1.219329
27-30	0.04457	0.048829	0.04752	0.060964	0.085625	0.0687614	1.367844	1.753582	1.447003
30-33	0.036725	0.039421	0.03738	0.050082	0.069018	0.0521898	1.363699	1.750761	1.396195
33-36	0.029062	0.027592	0.027857	0.038732	0.05543	0.0411062	1.332729	2.008941	1.475605
36-39	0.021712	0.015472	0.01898	0.031828	0.033538	0.0314215	1.46589	2.167694	1.655524
39-42	0.014945	0.006923	0.011795	0.020477	0.013156	0.0208759	1.370207	1.900381	1.769949
42-45	0.009219	0.002755	0.006422	0.011116	0.005823	0.0124825	1.205799	2.114114	1.943645
45-48	0.005014	0.001019	0.003003	0.007255	0.002696	0.0062413	1.446823	2.646233	2.07851
48-51	0.002473	0.000362	0.00124	0.003393	0.001078	0.0025826	1.372445	2.983034	2.082976
51-54	0.001135	0.000134	0.000457	0.00234	0.000216	0.0008609	2.061077	1.61475	1.883068
54-57	0.000491	5.51E-05	0.000158	0.000702		0.0009685	1.430395		6.111923
57-60	0.00021	2.52E-05	5.53E-05	0.000351		0.0002152	1.670629		3.893035
60-63	9.18E-05	1.26E-05	1.84E-05	0.000117		0.0001076	1.275038		5.852939

B-3

Table B-1-2. Frequency ratio analysis for elevation datasets (DEM) values at landslide location

| Bins(degree)	pixels in each bin (%)			Landslide pixels in each bin			Frequency ratio		
	10	hybrid	30	10m	hybrid	30m	10m	hybrid	30m
0-100	0.138936	0.129848	0.131359	0.224237	**0.233441**	0.214893	1.613962	1.9	1.635917
100-200	0.120679	0.112814	0.115931	0.166519	0.167314	0.1669	1.379856	1.28854	1.439642
200-300	0.111786	0.104369	0.098831	0.144516	0.140777	0.144733	1.29279	1.247865	1.464445
300-400	0.09676	0.090446	0.084766	0.099956	0.104746	0.103734	1.033024	1.003615	1.223766
400-500	0.079251	0.073449	0.070801	0.067337	0.06548	0.070591	0.849669	0.723968	0.997034
500-600	0.066397	0.060925	0.060478	0.047656	0.045523	0.049607	0.717743	0.619795	0.820253
600-700	0.060412	0.055698	0.055556	0.039695	0.037972	0.039492	0.657065	0.623258	0.710853
700-800	0.053741	0.050498	0.053198	0.039142	0.038296	0.039923	0.728348	0.687562	0.750448
800-900	0.047008	0.045158	0.052682	0.04069	0.040022	0.037986	0.865596	0.792533	0.721032
900-1000	0.041127	0.040077	0.045632	0.029965	0.029881	0.03196	0.728591	0.661703	0.700368
1000-1100	0.03458	0.034953	0.039679	0.028417	0.027077	0.027763	0.821762	0.675616	0.699694
1100-1200	0.02946	0.030469	0.034272	0.024436	0.024056	0.024212	0.829464	0.688242	0.706468
1200-1400	0.028346	0.038776	0.032856	0.017691	0.017044	0.01711	0.624126	0.559391	0.52075
1400-1600	0.020359	0.028831	0.025504	0.013379	0.01219	0.014204	0.657151	0.314366	0.556935
1600-1800	0.016386	0.02942	0.021215	0.008182	0.008414	0.008393	0.499338	0.291845	0.395632
1800-2000	0.013734	0.020554	0.018491	0.004423	0.004099	0.004627	0.322029	0.139335	0.250233
2000-2200	0.012459	0.017014	0.016146	0.002543	0.002481	0.002367	0.204127	0.120712	0.146619
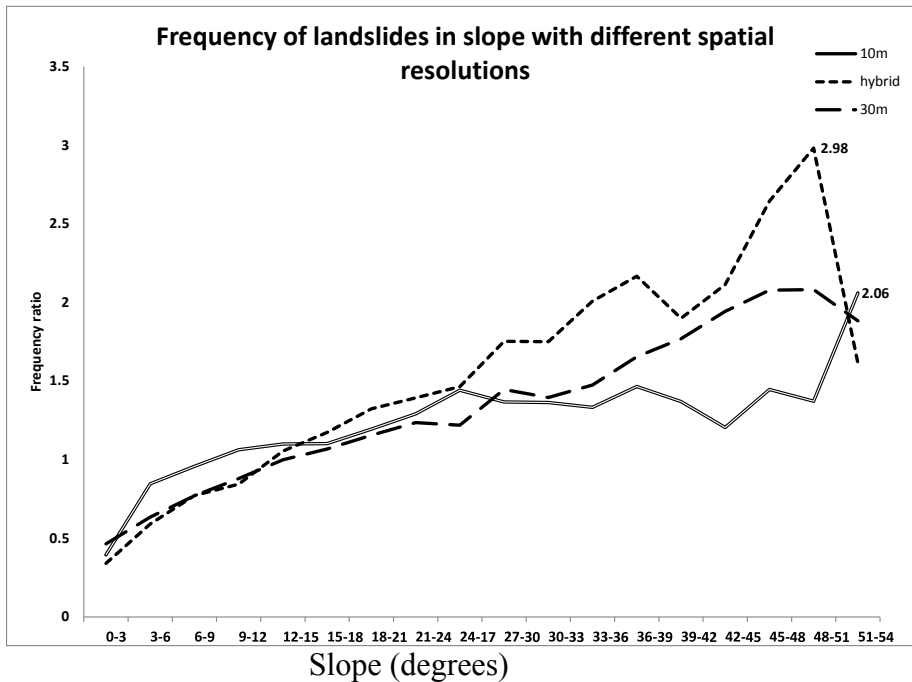
Figure B.1.1: Frequency ratio versus slope bins (degrees)

Frequency of landslides in elevation with different spatial resolutions
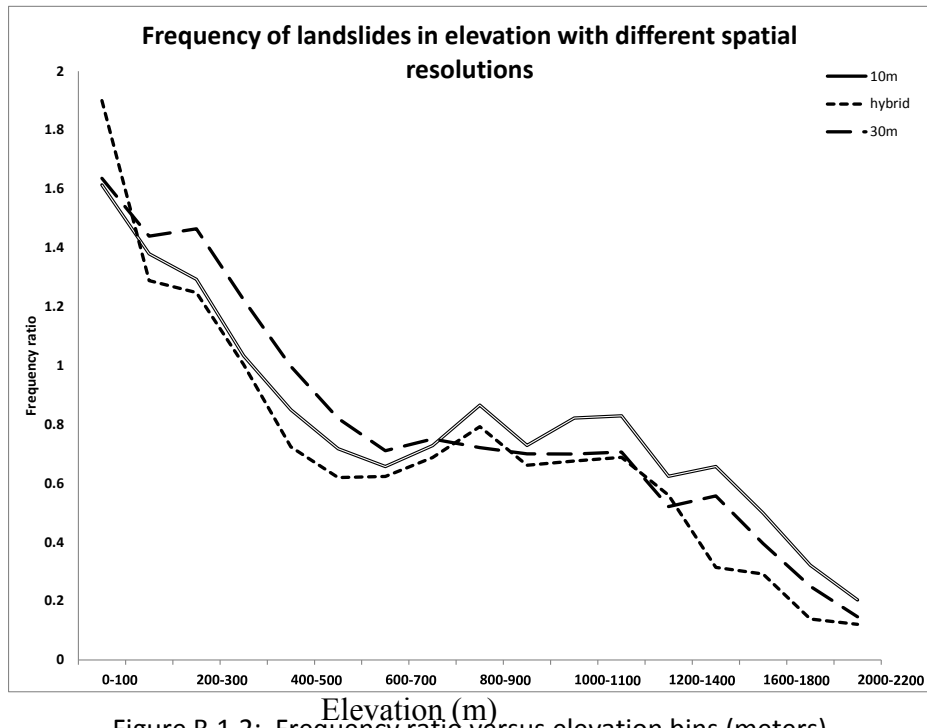
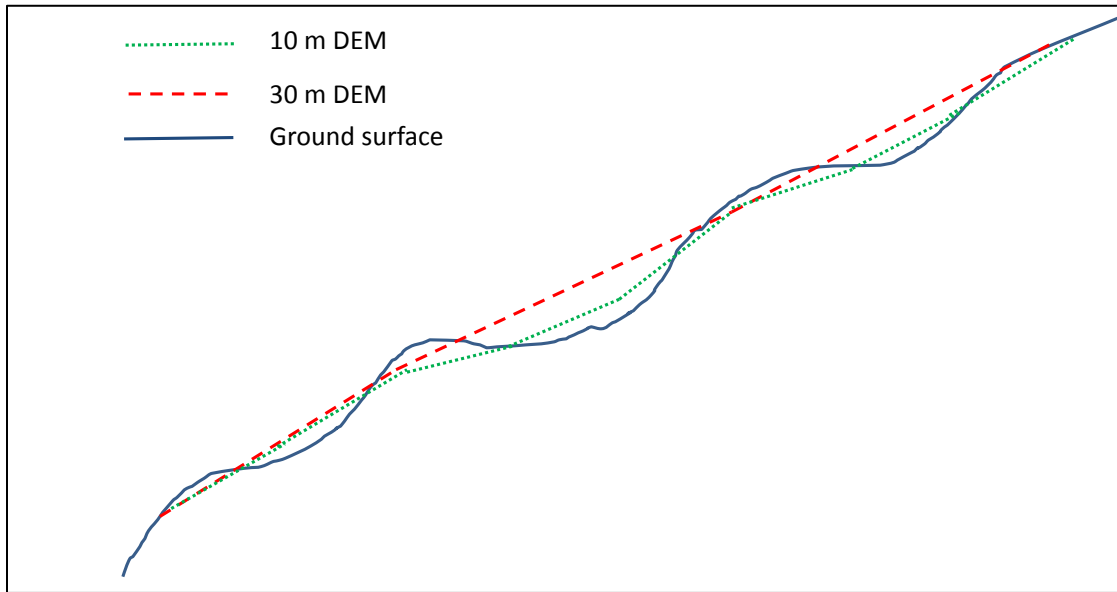Figure B.1.2: Frequency ratio versus elevation bins (meters)

Figure B.1.3: Illustrative example of DEM created using a 10 m and 30 m pixel size. Note that the 10 m can capture localized topographic variability better.

B.4 Influence on Slope Strength Histograms
As discussed in Chapters 6 and 10, strength parameter (e.g., friction angle) distributions for each lithological unit were estimated based on slope values at mapped landslide locations. Figures B.4 to B.9 present results derived from each of the grid types. Overall, the results are similar between each DEM. However, there are some differences worth noting for each of the lithological units:

Metamorphic. The ASTER slopes at landslide locations tend to be shallower compared to the hybrid and NED models. Also, in comparing the hybrid and NED model is a more distinct peak with the hybrid 30 m compared to the NED 10 m that seems to be spread more uniformly throughout the slopes. The NED also picks up several higher slopes (~50 degrees) that are not detected in the ASTER and HYBRID 30 m DEMs. This is likely because of the finer resolution detecting more localized changes in slope.

Plutonic – For the plutonic lithological unit, the ASTER slopes tend to show more landslides occurred at shallower slopes. The NED and HYBRID datasets tend to produce similar results, although the peak is more pronounced in the HYBRID dataset.

Sedimentary – The ASTER DEM tends to predict a lower strength compared to the HYBRID and NED. Again, the HYBRID dataset produces a more pronounced peak.

Surficial Sedimentary – Both the HYBRID and NED datasets show an increased number of landslides at very shallow slopes.

Tectonic - This unit has relatively few samples, and as such, the does not have significant results for comparison. However, the HYBRID DEM shows the least scatter and more resemblance to a normal distribution than the ASTER and NED datasets.

Volcanic – In this unit, the HYBRID slopes tends to have a more defined peak and show less landslide occurrences at shallow slopes. It also has less variance compared to the NED and ASTER slopes.

Overall, for most of the datasets, using the LIDAR in the hybrid DEMs helps define peaks and tends provides a cleaner histogram for using the slope at failure to estimate lithological strength. Hence, a full LIDAR DEM for the entire study area may be able to reduce uncertainty using this methodology even further.

Note that variability in horizontal accuracy of the DEMs can also play a role in the results, particularly in steep slopes.
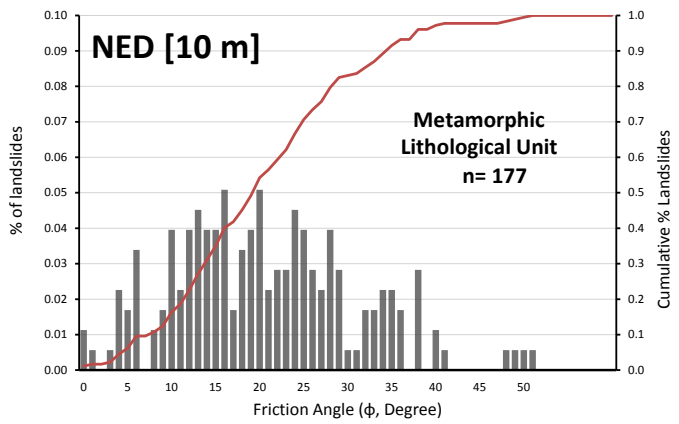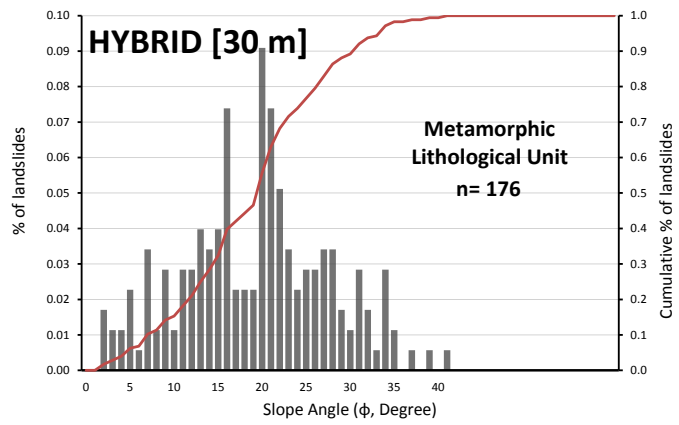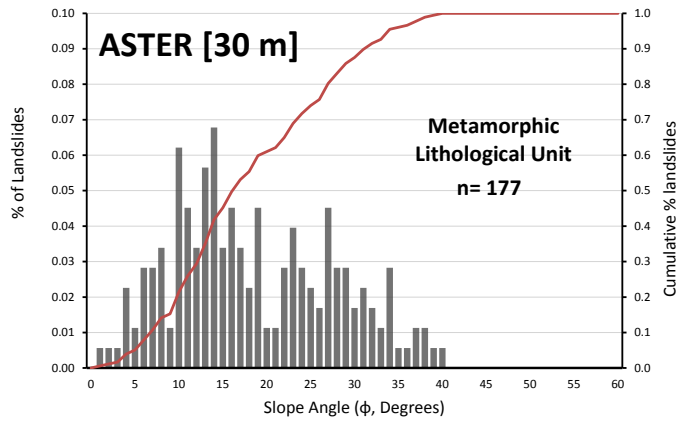
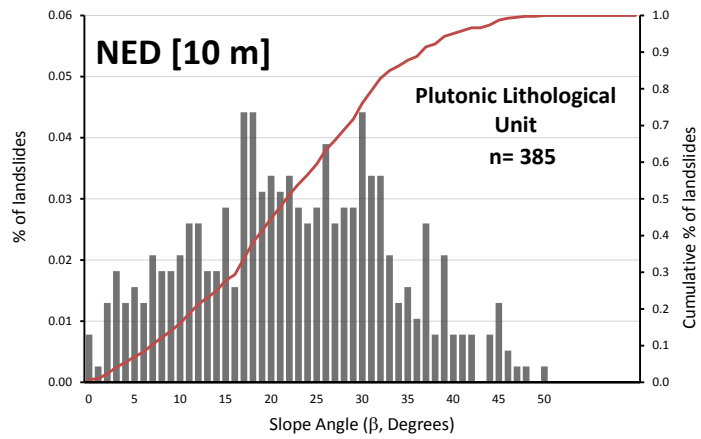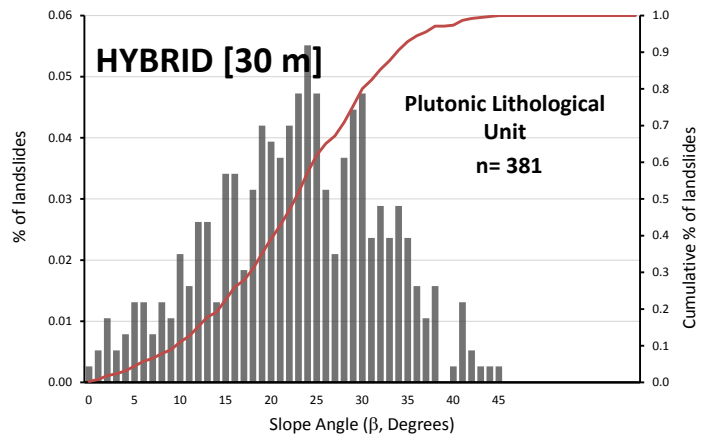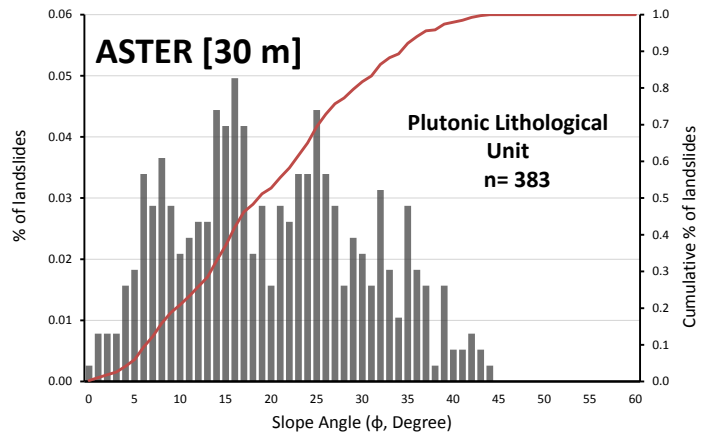Figure B.1.4: Histogram distribution of slopes for the metamorphic lithological unit.

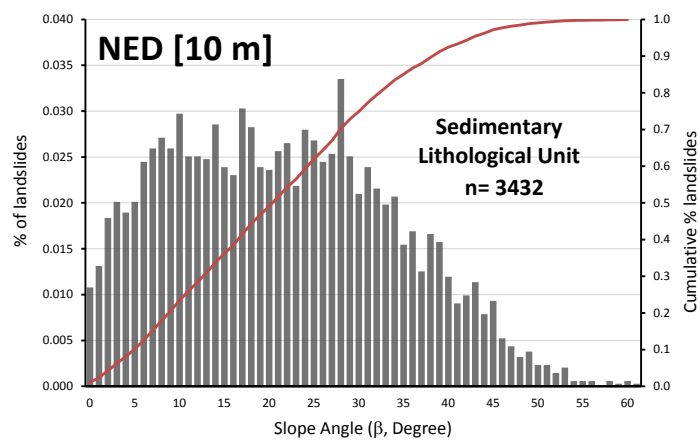Figure B.1.5: Histogram distribution of slopes for the plutonic lithological unit.
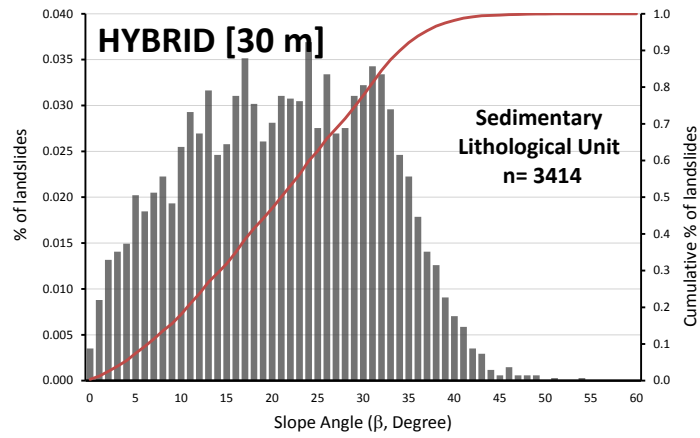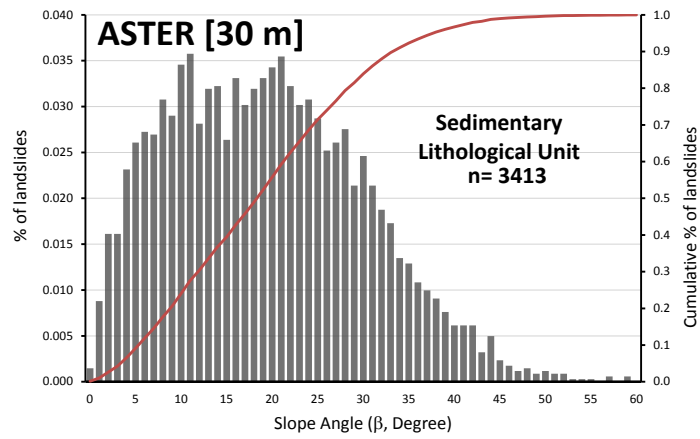
B-8

Figure B.1.6: Histogram distribution of slopes for the sedimentary lithological unit.
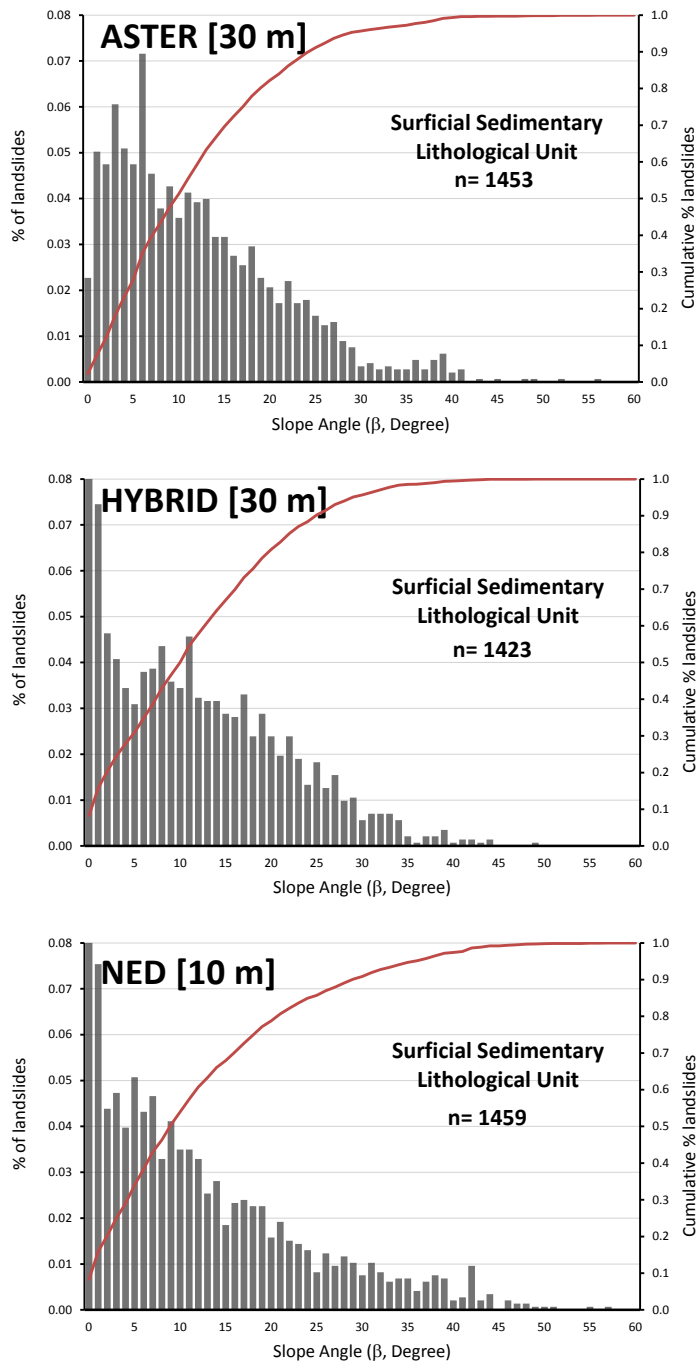
Figure B.1.7: Histogram distribution of slopes for the surficial sedimentary lithological unit.
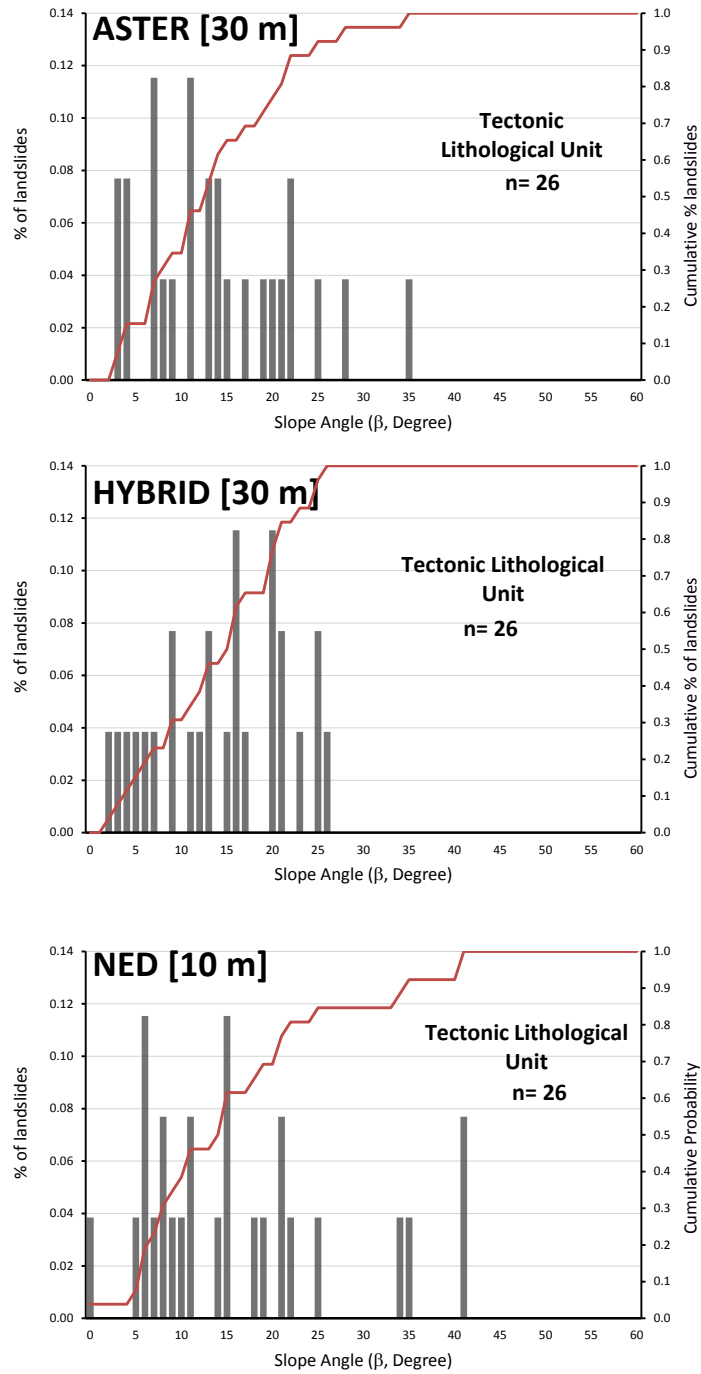
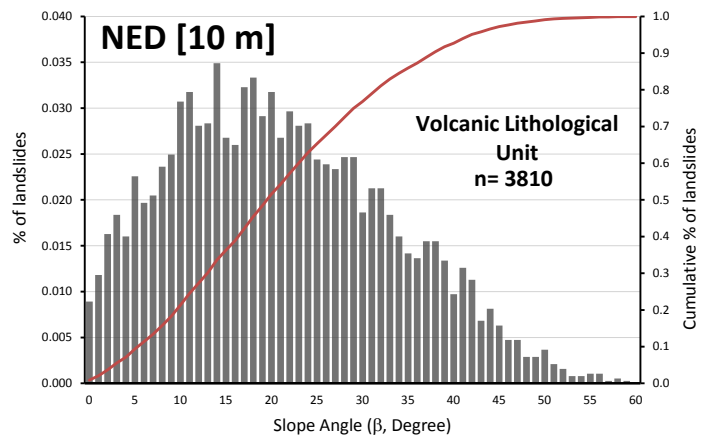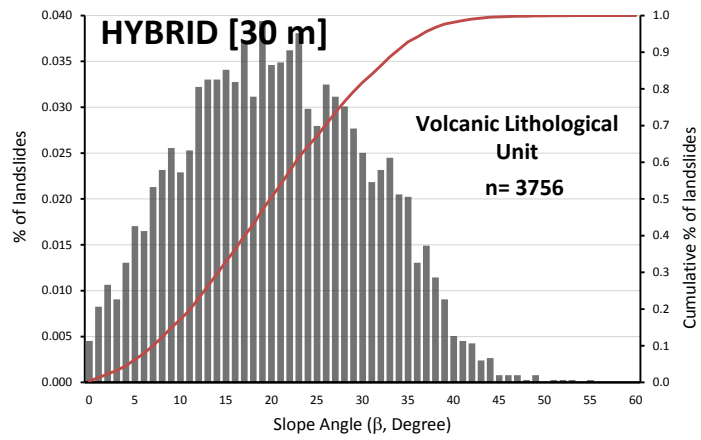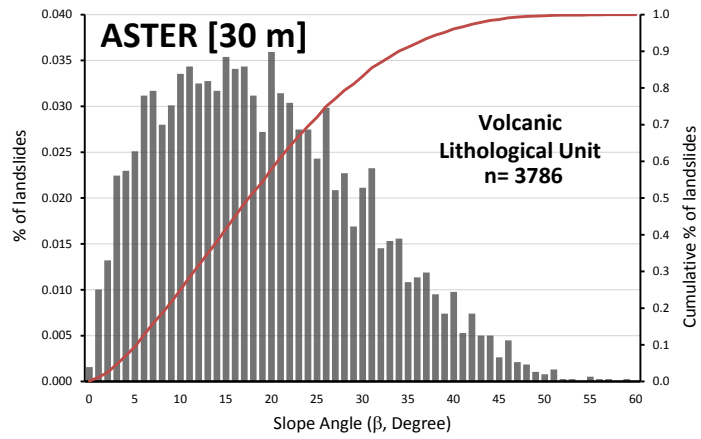Figure B.1.8: Histogram distribution of slopes for the tectonic lithological unit.

B-11

Figure B.1.9: Histogram distribution of slopes for the volcanic lithological unit.

B-12

APPENDIX C

A MAXIMUM ENTROPY APPROACH TO SEISMIC SLOPE STABILITY ANALYSIS AND MAPPING

APPENDIX C – A MAXIMUM ENTROPY APPROACH TO SEISMIC SLOPE STABILITY ANALYSIS AND MAPPING

C.1 INTRODUCTION

As an alternative to the multivariate technique described in Chapter 8, we are exploring the development of additional landslide susceptibility maps for Oregon using a maximum entropy based modeling approach, MaxEnt. This approach, developed by Steven J. Phillips of AT&T Labs along with Miroslav Dudik and Robert E. Schapire of Princeton University, has conventionally been used for species distribution modeling (*Phillips, 2006*). MaxEnt is based on a presence-only machine learning statistical methodology and can generate correlations between occurrence points and predictor variables by removing patterns to maximize randomness. Hence, it is ideally suited to analyze the variety of geospatial and geologic variables that contribute to landslide hazards. MaxEnt is proving to be a very powerful statistical prediction tool and with the exception to very recent work performed by Angel Felicisimo of University Center of Merida, Spain (*Felicisimo and Cuartero, 2012*) and Matteo Convertino of University of Florida (*Convertino, 2013*) it has not been used for landslide susceptibility modeling.

C.2 METHODS

For this work, the landslide susceptibility model was developed using geo-referenced landslide occurrence points from the Statewide Landslide Information Database for Oregon (SLIDO) and numerous predictor layers comprised of remote sensing data, categorical lithology distribution, and probabilistic seismic ground acceleration and velocity predictions. The remote sensing predictor layers include slope and aspect derived from a National Elevation Dataset 30m digital elevation model, annual mean precipitation from PRISM Climate Group and Normalized Difference Vegetation Index (NDVI) data. In addition, we included distance from faults and rivers layers derived from vector data obtained from the Oregon Spatial Data Library. These datasets are described in more detail in Chapter 5.

To determine the suitability of the chosen predictor variables for modeling landslide susceptibility, we developed comparative distribution plots (Figure C.1). These plots provide a graphical comparison of the distribution of values for a given predictor variable throughout the entire extent of the study area against values associated with the individual SLIDO occurrence points.
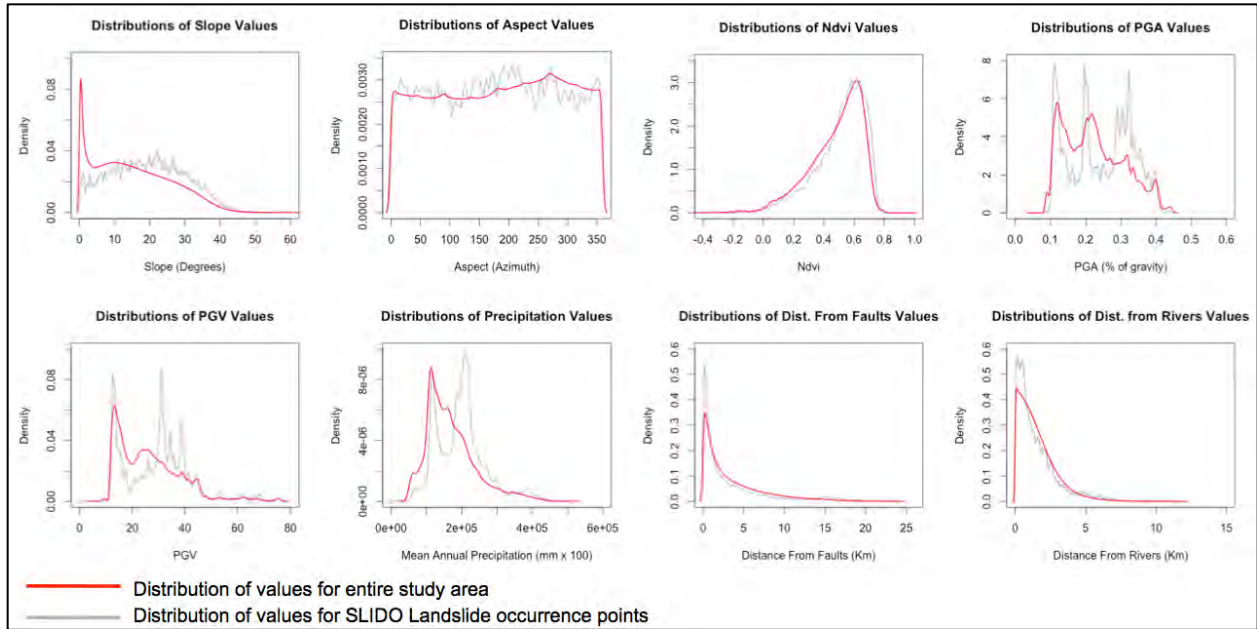
Figure C.1.10: Comparative Distribution Plots

Of these above plots, the NDVI and Distance from Rivers and Faults plots show very little contrast between the distribution of values for the SLIDO landslide occurrence points and the distribution of values for the entirety of the study area. This lack of contrast suggests that NDVI and Distance to Rivers and Faults will not function as a suitable predictor variable for this particular prediction model. In addition, we do not expect Aspect to contribute much to the model given the relatively even distribution of values for the SLIDO occurrence points and the environmental values. Due to the perceived inadequacy of the aforementioned predictor variables, we developed two MaxEnt models, one including all predictor variables (Model 1) and a second model only including the slope, precipitation, PGA and PGV layers (Model 2).

MaxEnt has many options and parameters that can be utilized to fine-tune a model. One of the more significant global parameters is the "regularization multiplier" which is used to control the parsimony of the model. The default regularization value is 1.0, anything lower will result in fitting the model very closely to the occurrence points (over fitting) and anything greater will progressively generalize the model and smooth out the response curves (under fitting). In order to optimize the chosen regularization multiplier for our models we ran numerous iterations of MaxEnt with the aide of BlueSpray, a Java based GIS software developed by SchoonerTurtles, Inc. (http://www.schoonerturtles.com.). BlueSpray contains a module that allows for batch processing of numerous MaxEnt models while systematically changing the regularization parameter. In addition, BlueSpray gathers results and performs calculations after each MaxEnt run, including the area under the receiver operating characteristic curve (AUC) and Akaike Information Criterion (AIC), which can be used to evaluate the quality of the model. Because we kept all but the regularization parameter constant, AIC is an ideal way to judge which regularization value results in the best model. AIC is a valuable tool for relative ranking of statistical models, however, all occurrence points and prediction variables associated with the

C-2

models must be the same in order for comparison of AIC values to be valid. For MaxEnt Models 1 and 2, regularization parameters of 1.4 and 0.7, respectively were found to result in the best AIC values.

C.3 PRELIMINARY RESULTS AND DISCUSSION

The thoroughness of the MaxEnt result output provides a surplus of information for aide in judging relative validity among models and understanding the affect predictor variables have on the result. A critical component of judging relative validity among models is the area under the receiver operating characteristic curve (AUC) which is provided in the beginning of the MaxEnt output (Figure C.2). The AUC is calculated using the receiver operator characteristic curve that plots the percentage of predicted occurrences that match actual occurrence samples versus the percentage of predicted occurrences that do not match. More specifically, The AUC compares the likelihood that the probability of landslide occurrence predicted by the model will be higher in a location shared by an actual landslide occurrence than a random location with no landslide occurrence (*Convertino, 2013*). Landslide susceptibility Model 1 received an AUC of 0.636 and Model 2 received and AUC of 0.630.
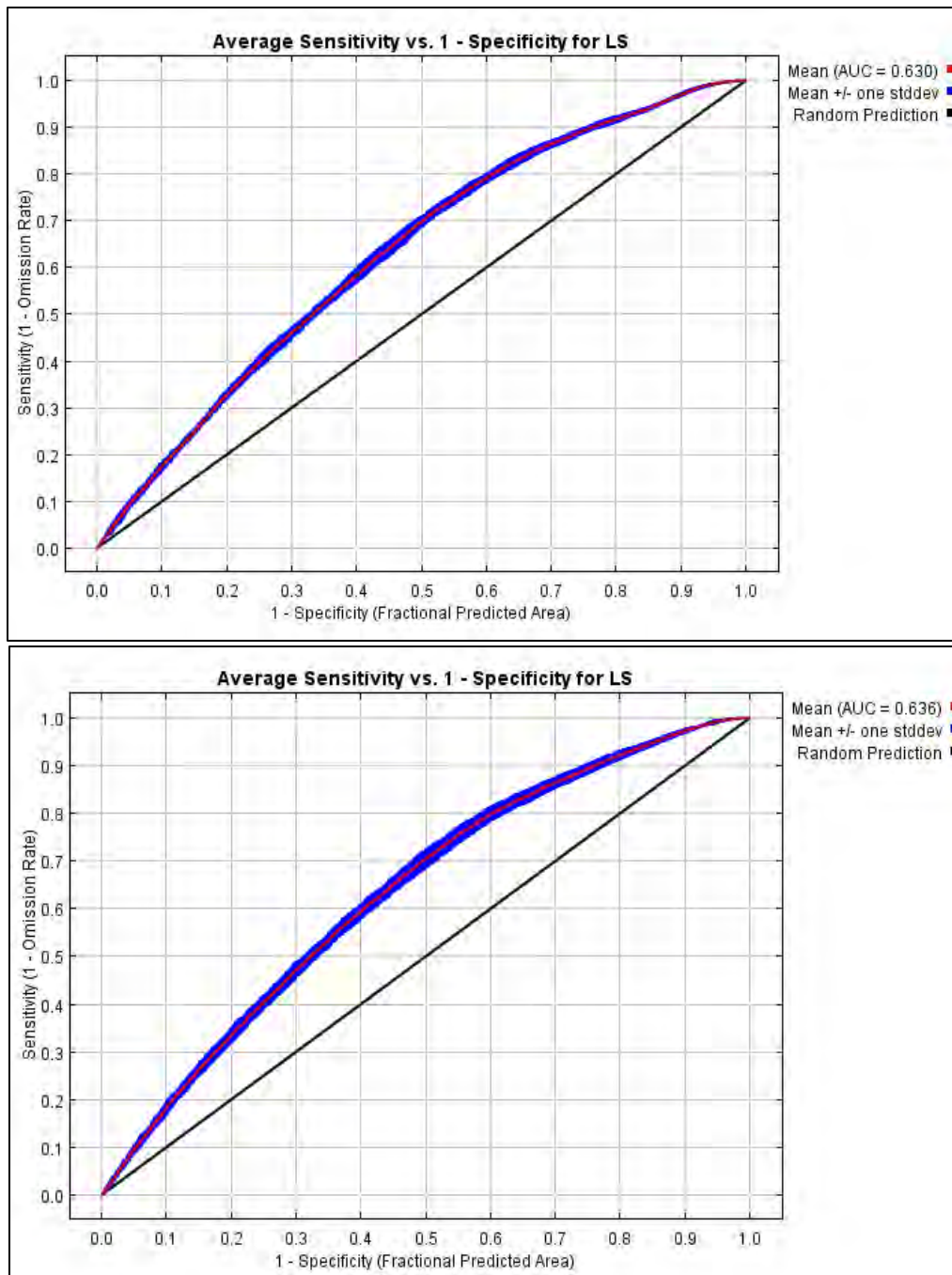
Figure C.1.11: Area under receiver operating characteristic curve plots for Model 1 (Top) and Model 2 (Bottom) (MaxEnt Output)

Another important output to evaluate is the response curves (Figure C.3). The response curves show how the model changes as each predictor variable is varied while all other prediction variables are held at their average sample value (*Phillips, 2006*). Each response curve has a +/- one standard deviation blue band which results from a cross validation performed by MaxEnt.

The cross validation tool randomly splits the occurrence data into a number of groups called "folds" based on the quantity of replicate runs input by the user. MaxEnt develops a model for each replicate run, leaving out one of the folds each time and using it for evaluation (*Elith et al., 2011*). As expected from our discussion of Figure C.1, we observe a relatively flat line response from the Aspect, NDVI, and Distance from Fault and Rivers predictor variables.

To further understand how the predictor variables affect the resulting model a jackknife test can be enabled in MaxEnt (Figure C.4). MaxEnt performs a jackknife test by generating numerous models for which each predictor variable is excluded in turn followed by creation of models where each predictor is used in isolation. A comparison between the jackknife models and a model including all predictor variables is then performed to identify the predictor with the highest gain when used in isolation and the predictor that decreases the gain the most when it is omitted. Gain in MaxEnt is closely related to deviance, a measure of goodness of fit used in generalized additive and generalized linear models. At the end of a MaxEnt run, the gain indicates how closely the model is concentrated around the occurrence points (*Phillips, 2010*).

Based on the jackknife results for Model 1, we can conclude that the Precipitation and Slope predictors provide the most useful information (Figure C.4, see dark blue bar) for development of the model, followed by PGV and then PGA. In addition, because the teal colored bar belonging to the Slope predictor is shortest (farthest from the right) we can conclude that the omission of Slope has the largest effect on the model. From this, we can infer that Slope contributes information distinct from the other predictors. The Jackknife test for Model 2 generated similar results.
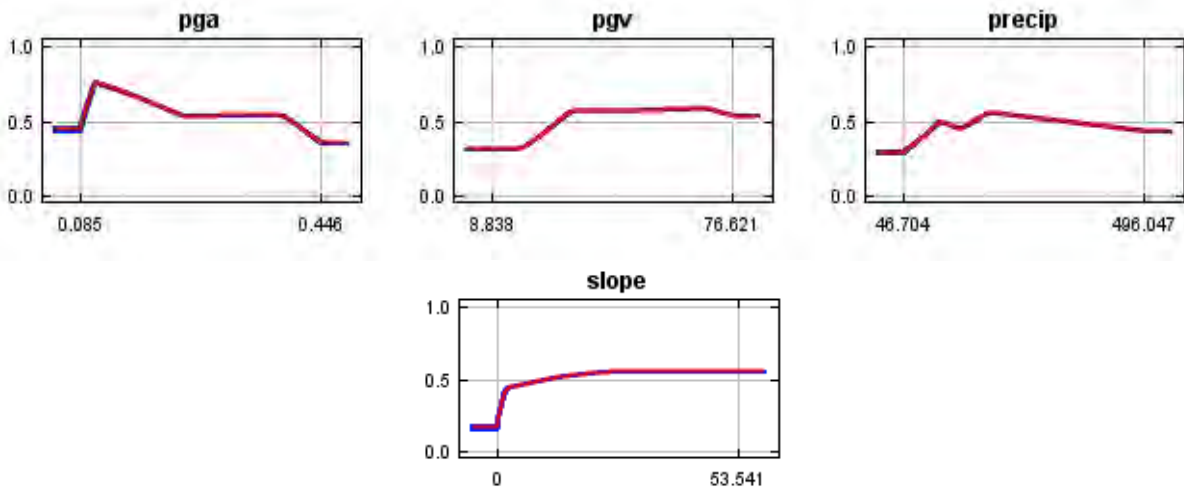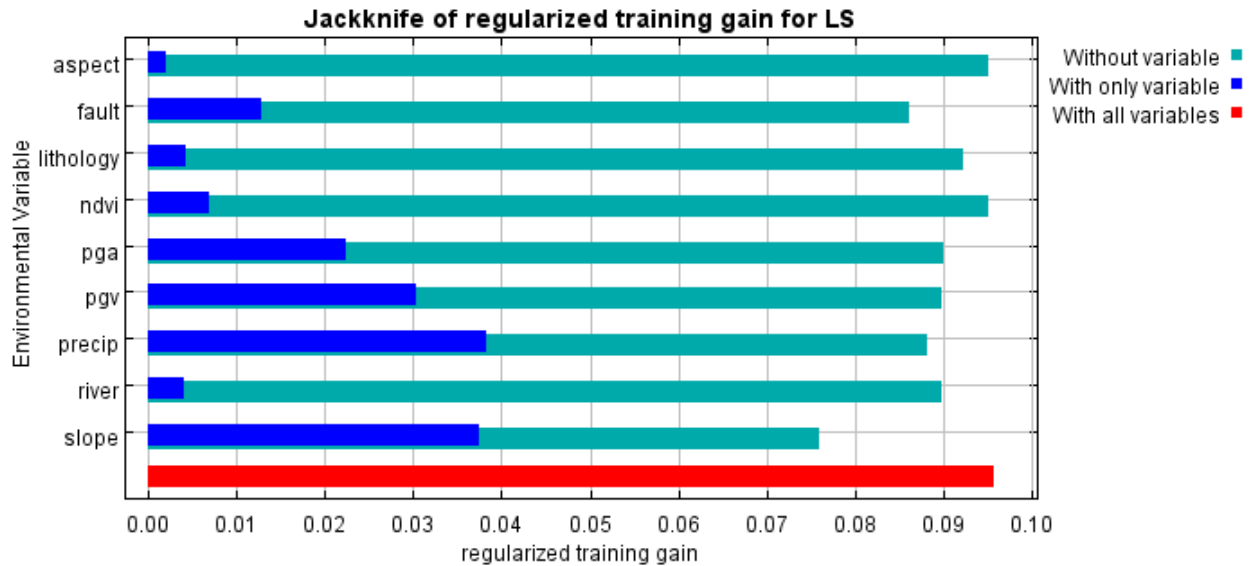
Model 1
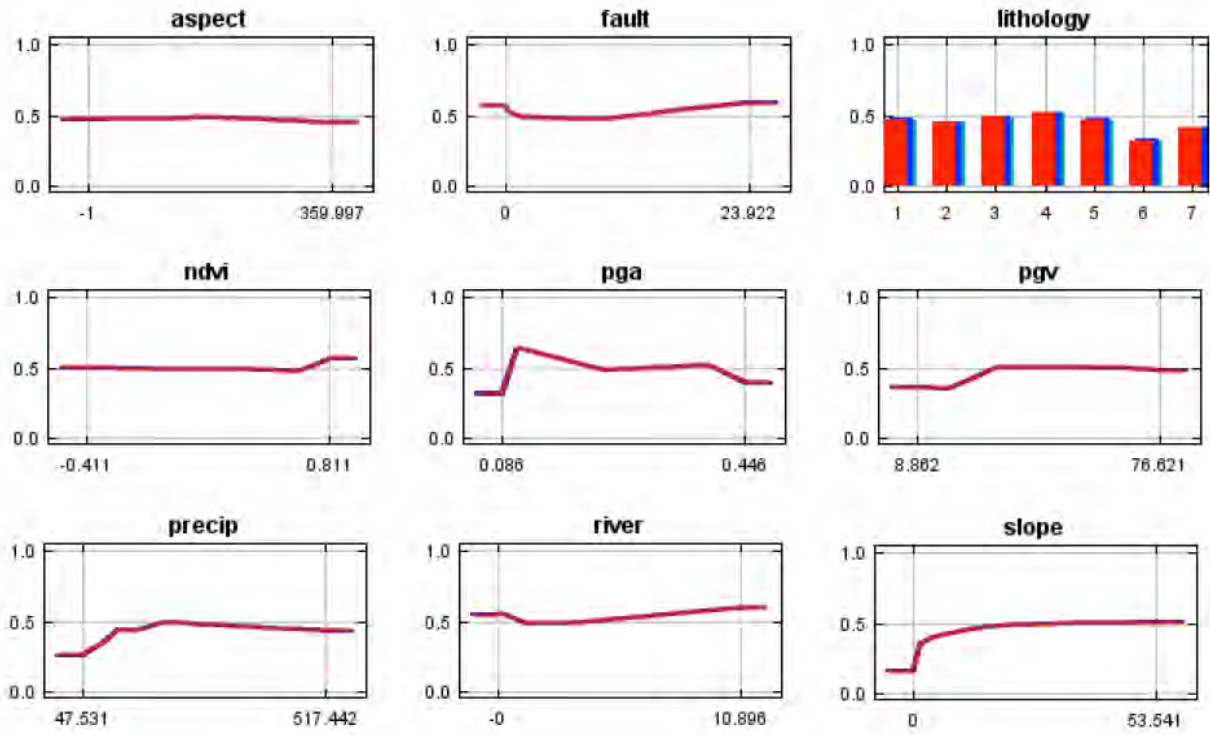
Model 2

Figure C.1.12: Model 2 Response Curves for Predictor Layers (MaxEnt Output)
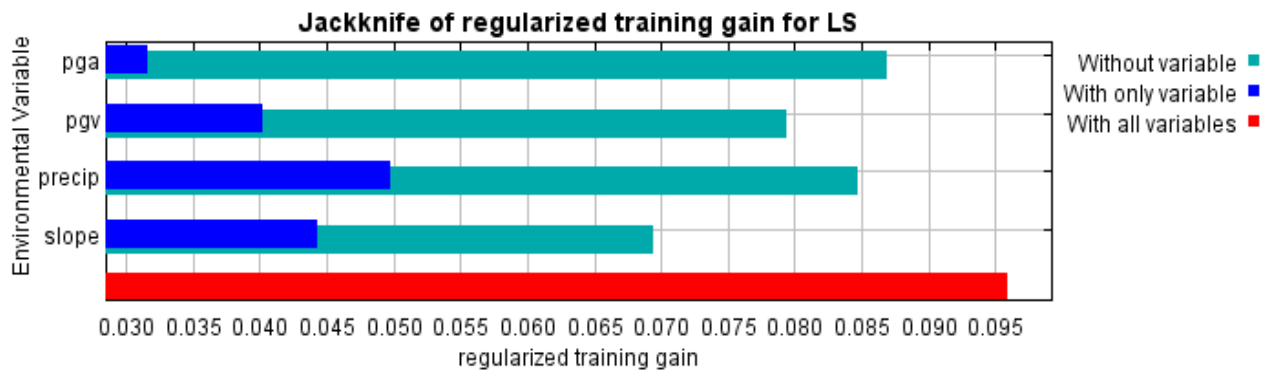
C-6

Model 1

Model 2

Figure C.13: Results of Jackknife Procedure (MaxEnt Output)

The final prediction surfaces derived from our MaxEnt models for landslide susceptibility are presented in Figure C.5. Slight differences can be observed amongst the two models. They both identify similar hotspots, however, Model 2, utilizing only the top four contributing predictor variables appears more concise in its distribution of landslide susceptibility zones.
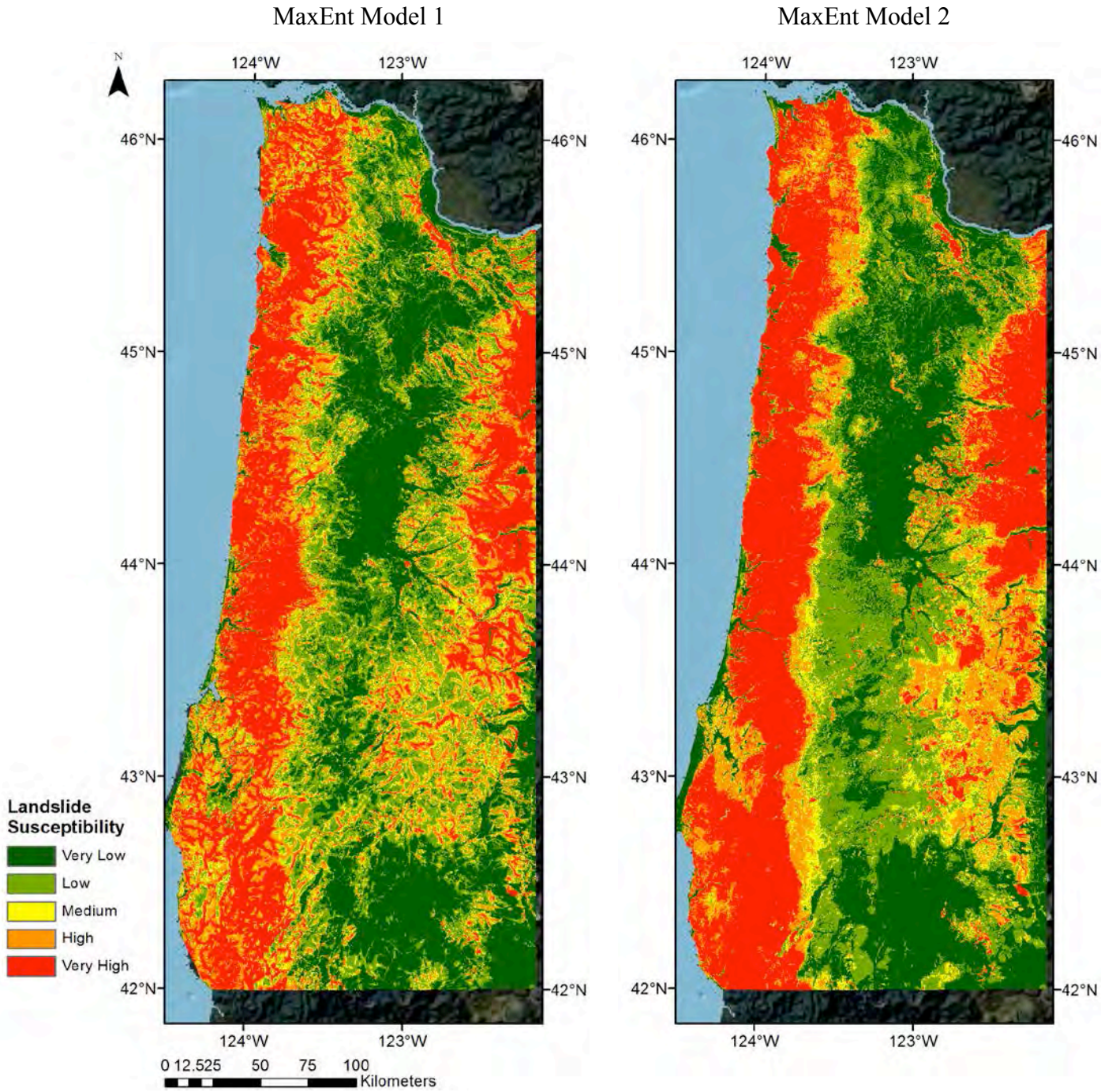
Figure C.1.14: Final MaxEnt Prediction Surfaces for Landslide Susceptibility

As a preliminary effort to validate the MaxEnt-derived model, we overlaid mapped landslide polygons from SLIDO on the prediction surface. Review of the side-by-side maps indicated a satisfactory correlation between polygon locations and areas of high probability of landslide occurrence indicated by MaxEnt (Figure 8.6). In some cases, high probability dark red zones

C-8

line up exactly with mapped landslide polygons (Figure C.7). This is a result of MaxEnt detecting the relationship between SLIDO occurrence points and the surficial sediments lithologic unit combined with the fact that many post landslide terrains have been mapped as surficial sediments. Also, mapped landslide polygons were classified as weak soils in the PGA and PGV maps created in the Oregon Resilience Plan.
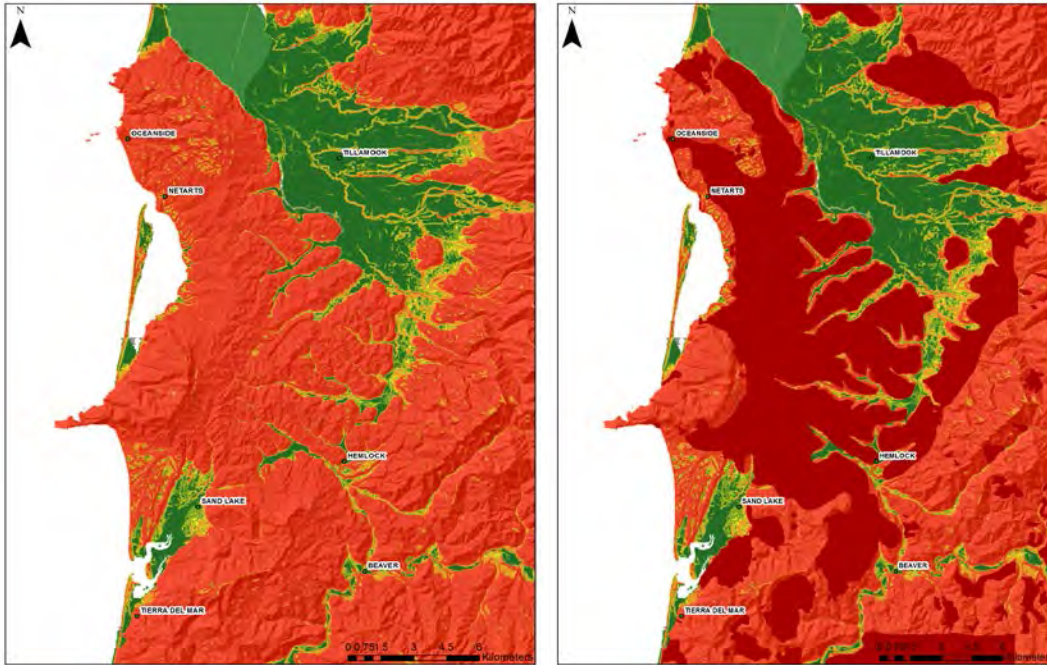

Figure C.1.15: Visual validation of MaxEnt prediction surface (Left) with SLIDO landslide polygons (Right) near Tillamook, Oregon.
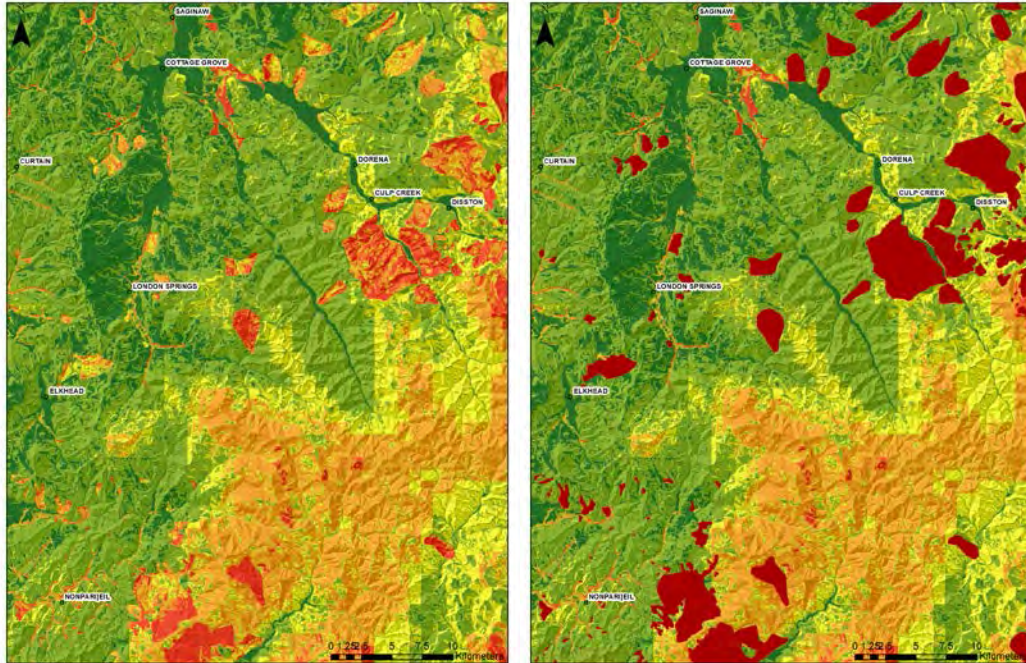
Figure C.11.16: Visual validation of MaxEnt prediction surface (Left) with SLIDO landslide polygons (Right)

C.4 CONCLUSION

Using MaxEnt as a modeling technique enables improved understanding of the contribution of causative factors and aids in judging the validity and consistency of output models. Our preliminary models derived using this approach compare well with results obtained from modeling using other techniques in Chapters 6 and 7. Future work will entail: further refinement of the MaxEnt model by way of parameter adjustment, a systematic comparison of MaxEnt prediction models with models developed using other methods, exploring results when using a 10 m resolution digital elevation model and lastly experimenting with the omission of certain types of landslides included in the SLIDO data.

APPENDIX D

OUTPUT AMBRASEYS AND MENU (1988) DISPLACEMENT REGRESSION MODEL

This section provides output maps using the AM displacement model for validation purposes only. These maps are not recommended for use.

APPENDIX D – OUTPUT AMBRASEYS AND MENU (1988) DISPLACEMENT REGRESSION MODEL
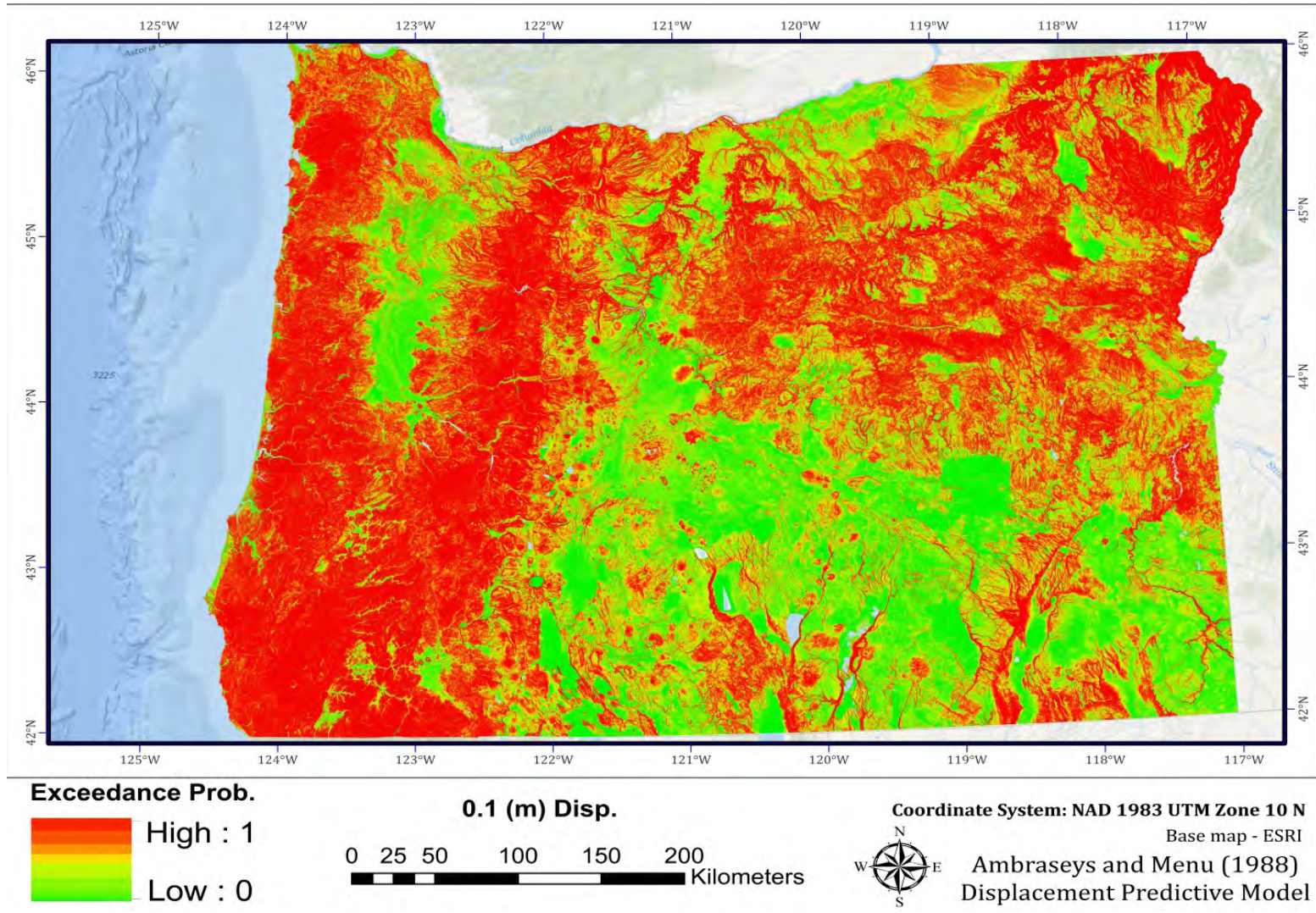

Figure D.1.17: 10 centimeter displacement exceedance hazard map for state of Oregon with Ambraseys and Menu (*1988*) predictive displacement regression model.
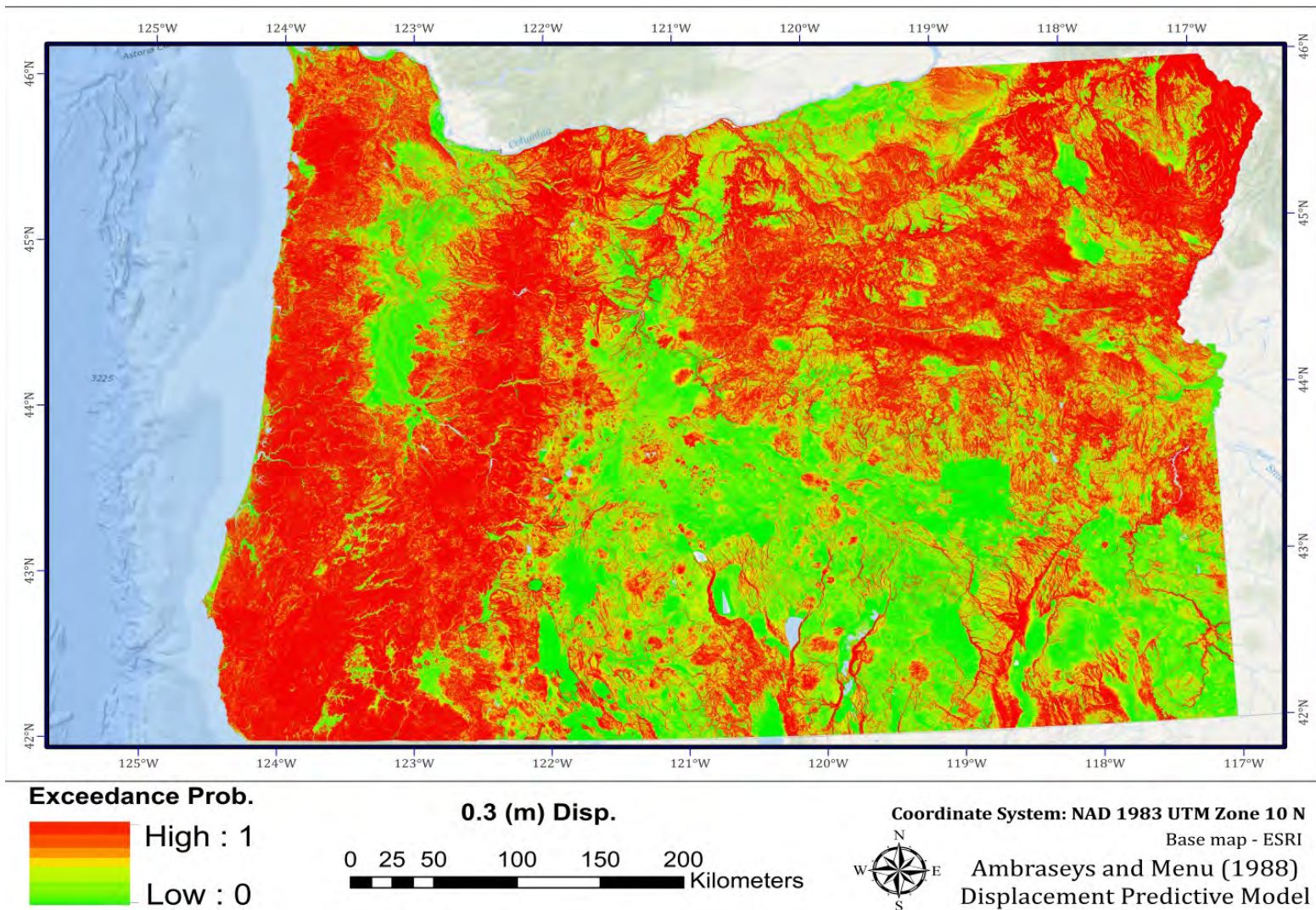
Figure D.1.18: 30 centimeter displacement exceedance hazard map for state of Oregon with Ambraseys and Menu (*1988*) predictive displacement regression model.
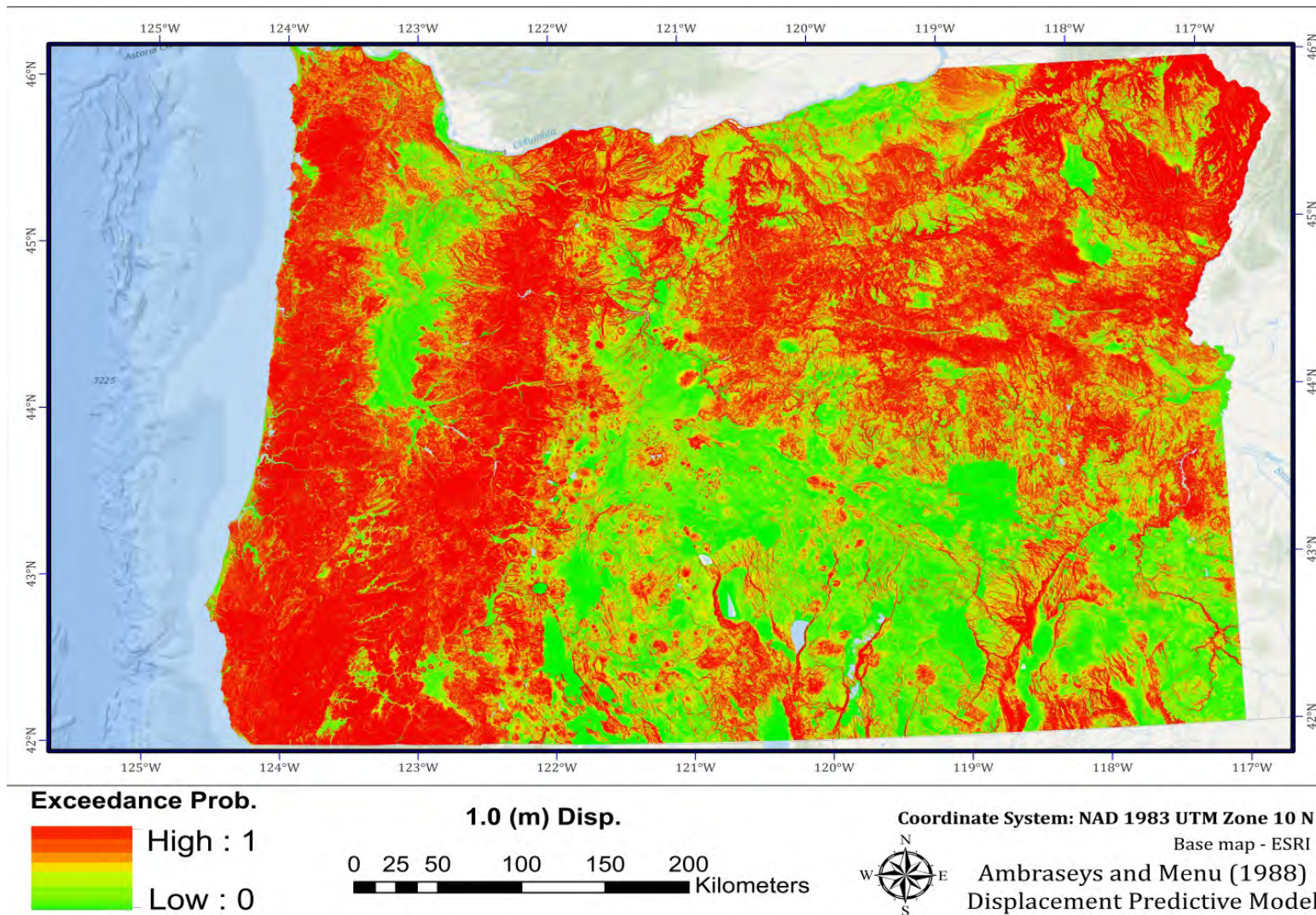
Figure D.1.19: 1 meter displacement exceedance hazard map for state of Oregon with Ambraseys and Menu (*1988*) predictive displacement regression model.
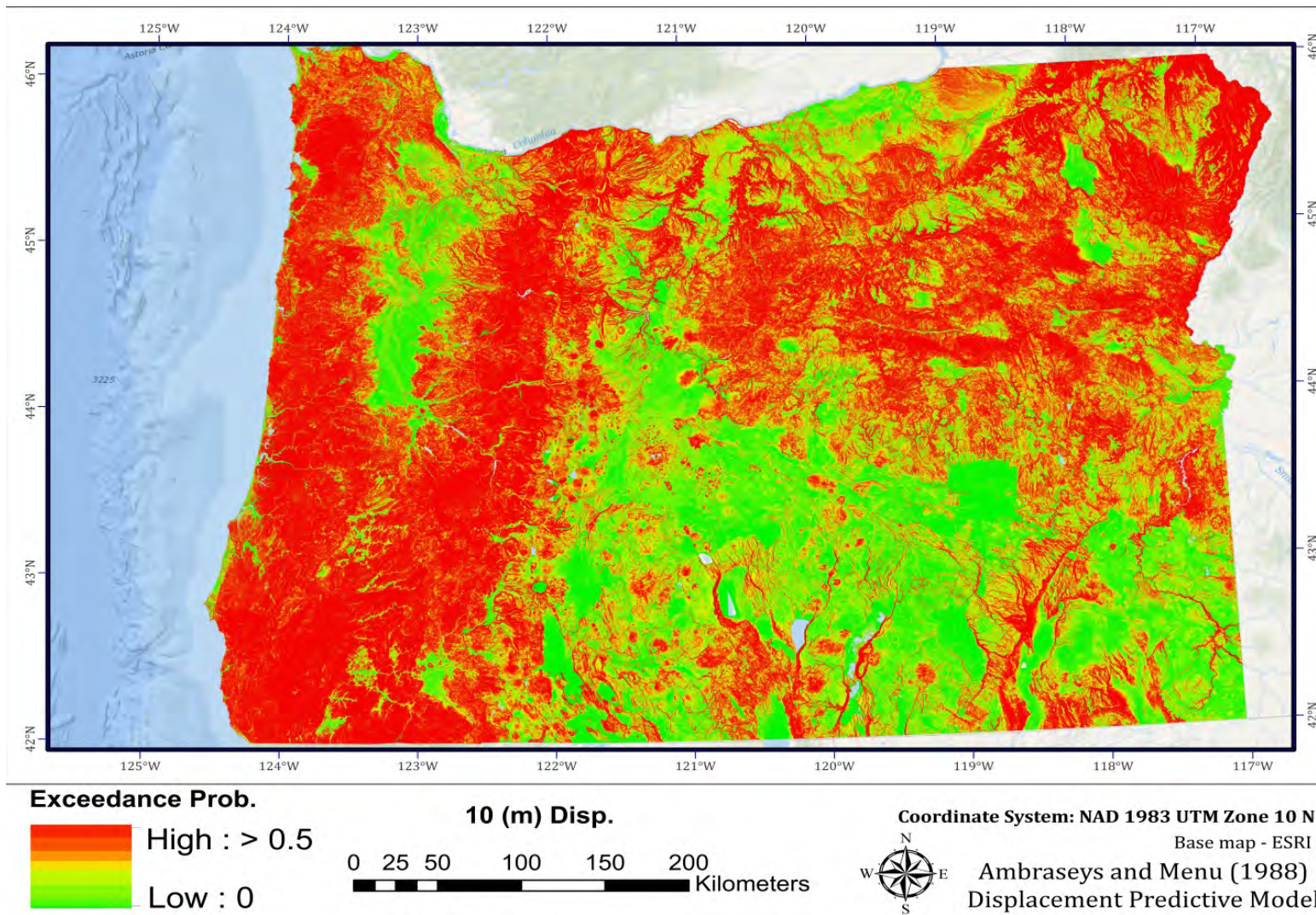
Figure D.1.20: 10 meter displacement exceedance hazard map for state of Oregon with Ambraseys and Menu (*1988*) predictive displacement regression model.
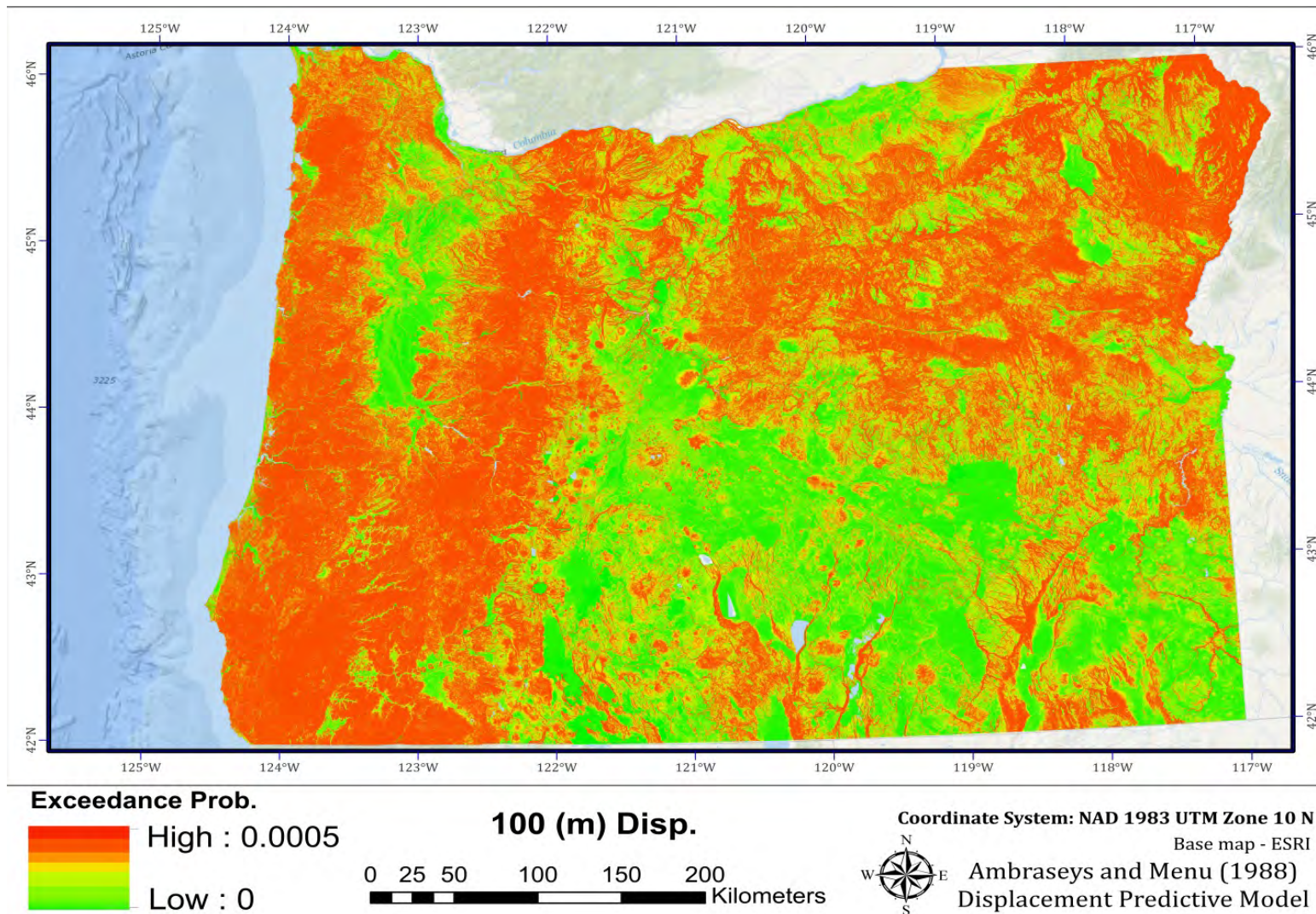
Figure D.11.21: 100 meter displacement exceedance hazard map for state of Oregon with Ambraseys and Menu (*1988*) predictive displacement regression model.

APPENDIX E

REMEDIATION TECHNIQUES

APPENDIX E - REMEDIATION TECHNIQUES

Slope management is a challenging task due to the high variability of conditions that are site specific. Table F-1 summarizes several techniques used for slope remediation based on findings of comprehensive reports. This appendix will also highlight key references that provide examples and guideline procedures for slope management and repair.
Canadian Ministry of Forests Land Management Handbook #18: "A Guide for Management of Landslide Prone Terrain in the Pacific Northwest, 2nd Edition". (*Chatwin et al., 1994*).

While this guide was developed for forestry applications, it has significant relevance to highway slope management.

The authors break down unstable slope control and management into four categories:

Avoiding the unstable situation

Preventing destabilization of marginally stable soils

Stabilizing unstable slopes

Protecting downslope resources when unstable situations cannot be corrected.

The wide variety of slope stabilization techniques can be divided into four basic categories:

Unloading the head of the slope

Draining groundwater

Loading the toe of the slope

Shifting the position of the potential failure surface

USGS Landslide Handbook (Circular 1325) – Appendix C "Introduction to Landslide Stabilization and Mitigation". This resource provides a very comprehensive overview of various types of techniques for landslide stabilization based on the type of landslide. This resource is a concise, updated summary of information that was taken from Chatwin et al. (*1994*), discussed above. However, this handbook also provides simple guidance for homeowners living near unstable slopes.

NCHRP Synthesis 430 "Cost-effective and sustainable road slope stabilization and erosion control."

Most roads (88% in the world, 75% in the US) throughout the world are low-volume, rural roads.

This synthesis conducted a literature review and questionnaire for current practices, effective practices, and emerging solutions for road slope management.

The appropriate stabilization technique depends highly on site characteristics including water (location, amount of rainfall, drainage and flow rates), soil properties (type, strength, plasticity, etc.), and topography.

Emphasis should be placed on proactive erosion prevention since it is easier and more cost effective than to fix a failed slope.

Multiple techniques can be used together.

More research is needed for benefit –cost analysis of products and techniques as well as the capabilities of various slope stabilization techniques.

This report presents several summary tables of pros and cons of various erosion control, biotechnical stabilization, mechanical stabilization, and earthwork techniques.

WA-RD 787.1 "Design Guidelines for Horizontal Drains used for slope stabilization." These guidelines were developed to provide a comprehensive reference to design horizontal drainage systems". Key findings and recommendations in this report include:

These guidelines consider translational and rotational failures, including fractured systems.

The guidelines provide an iterative approach to optimize the number of drains required while maintaining a FS > 1.2.

The guidelines consider both steady state and transient conditions for flat surfaces and slopes <10°.

The guidelines also conclude that drains installed in the upper regions of slopes are less effective compared to drains installed in deeper sections (Unless there is perched water in the slope). Installation of drains in the upper section also reduces the amount of concentrated water pouring out on the slope.

Translational failures for thin geologic sections were found to be more sensitive to increases in water levels in the upper slope (e.g. precipitation). Rotational failures were found to be more sensitive to rising pore pressures in the lower slope.

Effectiveness of horizontal drains decreases with increasing soil anisotropy.

NCHRP-IDEA Project 57 Final Report "Landslide stabilization using wick drains"

Wick drains resist clogging, are inexpensive, flexible, and easy to install.

The study is based on field studies of wick drains at eight sites across the central US and a literature review.

It provides guidance on appropriate depths (< 3-5 m beyond failure surface), installation angle (near horizontal), clustering of drains and fanning outward (to avoid concentration of water at one location), using an appropriate filter mesh based on soil fine content, and use of a pushing pipe for installation to reduce smear.

It also discusses limitations of wick drains including difficulty installing in dense soils and rock. Wick drains are ideal when SPT N (blows/ft.) values are less than 20 and are not feasible when N values are greater than 30.

Table F-1. Summary of common slope stabilization techniques (continued on next page).

		Description	Best use	Cost
Geometrical	**Excavation**	Increasing the stability by lowering the driving force	Deep Soils with rotational landslides	$
	Slope lowering	Moving out the brow of Slope and reducing weight of materials	Shallow instabilities	$
	Height Reducing	Reducing the weight of the soil mass and forming a lower slope by excavation	Not as efficient as other methods	$
	Benches	Reducing shallow failures not the total slope stability	Steep slopes or rock face	$
Hydrological	**Shallow drainage**	It will do the surface drainage at the slope head	Shallow soils overlying on an impermeable layer	$$
	Deep drainage	More effective than shallow,filtration routes in the ground	Steeper Slopes	$$$
	Isolated wells	Preparing a drainage pump for each well, lowering the water pressure	Moderate or Steeo Slopes	$$$$
	Drainpipes	Common in highway construction, most effective during the perliminery excavation	When it is designed based on the various slope properties	$$$

Table F-1 (continued). Summary of common slope stabilization techniques.

		Description	Best use	Cost
Reinforcement elements	**Retaining Walls**	Drainage behind the wall is essential	When it is designed based on the backfill and the slope properties	$$$$
	Anchors	Increasing the resistance to sliding by an active force	Moderate to Steep Slopes	$$$
	Shotcrete	Type of concrete by air jet which provide surfacial stability and avoid wethering	Local surfacial instabilities	$
	Mesh and Cable	Simple, cheap method to prevent falling of rock blocks in to the road	For fractures instable rocks	$
	Soil nailing	Increasing the properties of the ground	Deep potential failure surfaces	$$$
	Micropiles	Improving the ground characteristics by creating a 3D grid of micropiles tied to rigid reinforce concrete	When the potential landslide is not very extensive	$$$